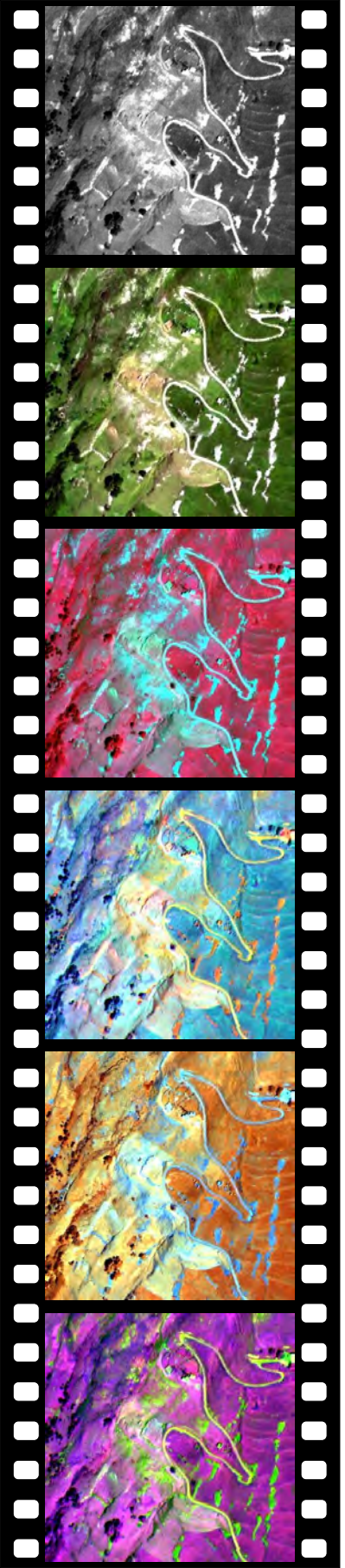

Imaging spectroscopy for ecological analysis in forest and grassland ecosystems

Lucie Homolová

Imaging spectroscopy for ecological analysis in forest and grassland ecosystems

Lucie Homolová

Thesis committee

Promotor
Prof. Dr M.E. Schaepman
Professor of Remote Sensing, University of Zürich, Switzerland
Professor of Geo-Information Science and Remote Sensing, Wageningen University

Co-promotor
Dr J.G.P.W. Clevers
Associate Professor, Laboratory of Geo-Information Science and Remote Sensing
Wageningen University

Other members
Prof. Dr H.B.J Leemans, Wageningen University, The Netherlands
Prof. Dr A.K Skidmore, University of Twente, The Netherlands
Prof. Dr J.H.C Cornelissen, VU University Amsterdam, The Netherlands
Prof. Dr L. Halounová, Czech Technical University of Prague, The Czech Republic

This research was conducted under the auspices of the C.T. de Wit Graduate School of Production Ecology & Resource Conservation (PE&RC)

Imaging spectroscopy for ecological analysis in forest and grassland ecosystems

Lucie Homolová

Thesis

submitted in fulfilment of the requirements for the degree of doctor
at Wageningen University
by the authority of the Rector Magnificus
Prof. Dr M.J. Kropff,
in the presence of the
Thesis Committee appointed by the Academic Board
to be defended in public
on Friday 10 January 2014
at 4 p.m. in the Aula.

Lucie Homolová
Imaging spectroscopy for ecological analysis in forest and grassland ecosystems
177 pages

PhD thesis, Wageningen University, Wageningen, NL (2014)
With references, with summaries in English, Dutch and Czech

ISBN 978-94-6173-824-0

Table of contents

1

Introduction

1.1 Introduction

The global human population exceeded seven billions in 2011 and it is expected to reach up to ten billions in 2100 according to the medium variant defined by the United Nations (UN, 2011). This causes an extreme pressure on the Earth's ecosystems to provide resources and services (e.g. provision of food, fresh water, fuel, etc.) to satisfy growing needs of the human population. According to the Millennium Ecosystem Assessment (MEA, 2005), the extent, structure and function of ecosystems have changed more rapidly since the 1950's than in any comparable period of time in human history. There is currently enough scientific evidence that human-induced activities have been contributing to changes in global environment (Doney et al., 2009; Galloway et al., 2008; IPCC, 2007; Joos and Spahni, 2008; Klein Goldewijk et al., 2011; Thomas et al., 2004).

Both increasing human-induced pressure on delivery of ecosystem services and rapidly changing environmental conditions threaten the extent, structure and function of the Earth's ecosystems. There is a chance of pushing ecosystems into a new state that might be less favourable to support human well-being (Rockström et al., 2009). For a sustainable functioning of ecosystems in future it is essential to understand how ecosystems respond to environmental and human-induced pressures. We already know that the typical response of plants to stress involves short-term physiological changes and long-term physiological, morphological and functional changes (Mooney et al., 1991). Therefore, it is important to monitor the magnitude and the extent of stress-induced changes, as well as to predict them to assess the future development of ecosystems. In this respect, remote sensing (RS) offers a unique opportunity for frequent monitoring of terrestrial as well as aquatic ecosystems from local to global scales. Since the advent of RS for Earth observation in the 1970's, repetitive and spatially continuous RS data have been providing valuable information on the actual status of ecosystems (Joiner et al., 2011; Myneni et al., 2002), helping to detect changes in land cover (Skole and Tucker, 1993; Stow et al., 2004) and to reveal trends (de Jong et al., 2012; Stöckli and Vidale, 2004). Moreover, RS data hold a strong potential to be used as input to models predicting ecosystem dynamics under changing environmental conditions (Nemani et al., 2009; Sitch et al., 2003). Nowadays, many national and international organizations and initiatives have already included RS data to support, e.g., land use management and nature conservation programs. Global monitoring systems such as GEOSS (Global Earth Observation System of Systems) or the European GMES (Global Monitoring of Environment and Security) show particular examples of infrastructures combining RS and in-situ data and redistributing them to a wide range of users.

1.2 Vegetation ecosystems of interest

This thesis contributes to scientific issues in the use of remote sensing in two structurally and ecologically contrasting ecosystems: evergreen coniferous forests and montane grasslands.

1.2.1 Evergreen coniferous forests

Evergreen coniferous forests spread from temperate to boreal regions of North America, Europe and Asia and cover approximately 10% of total land surface area (Bartholomé and Belward, 2005; Melillo et al., 1993). Forests in general have a tremendous value for human societies (Bonan, 2008). They provide timber, fuel wood and food resources, they support fresh water purification, cultural, spiritual and recreational services. Moreover, they play an essential role in the global carbon balance. They sequester carbon into plant biomass and mitigate this way the effect of global climate change. Temperate and boreal coniferous forests act as a substantial carbon sink with 0.6-0.7 Gt of carbon per year (Magnani et al., 2007; Myneni et al., 2001). This represents roughly 30% of the carbon annually sequestered by terrestrial ecosystems. Recent studies suggested that global environmental changes may substantially reduce the future carbon sequestration capacity of terrestrial ecosystems (Canadell et al., 2007). The sequestration capacity of the evergreen coniferous forests, as well as their capability to provide various services is driven by actual forest condition and its eco-physiological status. Monitoring of the eco-physiological forest status from local to global scale can benefit from variables retrieved from remote sensing data such as leaf chlorophyll content and leaf area index.

From a remote sensing point of view, coniferous forests represent one the most challenging ecosystems to work with because of their complex canopy structure (Ollinger, 2011; Rochdi et al., 2006). Coniferous forests are characterized by a typical three-dimensional shape of leaves and a hierarchical structure of leaves, shoots, branches and crowns. The complex canopy structure of conifers influences the reflected radiation flux, particularly in the near infra-red region. Solar radiation is more likely to be absorbed by conifers making them appear darker in the near infra-red region compared with their broadleaf counterparts (Rautiainen and Stenberg, 2005). Understanding the underlying mechanisms and confounding effects of canopy structure on spectral measurements and estimation of biochemical properties from RS gains more and more attention within the remote sensing research community (Knyazikhin et al., 2012).

This thesis contributes to the research of coniferous forest structure by investigating the area of individual needles, its measurement and implication for the remote sensing of forest chlorophyll content. In addition, procedures for estimating the chlorophyll content of coniferous forests still require improvement in terms of accuracy, which are addressed here.

1.2.2 Montane grasslands

Montane grasslands are the dominating vegetation coverage in subalpine and alpine regions. High mountain ecosystems represent the only biogeographical unit that can be found globally at all latitudes depending on altitude (Körner, 1999). The total vegetated alpine area covers only 3% of the total land surface (Körner, 1999). Despite this relatively small extent, montane ecosystems host roughly 10,000 higher plant species (corresponding to about 4% of all known higher plant species). About 40% of the global human population depends in some way on resources and services of mountain regions (Körner, 1999). Montane ecosystems are often perceived as economically non-profitable areas for mankind, but they actually provide vast ranges of goods and services such as fresh water purification, protection against natural hazards (erosion, landslides, avalanches), provision of fodder and timber, tourism and recreation (Grêt-Regamey et al., 2012). Montane ecosystems are well adapted to very distinct and sometimes extreme environmental conditions. These environmental conditions make these ecosystems exceptionally fragile. Their biodiversity and functioning are often sensitive to changes in climate and land use, habitat fragmentation and other human-induced disturbances (Dirnböck et al., 2003; Pauli et al., 2007; Roux-Fouillet et al., 2011). A complex topography and distinct environmental conditions in mountain regions influence the spatial distribution of species occurrence and valuable ecosystem services. Spatial assessment of multiple ecosystem services can be important for targeted land use management, nature conservation and sustainable maintenance of ecosystem services for human well-being (Naidoo et al., 2008; O'Farrell et al., 2010). In this thesis we investigate the role of remote sensing to map multiple ecosystem services in montane grasslands of the French Alps subalpine region.

1.3 Imaging spectroscopy of vegetation

1.3.1 Imaging spectroscopy

Imaging spectroscopy (or hyperspectral remote sensing) was introduced in the mid 1980’s and it brought an enhanced insight into spectral properties of Earth’s surfaces (Goetz, 2009). Imaging spectroradiometers, compared to multispectral remote sensing instruments, measure the reflected solar spectrum in the optical domain from 400 – 2500 nm into many narrow continuous spectral bands (Schaepman, 2009). Modern spectroradiometers offer excellent radiometric performance and spectral resolution (hundreds of spectral bands usually less than 10 nm wide). The continuous spectral response of vegetation helps to reveal biochemical- and structure-driven differences among species, plant communities and ecosystems (Kokaly et al., 2009; Ustin et al., 2009).

Several imaging spectroradiometers are nowadays available for laboratory-, ground-, and airborne-based sensing of vegetation spectral properties, but spaceborne imaging spectrometers are currently still only sparsely available (Malenovský et al., 2009; Schaepman, 2009). In this thesis we explore the use of airborne imaging spectroscopy data for vegetation ecological analysis. Thanks to both high spatial and spectral resolution, airborne imaging spectroscopy data are particularly useful for local case studies of heterogeneous vegetation surfaces. Airborne data help to develop, test and to upscale new algorithms for satellite-based RS, and to support validation of satellite-based RS products.

Data for this thesis were acquired by the AISA airborne imaging spectroradiometer (Specim, Spectral Imaging Ltd., Finland). AISA is a pushbroom instrument operating in the optical domain of the electromagnetic spectrum. The visible and near infra-red spectral range (400 – 970 nm) is covered by the AISA Eagle instrument. AISA Eagle can acquire up to 488 bands with a spectral sampling distance of 1.25 nm. The maximum signal-to-noise ratio reaches up to 1250:1. The near- and short-wave infrared spectral range (970 – 2500 nm) is covered by the AISA Hawk system. AISA Hawk can acquire up to 254 bands with a spectral sampling distance of 6.3 nm. The maximum signal-to-noise ratio reaches up to 800:1. Both instruments can be combined in a dual sensor bracket mount to collect a full datacube from 400 to 2500 nm. Depending on the flying altitude, the spatial resolution of acquired images can range from sub-meter to meters pixel size.

1.3.2 Remote sensing methods

Generally, methods studying vegetation properties using remote sensing data can be divided into three groups: i) empirical, ii) physical and iii) hybrid methods (a combination of empirical and physical methods) (Liang, 2004). Steadily increasing availability of accurate imaging spectroscopy data promoted development of algorithms that take advantage of a high spectral dimensionality and that are often applied to a specific, narrow spectral region (Ustin et al., 2009).

Empirical methods build on a simple regression relationship established between in-situ measured vegetation properties and spectral data (Ferwerda and Skidmore, 2007; Yoder and Pettigrew-Crosby, 1995). Typically, individual spectral bands are combined to form a vegetation index that enhances sensitivity to a specific vegetation property (Verstraete and Pinty, 1996). Multivariate statistical techniques (e.g. multiple linear regression) combine several spectral bands into a simple empirical model (Serrano et al., 2002). Spectral transformations such as the derivative or continuum removal are often used in empirical RS methods and they are particularly well suited for spectrally continuous imaging spectroscopy data.

By nature, empirical methods are computationally fast and effectively summarize local data, but they lack a cause-effect relationship. Consequently, predictive

statistical relationships often suffer from lack of robustness and portability, as they are site, species and time specific. The limitation of empirical methods can be partially overcome by using physically-based retrieval methods (Asner et al., 2003).

Physical methods are mostly based on radiative transfer theory. Radiative transfer models (RTMs) simulate plant-light interactions and provide an explicit link between the biochemical and structural characteristics of the major vegetation scattering elements (leaves) and the canopy reflectance (Jacquemoud et al., 2009; Ross, 1981). RTMs are used at the leaf and canopy level. Due to its simplicity, the PROSPECT model is probably the most widely used RTM to simulate leaf optical properties (Feret et al., 2008; Jacquemoud and Baret, 1990). The canopy RTMs range from the simplest homogeneous turbid medium (family of the SAIL models (Verhoef and Bach, 2007)) to detailed three-dimensional models (Disney et al., 2000; Gastellu-Etchegorry et al., 2004). In the forward mode, RTMs provide an effective means to investigate the influence of vegetation biochemical and structural properties on canopy reflectance. Inverse modelling is then used for retrieving vegetation properties from remote sensing data (Kimes et al., 2000).

Physical-based RS methods are more universally applicable as they account for the effects of canopy structure, topography, and observation geometry on canopy remotely sensed reflectance (Asner et al., 2003; Gastellu-Etchegorry and Bruniquel-Pinel, 2001). The major drawback of the RTM inversion is that the final solution is not necessarily unique (Combal et al., 2003) and some canopy RTMs can require many input parameters that limits their applicability.

Finally, hybrid methods take advantage of both empirical and physical methods. A hybrid inversion algorithm is a combination of extensive simulation using a leaf-canopy RTM and implementation of a parametric or non-parametric regression model (Bacour et al., 2006). In this thesis we employ the hybrid approach to estimate chlorophyll content of Norway spruce trees and use empirical methods to estimate vegetation properties of subalpine grasslands.

1.3.3 Vegetation properties from imaging spectroscopy

Not all vegetation properties can be retrieved using remote sensing based solutions (more discussion follows in Chapter 2). Especially biochemical (e.g. foliar pigments, water) and structure-related (e.g. leaf area index) vegetation properties, which play a key role in radiation absorption and scattering, can be retrieved from RS data with acceptable accuracy.

Complexity of plant-light interactions represents the major challenge in the remote sensing of vegetation. Many globally important processes occur at the leaf level and thus scaling schemes are required to interpret remotely sensed signals originating from complex plant communities (Malenovský et al., 2007). For example,

some vegetation indices sensitive to chlorophyll content that were developed at leaf level using laboratory measured spectra cannot be well transferred to the canopy level (Haboudane et al., 2002; Zarco-Tejada et al., 2001). The canopy structure plays the major role in scaling from leaf to canopy level. The effect of canopy structure can be incorporated into an RS method by using 3-D RTMs (Disney et al., 2000; Gastellu-Etchegorry et al., 2004). Recently, Knyazikhin et al. (2012) emphasized the crucial role of knowing well the canopy structure in RS of forest biochemical properties. They showed that previously reported correlations between nitrogen content and the near infra-red reflectance are actually a consequence of canopy structure variations rather than of nitrogen.

The high spectral resolution that is typical for imaging spectroscopy data is particularly suitable to study individual absorption features of plant biochemical components such as plant pigments (Ustin et al., 2009), water or dry matter (Kokaly et al., 2009). Among the plant pigments chlorophyll *a* and *b* are of highest importance, because they absorb incoming solar radiation in the visible region of the electromagnetic spectrum (400 – 700 nm) and transfer the energy to initiate photosynthesis. The concentration of chlorophyll a and b controls the amount of absorbed solar radiation available for photosynthesis and, consequently, plant primary productivity. The concentration in leaves decreases under stress and during the senescence phase. Therefore, many RS studies focused on the quantification of total chlorophyll as a valuable indicator of actual plant eco-physiological status (Blackburn, 2007; Haboudane et al., 2002; Ustin et al., 2009). As summarized by Blackburn (2007), many RS-based methods have been developed for the non-destructive measurement of chlorophyll content ranging from narrow-band vegetation indices, analysis of spectral derivatives or continuum-removed spectra, to the employment of physical methods based on RTMs. However, lack of uniformity between the RS methods and large variability of available chlorophyll-sensitive vegetation indices suggest that certain challenges and unresolved issues remain in RS of chlorophyll. Issues such as canopy structural effects are especially relevant for coniferous forest studies as demonstrated in this thesis. Moreover, this thesis addresses estimation of other vegetation properties such as green biomass, litter mass and species diversity in subalpine grasslands.

1.4 Research questions

This thesis builds on interdisciplinary research and it contributes to bridging gaps between the remote sensing and plant ecology research communities. The main objective of this thesis is *"to explore high spatial and spectral resolution imaging spectroscopy for ecological applications in two structurally and functionally different ecosystems: coniferous forests and montane grasslands"*. To reach the objective we carried out an analysis at the level of individual leaves, plants and communities. The major challenges are addressed by the following research questions:

1. *What is the current state-of-the-art in using optical remote sensing for estimation of key plant traits used widely in plant ecology research?*

2. *What is the variability of total to projected leaf area ratio of Norway spruce needles and what is the implication for remote sensing based estimates of crown averaged biochemical properties?*

3. *What is the potential use of the continuum removal transformation for quantitative mapping of chlorophyll content of Norway spruce crowns using airborne data and radiative transfer modelling?*

4. *What is the potential of airborne imaging spectroscopy to map ecosystem properties and services in subalpine grasslands in comparison with a plant-trait based modelling approach?*

1.5 Structure

The thesis is based on four peer-reviewed papers (Chapters 2-5). Each of those chapters represents an answer to the research questions presented in section 1.4. Chapter 2 reviews the use of remote sensing for estimation of important plant traits. Chapters 3 & 4 address remote sensing applications in coniferous forests. Chapter 5 focuses on remote sensing of ecosystem services in subalpine grasslands.

Chapter 1 introduces the ecosystems of interests, key principles about the remote sensing of vegetation and summarizes the main research questions. More details on linking remote sensing with plant ecology research are given in the next chapter.

Chapter 2 reviews recent achievements as well as challenges in remote sensing of individual plant traits that has been recognized as being important for ecosystem function studies (namely plant growth and life forms, flammability properties, photosynthetic pathway and activity, plant height, leaf lifespan and phenology, specific leaf area, leaf nitrogen and phosphorous).

Chapter 3 addresses an important, but also challenging, aspect in remote sensing of coniferous canopies – the role of leaf shape. We describe our own geometrical model to estimate total leaf area of spruce needles and decompose the variability of leaf area within a crown. We study the influence of biased total leaf area measurements on the accuracy of remote sensing based crown averaged biochemical properties.

Chapter 4 explores the continuum removal technique applied on high resolution airborne imaging spectroscopy data to estimate chlorophyll content of Norway spruce trees. We use radiative transfer modelling to develop a new vegetation index based on the continuum removal transformation of the red-edge reflectance (650 – 720 nm).

Chapter 5 presents a case study that explores the potential of imaging spectroscopy beyond traditional mapping of vegetation properties. We map ecosystem properties that underpin ecosystem services supplied by subalpine grasslands and compare it with results of plant trait-based statistical modelling. Furthermore, we discuss advantages and disadvantages of both approaches. This research opens a door to assessment of multiple ecosystem services using non-destructive remote sensing methods.

Chapter 6 summarizes the main results for each research question (Chapters 2 – 5), puts them into a broader context and suggests directions for future research efforts.

The thesis is complemented by all references used throughout this work, appendices, acknowledgements, and curriculum related information.

2

Review of optical-based remote sensing for plant trait mapping

This chapter is based on:

Homolová L, Malenovský Z, Clevers JGPW, García-Santos G, Schaepman ME (2013)
Review of optical-based remote sensing for plant trait mapping.
Ecological Complexity 15: 1-16
DOI 10.1016/j.ecocom.2013.06.003

Abstract

Plant trait data have been used in various studies related to ecosystem functioning, community ecology, and assessment of ecosystem services. Evidences are that plant scientists agree on a set of key plant traits, which are relatively easy to measure and have a stable and strong predictive response to ecosystem functions. However, the in-situ measurements of plant trait data are still limited to small area, to a certain moment in time and to certain number of species only. Therefore, remote sensing (RS) offers potential to complement or even replace in-situ measurements of some plant traits. It offers instantaneous spatially contiguous information, covers larger areas and in case of satellite observations profits from their revisit capacity.

In this review, we first introduce RS concepts of light – vegetation interactions, RS instruments for vegetation studies, RS methods, and scaling between in-situ measurements and RS observations. Further we discuss in detail current achievements and challenges of optical RS for mapping of key plant traits. We concentrate our discussion on three categorical plant traits (plant growth and life forms, flammability properties and photosynthetic pathways and activity) and on five continuous plant traits (plant height, leaf phenology, leaf mass per area, nitrogen and phosphorous concentration or content). We review existing literature to determine the retrieval accuracy of the continuous plant traits. The relative estimation error using RS ranged between 10% and 45% of measured mean value, i.e. around 10% for plant height of tall canopies, 20% for plant height of short canopies, 15% for plant nitrogen, 25% for plant phosphorus content/concentration, and 45% for leaf mass per area estimates.

The potential of RS to map plant traits is particularly high when traits are related to leaf biochemistry, photosynthetic processes and canopy structure. There are also other plant traits, i.e. leaf chlorophyll content, water content and leaf area index, which can be retrieved from optical RS well and can be of importance for plant scientists.

We underline the need that future assessments of ecosystem functioning using RS should require comprehensive and integrated measurements of various plant traits together with leaf and canopy spectral properties. By doing so, the interplay between plant structural, physiological, biochemical, phenological and spectral properties can be better understood.

2.1 Introduction

Plant traits are structural, physiological, biochemical or phenological features, e.g. plant height, photosynthesis rate, nitrogen content or leaf phenology, respectively, which are being increasingly used in ecology research (Cornelissen et al., 2003; Kattge et al., 2011). Due to the fact that groups of plants sharing a similar function within an ecosystem also tend to exhibit similar plant traits, plant traits are used to study the response of plants to various environmental pressures (e.g. changes in climate and land use) and the effect of plants on important ecosystem processes (e.g. biogeochemical cycles) (Díaz and Cabido, 1997; Lavorel and Garnier, 2002). Moreover, they have been successfully used in various studies related to ecosystem functioning (Díaz et al., 2004; Orwin et al., 2010; Wright et al., 2004), community ecology (Kraft et al., 2008), plant response to environmental pressures (de Bello et al., 2006; Garnier et al., 2007), plant invasion (Kurokawa et al., 2010; van Kleunen et al., 2010) and assessment of ecosystem services (Lavorel et al., 2011).

Nowadays there are hundreds of plant traits identified and measured by ecologists (Kattge et al., 2011). Plant trait data are measured at the level of individual plants and further upscaled to canopy properties (Violle et al., 2007) and data are often being compiled in various local (Kleyer et al., 2008; Paula et al., 2009) and global (Kattge et al., 2011) databases. Evidences are that plant scientists agree on a set of key plant traits, which are relatively easy to measure and have a stable and strong predictive response to ecosystem functions at various scales (Cornelissen et al., 2003; Díaz et al., 2004; Wright et al., 2004). Although data on key plant traits can be relatively well obtained from in-situ measurements, the measurements are still limited to small area, to a certain moment in time and to certain number of species only. Therefore, remote sensing (RS) offers potential to complement or even replace in-situ measurements of some plant traits (Kokaly et al., 2009) at larger areas.

Capabilities to retrieve plant traits and canopy properties from optical RS have evolved hand in hand with the technological development of RS spectroradiometers (Milton et al., 2009). Early RS spectroradiometers providing data of coarser spatial and spectral resolutions have supported mainly vegetation classification into broader functional groups (Ustin and Gamon, 2010) and the development of simple vegetation indices (VIs) that were sensitive to broad variations in canopy properties (Cohen and Goward, 2004; Turner et al., 1999). Next generation of medium spectral and spatial resolution spectroradiometers together with development of radiative transfer models (Liang, 2004) have facilitated quantitative estimation of some plant traits (e.g. chlorophyll content (Dash and Curran, 2004) and water content (Cheng et al., 2006)) and canopy properties (e.g. leaf area index (Myneni et al., 2002)). Development of high spectral resolution imaging spectroradiometers encouraged even more the quantitative estimation of plant traits related to physiology and

biochemistry. Plant pigments are the most studied traits (Blackburn, 2007; Ustin et al., 2009) and among them chlorophylls a and b (C_{ab}) have received most attention (Haboudane et al., 2002; le Maire et al., 2004; Malenovský et al., 2013; Schlerf et al., 2010; Zarco-Tejada et al., 2004), whereas carotenoids (Gitelson, 2002; Hernández-Clemente et al., 2012) and anthocyanins (Gitelson et al., 2006) have been studied less. Other biochemical traits retrieved from optical RS data are plant macronutrients (N, P, K, Mg, Ca) (Mutanga et al., 2004; Pimstein et al., 2011) and there is clear dominance of N and P related studies (both traits discussed in details later). Furthermore, leaf water content (Clevers et al., 2010; Colombo et al., 2008), leaf mass per area (discussed in details later), lignin and cellulose (Kokaly et al., 2009) or polyphenols (Skidmore et al., 2010) can be potentially retrieved from optical spectral data too.

Advantages of using RS are its capability to provide spatially contiguous and – for certain observations – high revisit frequency at the typical length scale of the trait processes observed. Moreover, it offers different sampling scheme to trait mapping, determined by combination of pixel size, spatial extent and revisit time of RS observations, than in-situ measurements. The major challenge in quantitative RS of plant traits plays the canopy structure. It affects interpretation of canopy reflectance and has negative impact on the retrieval accuracy of biochemical traits (Knyazikhin et al., 2012; le Maire et al., 2008). Therefore approaches accounting for integral effects of canopy structure (Knyazikhin et al., 2012) or measurements of canopy structure itself (van Leeuwen and Nieuwenhuis, 2010) have recently gained more attention.

The potential of RS data for ecological applications is large, however, we see that successful integration of RS observations and ecological applications still requires bridging gaps in the perception of traits importance, scientific terminology (Schaepman-Strub et al., 2006; Violle et al., 2007) and scaling among leaf, plant and canopy levels (Malenovský et al., 2007; Messier et al., 2010). In this review, we want to demonstrate the potential of RS for estimating individual plant traits as defined by ecologists and therefore strengthen links between plant ecology and remote sensing research communities. First, we introduce RS concepts of light – vegetation interactions, RS instruments for vegetation studies, RS methods, and scaling between in-situ and RS data. Further, we discuss in detail current achievements and challenges when using optical RS to estimate key plant traits. We used Cornelissen et al. (2003) as baseline reference for key traits. These included plant growth and life forms, flammability properties, photosynthetic pathways and activity, plant height, leaf lifespan and phenology, specific leaf area, leaf nitrogen and phosphorous. Regenerative (e.g. seed mass) and belowground (e.g. rooting depth) traits are deliberately excluded, since they cannot be estimated using direct measurements from optical RS. We put emphasis on optical, passive RS, but mention active RS (laser scanning and microwave radar) to trait mapping whenever appropriate.

2.2 Material and methods

2.2.1 Light-vegetation interactions

Interactions between incident radiation and canopy elements are extremely complex and are described by three main physical mechanisms: absorption reflection, and transmission. The solar reflected radiation in the optical domain (i.e. between 380 and 2500 nm) is commonly used in vegetation studies, because most of the diagnostic absorption features of green vegetation are located in this part of the spectrum (Kokaly et al., 2009; Ustin et al., 2009). Reflectance of vegetation canopies depends on radiative properties of leaves, other non-photosynthetic canopy elements and their spatial organisation. Leaf reflectance spectra are mainly characterized by i) strong and well described absorption of foliar photosynthetic pigments, dominated by chlorophylls, in the visible region (400 – 700 nm, VIS), ii) leaf structure in the near infrared region (700 – 1300 nm, NIR), and iii) prevailing water and protein absorptions (as well as other biochemicals) in the shortwave infrared region (1300 – 2500 nm, SWIR). Mechanisms influencing leaf reflectance are well understood (Kumar et al., 2001), but interpretation of canopy level reflectance remains challenging due to multiple light interactions between canopy elements and background (Disney et al., 2006; Ross, 1981; Widlowski et al., 2004). The key factor influencing canopy reflectance is the canopy structure (Disney et al., 2006; Rautiainen et al., 2004). The most widely used descriptor of a canopy structure in RS studies is leaf area index (LAI) (Fernandes et al., 2004; Turner et al., 1999). LAI alone cannot fully describe the effects of the canopy structure. There are many other leaf level traits (e.g. ratio of mesophyll cell surface to intercellular air spaces, leaf thickness) and canopy properties (e.g. leaves orientation in a canopy characterized by leaf angle distribution, leaves aggregation characterized by clumping index) that strongly influence remotely sensed canopy reflectance. Lack of in-situ measurements and complex interplay among structural leaf traits and canopy properties prevents to decouple their individual effects on RS reflectance data. Furthermore, presence of background and understory components (Eriksson et al., 2006), presence of non-photosynthetic elements (Verrelst et al., 2010), and varying observation geometries (Lobell et al., 2002) also influence canopy reflectance. Therefore RS methods try to minimize these confounding effects (Knyazikhin et al., 2012) and enhance the sensitivity of reflectance data towards a trait or a property of interest (Haboudane et al., 2002; Verstraete and Pinty, 1996). Alternatively, combined retrieval schemes are optimizes to use spectral, spatial and directional domains simultaneously (Laurent et al., 2011b; Schaepman, 2007).

2.2.2 Remote sensing instruments

Environmental studies can nowadays benefit from a large variety of RS data provided by different passive and active RS systems. We first discuss optical, passive RS systems, because they are being prevailingly used to study vegetation properties. Optical spectroradiometers on satellite-, airborne- and ground-based platforms represent a trade-off among spatial, spectral and temporal resolutions. Spectroradiometers onboard satellite platforms acquire data of regional to global coverage with spatial resolution of tens to hundreds meters and revisit time typically between 2 and 16 days. From the advent of broad-band, multispectral and coarse spatial resolution spectroradiometers (e.g. advanced very high resolution spectroradiometer AVHRR onboard NOAA) in the 1970's and 80's we have moved towards spectroradiometers of increasing resolutions. Currently operational satellite-based spectroradiometers suitable for vegetation monitoring are of moderate spectral and spatial resolutions (e.g. moderate resolution imaging spectroradiometers MODIS onboard Aqua and Terra, the recently terminated Envisat mission with MERIS, and Enhanced Thematic Mapper ETM+ onboard Landsat). New advanced data for systematic, long-term observation of the Earth systems will be provided from 2013 onwards by the prospective future ESA Sentinel missions (Malenovský et al., 2012).

The major disadvantage of satellite-based multispectral spectroradiometers is that they sample the electromagnetic spectrum only with a few spectral bands. Therefore imaging spectroscopy has emerged to overcome spectral limitations of multispectral systems (Goetz, 2009; Schaepman, 2009). Imaging spectroscopy (often referred as hyperspectral RS) acquire data of unprecedented radiometric quality and high spectral resolution – typically the number of overlapping narrow spectral bands exceeds one hundred, providing therefore almost contiguous spectral information (Schaepman, 2009). Spaceborne imaging spectrometers are still only sparsely available (Hyperion on EO1 and CHRIS on PROBA platforms). Most of the existing imaging spectroradiometers are therefore operated on airborne platforms, which enables acquiring data of high spatial resolution too (the ground pixel size is usually less than a few meters). A great advantage of airborne RS is high versatility to meet user requirements on target selection, spatial and spectral resolutions, and acquisition date. Additionally, it allows combining imaging spectroradiometers with other type of RS instruments (Asner et al., 2012). One drawback of is reduced multi-temporal feasibility due to costs and logistics.

Mounting an imaging (or non-imaging) spectroradiometer on ground-based constructions (proximal sensing) certainly increases the temporal frequency, which is ideal to study diurnal changes in vegetation activity, but limits the spatial coverage to very small areas or individual plants only (Ač et al., 2009).

Comprehensive overviews of currently operational and future satellite multispectral and airborne imaging spectroradiometers and their specifications are

published elsewhere (Ayanu et al., 2012; Grace et al., 2007; Malenovský et al., 2009; Schaepman, 2009).

Other RS systems like multi-directional and active RS systems, which have supported studies of vegetation structue (Widlowski et al., 2004), are introduced only briefly. Multi-directional optical systems (e.g. CHRIS on the PROBA platform) provide observations of the same target from multiple viewing directions over a short timeframe provides. This measurement setup captures the anisotropy of reflected solar radiation in different wavelengths, which conveys information about canopy structure (Chopping, 2008; Widlowski et al., 2004).

Laser scanners (often referred as lidars) emit and record backscattered signal in the optical part of the electromagnetic spectrum (0.01 – 10 µm) and measure runtime from the instrument to the ground surface and back. There are two types of laser scanners: discrete return systems that record either single or multiple backscatter echoes and full waveform systems that record the entire backscatter signal from a return (Mallet and Bretar, 2009; Wulder et al., 2012). Up to date vegetation structural properties derived from laser scanning include vegetation height (see section 3.4 for detailed discussion), canopy volume, leaf area index, gap fraction and vegetation profiles (Lefsky, 2002; Lindberg et al., 2012; van Leeuwen and Nieuwenhuis, 2010). Recent development have advanced towards a multispectral full waveform system, which provide additional information on the 3D distribution of plant physiological properties (Hakala et al., 2012).

Imaging synthetic aperture radars (SAR) emit and record backscattered signal at one or more polarizations in the microwave part of the electromagnetic spectrum (cm to multiple m). Their greatest advantage over the optical instruments is of being able to acquire images independently of cloud cover. However, challenges remain to interpret radar data from very dense or moist canopies, where backscatter signal saturates (Mitchard et al., 2009). The major application domain of radar data is to estimate vegetation height and biomass (partly reviewed by Koch et al. (2010) and Patenaude et al. (2005)). This will be strongly supported by the future ESA radar mission BIOMASS (le Toan et al., 2011).

Studies whereby data from optical spectroradiometers, laser scanners and radar are combined are becoming more common and promising for complex vegetation studies (Asner et al., 2012; Cartus et al., 2012; Hyde et al., 2006; Montesano et al., 2013)

2.2.3 Remote sensing methods

Plant traits and canopy properties may be assessed qualitatively or quantitatively from RS data. Qualitative methods – classification techniques use a set of decision rules assigning image pixels with similar spectral properties into discrete thematic vegetation classes (Xie et al., 2008). Qualitative methods used to interpret optical RS data can be divided into two broad groups: empirical and physical methods (or

combination of both) (Liang, 2004). Empirical methods build on statistical relationships established between limited number of in-situ trait measurements and RS data using regression techniques (Ferwerda and Skidmore, 2007; Smith et al., 2002). The sensitivity of RS data towards traits or properties of interests is often enhanced by calculating VIs (Chen et al., 2010b; le Maire et al., 2004; Turner et al., 1999) or spectral transformations in case of contiguous hyperspectral data (Schlerf et al., 2010). By nature, empirical methods are computationally fast and effectively summarize local data, but they lack cause-effect relationships. Consequently, predictive statistical relationships often suffer from lack of robustness and transferability as they are usually site, species and time specific (Colombo et al., 2003; Grossman et al., 1996).

Limitations of empirical methods can be partly overcome by using physical RS methods. These methods are based on radiative transfer models (RTMs), which simulate light absorption and scattering inside vegetation canopies accounting for leaf biochemical composition and canopy structural properties (Gastellu-Etchegorry et al., 2004; Jacquemoud et al., 2009; Rautiainen et al., 2010; Verhoef and Bach, 2007). The role of coupled soil-leaf-canopy RTMs (Jacquemoud et al., 2009) in RS is two-fold. First, they help to study the effects of additional perturbing factors (soil background, non-photosynthetic materials and observation geometry) on canopy reflectance. Second, they enable direct estimation of leaf traits and canopy properties that are directly involved in the radiative transfer by using inversion techniques (Baret and Buis, 2008). Further, when combined with atmospheric RTMs, they hold the promise to estimate many leaf traits and canopy properties simultaneously (Laurent et al., 2011a). Some traits and properties can be estimated with high accuracy and fidelity, e.g. leaf chlorophyll content (Sampson et al., 2003; Zarco-Tejada et al., 2004), leaf water content (Clevers et al., 2008; Colombo et al., 2008) and leaf area index (Myneni et al., 2002; Schlerf et al., 2005). Still, other canopy structural properties (e.g. leaf aggregation, leaf angle distribution) present a substantial challenge for RTMs parameterization and interpretation from RS data (Ollinger, 2011). The major drawback of the physical methods is that different combinations of RTM input parameters may produce the same reflectance spectra, which makes estimation of canopy properties from RS data ambiguous (Baret and Buis, 2008; Combal et al., 2003).

2.2.4 Scaling and terminology

Spatial scale of in-situ measured plant traits and RS data often disagrees. Here we want to demonstrate how to match scaling terminology used in ecology and RS (Figure 2.1). An ultimate requirement for RS of plant traits shall be to match the spatial scales of trait with RS data. We exemplify this using a key plant trait – nitrogen (N) and demonstrated simple scaling of in-situ measurements from leaf to canopy level and overlap it with scaling approaches applied to RS data (Table 2.1).

Quantitative traits such as N are usually measured at the level of individual leaves of dominant plant species and expressed either as concentration (mass fraction per unit dry leaf mass) or content (mass fraction per unit leaf area) (here we refer to the terminology introduced by Datt (1998)). Assuming the mass ratio hypothesis (Grime, 1998), the leaf level measurements can be further upscaled to the community (canopy) level by calculating a weighted mean using relative abundances of the most dominant species (Lavorel et al., 2008). This community weighted mean of a leaf trait is not directly comparable with RS, unless a physical scaling using leaf-canopy RTMs is applied to interpret RS data (Malenovský et al., 2007). If the community weighted mean is multiplied by biomass or LAI, one obtains a canopy integrated value (i.e. canopy property) expressed per unit surface area (Table 2.1), which can be directly compatible with remotely sensed canopy reflectance. Ultimately, RS spectroradiometers measure a mixed signal reflected from entire plants (including woody and dry elements) and soil background. Information content originating from the green vegetation fraction can be enhanced by downslcaing techniques – spectral unmixing or data fusion (Malenovský et al., 2007). However, interpretation of RS data in areas with fractional vegetation cover below 30% remains extremely difficult (Okin et al., 2001) and largely non-conclusive.

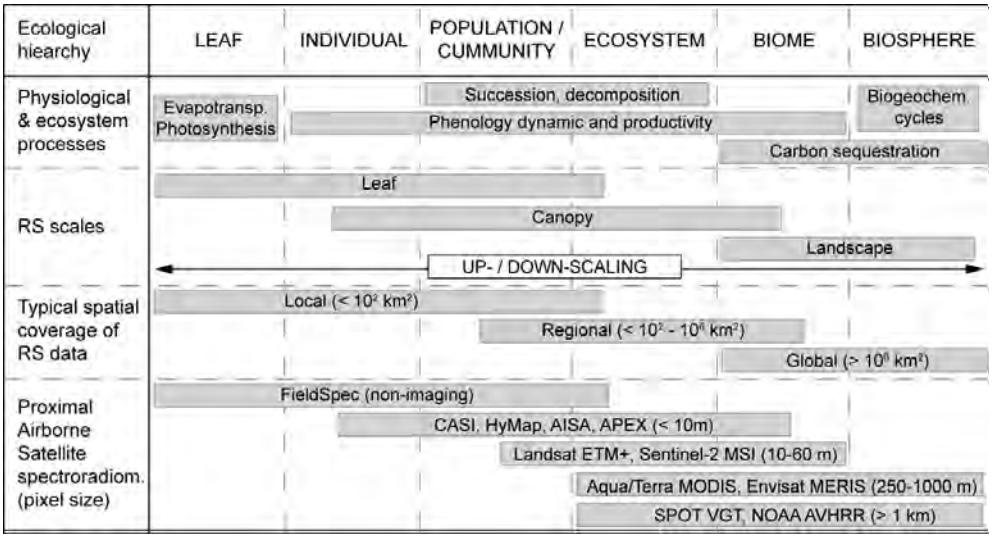

Figure 2.1 Link between ecological and remote sensing spatial scales with examples of typical remote sensing spectroradiometers operational at variety of spatial scales.

Table 2.1 Example of scaling of leaf nitrogen concentration and content from the leaf to the canopy level.

Trait	Leaf trait of species *i*	Leaf trait of a community	Canopy trait of a community (~ property)
N concentration [units]	Ni [mg g^{-1} of leaf mass]	N_{CWM} = SUM(N_i * F_i) [mg g^{-1} of leaf mass]	N_{CWM}[mg g^{-1}] * BIO[g m^{-2}] [mg m^{-2} of surface area]
N content [units]	Ni [mg cm^{-2} of leaf area]	N_{CWM} = SUM(N_i * F_i) [mg m^{-2} of leaf area]	N_{CWM}[mg m^{-2}] * LAI[m^2 m^{-2}] [mg m^{-2} of surface area]
		RS up/downscaling (Malenovský et al., 2007)	
Reflectance data	Laboratory or proximal sensing	RS data combined with RTM upscaling	RS data optionally combined with up/downscaling

N_i – nitrogen concentration or content of a species *i*, CWM – community weighted mean, F_i – relative abundance of species *i*, BIO – biomass, LAI – leaf area index, RTM – radiative transfer model

2.3 Remote sensing of plant traits

In the following sections we will introduce individual plant traits and possible RS solutions (summarized in Table 2.2 at page 31), including strengths and drawbacks of currently available RS methods. In order to support our discussion about RS of plant traits we compiled a database of reviewed scientific articles (Appendix A1). We reviewed scientific papers about RS of leaf mass per area (LMA), nitrogen (N) and phosphorus (P) concentration or content. These are three frequently used traits in plant ecology analysis with strong potential to be derived from RS data. Moreover, we discuss plant growth and life forms, plant flammability properties, plant photosynthetic pathway and photosynthesis, plant or canopy height, leaf lifespan and phenology. From the reviewed articles (Appendix A1) we extracted two accuracy indicators: coefficient of determination (R^2) and relative root mean square error (RMSE) to evaluate the accuracy of RS methods estimating N, P and LMA (Figure 2.2).

2.3.1 Plant growth and plant life forms

Plant growth form and plant life form classifications (Cornelissen et al., 2003) are considered as one of many existing plant functional classification schemes (Ustin and Gamon, 2010). There is no comprehensive assessment of plant growth forms or plant life forms as defined in Cornelissen et al. (2003) using RS. But current moderate resolution RS spectroradiometers (e.g. MODIS, MERIS) have been providing global data for land cover classifications, where vegetation is classified into broader functional classes (Arino et al., 2008; Bartholomé and Belward, 2005; Friedl et al., 2010). Existing global vegetation classifications are by definition closer to plant growth forms than to plant life forms, because they determine the vegetation classes based on canopy phenology and structure. Additionally, local studies demonstrated capabilities of RS to map specific plant growth forms or even individual species.

Martin et al. (1998) determined forest species composition using maximum likelihood classification. Kokaly et al. (2003) mapped vegetation types in Yellowstone national park using continuum removal. Hamada et al. (2007) detected an invasive Tamarisk shrub species in riparian vegetation using hierarchical clustering. Kalacska et al. (2007) discriminated between forest lianas and their host trees in tropical forest. Underwood et al. (2006) and Hestir et al. (2008) mapped invasive aquatic vegetation using spectral mixture analysis. The common feature of RS data used in the above mentioned studies is the pixel size smaller than 20 meters.

The overall accuracy of the global land cover classifications varies between 68% and 75% (Friedl et al., 2010; Mayaux et al., 2006), whereas the accuracy of local RS studies varies between 65% and 95% and for some cases it drops below 50% (Underwood et al., 2006). Despite improving spectral and spatial resolution of RS instruments, it seems that RS reaches certain limits in accuracy and number of vegetation classes that can be distinguished. This is due to large variability within and among species, which decreases spectral separability among plant growth forms (Ustin and Gamon, 2010), as well as limited increase in dimensionality of RS data with increasing number of spectral bands (Schimel et al., 2013).

2.3.2 Plant flammability properties

Individual components of the flammability trait are twig and leaf dry matter content, degree of ramification, leaf size, presence of standing litter, oils and waxes (Cornelissen et al., 2003). RS cannot quantify individual components of the flammability trait, but it can be used to assess combustibility of entire plant communities, which is driven by the amount of dry biomass and canopy structure. RS data have been used to support fire risk assessment and served as basis for fire monitoring schemes at the landscape level (Arroyo et al., 2008). Optical RS data have been used to derive vegetation properties such as the proportion between live and dead biomass (Jia et al., 2006) and fuel moisture content (ratio between water and dry leaf mass) (Chuvieco et al., 2002; Koetz et al., 2004). Both are relevant attributes for classification of fuel types (Arroyo et al., 2008; Lasaponara and Lanorte, 2007). The major limitation of passive optical RS for fire risk assessment is its inability to i) estimate vegetation height, which is critical for fuel type discrimination, and ii) to penetrate deeper into multi-layered canopies and therefore cannot provide information about understory, which plays an important role for fire spreading (Arroyo et al., 2008). Using active radar RS systems (Saatchi et al., 2007) and the fusion of optical RS data with laser scanning (Erdody and Moskal, 2010; Mutlu et al., 2008) or radar data (Treuhaft et al., 2004) represent a promising approach for fire risk assessment in terms of precise canopy structure and biomass mapping.

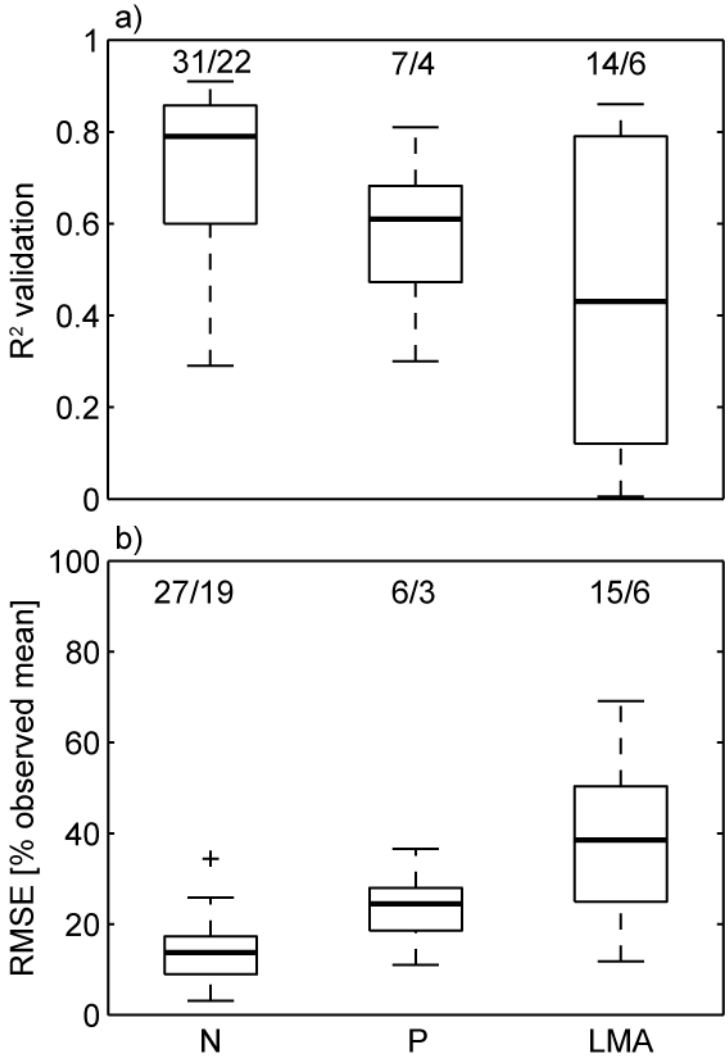

Figure 2.2 Performance of remote sensing methods evaluated by (a) the coefficient of determination R^2 and (b) the relative root mean square error RMSE for the estimation of nitrogen (N), phosphorus (P) concentration and content, and leaf mass per area (LMA) from various type of remote sensing data. (Legend: Central line in a box is median, box height is the interquartile range (i.e. 50% of the data) and whiskers represent minimum and maximum unless the observed values exceed 1.5 of the interquartile range and in that case they are marked as outliers (crosses). Number (in format of x/y) above each box indicates number of reported accuracy indicators (x) and corresponding number of scientific articles (y) they were extracted from).

2.3.3 Plant photosynthetic pathway and photosynthesis

Spatial distribution of the plant photosynthetic pathway, i.e. C3, C4 and CAM metabolism, is relevant for simulating global carbon budget, because C4 plants tend to benefit from increasing temperature and atmospheric CO_2 (Ehleringer et al., 1997; Still et al., 2003). C3 and C4 leaves differ in internal leaf structure and biochemical composition (Hatch, 1987) and therefore a possibility of spectral discrimination between C3 and C4 plants exists. Siebke and Ball (2009) discriminated C3 and C4 grass species using a simple ratio between leaf reflectance at 696–709 and 545–567 nm that was sensitive to various concentrations of chlorophyll a and b. Irisarri et al. (2009) found that proximal reflectance can distinguish between a pure plantation of C3 and C4 grass species. However, observed spectral differences can be partly attributed to differences in leaf orientation, because C3 species in the study of Irisarri et al. (2009) had more erect leaves than C4 species. Airborne or satellite based RS studies used multi-temporal RS observations that captured asynchronous seasonality of C3 and C4 grass species (Davidson and Csillag, 2001; Foody and Dash, 2007) and could explain about 60% of the variability in C3/C4 grassland species composition.

Complementary to RS based mapping of plant photosynthetic pathways, we can profit from intensive and ongoing research of RS of global plant photosynthesis known as gross primary productivity (GPP) (Coops et al., 2010; Grace et al., 2007; Hilker et al., 2008b). The most widely applied approach of GPP modelling is based on the light use efficiency concept of Monteith (1972), which calculates GPP as the product of two plant growth limiting factors: the amount of absorbed photosynthetic active radiation (APAR) between 400 and 700 nm and plant light use efficiency (LUE) converting APAR into biomass (Field et al., 1995; Hilker et al., 2008b).

APAR is approximated by unitless fraction expressing how much of incoming photosynthetic active radiation is absorbed by vegetation (fAPAR). FAPAR was recognized as one of the essential climate variables by FAO Global Terrestrial Observing System (Gobron and Verstraete, 2009) and it is being currently estimated from global satellite RS data. The simplest empirical solutions relate fAPAR to the vegetation greenness using NDVI (Myneni and Williams, 1994) and EVI (Xiao et al., 2004) indices. EVI tends to outperform NDVI in denser canopies, where NDVI saturates (Huete et al., 2002). Empirical retrievals of fAPAR are sensitive to perturbing effects of soil background, observing geometry and atmospheric conditions (Fensholt et al., 2004). Alternatively, many operational RS-based fAPAR algorithms rely nowadays on physically-based approaches using RTMs (Baret et al., 2007; Gobron et al., 2000; Myneni et al., 2002). Recent comparative studies (D'Odorico et al., 2013; Martínez et al., 2013; McCallum et al., 2010), however, found inconsistencies among fAPAR products. The largest discrepancies were reported for coniferous forests (D'Odorico et al., 2013; McCallum et al., 2010), which is mainly attributed to simplified representation of canopy structure in existing RTMs.

Possibility of LUE estimation from RS increased only in the past decade because of the development of fine spectral resolution instruments. We concentrate our discussion on direct RS approaches, which quantify LUE by measuring subtle changes in leaf and canopy reflectance resulting from two photoprotective mechanisms: non-photochemical quenching and chlorophyll fluorescence (Grace et al., 2007). Non-photochemical quenching dissipates the excess energy into heat by inducing changes in the xantophyll pigment cycle. Different composition of xantophyll pigments results into changes of leaf reflectance at 531 nm, which lead to the formulation of the photochemical reflectance index (PRI) (Gamon et al., 1992; Peñuelas et al., 1995). PRI exponentially increases with increasing LUE and is able to explain about 42% of LUE variability at the leaf level and 59% at the canopy level (Garbulsky et al., 2011). According to Garbulsky et al. (2011) PRI seems to perform better at the canopy level, but some studies argued that the PRI-LUE relationship is negatively affected by the canopy structure, soil background and observation geometry (Barton and North, 2001; Hernández-Clemente et al., 2011; Hilker et al., 2008a). Moreover, PRI values vary between species with the same photosynthetic capacity (Guo and Trotter, 2004). Therefore the use of PRI as the LUE proxy in complex canopies needs to be further investigated.

Sun induced chlorophyll fluorescence (SiF) is recently being explored as an indicator of LUE and actual photosynthesis (Damm et al., 2010; Malenovský et al., 2009; Meroni et al., 2009). SiF is a flux of photons that were not used for photosynthesis, but re-emitted at 685 nm and 740 nm (Buschmann, 2007). This adds a weak≤(3%), but detectable, signal to the remotely sensed leaf and canopy reflectance (Meroni et al., 2009; Moya et al., 2004). SiF was first estimated using proximal reflectance data by analysing double-peak reflectance feature between 690 and 710 nm (Zarco-Tejada et al., 2003) or the narrow oxygen absorptions – Fraunhofer lines (Meroni and Colombo, 2006). The later principle was recently applied on airborne and satellite RS data. Zarco-Tejada et al. (2009) estimated SiF of individual trees under water stress using RS data of very high spatial (15 cm) and spectral (1 nm) resolutions. Joiner et al. (2011) and Guanter et al. (2012) presented the first global map of plant steady state SiF as monthly averages in 2° x 2° grid derived from Fourier Transform Spectrometer (FTS) on board of the Greenhouse gases Observing SATellite (GOSAT). Despite the recent evidence of SiF retrievals from optical RS data, the operational approaches will require rigorous spectral calibrations and atmospheric corrections (Guanter et al., 2007) and to fully understand the effects of environmental variables on SiF (Malenovský et al., 2009).

2.3.4 Plant height

Plant height is an important trait associated with plant competitive abilities. Laser scanning has emerged to be the most accurate RS technology for the measurement of plant and canopy height (Danson et al., 2009; Lefsky, 2002; van Leeuwen and

Nieuwenhuis, 2010). Discrete return laser scanning have been successfully used for height estimation mainly of tall canopies such as boreal coniferous (Hopkinson et al., 2004; Næsset et al., 2004), temperate deciduous (Brandtberg et al., 2003) or tropical (Clark et al., 2004) forests. Less often it has been used in smaller canopies, such as shrubs (Glenn et al., 2011), crops (Davenport et al., 2000) or grasslands (Straatsma and Middelkoop, 2007). The best absolute accuracies achieved in tree height estimation from airborne discrete return laser scanners are between 0.5 and 1.0 m irrespective to a tree height (Kaartinen et al., 2012). According to Næsset et al. (2004) the accuracy in height estimation from discrete return laser scanning is higher for individual trees (relative RMSE of 5±2.5%) than for forest canopies (relative RMSE of 7±2.5%). Generally, a relative error of height estimation in tall forest canopies is usually less than 10% of the measured mean canopy height (Kaartinen et al., 2012; Næsset et al., 2004), while for lower canopies it reaches up to 20% (Davenport et al., 2000; Kaartinen et al., 2012).

Canopy height estimation using discrete return laser scanning faces three major issues. First is the determination of the terrain elevation, which is difficult in very low or too dense canopies, where emitted signal cannot penetrate to the ground (Falkowski et al., 2008; Lefsky, 2002). Second is the accurate detection of the uppermost canopy layer, which depends on the sampling pulse density (Jakubowski et al., 2013; Magnusson et al., 2007). Tree height accuracy decreases with decreasing sampling pulse density, but remains relatively constant and high until the densities drops below 1 pulse/m^2 (Jakubowski et al., 2013). The last issue is related to the selection of an extraction method. A recent international comparison revealed large variability among 14 extractions methods (RMSE varied between 0.5 and 4.5 m) to estimate height of individual coniferous trees (Kaartinen et al., 2012).

Full waveform lasers (Mallet and Bretar, 2009) provide certainly better insight into the 3D vegetation structure (Lindberg et al., 2012), but they do not necessarily yield more accurate plant and canopy height estimates than discrete return systems. Benefits of full waveform systems are improved detection of the ground surface elevation in denser canopies and possibly more accurate height estimates for plants underneath the main canopy layer.

2.3.5 Lifespan and phenology

Leaf lifespan (longevity) and phenology (seasonal timing) are closely related to plant nutrition conservation and competitive strategies and are influenced by local meteorological, topographic and soil variations (Dahlgren et al., 2007). It is beyond the capabilities of RS to measure leaf lifespan of evergreen species. But for plant communities that periodically change their foliar apparatus, time series of RS data provide an effective means of extracting land surface phenology (LSP) indicators including start, end, duration and maximum peak of the vegetation season (Liang and Schwartz, 2009; Reed et al., 1994). Considering strictly the definition of leaf

phenology by Cornelissen et al. (2003) then the length of the vegetation season is the equivalent RS proxy of leaf phenology. It is important to realized that LSP indicators are related, but not identical, to field observed plant phenology indicators such as budburst, leaf unfolding, flowering (Liang and Schwartz, 2009).

Typical temporal and spatial resolutions of RS data used for LSP analysis are biweekly composites of VIs of global spatial extent and a pixel size ranging from 0.25 to 8 km (e.g., MODIS land products (Huete et al., 2002), AVHRR NDVI time series (Tucker et al., 2005)). The estimation of the LSP indicators from the satellite RS is influenced by four factors: i) temporal resolution (Kross et al., 2011), ii) missing or noisy data due to clouds or snow cover (Delbart et al., 2006), iii) magnitude of the seasonal amplitude in vegetation greenness to override other sources of variation (e.g. earlier greening of understory), and iv) a method extracting the phenology indicators (de Beurs and Henebry, 2010; White et al., 2009). White et al. (2009) demonstrated that different extraction methods (e.g. global and local threshold values, inflection points in time series curves) applied on NDVI time series can yield differences up to 60 ± 20 days in the estimation of the start of the vegetation season. This suggests that there is no agreement on a single, globally appropriate extraction method of LSP (Schwartz and Hanes, 2010; White et al., 2009).

Consistent and long time series of RS data enable analyzing inter-annual variability in vegetation trends (de Jong et al., 2012) and land surface phenology (White et al., 2009) (see Remote Sensing special issue on monitoring global vegetation with AVHRR NDVI3g Data (1981-2011); http://www.mdpi.com/journal/remotesensing/special_issues/monitoring_global). Particular attention has been drawn on high latitude regions (Delbart et al., 2006), where climatic changes have been pronounced. Prolongation of the vegetation season has been revealed in Europe (Stöckli and Vidale, 2004) and globally (Julien and Sobrino, 2009) in 1980's and 90's, but the extent and quantification of these changes are still under discussion.

2.3.6 Specific leaf area and leaf dry matter content

Plant scientists consider leaf dry matter content (LDMC in mg g^{-1}) and specific leaf area (SLA in m^2 g^{-1}) as two separate traits. LDMC negatively correlates with SLA (Garnier et al., 2001; Shipley and Vu, 2002; Vile et al., 2005) and both traits are related to plant growth rate and leaf resistance to physical damage. We want to clarify first that some RS studies use terms "leaf dry matter content" or "dry matter content" when actually referring to leaf mass per area (LMA) – the inverse ratio of SLA (Riaño et al., 2005; Schaepman et al., 2004; Vohland et al., 2010). LMA can be retrieved from RS data using empirical, as well as physical methods, because LMA is an input into leaf RTM (Jacquemoud et al., 2009). Despite this fact, only a few RS studies specifically targeted LMA estimation from proximal or remote sensing data achieving rather inconsistent results. Based on our literature review (Appendix A1)

and Figure 2.2, we can conclude that LMA can be retrieved with low to moderately good accuracy. The average R^2 between RS-estimated and measured LMA was equal to 0.45 ± 0.34 and the average relative RMSE was equal to $45 \pm 30\%$. Higher estimation accuracies were achieved for the canopy integrated estimates (i.e. LMA*LAI) than for leaf-level estimates (Schaepman et al., 2004; Vohland et al., 2010). Physically-based retrieval methods dominate and we found little agreement among empirical methods on the best spectral wavelengths for LMA estimation. Interestingly, Wang et al. (2011) found that the most optimal spectral bands for LMA estimation are located at 1649 and 1722 nm, but almost identical bands were used to estimate phosphorus content of wheat canopies (Pimstein et al., 2011). Question remains whether these studies observed direct variations in LMA and P, or whether both traits correlate with another canopy property, which influences the reflectance in 1650 – 1720 nm. Only a few studies attempted to estimate single leaf dry matter components such as cellulose or lignin using empirical methods. For example, Zagolski et al. (1996) could explain around 60% of lignin and cellulose variability in a pine forest, Serrano et al. (2002) could explain up to 80% of lignin variability in chaparral communities.

SWIR wavelengths are most important for LMA estimation (Asner et al., 2011; Kokaly et al., 2009), but they are also strongly influenced by water absorption (Riaño et al., 2005). The masking effect of water and canopy structure decreases the accuracy of LMA estimates from optical RS. Therefore a water removal algorithm is required or one could estimate leaf water content instead, because it is a complementary measure of LMA and can be retrieved with higher accuracy than LMA using RTM inversion (Clevers et al., 2008; Colombo et al., 2008).

2.3.7 Leaf and canopy nitrogen

Nitrogen (N) is an important component in proteins, nucleic acids and chlorophylls and therefore strongly linked to plant photosynthesis (Reich et al., 1995) and gross primary productivity (LeBauer and Treseder, 2008; Smith et al., 2002). Currently the best way to estimate N from optical RS is by means of empirical methods, because physically-based retrievals are not well established. The only leaf RTM having N as an input is the LIBERTY model (Dawson et al., 1999). This model is not often used among the RS research community, which prefers using a simpler model – PROSPECT (Jacquemoud et al., 1996). Though there were attempts to incorporate N into PROSPECT, they were abandoned due to its strong covariance with other N containing compounds leading to inconsistent results (Jacquemoud et al., 1996; Kokaly et al., 2009). Among many empirical approaches, several VIs were proposed specifically to estimate leaf N and they were mainly established for crops (Chen et al., 2010b; Tian et al., 2011). Also band selection techniques, such as stepwise or partial least square regressions, were successfully applied on transformed reflectance spectra (Smith et al., 2003; Yoder and Pettigrew-Crosby, 1995). Based on our

literature review (Appendix A1) and Figure 2.2, we can conclude that empirical RS methods can retrieve N with high accuracy. The average R^2 between RS-estimated and measured N was equal to 0.72 ± 0.16 and the average relative RMSE was equal to 15 ± 7%.

Wavelengths that were frequently reported as important for N estimation are summarized in Figure 2.3. These wavelengths can be integrated into three broad spectral regions: i) red-edge region (680-780 nm) that is characterized by low reflectance in red due to strong C_{ab} absorption and high reflectance in NIR due to leaf internal scattering , ii) NIR region around 1200 nm that is associated also with water absorption, and iii) SWIR region where three main protein absorption features are located around 1680 nm, 2050 nm and 2170 nm (Kumar et al., 2001). Recent work of Knyazikhin et al. (2012) showed that a positive correlation between N and NIR reflectance, which was previously found in some temperate and boreal forests (Ollinger et al., 2008), is actually a result of canopy structure effects. They emphasized that quantification of biochemical traits from NIR in general is strongly influenced by radiation scattering processes, which have to be accounted for in order to achieve correct results.

Moreover, we bring evidence that a moderately strong correlation between leaf N and C_{ab} exists across different species (Table 2.3 and Appendix A2). The average Pearson correlation coefficient is equal to 0.65 ± 0.15, and it varies between 0.4 and 0.9 for individual species. This finding supports our hypothesis that remotely sensed C_{ab} can be potentially used as an operational approach to estimate N. Many C_{ab} sensitive VIs (Sims and Gamon, 2002), simple spectral models (Gitelson et al., 2006) and spectral transformations (Kokaly and Clark, 1999) have been developed and tested to estimate C_{ab} from the leaf reflectance data. Their robustness and upscaling to the canopy level have been thoroughly tested using RTM (Haboudane et al., 2002; le Maire et al., 2004). Additionally, physical RS methods using RTM enable direct estimation of C_{ab} (Jacquemoud et al., 2009). This is particularly an advantage in structurally complex canopies such as conifers (Malenovský et al., 2013; Zarco-Tejada et al., 2004), where simple empirical methods often fail. When using RS-based C_{ab} as proxy of N, one has to keep in mind that the positive N-C_{ab} relationship is species specific (Hallik et al., 2009; Appendix A2) and therefore more suitable for communities with lower species diversity.

Table 2.3 Pearson's correlation coefficient (R) between measured leaf chlorophyll (C_{ab}) and leaf nitrogen (N) concentration or content as reported for some plant species in literature and from our own field measurements. The number of stars in the superscript indicates the statistical significance of the reported correlations (****$p \leq 0.001$, ***$p \leq 0.01$, **$p \leq 0.05$, *$p \leq 0.1$, in case the statistical significance was not reported the R value is without a superscript).

Species name		Units		
(No. of observations)	R	C_{ab}	N	Reference
Trees				
Larix decidua (18)	0.60***	μg cm^{-2}	mg cm^{-2}	(Appendix A2)
Populus tremula (19)	0.71****	g m^{-2}	g m^{-2}	(Hallik et al., 2009)
Tilia cordata (20)	0.75****	g m^{-2}	g m^{-2}	(Hallik et al., 2009)
Acer macrophyllum (80)	0.65	mg g^{-1}	mg g^{-1}	(Yoder and Pettigrew-Crosby, 1995)
Picea abies (78)	0.37***	mg g^{-1}	%	(Schlerf et al., 2010)
Fagus sylvatica (70) and Quercus spp. (75)	0.81****	μg cm^{-2}	mg g^{-1}	(le Maire et al., 2008)
Tsuga heterophylla (11), Pinus ponderosa (6), Pseudotsuga menzeisii (3), Juniperus occidentalis (3)	0.60***	mg cm^{-2}	mg cm^{-2}	(Johnson et al., 1994)
Tropical forest species (n.a.)	0.70-0.84	-	-	(Asner and Vitousek, 2005)
Shrubs				
Juniperus nana (11)	0.70*	μg cm^{-2}	mg cm^{-2}	(Appendix A2)
Vaccinium myrtillus (14)	0.51*	μg cm^{-2}	mg cm^{-2}	(Appendix A2)
Gossypium hirsutum (18)	0.68	mmol m^{-2}	mmol m^{-2}	(Evans, 1989)
Graminoides				
Dactylis glomerata (13)	0.78***	μg cm^{-2}	mg cm^{-2}	(Appendix A2)
Dactylis glomerata (32)	0.38**	g m^{-2}	g m^{-2}	(Hallik et al., 2009)
Kobresia myosuroides (14)	0.47**	μg cm^{-2}	mg cm^{-2}	(Appendix A2)
Festuca violacea (6)	0.74*	μg cm^{-2}	mg cm^{-2}	(Appendix A2)
Bromus erectus (18)	0.42***	μg cm^{-2}	mg cm^{-2}	(Appendix A2)
Phleum pratense (33)	0.64****	g m^{-2}	g m^{-2}	(Hallik et al., 2009)
Forbs/herbs				
Laserpitium latifolium (14)	0.65*	μg cm^{-2}	mg cm^{-2}	(Appendix A2)
Rhinanthus alectorolophus (28)	0.84****	μg cm^{-2}	mg cm^{-2}	(Appendix A2)
Crepis pyrenaica (15)	0.84****	μg cm^{-2}	mg cm^{-2}	(Appendix A2)
Leonthodon hispidus (20)	0.47*	μg cm^{-2}	mg cm^{-2}	(Appendix A2)
Centaurea scabiosa (15)	0.81****	μg cm^{-2}	mg cm^{-2}	(Appendix A2)
Gentiana luthea (14)	0.61*	μg cm^{-2}	mg cm^{-2}	(Appendix A2)
Plantago media (15)	0.57*	μg cm^{-2}	mg cm^{-2}	(Appendix A2)
Cirsium arvense (9)	0.75**	g m^{-2}	g m^{-2}	(Hallik et al., 2009)
Phaseolus vulgaris (21)	0.84	mmol m^{-2}	mmol m^{-2}	(Evans, 1989)
Spinacia oleracea (12)	0.96	mmol m^{-2}	mmol m^{-2}	(Evans, 1989)
Alocasia macrorrhiza (15)	0.50	mmol m^{-2}	mmol m^{-2}	(Evans, 1989)
Crops				
Triticum spp. (21)	0.86****	g cm^{-2}	g m^{-2}	(Boegh et al., 2002)
Triticum spp. (123)	0.50**	mg g^{-1}	%	(Oppelt and Mauser, 2004)
Triticum aestivum (51)	0.89	mmol m^{-2}	mmol m^{-2}	(Evans, 1989)

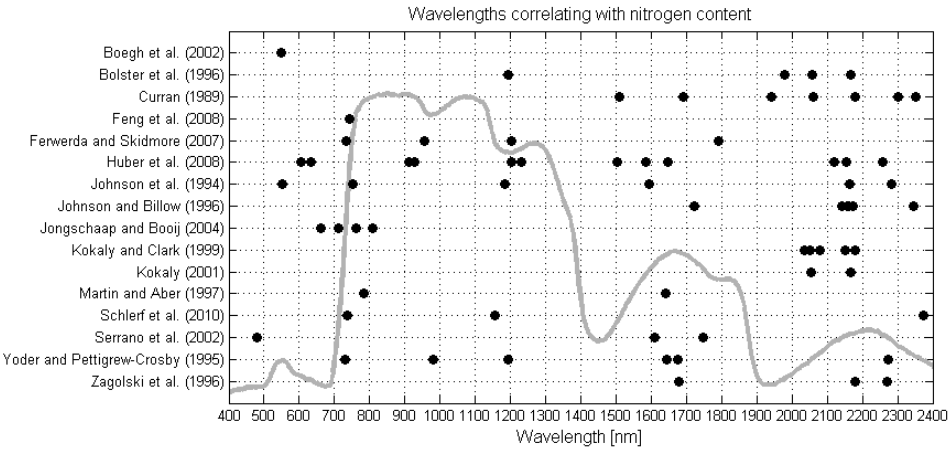

Figure 2.3 Overview of spectral wavelength used in scientific literature for estimation of nitrogen concentration and content in green and dry plant leaves. Each dot represents a reported spectral wavelength. A typical reflectance response of green vegetation (grey line) is plotted for clarity.

2.3.8 Leaf and canopy phosphorus

Leaf phosphorus (P) is an indicator of plant growth rate and nutrient quality. We found only limited number of studies that estimated P from RS data (Appendix A1). Only Porder et al. (2005) used airborne RS to estimate canopy P concentration of broadleaf tropical forest. The rest of the reviewed studies used airborne-based or proximal sensing to estimate P concentration in structurally homogeneous canopies, such as crops and grasslands. Based on results of our literature review (Appendix A1) and Figure 2.2, we can conclude that P can be retrieved from optical RS with lower accuracies than N. The average R^2 between RS-estimated and measured P was equal to 0.57 ± 0.16 and the average relative RMSE was equal to 23 ± 7%. In all cases empirical retrieval methods were used. The selection of spectral bands used in regression models was inconsistent among the reviewed studies, which can be mainly attributed to the low P concentration in leaves (less than 1% of dry leaf mass) and the absence of pronounced P absorption features. NIR and SWIR spectral bands were often included in the regression models, but these bands are strongly influenced by water absorption and canopy structure. When the effect of leaf water content was suppressed by applying a water removal technique (Schlerf et al., 2010), the accuracy of the P prediction in savana grasslands from proximal sensing increased (Ramoelo et al., 2011). We have not found any VI that is specifically designed for P estimation and previously designed indices for C_{ab} or N estimation did not perform satisfactorily (Pimstein et al., 2011). Similar to nitrogen, the biomass weighted canopy P concentration can be retrieved with higher accuracy than leaf-level concentration (Pimstein et al., 2011).

Table 2.2 Link between plant traits as described by Cornelissen et al. (2003) and possible remote sensing counterparts

Plant traits from Cornelissen et al. (2003) [typical units]	Trait definition	RS methods	RS references	Operational scale: Leaf	Individual	Pop./Com.	Ecosystem	Biome	LOSU[1]
Plant growth form [categories]	Determined by canopy structure and height	Global land cover classification, where several growth forms can be combined in one class	(Arino et al., 2008; Bartholomé and Belward, 2005; Friedl et al., 2010)				*	*	4
		Direct detection of some specific plant growth forms:							
		Shrubs	(Chopping et al., 2006; Hamada et al., 2007)		*	*	*	*	3
		Trees	(Kokaly et al., 2003; Martin et al., 1998)		*	*	*	*	4
		Lianas	(Kalacska et al., 2007; Sánchez-Azofeifa et al., 2009)	*	*				1-2
		Aquatic vegetation	(Hestir et al., 2008; Underwood et al., 2006)		*	*			2
Plant life form [categories]	Determined by position of perenating tissue to the ground surface	Not available	Not available						
Plant flammability (combined trait) [categories]	Combination of six traits determining how easily a plant produces flames	Not available	Not available						
		But RS can asses vegetation fire properties:							
		Canopy moisture content	(Chuvieco et al., 2002; Koetz et al., 2004)			*	*		3
		Proportion between dead and live biomass	(Erdody and Moskal, 2010; Jia et al., 2006)			*	*		3
Photosynthetic pathway [categories]	C3, C4, CAM metabolism	Chlorophyll b/a ratio	(Siebke and Ball, 2009)	*					1-2
		Canopy structure	(Irisarri et al., 2009)		*	*			1
		Multi-temporal satellite RS detecting asynchronous seasonality of C3 and C4 species	(Davidson and Csillag, 2001; Foody and Dash, 2007)				*	*	2-3
Clonality [categories]	Ability to reproduce vegetatively.	Not available	Not available						
Spinescence [categories]	Presence, type, size and density of spines	Not available	Not available						

Table 2.2 Continues

Plant traits from Cornelissen et al. (2003) [typical units]	Trait definition	RS methods	RS references	Operational scale: Leaf	Individual	Pop./Com.	Ecosystem	Biome	LOSU[1]
Plant / canopy height [m]	Distance between ground and the upper boundary of the main photosynthetic tissue	Directly derived from laser scanning data	(Holmgren et al., 2003; Næsset et al., 2004; Kaartinen et al., 2012; Straatsma and Middelkoop, 2007)		*	*	*		4-5
		Indirectly related to leaf area index	(Chopping et al., 2008; Van Wijk and Williams, 2005)			*	*		2
Leaf lifespan [months]	Period when an individual leaf is physiologically active	See leaf phenology	Not available						
Leaf phenology [months]	Number of months per year when canopy is green	For plant periodically changing leaves the length of growing season is derived from							
		Satellite multi-temporal data	(Reed et al., 1994; White et al., 2009)				*	*	4
		Proximal phenological cameras	(Richardson et al., 2009)		*	*			4
Leaf size [m^2]	One-sided surface area	Not available	Not available						
		But for entire plant communities it can be linked to leaf area index	(Chen et al., 2002; Fernandes et al., 2004; Garrigues et al., 2008)			*	*	*	4
Specific leaf area [m^2 kg^{-1}]	One-sided area of a fresh leaf divided by its dry mass	Directly estimated as leaf mass per area (1/SLA) from RTM inversion	(Fourty and Baret, 1998; Riaño et al., 2005; Vohland et al., 2010)			*	*		2-3
		Related to leaf water content that can be estimated from RTM inversion or empirical methods	(Clevers et al., 2008; Colombo et al., 2008)		*	*	*	*	3-4
Leaf dry matter Content [mg g^{-1}]	Dry mass of leaf divided by its fresh mass	Empirical methods estimating individual components such as lignin or cellulose	(Kokaly et al., 2009; Serrano et al., 2002)		*	*	*		2
		Related to specific leaf area (see above)							
Leaf nitrogen concentration/content [mg g^{-1} / mg m^{-2}]		Directly estimated using empirical RS methods	(Martin et al., 2008; Oppelt and Mauser, 2004; Serrano et al., 2002)		*	*	*		3
		Indirectly related to chlorophyll content that can be estimated using RTM inversion	(Dash and Curran, 2004; Zarco-Tejada et al., 2004)	*	*	*	*		4-5

Table 2.2 Continues

Plant traits from Cornelissen et al. (2003) [typical units]	Trait definition	RS methods	RS references	Operational scale					LOSU[1]
				Leaf	Individual	Pop./Com.	Ecosystem	Biome	
Leaf phosphorus concentration/content [mg g^{-1} / mg m^{-2}]		Directly estimated using empirical RS methods	(Mutanga and Kumar, 2007; Porder et al., 2005)		*	*	*		2-3
Leaf physical strength [N]	Leaf resistance to fracture	Not available	Not available						

[1]LOSU (Level of Scientific Understanding) indicates the fidelity of RS methods and RS-based products used in vegetation studies. It represents a weighted average of scores for the number of reported studies and obtained accuracy of RS methods (1 is low, 2 is low-medium, 3 is medium, 4 is medium-high, and 5 is high level of the scientific understanding).

2.4 Concluding remarks

In this review, we provided an extensive summary of RS methods for the estimation of key plant traits as defined by Cornelissen et al. (2003). Main conclusions and future outlooks for the individual traits are listed as follows:

- Classification of plant growth and plant life forms cannot be entirely reproduced by RS. Global RS-based land cover classification schemes classify vegetation to broad classes, which are by definition closer to plant growth forms. Their classification accuracy is around 70%. High resolution RS facilitate local classifications of some plant growth forms or even individual species, but the classification accuracy vary between 50 and 95%. Combination of optical RS with multi-directional RS or laser scanning can improve existing plant classifications by increasing the separability among vegetation types.
- Plant flammability as a combined trait cannot be quantified using optical RS observations. However, when combining optical passive and active RS then the combustibility of entire plant communities can be well assessed. RS data are currently being used to quantify fire properties such as moisture content, plant height and the proportion between live and dead biomass. These are valuable input data for fire models and fuel classification schemes.
- Use of optical RS for mapping C3 and C4 photosynthetic pathways remains rare. Instead, RS data has been widely exploited for spatio-temporal mapping of plant photosynthetic activity using proxies of fraction of absorbed photosynthetic radiation and light use efficiency. Direct estimation of light use efficiency by means of chlorophyll fluorescence has emerged as a very promising approach. Though major challenges in RS of chlorophyll fluorescence are currently being investigated, recent results already demonstrated that large scale mapping of chlorophyll fluorescence from RS is possible.
- Plant height can be directly and most accurately estimated from active laser scanning data. The relative error of height estimation from discrete return laser systems is usually bellow 10% in tall forest canopies and increases up to 20% in lower canopies. Full waveform lasers do not necessarily provide improvement in absolute height estimation, but they certainly offer better insight into the 3D vegetation structure. Understanding the effects of canopy structure on reflectance is a major challenge in RS of vegetation.
- Multi-temporal satellite RS can deliver relevant land surface phenological indicators, such as start, end, maximum peak and duration of the vegetation season for plant communities periodically changing their foliage. Recent comparative studies suggested that there is no agreement on a single, globally appropriate method to extract land surface phenology. There is critical need to effectively validate RS-based phenology indicators and therefore in-situ data are required across global biomes. Future studies should attempt to employ data

from active RS systems to separate asynchronous phenology of understory and the main canopy. Moreover, the future chlorophyll fluorescence observations from space can provide an accurate identification of the photosynthesis onset and offset.

- Specific leaf area or its inverse ratio leaf mass per area can be estimated from the optical RS data using empirical, as well as physical methods. Despite this possibility, the retrieval accuracy substantially varied and it was the lowest among the reviewed plant biochemical traits. Inconsistencies are mainly due to confounding effects of water present in the plant tissue and the atmosphere. An algorithm that significantly suppresses the absorption effect of water or improvements in atmospheric corrections is prerequisite for an accurate retrieval of leaf mass per area from optical RS.
- Nitrogen can be estimated from optical RS using empirical methods achieving the highest accuracies among the reviewed plant biochemical traits. The highest uncertainty was observed in coniferous canopies, which is due to their complex canopy structure. Therefore there is an urgent need for improved RS methods accounting and correcting for canopy structure effects. We supported the hypothesis that RS of chlorophyll content can be used as an operational proxy for N estimation, since moderately strong relationship between nitrogen and chlorophyll exists. Moreover, the future multi-temporal observations of chlorophyll fluorescence might also improve N retrieval methods.
- Finally, phosphorus can be estimated from optical RS using empirical methods only. The achieved accuracies are moderately good, but lower than for nitrogen. Due to low concentration of P in leaves and confounding effects of canopy structure and water content we do not expect that operational large scale mapping of P from RS will be achievable in a near future.

In addition, the applicability of RS methods goes beyond the traits discussed in this review. Several well-established and thoughtfully validated RS-based traits can support or even extend the collection of current key plant traits used in ecology. Those are mainly leaf/canopy chlorophyll and water content, LAI, fAPAR and fractional vegetation cover.

We see an urgent need to address in a more comprehensive fashion the effects of vegetation structure in interpretation of RS data. Therefore advanced measurements of traits such as the volume of intracellular air spaces, leaf thickness, leaf angle distribution, proportion of non-photosynthetic biomass within canopy light acclimation are required. Generally, more coherent collection of in-situ trait measurements together with proximal and remote sensing observations will be required to develop robust scaling schemes and support airborne and satellite based RS methods of trait estimation. Such an interdisciplinary cooperation resulted recently in a novel concept of “optical traits”, i.e. assessing combined effects of

vegetation physiological, structural and phenological properties on reflectance measurements (Ustin and Gamon, 2010).

The most important advantage of using RS is its ability to provide spatially explicit and continuous maps of relevant traits repeatedly during the vegetation season. If combined with eco-physiological models that are designed having the current and future capabilities of RS data in mind, substantial progress will be achieved in spatio-temporal mapping of ecosystem functioning.

Acknowledgements

This work was supported by following projects: Ecochange (FP6-2006-GOCE-036866) and Hyper-I-Net (EC Marie Curie Action, MRTN-CT-2006-035927). We appreciate comments on earlier versions of the manuscript by A. Damm, R. de Jong, P. D'Odorico, I. Garonna, R. Leiterer and D. Small. We appreciate excellent reviewers' comments, allowing to substantially improving the manuscript

3

Measurement methods and variability assessment of the Norway spruce total leaf area: implications for remote sensing

This chapter is based on:

Homolová L, Lukeš P, Malenovský Z, Lhotáková Z, Kaplan V, Hanuš J (2013) Measurement methods and variability assessment of the Norway spruce total leaf area: implications for remote sensing. Trees Structure and Functions 27:111-121 DOI 10.1007/s00468-012-0774-8

Abstract

Estimation of total leaf area (LA_T) is important to express biochemical properties in plant ecology and remote sensing studies. A measurement of LA_T is easy in broadleaf species, but it remains challenging in coniferous canopies. We proposed a new geometrical model to estimate Norway spruce LA_T and compared its accuracy with other five published methods. Further, we assessed variability of the total to projected leaf area conversion factor (CF) within a crown and examined its implications for remotely sensed estimates of leaf chlorophyll content (C_{ab}). We measured morphological and biochemical properties of three most recent needle age classes in three vertical canopy layers of 30 and 100-year-old spruce stands. Newly introduced geometrical model and the parallelepiped model predicted spruce LA_T with an error < 5% of the average needle LA_T, whereas two models based on an elliptic approximation of a needle shape underestimated LA_T by up to 60%. The total to projected leaf area conversion factor varied from 2.5 for shaded to 3.9 for sun exposed needles and remained invariant with needle age class and forest stand age. Erroneous estimation of an average crown CF by 0.2 introduced an error of 2 – 3 µg cm^{-2} into the crown averaged C_{ab} content. In our study, this error represents 10 – 15% of observed crown averaged C_{ab} range (33 – 53 µg cm^{-2}). Our results demonstrate the importance of accurate LA_T estimates for validation of remotely sensed estimates of C_{ab} content in Norway spruce canopies.

3.1 Introduction

Measurements and monitoring of forest structural and biochemical properties (e.g., leaf area index, leaf foliar pigment, nitrogen or water content) and physiological processes (e.g., gas exchange, photosynthesis) are important for the understanding of forest carbon sequestration (Luyssaert et al., 2007). In-situ measurements of forest properties and processes are usually spatially and timely limited, labor demanding particularly in complex canopies such as mixed boreal or tropical forests. Thus, in-situ measurements become impractical for large-scale applications. Emerging remote sensing (RS) imaging spectroscopy (often referred to as hyperspectral RS) has a great potential for regular monitoring of forest properties and processes at larger spatial scales (Kokaly et al., 2009; Rautiainen et al., 2010; Ustin et al., 2004). Currently, imaging spectroscopy data have been used to estimate leaf and canopy biochemical properties such as chlorophyll (Malenovský et al., 2006b; Moorthy et al., 2008; Zarco-Tejada et al., 2004), nitrogen (Huber et al., 2008; Schlerf et al., 2010) and water content (Clevers et al., 2010; Koetz et al., 2004), canopy structural properties such as leaf area index (Fernandes et al., 2004), and eco-physiological processes such as mapping of net primary productivity (Ollinger and Smith, 2005). Successful calibration and validation of the RS methods, however, depend on accurate and reliable in-situ measurements of canopy biochemical properties that are often expressed at leaf area basis. While estimation of leaf area of broadleaf species is straightforward, it is a challenging task for non-flat coniferous needles. In case of conifers, total leaf area (LA_T) or hemisurface leaf area ($LA_H = ½\ LA_T$) seems to be a more appropriate expression for gas exchange or photosynthesis-related studies than projected leaf area (LA_P), as stomata are located all around the needle surface (Smith et al., 1991).

The LA_T for broadleaf species is computed as two times LA_P, which can easily be measured by planimeters, desktop scanners, or leaf area meters (Beerling and Fry, 1990). These techniques can be used to measure LA_P of coniferous species, but they are not suitable for LA_T (or LA_H) measurements due to the three-dimensional shape of needles. Needle LA_T has been determined by a volume displacement method (Johnson, 1984) or from absorbance measurements of entire shoots (Serrano et al., 1997), but both methods are used rarely. More frequently, needle LA_T is computed from an approximation of the needle shape by a simple geometrical primitive (Niinemets and Kull, 1995; Sellin, 2000). Pine needles can be represented as half-cylinders or half-ellipsoids (Svenson and Davies, 1992), spruce needles are usually modeled as parallelepipeds or ellipsoids (Sellin, 2000). Dimensions of geometrical primitives are based on directly measurable morphometric variables, such as needle length and diameter. For example, Perterer and Körner (1990) proposed a complex model based on 9 different measures for spruce and 12 for pine needles, which

significantly limits its practical use in forest research. Nevertheless, a detailed and accurate needle geometrical model is fundamental for developing simpler, feasible, but still reliable, methods to estimate LA_T of coniferous species.

Once LA_T is accurately determined, a conversion factor (CF) between LA_T and LA_P can be derived and used to estimate LA_T from easily measureable LA_P. Conversion factor is species specific, but it also varies within a canopy of the same species due to changing irradiance inside a canopy (Niinemets and Kull, 1995; Sellin, 2000). The characteristic organization of branches and shoots in coniferous canopies produces a heterogeneous radiation regime in a canopy vertical profile (Chmura and Tjoelker, 2008; Špunda et al., 1998; Waring, 1983). For example lower parts of a young spruce canopy can receive only about 10% of irradiance when compared to the top of the canopy (Kalina et al., 2001). Light availability modulates leaf morphological properties (Bond et al., 1999; Hallik et al., 2009; Niinemets, 2007); the shaded needles are usually more flat compared to sun exposed needles with more circular or rhomboidal cross-section (Cescatti and Zorer, 2003). Usability of CF for LA_T estimation is, therefore conditioned by understanding its variability between and within individual tree crowns.

Taking the advantage of high resolution digital photography and computer image processing techniques, the first objective of this study was to propose an accurate geometrical model to estimate LA_T of Norway spruce needles and compare it with five previously published LA_T estimating methods. The second objective was to investigate variability of the total to projected leaf area conversion factor (CF) taking into account three sources of variability: (1) needle position within a crown vertical profile, (2) needle age, and (3) canopy structure due to different forest stand age. Finally, the third objective was to quantify the influence of biased LA_T measurements on the estimation accuracy of crown averaged biochemical properties, which are being used for calibration and validation of remote sensing derived products.

3.2 Materials and methods

3.2.1 Study area and needle sampling

Morphological and biochemical properties of Norway spruce needles were analyzed for needle samples collected at the Bílý Kříž experimental research site (Moravian-Silesian Beskydy Mts. at the eastern part of the Czech Republic bordering with Slovakia; 18.53°E, 49.50°N, mean altitude of 880 m a.s.l.). The microclimatological conditions of the site are described in Urban et al. (2007).

Two montane Norway spruce (*Picea abies* (L.) Karst) forest stands of different age and structure were selected for this experiment: a 30-year-old regular plantation (further referred to as the “immature” stand), and an about 100-year-old stand (further referred to as the “mature” stand), both growing on a moderate slope (13°)

with S-SE orientation. In 2006, the average tree height was 12.5 m in the immature and 40 m in the mature stand, the average diameter at breast height was 14 and 53 cm, respectively, the canopy density was about 1,400 and 160 trees ha^{-1}, respectively, and the approximate stand area was 7.5 and 2.5 ha, respectively.

Ten immature and 20 mature representative trees were selected for the needle sampling. Double number of mature trees was considered, because we expected higher variability in needle morphological and biochemical properties due to a larger structural heterogeneity of the mature stand. One branch was collected from the upper (sun exposed zone, E), middle (transition zone, T), and bottom (sun shaded zone, S) canopy layer to capture varying irradiation conditions inside the canopies. From each branch, the last three needle age classes were sampled resulting in nine needle samples per tree. About 5 – 7 representative and visually healthy shoots (i.e., the annual growth segments) per needle age class were selected and about 30 individual needles were randomly sampled from the central part of shoots. Each needle sample was divided into three subsets including about ten needles each: the first subset was used for estimation of needle LA_T and LA_T/LA_P conversion factor, the second subset for needle water content and specific leaf area, and the third subset for photosynthetic pigment analysis. In total we collected three times 270 needle samples.

Posterior statistical assessment of the optimal sample size using the Power t-test (Erdfelder et al., 1996) indicated a minimum sample size of 21 trees to assess the total variance of CF, which was exceeded with total of 30 trees sampled.

3.2.2 Estimation of needle LA_T and CF

The needles from the first subset for LA_T estimation were kept deep-frozen until the laboratory processing. Individual needle samples were first scanned on a desktop scanner to measure LA_P and then five needles were randomly selected for further processing (preceding analysis indicated that 5 needles is sufficient to obtain LA_T representative for the entire needle sample; results not shown). Five needles were scanned on a desktop double-lamp scanner to determine their individual LA_P and length along curvature (L). Then three cross-sections (approximately 100 µm thick) were obtained from the base, middle and top part of a needle using a hand microtome. Micrographs of cross-sections were acquired with the Canon EOS 450D digital camera, which was mounted on the Novex BT PL microscope. The micrographs were captured uncompressed with maximum possible resolution of 12 MPix to ensure high precision of image analysis. Perimeter and length of both the major (D_1) and the minor (D_2) diameters were measured automatically for each cross-section using a self-developed image analysis procedure [combination of Python 2 and GNU (General Public Licence) Image Manipulation Program (GIMP, v. 2.6)].

The total leaf area of spruce needles was estimated using six methods. We proposed a new geometrical model for LA_T estimation of spruce needles (method I),

which was based on the model of Perterer and Körner (1990). Our model approximated the spruce needle shape to three geometric primitives: two adjacent circular cone frustums, and a cone cap representing a tapered needle's top (Figure 3.1). The total leaf area of a needle was calculated according to the following equation:

$$LA_T I = \frac{P_B + P_M}{2}.\, L'_{B-M} + \frac{P_M + P_T}{2}.\, L'_{M-T} + \frac{P_T.L'_T}{2}, \tag{3.1}$$

where P_B, P_M, and P_T are the measured perimeters of three cross-sections placed at the base ($_B$), middle ($_M$) and top ($_T$) of a needle, respectively. L'_{B-M} is a slant height of the cone frustum between the base and the middle cross-sections calculated from the measured cone height L_{B-M} as $L'_{B-M} = \sqrt{L^2_{B-M} + (P_B/2\pi - P_M/2\pi)^2}$. L'_{M-T} is a slant height of the cone frustum between the middle and the top cross-section calculated analogous to L'_{B-M}. L'_T is a slant height of a cone cup calculated as $L'_T = \sqrt{L^2_T + (P_T/2\pi)^2}$. We assumed that L_T = 1.5 mm, $L_{B-M} = L_{M-T}$ and the sum of the three lengths was equal to the total needle length measured along the curvature of the needle central axis (L) as illustrated at Figure 3.1b.

The other five methods for estimation of needle LA_T were previously published in scientific literature. More details on methods II – V can be found in Sellin (2000) and on method VI in Pokorný (2002). Here, we provide only the final formulas and the variables are explained at Figure 3.1:

Method II: A needle side approximated to a parallelepiped:

$$LA_T II = 2.L.\sqrt{D_1^2 + D_2^2} \tag{3.2}$$

Method III: A needle side approximated to an ellipse:

$$LA_T III = \frac{\pi.L.\sqrt{D_1^2 + D_2^2}}{2} \tag{3.3}$$

Method IV: A needle approximated to an ellipsoid:

$$LA_T IV = \pi.\sqrt[3]{D_1^2.D_2^2.L^2} \tag{3.4}$$

Method V: A needle side approximated to a rectangle with tapering ends to a half-ellipse:

$$LA_TV = \frac{4.r.L.\sqrt{D_1^2+D_2^2}+(1-r).\pi.L.\sqrt{D_1^2+D_2^2}}{2} \quad (3.5)$$

(r is the relative length of the rectangular part of a needle and it was equal to 0.75).

Method VI: CF derived as the ratio of the middle cross-section perimeter and major diameter:

$$LA_TVI = \frac{P_M}{D_1}.LA_P \quad (3.6)$$

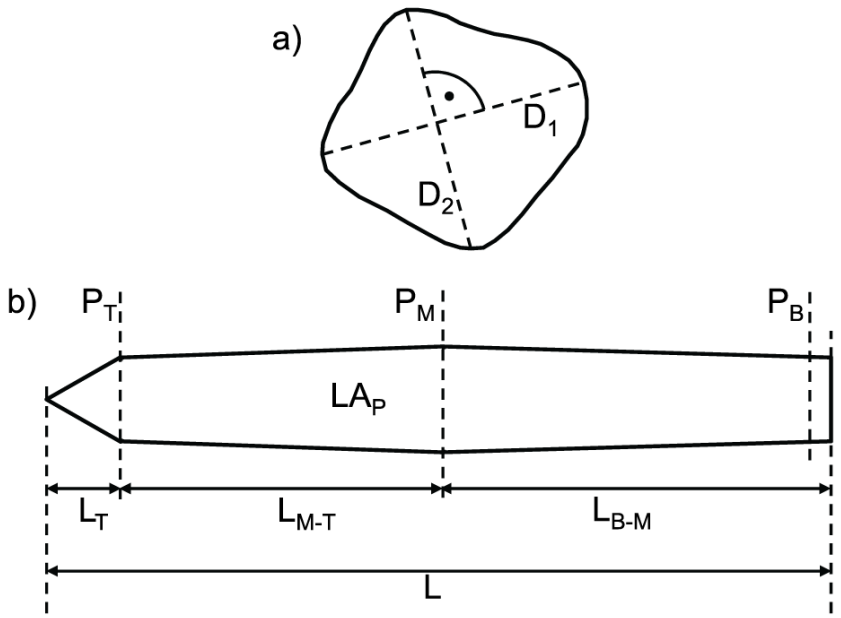

Figure 3.1 Geometrical model developed in this study to calculate total leaf area of Norway spruce needles and its inputs: a) needle cross-section and its major (D_1) and minor (D_2) diameter, b) schematic position of three cross-sections (P_T, P_M, P_B are perimeters of a cross-section at the top, middle, and bottom part of a needle, respectively; L_{B-M}, L_{M-T} are lengths of segments between two cross-sections assuming that $L_{B-M} = L_{M-T}$; L_T is height of cone cap, which was approximately 1.5mm; L is total needle length measured along the curvature of the needle central axis; LA_P is projected leaf area of a needle).

Six LA_T estimating methods (Eq. 3.1 – 3.6) were compared at the individual needle level against the same reference ($\overline{LA_T}$). The reference total leaf area was calculated for 21 needles, which were selected across the entire sample pool to capture the variability of a needle shape. We took 9 – 15 cross-sections per needle, depending on its length, and calculated $\overline{LA_T}$ using the same principle as presented for method I (Eq. 3.1), but instead of two we integrated surface area of up to 14 cone frustums.

Finally, the conversion factor between total (method I) and projected (scanned) leaf area was calculated as a simple ratio: $CF = LA_T / LA_P$. We applied a three-way analysis of variance (ANOVA) at the significance level $\alpha = 0.01$ and with a prior normality test to analyze CF variability between and within spruce crowns considering three potential sources of CF variability: (1) needle position within a crown vertical profile, (2) needle age, and (3) forest stand age.

3.2.3 Measurement of needle biochemical properties and upscaling to a crown level

The second and the third needle subsets were used to analyze the following needle biochemical properties: specific leaf area (SLA), water (C_w), chlorophyll *a* and *b* (C_{ab}) and carotenoid (C_{xc}) content. Needles for SLA and C_w content determination were weighted immediately after clipping, stored in paper bags, dried in an oven at 60 °C for 48 h, and weighted again after drying. Needles for photosynthetic pigments (C_{ab} and C_{xc}) were kept in deep freeze and dark until being processed in a laboratory. Pigments were extracted according to the method of Porra et al. (1989) using the dimethylformamide solvent and the pigment concentration was determined spectrophotometrically according to the equations of Wellburn (1994). Following the terminology proposed by Datt (1998), we define constituent concentration as mass fraction per unit dry leaf mass (in mg g^{-1}) and constituent content as mass fraction per unit leaf area (in mg cm^{-2}). Equation 3.7 shows the conversion between concentration and content of a constituent X (C_w, C_{ab} or C_{xc}) using specific leaf area [SLA_H, the ratio of hemisurface leaf area (cm^2) to the corresponding dry mass weight (g)].

$$X\,[\mathrm{mg\ cm^{-2}}] = \frac{X[\mathrm{mg\ g^{-1}}]}{SLA_H[\mathrm{cm^2 g^{-1}}]} \tag{3.7}$$

The upscaling from the leaf to the crown level was done by simply averaging nine values of leaf level biochemical content per tree (i.e., combination of needle samples from three crown vertical layers and three needle age classes). The mean value per crown is hereafter referred to as “crown averaged content”. We selected this simple upscaling approach, because it is often used in remote sensing studies (Huber et al., 2008; Schlerf et al., 2010; Zarco-Tejada et al., 2004).

In order to evaluate the effect of LA_T estimation on crown averaged biochemical content of SLA, C_w, C_{ab} and C_{xc}, first, we calculated crown averaged biochemical

content using six LA_T estimating methods (Eqs. 3.1 – 3.6). SLA_H computed from six different LA_T values served as the basis for conversion from needle biochemical concentrations to contents (Eq. 3.7). Second, we considered a theoretical case, where needle biochemical concentration (mg g^{-1}) and corresponding LA_P are known, but a sample LA_H is unknown. Missing LA_H was then calculated as $LA_P \times CF \times 0.5$, where LA_P is the measured projected leaf area of a sample and CF is a theoretical value of the total to projected leaf area conversion factor. The theoretical CF varied within a physically meaningful range from 2 (flat needles) to 4 (square shaped needles) with steps of 0.2, while assuming a constant theoretical CF value for entire crown vertical profile. Once again, we computed crown averaged biochemical content (X_{CF}) as a simple average of nine needle biochemical contents, but this time using the theoretical CF to estimate a sample LA_H. X_{CF} was then compared with crown averaged biochemical content (X_{REF}), based on the LA_T estimating method I (Eq. 3.1), using root mean square error (RMSE):

$$\mathrm{RMSE} = \sqrt{\frac{1}{n}\sum_{i=1}^{n}\left(X_{i,CF} - X_{i,REF}\right)^2}\,, \tag{3.8}$$

where n is the number of trees.

3.3 Results

3.3.1 Accuracy of LA_T estimating methods

The accuracy of six LA_T estimating methods was assessed at the level of individual needles (in total 21 needles selected from the entire sample pool) by comparing all methods against one reference (Figure 3.2). The reference total leaf area ($\overline{LA_T}$) was calculated from 9 – 15 cross-sections taken along the needle length using similar principle as presented in Eq. 3.1. The average total area of a single needle was 52.2 (±9.5) mm^2. Detailed cross-sections analysis showed that the minor diameter of needle cross-sections is almost invariant along the entire needle length, whereas the major diameter decreases towards the needle ends (Figure 3.3). The coefficient of determination (R^2) between the LA_T estimating methods and the reference was generally high, varying between 0.79 and 0.99. Methods I and II provided accurate estimates of LA_T, R^2 was higher than 0.98 and RMSE was equal to 2.4 and 1.6 mm^2, respectively. In both cases, the relative RMSE was smaller than 5% of the average needle LA_T. Method III, which modeled needle side as an ellipse, and method IV, which modeled needle as an ellipsoid, systematically underestimated LA_T, with RMSE of 12.1 and 31.4 mm^2, respectively. Relative RMSE was up to 60% of the average needle LA_T.

Table 3.1 Morphological and biochemical properties of Norway spruce needles obtained from sampling of 10 immature and 20 mature trees from three canopy vertical layers (exposed, transition and shaded) and three most recent needle age classes (1 – most recent, 2 – last year, 3 – two-year-old needles). The values are presented as mean ± standard deviation.

	Age	Immature			Mature		
	class	Exposed	Transition	Shaded	Exposed	Transition	Shaded
Needle	1	15.9±1.2	16.3±2.6	13.3±2.0	15.8±2.2	17.7±2.0	17.1±2.5
length	2	16.5±1.1	15.3±1.7	14.8±1.4	18.1±2.2	16.6±2.5	16.0±2.8
[mm]	3	18.8±1.8	16.9±2.3	17.1±2.4	17.3±2.5	18.4±2.7	17.6±2.9
Major	1	1.19±0.06	1.16±0.07	1.07±0.10	1.29±0.14	1.13±0.07	1.10±0.09
diam. D_1	2	1.23±0.09	1.18±0.04	1.15±0.05	1.38±0.10	1.12±0.08	1.07±0.08
[mm]	3	1.26±0.07	1.22±0.04	1.16±0.06	1.25±0.13	1.18±0.10	1.11±0.09
Minor	1	1.04±0.12	0.67±0.13	0.61±0.25	1.10±0.07	0.64±0.08	0.54±0.06
diam. D_2	2	1.08±0.09	0.84±0.15	0.61±0.17	1.18±0.13	0.66±0.10	0.64±0.11
[mm]	3	1.03±0.15	0.88±0.14	0.67±0.19	1.19±0.09	0.59±0.05	0.55±0.06
LA_T / LA_P	1	3.46±0.23	3.09±0.25	2.83±0.27	3.51±0.18	2.89±0.15	2.85±0.24
CF	2	3.55±0.09	3.25±0.29	2.92±0.37	3.40±0.19	2.94±0.28	2.87±0.19
[-]	3	3.41±0.21	3.30±0.23	2.77±0.24	3.43±0.20	2.89±0.19	2.85±0.17
C_{ab} conc.	1	1.47±0.28	2.33±0.65	3.29±0.96	1.86±0.35	2.68±0.52	2.77±0.40
[mg g^{-1}]	2	2.06±0.32	2.63±0.48	3.11±0.58	2.36±0.49	3.15±050	3.30±0.48
	3	2.21±0.45	2.57±0.33	3.38±0.54	2.23±0.47	3.46±0.51	3.76±0.52
C_{ab} content	1	23.7±4.5	32.3±12.3	38.7±6.6	32.2±6.8	32.7±3.3	30.1±4.0
[µg cm^{-2}]	2	40.4±6.2	41.3±8.4	48.2±9.0	48.8±9.6	43.8±7.4	41.0±5.8
	3	43.0±8.4	43.4±5.5	50.4±13.6	46.6±12.5	49.2±8.2	45.2±5.6
C_{xc} conc.	1	0.26±0.05	0.36±0.12	0.46±0.15	0.30±0.05	0.36±0.06	0.37±0.05
[mg g^{-1}]	2	0.35±0.06	0.41±0.07	0.46±0.09	0.38±0.07	0.44±0.07	0.46±0.07
	3	0.37±0.08	0.42±0.05	0.51±0.06	0.38±0.07	0.50±0.07	0.54±0.07
C_{xc} content	1	4.1±0.8	5.0±2.3	4.3±1.0	5.2±0.9	4.4±0.4	4.1±0.5
[µg cm^{-2}]	2	6.9±1.1	6.4±1.1	5.6±1.6	7.8±1.5	6.2±1.1	5.8±0.9
	3	7.3±1.4	7.1±0.8	7.3±1.9	7.8±1.9	7.1±1.3	6.5±0.9
C_w conc.	1	0.59±0.02	0.62±0.02	0.63±0.02	0.55±0.02	0.61±0.02	0.61±0.03
[g g^{-1}]	2	0.56±0.02	0.59±0.02	0.61±0.03	0.53±0.02	0.58±0.05	0.57±0.02
	3	0.56±0.01	0.58±0.01	0.61±0.03	0.50±0.03	0.56±0.03	0.57±0.03
C_w content	1	23.8±1.6	22.8±3.2	16.7±2.4	22.0±3.1	20.2±5.8	17.9±4.7
[mg cm^{-2}]	2	25.1±1.9	23.0±3.4	19.3±3.1	23.5±3.0	19.0±3.5	16.7±3.0
	3	25.4±2.7	23.3±1.9	22.0±5.5	21.2±3.2	18.1±2.6	16.4±1.7
SLA_H	1	61.8±3.3	74.2±10.6	105.8±24.9	58.7±9.4	82.4±15.3	91.0±17.3
[cm^2 g^{-1}]	2	51.3±5.1	64.5±8.5	82.7±17.5	48.6±5.2	73.1±12.7	81.6±13.1
	3	51.5±4.7	59.6±6.5	75.6±23.2	48.7±5.1	71.1±10.2	83.8±10.8

3.3.2 Variability of total to projected leaf area conversion factor for method I

The sample specific conversion factor (CF) computed between LA_T (method I, Eq. 3.1) and scanned LA_P varied from 2.5 to 3.8 (95^{th} percentile). We examined three sources of CF variability: i) needle position within a crown vertical profile, ii) needle age, and iii) forest stand age (Figure 3.4 and Table 3.1). CF of the sun exposed

needles was higher than the CF of transition and shaded needles ($p \leq 0.01$). The mean values of CF were 3.47 (sun exposed needles), 3.18 (transition), and 2.84 (shaded needles) for the immature canopy and 3.44, 2.90, and 2.85, respectively, for the mature canopy. We did not find any statistically significant differences among three investigated needle age classes. The CF was nearly invariant between the immature and mature stand, except the transition canopy level, where CF of mature trees was lower compared to immature trees.

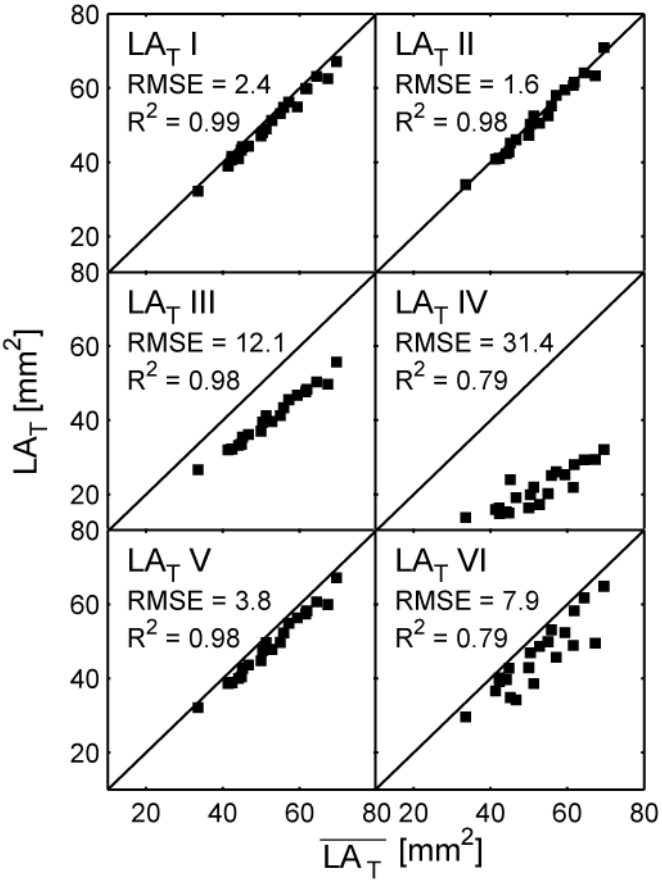

Figure 3.2 Comparison of six methods for estimation of total leaf area (Eq. 3.1 – 3.6) for individual spruce needles (n = 21) with the reference method ($\overline{LA_T}$). Root mean square error (RMSE) between each method and the reference, and coefficient of determination (R^2) are indicated for each method.

Finally, the CF was closely related to the ratio of the middle cross-section perimeter (P_M) and its major diameter (D_{1M}), with R^2 equal to 0.73, and thus CF could be reasonably modelled as:

$$CF = 0.47 (P_M / D_{1M}) + 1.3 \quad (3.9)$$

3.3.4 Impact of LA_T on upscaling of foliar biochemistry from leaf to crown level

At the needle level, biochemical concentration and content varied with needle age and canopy vertical position as summarized in Table 3.1. Pigment concentration (i.e. normalized by the dry mass) increased with increasing needle age and shadowing, whereas content (i.e. normalized by LA_H according to Eq. 3.7) increased only with needle age and remained nearly invariant among canopy vertical layers. Needle water content did not vary with needle age, but the typically sun shaded needles had lower C_w content than exposed needles. Specific leaf area, the ratio between needle LA_H and the dry mass, was the most variable needle property. It varied between 30 and 140 $cm^2 g^{-1}$ and it decreased with needle age and increased with increasing shadowing inside the canopy.

At the crown level, we first examined the influence of different LA_T estimating methods on the crown averaged biochemical content (Figure 3.5). Second, we examined whether the crown averaged biochemical content is sensitive towards biased LA_T estimates due to variable CF (Figure 3.6). Although we analyzed all biochemical properties, for brevity, we present results only for the chlorophyll content, because it is one of the most frequently studied vegetation property by remote sensing (le Maire et al., 2004; Ustin et al., 2009) and all biochemical properties showed similar response to different LA_T estimating methods.

An average crown averaged C_{ab} was equal to 39 µg cm^{-2} for the immature and 42 µg cm^{-2} for the mature spruce trees and it varied between 33 and 53 µg cm^{-2} (values based on LA_T estimations using our adjusted geometrical model, i.e. method I, hereafter used as the reference crown averaged C_{ab}). Figure 3.5 shows how different LA_T estimating methods yielded different crown averaged C_{ab} values. Methods II, V and VI, which estimated LA_T similar to our geometrical model (method I) produced crown averaged C_{ab} within the similar range (33 – 53 µg cm^{-2}). Methods III and IV, which underestimated LA_T, overestimated crown averaged C_{ab} up to 1.5 times. For illustration purposes we also show that the crown averaged C_{ab} normalized by LA_P is about 50% higher than C_{ab} normalized by LA_T (cf. the first and the last box of Figure 3.5).

The small case study with the theoretical CF, which varied between two and four with steps of 0.2, demonstrated how crown averaged C_{ab} content is sensitive to potentially biased LA_T estimates. Crown averaged chlorophyll content was exponentially increasing with decreasing theoretical CF (Figure 3.6b). The smallest RMSE (Eq. 3.8) between the reference crown averaged C_{ab} and C_{ab} estimated using

the theoretical CF was found for the value equal to 3.0 (Figure 3.6a). The smallest RMSE agreed well with the mean measured conversion factor for the immature (CF = 3.2) and the mature (CF = 3.1) spruce crowns. Large errors up to 25 µg cm^{-2} in crown averaged C_{ab} were observed for the lower values of the theoretical CF (closer to flat needles). A bias of 0.2 from the true conversion factor introduced an error of 2 – 3 µg cm^{-2} in crown averaged C_{ab} estimates.

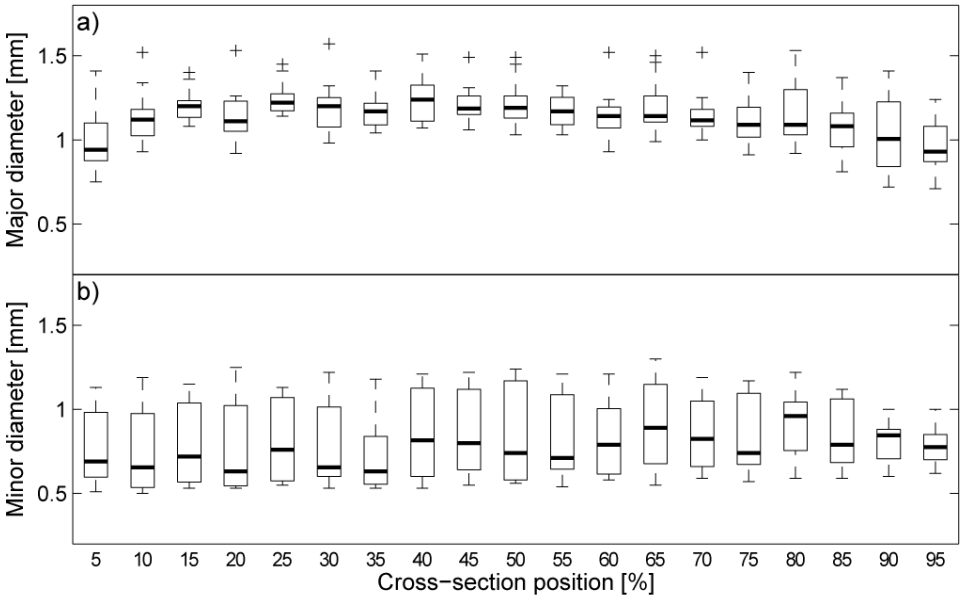

Figure 3.3 Changes on needle cross-section major diameter (a) and minor diameter (b) along the needle length. The position of needle cross-section (x-axis) is expressed in relative units, where 0% refers to the needle base and 100% to the needle top. Legend: central line in a box represents median, box height represents 50% of the data (interquartile range), whiskers represent the minimum and the maximum values, and crosses represent outliers (when an observed values exceeded 1.5 times the interquartile range).

3.4 Discussion

3.4.1 Accuracy of LA_T estimating methods

Modeling a spruce needle using our new geometrical model (method I), parallelepipeds as a proxy of needle sides (method II), or parallelepipeds with half-elliptic tapering (method V) resulted in LA_T estimates closely comparable with the true reference $\overline{LA_T}$ (Figure 3.2). Only methods I and II estimated LA_T of a single needle with relative RMSE less than 5% of the average LA_T. According to study of Frey (as cited in Niinemets (1997)), method II systematically underestimated real Norway spruce LA_T by 5 – 8%, but we did not observe any systematic

underestimation. Contrary to the accurate LA_T estimates by methods I and II, method III (needle sides modeled as an ellipse) and method IV (a needle modeled as an ellipsoid) systematically underestimated needle LA_T by 23% and 60%, respectively. Similar result was reported by Sellin (2000), who modeled a needle shape as an ellipse, which underestimated spruce needle LA_P by up to 20%. Our results suggest that an elliptic approximation is not suitable for modeling Norway spruce needles, because it introduces unrealistic tapering starting already at the middle part of a needle. Analysis of needle cross-sections for computing the reference total leaf area ($\overline{LA_T}$) confirmed that the major and the minor cross-section diameters are nearly invariant for 75% of the needle length and only the major diameter decreases towards needles' ends (Figure 3.3). Thus modeling Norway spruce needle shape as suggest by methods I, II and IV seems to be more suitable for LA_T estimation.

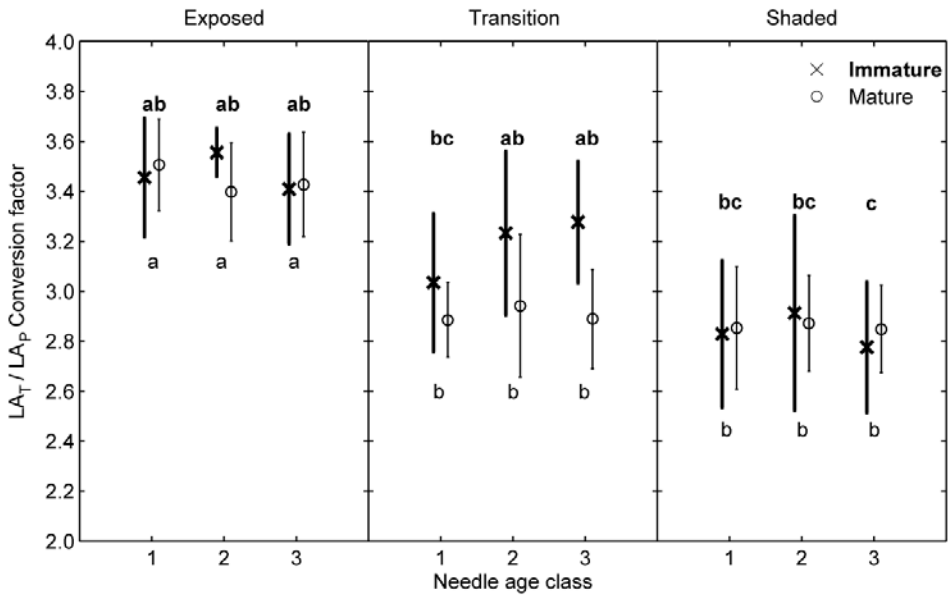

Figure 3.4 Total to projected leaf area conversion factor (CF) of two experimental Norway spruce stands, immature (×) and mature (○). The symbols represent mean values per needle category (combination of three needle age classes and three canopy vertical layers – sun exposed, transition and shaded). The whiskers represent the two-sided standard deviation. Equal letters above (immature stand) and bellow (mature stand) data points connect homogeneous groups within each forest stand, i.e. statistically insignificant differences between data groups at $p \leq 0.01$ (ANOVA, Tukey's post hoc test).

A reliable predictor of the total to projected leaf area CF seems to be the ratio between the middle cross-section perimeter and its diameter (R^2 = 0.73). The same approach uses method VI (Pokorný, 2002) to estimate LA_T from LA_P measurements, which was in reasonably good agreement with the reference $\overline{LA_T}$, as well as, with our geometrical model Method VI underestimated a single needle LA_T by less than 15%.

3.4.2 Variability of total to projected leaf area conversion factor for method I

The values of total to projected leaf area CF varied from 2.5 to 3.8 (Figure 3.4), which is in agreement with previously published CF values for various Norway spruce canopies. A CF between 2.3 and 3.1 (mean of 2.4) was observed for a 15-year-old experimental plantation in the Czech Republic (Pokorný, 2002), 2.3 – 3.7 (median around 2.5) was observed for current-year needles of 12 to 32-year-old trees in Germany (Niinemets, 1997), 3.0 – 3.3 (mean of 3.1) was observed for a 30-year-old forest in Estonia (Sellin, 2000), or slightly higher CF values in the range of 3.0 – 4.0 (mean of 3.6) were observed for current-year needles of a 40-year-old plantation in Northern Sweden (Stenberg et al., 1999). Our results showed, nevertheless, higher CF values than the average CF presented by Pokorný (2002), who studied the same immature Norway spruce stand in 1999. He reported an average CF of 2.6, whereas mean of our CF measurements was equal to 3.2. The discrepancy can be attributed to different methodologies and possibly also to higher light availability due to increasing canopy openness with the time induced by natural disturbances and managed thinning.

The majority of studies measuring the CF of Norway spruce were carried out on trees with an age less than 40 years and the results from those studies indicate that CF increases with increasing canopy age. In our study we sampled trees in their mature age (around 100 years old) and we found that the average CF was almost equal to the one measured in the 30-year-old spruce canopy. Our results indicated that CF values of entirely sun exposed and shaded needles were not significantly different in both stands. Some differences in CF were observed in the transition canopy vertical layer (Figure 3.4), which can be characterized by more variable irradiation conditions. The needles from the transition zone of the mature canopy tended to have CF similar to shaded needles. This indicates that the transition needles of the mature trees were actually sampled deeper in the canopy, i.e. from locations with less available light, than the transition needles of the immature stand. A more accurate physical based delineation of canopy sampling positions, e.g. using measurements of incident radiation, might solve this mismatch and assure inter-comparability of needle samples collected from different forest stands.

The decreasing trend of CF in the canopy vertical profile is attributed to the decreasing light availability in the lower parts of the canopy. Lower CF values together with more horizontally oriented foliage result in larger foliar surface, which helps trees to improve the light harvesting capacity of shaded branches. Similar trend

of decreasing CF with decreasing light availability has been reported for Central European Norway spruce by Niinemets (1997) and by Niinemets and Kull (1995), and for Silver fir dominated stands by Cescatti and Zorer (2003). Contrasting result, i.e. no trend between CF and light availability, was reported by Palmroth et al. (2002) for spruces growing in central Sweden. This independency can be attributed to the narrower crown habitus and typically more open canopies in higher latitudes, which ensure more equal distribution of light within the crown vertical profile. Furthermore, suppressed shade-tolerant Silver firs (Cescatti and Zorer, 2003) and shade-intolerant Scots pines (Niinemets, 2010) did not exhibit any clear trend either. This indicates that local ecological factors and tree social position plays important role in foliage adaptations towards varying irradiance intensities.

Finally, we did not observe significant differences in CF among three recent needle age classes, which is in agreement with results previously published by Sellin (2000).

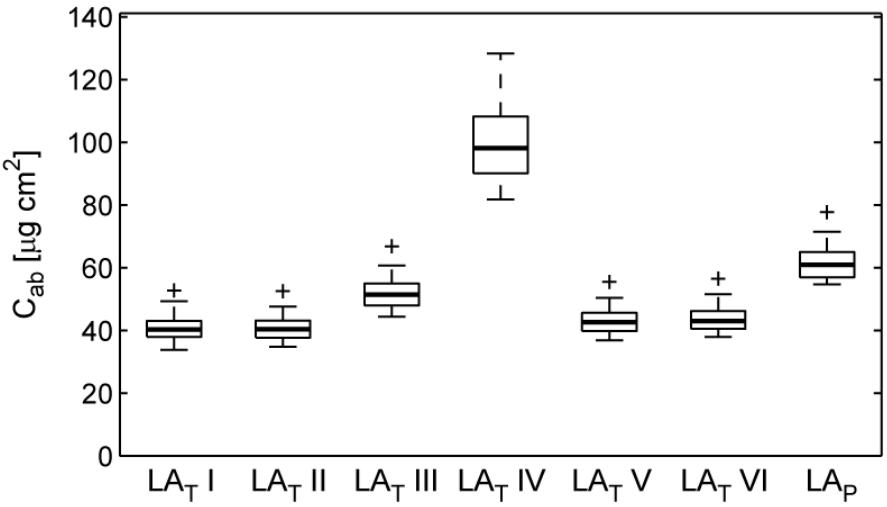

Figure 3.5 Summary statistics of crown averaged chlorophyll content for 30 Norway spruce trees. Six methods to estimate total leaf area (LA_T) and directly measured projected leaf area (LA_P) were used to express measured chlorophyll per leaf area. Detailed explanation of box plots can be found in the legend of Figure 3.3.

3.4.3 Impact of LAT on upscaling of foliar biochemistry from leaf to crown level

Leaf biochemical properties, such as chlorophyll and water, are in quantitative remote sensing studies often expressed per leaf area (Jacquemoud et al., 1996). Consequently, biochemical properties of non-flat spruce needles with a quadratic cross-section can significantly differ if being expressed against the projected or the total leaf area (Niinemets (2010) and Figure 3.5 in this study). As demonstrated in Figure 3.4, CF is decreasing with decreasing light availability inside the spruce canopies. Assuming a single, average CF value around 3.0 for the entire canopy profile, CF causes an overestimation of LA_T for shaded and an underestimation of LA_T for sun exposed needles. This error is further propagated into the measurements of biochemical content at the leaf level, as well as, into crown averaged values. Based on Figure 3.6a, erroneous estimation of the mean crown CF by 0.2 introduces already an error of 2 - 3 µg cm^{-2} in crown averaged chlorophyll content. Considering that observed range of crown averaged C_{ab} was only 20 µg cm^{-2} (i.e. it varied between 33 and 53 µg cm^{-2}), the error represents 10 - 15% of the observed range.
However, the variability of observed crown averaged C_{ab} was small as it can vary between 20 and 100 µg cm^{-2} (Malenovský et al., 2006b). The maximum RMSE due to erroneous estimation of the CF was up to 25 µg cm^{-2}. This error is even higher than the accuracy of common remote sensing methods estimating crown averaged chlorophyll content in coniferous canopies, which is usually around 10 µg cm^{-2} (Malenovský et al., 2006b; Moorthy et al., 2008; Zarco-Tejada et al., 2004).

Attention should be paid to methods of upscaling from the leaf biochemical properties to the crown or even canopy levels. In this study, we used simple averaging of leaf measurements, because it is the most frequent approach used in remote sensing studies investigating forest biochemical properties (Huber et al., 2008; Schlerf et al., 2010; Zarco-Tejada et al., 2004). Nevertheless, more sophisticated upscaling schemes, which would take into account real distribution of leaf biomass within the crown vertical profile, can likely provide more representative crown integrates. For example, Lukeš et al. (2009) combined the vertical distribution of leaf biomass and extinction of photosynthetically active radiation into a scaling scheme, which produced more realistic ground truth for validation of remotely sensed chlorophyll content of spruce crowns. Forthcoming upscaling studies should consider employing the rapidly developing methods of terrestrial and airborne laser scanning. Laser scanning enables mapping of 3D foliage distribution of individual tree crowns (van der Zande et al., 2006) and of complex forest stands (Morsdorf et al., 2010).

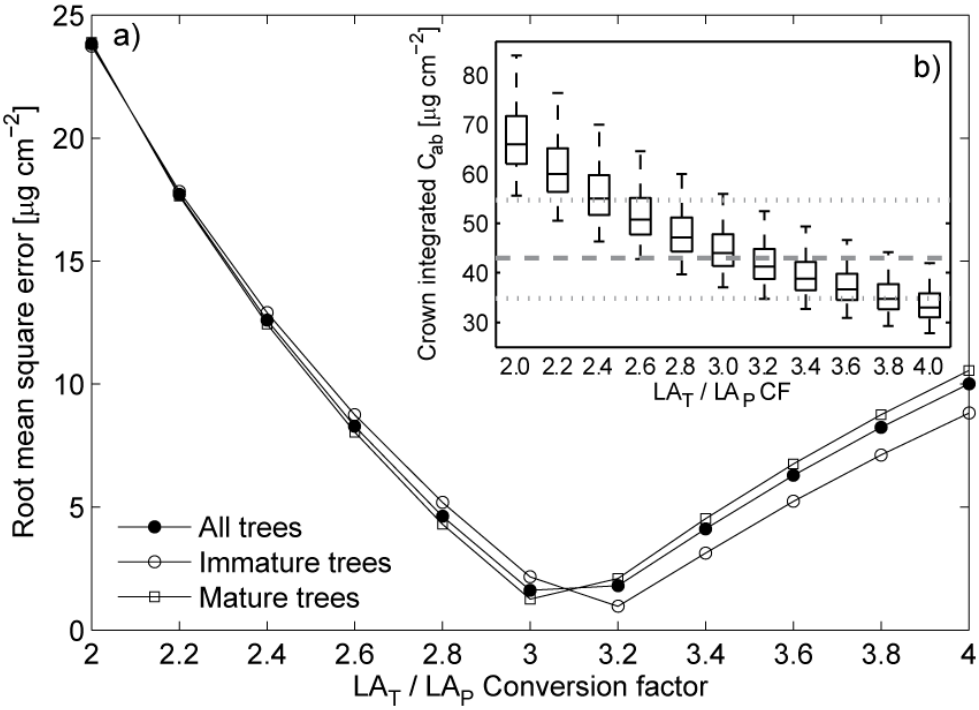

Figure 3.6 (a) RMSE (Eq. 3.8) between crown averaged leaf chlorophyll (C_{ab}) content normalized by LA_H calculated using sample specific CF (based on the LA_T estimating method I) and theoretical CF (i.e. single value for entire crown vertical profile, which varies between 2 and 4 with steps of 0.2). The mean RMSE values were calculated for 30 Norway spruce crowns (black dots), i.e. 10 immature (squares), and 20 mature (circles). The inserted figure (b) demonstrates how crown averaged C_{ab} decreases with increasing theoretical CF. The grey dashed line represents the median and the dotted grey lines indicate min. – max. range of the crown averaged content based on our LA_T estimating method I. Detailed explanation of box plots can be found in the legend of Figure 3.3.

3.5 Conclusions

Two out of six evaluated LA_T estimating methods, our newly proposed geometrical model based on three needle cross-sections (method I) and the parallelepiped model (method II), predicted Norway spruce needle LA_T with an error less than 5% of the average needle LA_T. Considering the overall feasibility of both methods, we can conclude that the parallelepiped model seems to be more suitable for an operational LA_T estimation in eco-physiology and applied remote sensing research, because it requires less inputs than the new geometrical model. Methods III and IV, which suggest an elliptic approximation of a needle shape, underestimated LA_T by up to 60%, and thus are not suitable for prediction of spruce needle LA_T. The conversion factor between total and projected leaf area (CF) was estimated with a reasonable

accuracy ($R^2 = 0.73$) using the ratio between the needle perimeter and the major diameter of a cross-section taken from the middle of a needle. CF varied from 2.5 (shaded needles) to 3.8 (sun exposed needles). The variability of CF was mainly driven by the position of needles in the vertical canopy profile, or in other words by the decreasing irradiation in the lower canopy layers. Influence of the needle and the stand age on the CF variability was insignificant. Therefore, for future in-situ measurements of CF we recommend sampling needles irrespective of their age (i.e. a mixed sample of several needle age classes), but taking into account several canopy vertical layers.

Since leaf area normalized biochemical properties (e.g. leaf chlorophyll and water content) of forest canopies can be estimated using the airborne and satellite imaging spectroscopy methods, representative and accurate in-situ measurements are required for calibration and validation of the remote sensing methods. We demonstrated that crown averaged chlorophyll (C_{ab}) content normalized by LA_P is about 50% higher than LA_T normalized C_{ab} content. Moreover, inaccurately estimated LA_T due to biased CF can introduce an error into crown averaged chlorophyll content reaching up to 25 µg cm^{-2}. If we consider a possible range of crown averaged C_{ab} between 20 and 100 µg cm^{-2}, the error can represent up to 30% of the total C_{ab} range, which can seriously affect the reliability of remote sensing methods.

Acknowledgements

This work has been supported by the ESA/PECS project no.98029, the Marie Curie research training network Hyper-I-Net (MRTN-CT-2006-035927), and Czech Science Foundation (No. 205/09/1989). We would like to thank Pavel Cudlín and František Havlíček for their assistance during the data collection, Stanislava Hasoňová for her outstanding patience with the needle cross-section cuts, Ivana Tomášková for her statistical advice, and Jan Clevers for language correction.

4

Retrieval of spruce leaf chlorophyll content from airborne image data using continuum removal and radiative transfer

This chapter is based on:

Malenovský Z, Homolová L, Zurita-Milla R, Lukeš P, Kaplan V, Hanuš J, Gastellu-Etchegorry J-P, Schaepman ME (2013) Retrieval of spruce chlorophyll content from airborne image data using continuum removal and radiative transfer.*
Remote Sensing of Environment 131: 85-102
DOI: http://dx.doi.org/10.1016/j.rse.2012.12.015

*Author's contribution to research design (10%), data collection (35%), analysis (25%) and writing (15%)

Abstract

We investigate combined continuum removal and radiative transfer (RT) modelling to retrieve leaf chlorophyll *a* and *b* content (C_{ab}) from the AISA Eagle airborne imaging spectrometer data of sub-meter (0.4 m) spatial resolution. Based on coupled PROSPECT-DART RT simulations of a Norway spruce (*Picea abies* (L.) Karst.) stand, we propose a new C_{ab} sensitive index located between 650 and 720 nm and termed $ANCB_{650–720}$. The performance of $ANCB_{650–720}$ was validated against ground-measured C_{ab} of ten spruce crowns and compared with C_{ab} estimated by a conventional artificial neural network (ANN) trained with continuum removed RT simulations and also by three previously published chlorophyll optical indices: normalized difference between reflectance at 925 and 710 nm ($ND_{925\&710}$), simple reflectance ratio between 750 and 710 nm ($SR_{750/710}$) and the ratio of TCARI/OSAVI indices. Although all retrieval methods produced visually comparable C_{ab} spatial patterns, the ground validation revealed that the $ANCB_{650–720}$ and ANN retrievals are more accurate than the other three chlorophyll indices (R^2 = 0.72 for both methods). $ANCB_{650–720}$ estimated C_{ab} with an RMSE = 2.27 μg cm^{-2} (relative RRMSE = 4.35%) and ANN with an RMSE = 2.18 μg cm^{-2} (RRMSE = 4.18%), while $SR_{750/710}$ with an RMSE = 4.16 μg cm^{-2} (RRMSE = 7.97%), $ND_{925\&710}$ with an RMSE = 9.07 μg cm^{-2} (RRMSE = 17.38%) and TCARI/OSAVI with an RMSE = 12.30 μg cm^{-2} (RRMSE = 23.56%). Also the systematic RMSE was lower than the unsystematic one only for the $ANCB_{650–720}$ and ANN retrievals. Our results indicate that the newly proposed index can provide the same accuracy as ANN except for C_{ab} values below 30 μg cm^{-2}, which are slightly overestimated (RMSE = 2.42 μg cm^{-2}). The computationally efficient $ANCB_{650–720}$ retrieval provides accurate high spatial resolution airborne C_{ab} maps, considerable as a suitable reference data for validating satellite-based C_{ab} products.

4.1 Introduction

Chlorophyll macromolecules are evolutionarily one of the most stable structures used by photosynthetically active organisms for light harvesting and energy transduction (Ustin et al., 2009). Therefore, they are playing an important role in the assimilation of carbon by green vegetation, accounting for 57 Gt of carbon per year (Normile, 2009). The total amount of chlorophyll pigments, which is reacting on surrounding environmental conditions and stress agents including anthropogenic pollutants (Buonasera et al., 2011), indicate the actual physiological status of plants (i.e. their current health and/or phenological states).

Chlorophyll molecules (mainly *a*, *b*, but also *c*, *d*, and *f*) demonstrate a strong spectral absorption in the blue and red part of the electromagnetic spectrum (Chen et al., 2010a). These absorption features allow space-borne mapping of vegetation chlorophyll *a* and *b* content (C_{ab}) from high spectral resolution data acquired by spectrometers (Harris and Dash, 2010). A challenging task is, however, to validate the accuracy of satellite maps that are derived at broad spatial resolutions ranging from tens to hundreds of meters (Dash et al., 2010; Stagakis et al., 2010). Although C_{ab} is relatively stable during the high vegetation season, it changes rapidly at the beginning and at the end of the season. Therefore, traditional ground based validation of satellite maps is not only time consuming and expensive, but also potentially inaccurate due to the need of collecting many chlorophyll samples in a relatively short time. An alternative solution for spatial validation of satellite products might be the use of high spatial resolution chlorophyll maps retrieved from airborne imaging spectrometers (Moorthy et al., 2008; Zarco-Tejada et al., 2004; Zhang et al., 2008).

High spatial resolution mapping of forest C_{ab} needs to account for the spatially heterogeneous structure of the forest environment (Verrelst et al., 2010). The hierarchical canopy architecture, resulting from foliage clumping at several spatial scales (Písek et al., 2011; Smolander and Stenberg, 2003; Stenberg, 1996), and the presence of various non-photosynthetic scatterers (e.g. branches and trunks) induces strong reflectance anisotropy and high spatial variability (Malenovský et al., 2008). The confounding influence of forest structure on imaging spectrometer-based retrievals of foliar biochemistry can be minimized by combining a continuum removal method (Clark and Roush, 1984) with vegetation canopy radiative transfer (RT) modelling (Myneni, 1991).

The reflectance continuum removal transformation enhances and standardizes specific absorption features of the foliar biochemical constituents (Broge and Leblanc, 2001), in our case chlorophylls. Kokaly and Clark (1999) used normalized band depths calculated from specific continuum-removed (CR) absorption features of leaf reflectance to estimate concentrations of nitrogen, lignin, and cellulose. Curran et al. (2001) refined this methodology and employed CR band depths normalized to

i) the band depth at the centre of the absorption feature (abbreviated BNC) or ii) the area of the absorption feature (abbreviated BNA) to estimate C_{ab}. Underwood et al. (2003) used the CR technique for mapping invasive plant species, Kokaly et al. (2003) for discriminating different vegetation types in the Yellowstone National Park, and Schmidt and Skidmore (2003) for differentiating saltmarsh vegetation types. More recently, the CR based methods have been successfully applied to map subgenera of two Australian Eucalyptuses (Youngentob et al., 2011), or to quantify grass forage nutrients of an African savanna (Knox et al., 2011).

Three-dimensional (3D) RT models simulate photon interactions with objects within the solar reflective and/or emissive part of the electromagnetic spectrum (Kimes and Kirchner, 1982; Myneni et al., 1992). Radiative transfer of complex natural and urban landscapes is modelled using various computing techniques such as ray tracing or discrete ordinate methods (Disney et al., 2000; Gastellu-Etchegorry et al., 2004). Several 3D models were designed with an intention to simulate physically RT within forest environments of high structural complexity (Disney et al., 2006; Schaepman et al., 2009; Widlowski et al., 2006; Widlowski et al., 2008). This ability makes them ideal to develop methods that can separate and suppress the confounding influence of forest structure on estimates of foliar biochemistry (Zarco-Tejada et al., 2001).

Several previously published studies have introduced a concept of estimating C_{ab} from airborne high spatial resolution imaging spectroscopy data with optical indices upscaled from leaf to canopy level using vegetation radiative transfer modelling (Haboudane et al., 2002; le Maire et al., 2008; Moorthy et al., 2008; Zhang et al., 2008). Following this concept, the objective of our study is to investigate the potential use of continuum removal transformation for quantitative C_{ab} mapping from airborne data of sub-meter spatial resolution. For this purpose, we use reflectance spectra of Norway spruce (*Picea abies* (L.) Karst.) crowns simulated using a coupled PROSPECT-DART leaf-canopy RT model and we propose a new continuum removal based optical index termed $ANCB_{650–720}$.

4.2 Material and methods

As this study exploits several interconnected remote sensing / ground observations, laboratory analyses, and computationally intensive methods, we first describe a general synopsis of principal methodological steps shown in Figure 4.1. In-situ measurements collected during a ground/flight campaign were used: i) to process spectral images acquired with an airborne imaging spectrometer, ii) to parameterize PROSPECT-DART radiative transfer modelling, and also iii) to produce the validation dataset (ground truth) for ten sampled spruce trees. The spectral bands simulated by the DART model allowed us to establish a statistical relationship between C_{ab} and four C_{ab} sensitive optical indices, i.e. a new optical index named

Area under continuum-removed curve Normalized to the Chlorophyll absorption Band depth between 650 and 720 nm ($ANCB_{650–720}$) and three published indices: Normalized Difference between reflectance at 925 and 710 nm - $ND_{925\&710}$ (le Maire et al., 2008), Simple reflectance Ratio between 750 and 710 nm - $SR_{750/710}$ (Zarco-Tejada et al., 2004) and TCARI/OSAVI ratio (Haboudane et al., 2002). The RT simulations were also used to train a C_{ab} estimating artificial neural network (ANN) (Bacour et al., 2006; Combal et al., 2003). C_{ab} of sunlit parts of Norway spruce crowns were estimated from geocoded, radiometrically and atmospherically corrected airborne spectral images of an AISA Eagle spectrometer by applying the following methods: i) the statistical relationships established between C_{ab} and the optical indices and ii) the properly trained ANN. The ANN results are cross-compared with estimates of the optical indices, including the newly proposed $ANCB_{650–720}$ index. Finally, the accuracy of the C_{ab} retrievals is validated with ground (laboratory) measured C_{ab}, extracted from needle samples of ten spruce tree crowns. The following subsections are further describing each methodological step illustrated in Figure 4.1.

4.2.1 Experimental test site

A Norway spruce monoculture located nearby the permanent experimental ecophysiological research station Bílý Kříž in the Moravian-Silesian Beskydy Mountains (eastern part of the Czech Republic; 18.54°E, 49.50°N, altitude 936 m above sea level) was chosen as test site of this study. In 2004 the regularly spaced 26-year-old spruce stand had a canopy height between 10 and 12 m, an average diameter at breast height (DBH) of about 13 cm and a leaf area index (LAI) ranging between 7 and 9 $m^2 m^{-2}$. The Norway spruce monoculture was subject of an intensive ground investigation characterizing spatially canopy structure, optical properties of leaves and other canopy elements, and foliar biochemistry including C_{ab}. Detailed abiotic and biotic characteristics of the Bílý Kříž study site and all ground measurement methods are described in Malenovský et al. (2008).

4.2.2 Processing and classification of the airborne AISA Eagle spectral images

Imaging spectroscopy data of the Bílý Kříž experimental stand was acquired under clear sky conditions by a pushbroom VNIR Airborne Imaging Spectroradiometer (AISA) Eagle (Spectral Imaging, Specim Ltd., Finland) on September 18th 2004 (around solar noon). The acquired digital numbers of 64 spectral bands between 398.39 and 983.06 nm (spectral sampling distance of about 10 nm) were transformed into radiance values using the sensor specific calibration equations in the CaliGeo software (Spectral Imaging, Specim Ltd., Finland). An empirical line atmospheric correction (Smith and Milton, 1999) and nadir image normalization was carried out using ground-measured spectra of five fabricated Lambertian calibration panels in the ATCOR-4 software (Richter and Schlapfer, 2002). The atmospherically corrected

AISA Eagle images of 0.4 m spatial resolution were then geo-orthorectified into the Universal Transverse Mercator (UTM) geographic projection (zone 34 North) using a digital elevation model of 2 m vertical resolution (0.4 m horizontal spatial resolution) and the aircraft positional data recorded by the Aerocontrol IIB inertial navigation system (Ingenieur-Gesellschaft für Interfaces, IGI GmbH, Germany). A detailed description of the radiometric, atmospheric, and geometric corrections and also the accuracy of the resulting AISA Eagle hemispherical directional reflectance function (HDRF; Schaepman-Strub et al., 2006) assessed from clay bare soil, gravel road, and grass canopy spectral measurements, is available in Malenovský et al. (2008).

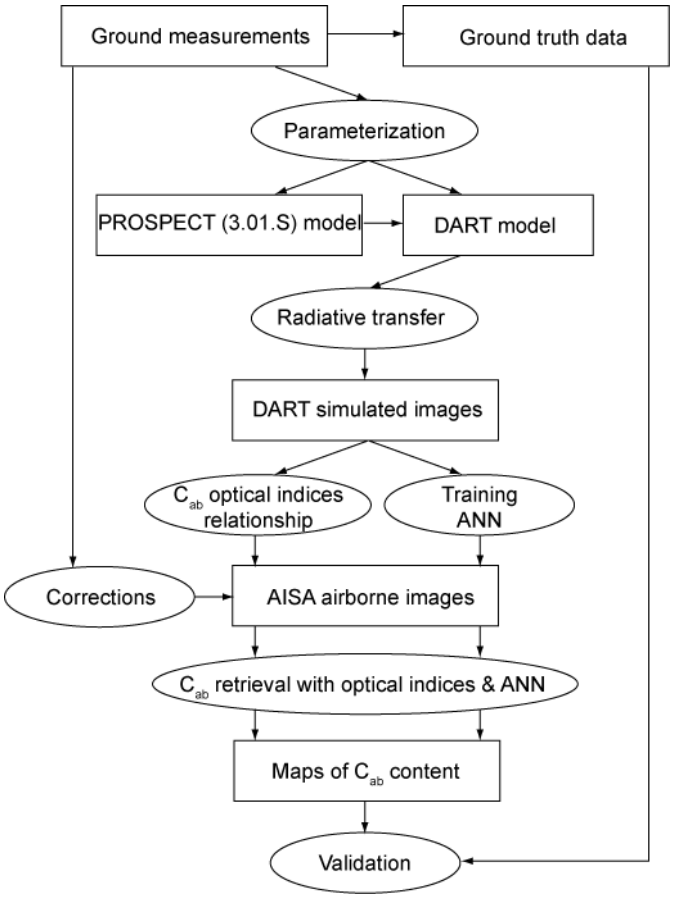

Figure 4.1 Basic methodological steps of the study. Rectangular objects represent the input/output data or models, while ellipsoidal objects represent the data processing and other operations (C_{ab} – leaf chlorophyll *a* and *b* content, ANN – artificial neural network, AISA – airborne imaging spectroradiometer).

A subset of approximately 200 by 320 m, covering the extent of the experimental forest stand, was extracted from the AISA Eagle image mosaic. The 0.4 m spatial resolution of AISA imagery allowed the identification of individual tree crowns and differentiation of their sunlit and shaded parts using a supervised maximum likelihood classification (ENVI software; ITT Visual Information Solutions) (Figure 4.2). Three optical indices sensitive to the vegetation structure (LAI): i) Normalized Difference Vegetation Index NDVI = $(R_{775} - R_{680})/(R_{775} + R_{680})$ (Tucker, 1979), ii) Weighted Difference Vegetation Index WDVI = $R_{755} - 1.376 \times R_{680}$ (Clevers, 1989), and iii) Simple Ratio SR = R_{775}/R_{708} (Jordan, 1969) were computed and added to the original set of AISA spectral bands to enhance spectral differences between the ground with understory and the spruce crowns. The AISA Eagle image was at first classified into five spectrally distinguishable classes: i) sunlit tree crowns, ii) shaded tree crowns, iii) sunlit ground and understory, iv) shaded bare ground, and v) shaded understory vegetation. In the second step, a local majority filter with a moving window of 3×3 pixels was applied to remove the single misclassified pixels. Finally, classes iii), iv) and v) were merged into a general class of 'background' (Figure 4.2). Five hundred validation pixels were randomly selected from nine digitized regions of interests that were evenly distributed over the forest site for an accuracy assessment purpose. Each selected pixel was visually assigned to one of the three classes and used to compute the classification confusion error matrix. An overall maximum likelihood classification accuracy of 92% (producer accuracies from 90% to 98% and user accuracies from 82% to 96%) with a Kappa coefficient of 0.864 was achieved. Similarly to Zarco-Tejada et al. (2004), we selected only sunlit crown pixels (classification accuracy of 96%) to be used in the subsequent C_{ab} estimation. The motivation for using just sunlit pixels is to include only remotely sensed HDRF of a high intensity that possess a high signal-to-noise ratio. The mean HDRF of AISA shaded crown pixels gaining about half intensity of the sunlit crown HDRF signal (Figure 4.3) is likely to result in a lower C_{ab} accuracy.

4.2.3 Reflectance continuum removal and selection of the suitable spectral range

The purpose of the reflectance continuum removal transformation is to enhance and standardize the specific absorption features of the biochemical constituents (Kokaly and Clark, 1999). To achieve this, the CR spectral interval must contain wavelengths that are most sensitive to the concentration changes of the particular biochemical absorbent. Proper location and width (i.e. starting and ending wavelength) of the CR part of spectra is, therefore, crucial for the quantification of the retrieved biochemical compounds. Figure 4.4 shows the mean C_{ab} specific absorption coefficients (k_{ab}) of the PROSPECT radiative transfer model for Norway spruce needles (Malenovský et al., 2006a) with a distinct absorption feature between 550 and 750 nm caused by the electron transition of the photosynthetic processes (Curran, 1989). According to

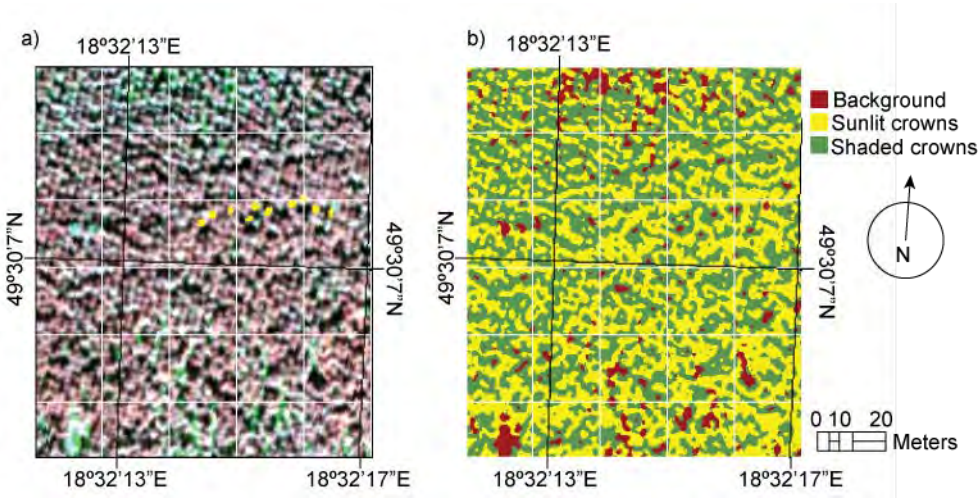

Figure 4.2 AISA Eagle image subset of Norway spruce forest stand at the research site Bílý Kříž (a) (yellow polygons indicate the locations of the sunlit tree crowns selected for ground truth sampling) and the maximum likelihood automatic classification separating sunlit and shaded crowns from the background (b).

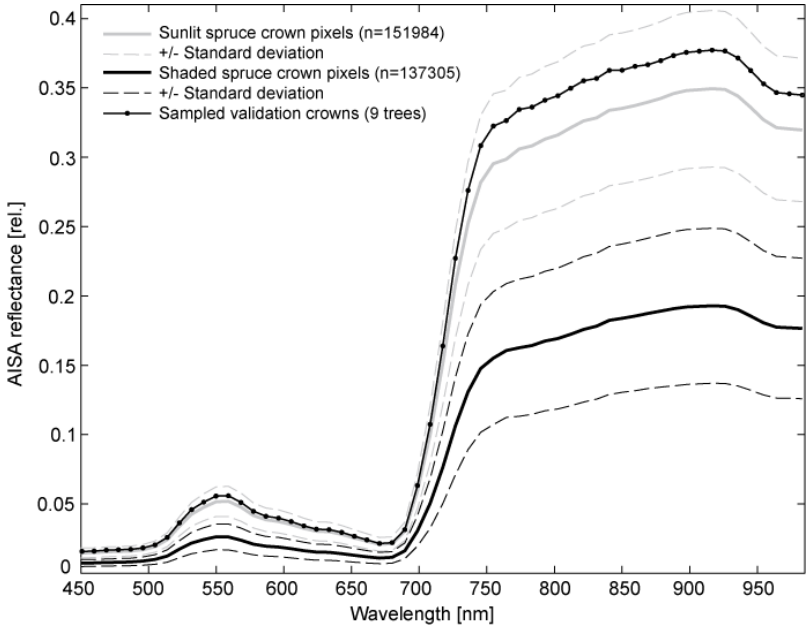

Figure 4.3 The mean top-of-the-canopy reflectance factor of 60 AISA Eagle spectral bands for all pixels classified as sunlit and shaded spruce crowns (n = 151984 and 137305, respectively).

Gitelson et al. (1996), the red edge wavelengths most sensitive to C_{ab} are located between 690 and 710 nm. The C_{ab} absorption is strongly influencing the shorter wavelengths of the red edge region, while the longer wavelengths are driven by canopy structural characteristics like leaf area index (LAI) and leaf angle distribution (LAD) (Liu et al., 2004). To include the most sensitive C_{ab} absorption wavelengths and to avoid in the same time negative interferences of the canopy structure, we decided to start the continuum removal interval in the middle of the red chlorophyll absorption feature (550 – 750 nm), i.e. at the wavelength of 650 nm, and to end it in the middle of the red edge region between 680 and 760 nm, i.e. at the wavelength of 720 nm (see Figure 4.4). The forest RT modelling (Section 4.2.4) was, therefore, restricted to simulate only the AISA Eagle spectral bands located in the spectral region between 650 and 720 nm.

4.2.4 PROSPECT-DART radiative transfer modelling

The leaf optical properties were simulated using the PROSPECT leaf RT model (version 3) (Jacquemoud and Baret, 1990), adjusted for Norway spruce needles by Malenovský et al. (2006a).They were upscaled to the level of forest canopy with Discrete Anisotropic Radiative Transfer DART (Gastellu-Etchegorry et al., 1996); a 3D RT model developed in CESBIO (Center for the Study of the Biosphere from Space, UPS-CNRS-CNES-IRD, France). A detailed description of specific DART functions and input parameters required to perform an ecologically sound 3D radiative transfer of a representative Norway spruce stand is provided in Malenovský et al. (2008). Herein we summarize only the most important aspects of our RT modelling that resulted in a database of simulated airborne spectral images. We subsequently use the term Look-Up-Table (LUT) for these simulated data.

Input parameters of our RT modelling were derived from the in-situ measurements collected at the Bílý Kříž test site during a join flight/field campaign in 2004 and destructive tree sampling performed in the previous years (Pokorný and Marek, 2000). Table 4.1 summarizes the key fixed and varied input parameters required to build a representative virtual 3D spruce forest stand. The number of tree crowns in a simulated scene varied according to the desired canopy cover (CC) of two predefined tree distributions as follows: i) four (CC= 75%), five (CC =85%), and six (CC =95%) trees in case of a regular tree distribution, and ii) five (CC=75%), six (CC=85%), and seven (CC=95%) trees in case of an irregular (clumped) tree distribution. Also, the LAI of the simulated stands was kept as a free variable, varying in accordance with ground measurements between 4 and 9 $m^2\ m^{-2}$ with a step of 1 $m^2\ m^{-2}$. Crowns with heights from 9 to 11 meters were constructed out of 11 horizontal levels of foliage turbid cells, characterized by the specific leaf average angle ranging from 25° to 40°. The vertical and horizontal foliage distributions within a crown, the trunk parameters, geometry of branches of the first order, and the distribution of fine woody twigs were adjusted according to destructive in-situ

measurements (for detailed description see Malenovský et al. (2008)). The forest stand background, covering a continuous slope of 13.5°, was modelled as a mixture of bare soil and senescent needle litter.

The directional-hemispherical optical properties of the scene surfaces (i.e. bark of trunks and branches, forest litter and soil) were defined in DART as being of a Lambertian nature. Several samples of these surfaces were collected during fieldwork and their reflectance was measured in laboratory using an optical integrating sphere Li-1800-12 (Li-Cor, Inc., USA) coupled with a FieldSpec PRO spectroradiometer (ASD, Inc., USA) according to the standard Li-Cor sphere measurement protocol. The optical properties (i.e. directional-hemispherical reflectance and transmittance) of the three spruce needle age-classes: i) needles of the current growing season (C), ii) needles of the previous growing season (C+1), and iii) needles older than the previous growing season (C++) were also measured in the Li-1800-12 integrating sphere according to the protocol developed and described in Malenovský et al. (2006a). These measurements were used to adjust the PROSPECT model for three age-classes of sunlit and shaded spruce needles (Malenovský et al., 2006a) and consequently used to retrieve the PROSPECT mesophyll structure parameter ~ N (Table 4.2) according to the method described in Jacquemoud et al. (1996). Needle optical properties entering the DART simulations were obtained from the adjusted PROSPECT model parameterized with the inputs summarized in Table 4.2. The retrieved variable of interest (C_{ab}) was kept free, ranging between the lowest (10 μg cm^{-2}) and the highest (100 μg cm^{-2}) value with an increment of 10 μg cm^{-2}, while leaf mass per area ~ C_m, water content ~ C_w and optical structural parameter N were fixed based on the needle sample laboratory measurements. Further details on leaf biochemistry measurements are provided in Section 4.2.6.

All combinations of free PROSPECT-DART input parameters (i.e. two tree distributions, three CC, six LAIs, and ten C_{ab} values) resulted in 360 simulations of Bidirectional Reflectance Factor (BRF) images containing eight AISA Eagle spectral bands between 650 and 720 nm (Table 4.1). Since the DART discrete ordinate RT simulations were performed without specifying the atmosphere between the stand canopy and the airborne sensor, the resulting top of canopy BRF values are comparable with the atmospherically corrected AISA Eagle spruce canopy reflectance images. The maximum likelihood classification method was applied once again on the PROSPECT-DART simulated spectral images to separate sunlit crown parts from shaded and from forest background pixels. After that, the BRFs of sunlit crown pixels of each simulated scene were averaged, continuum-removed, and stored together with the corresponding RT input parameters in the LUT.

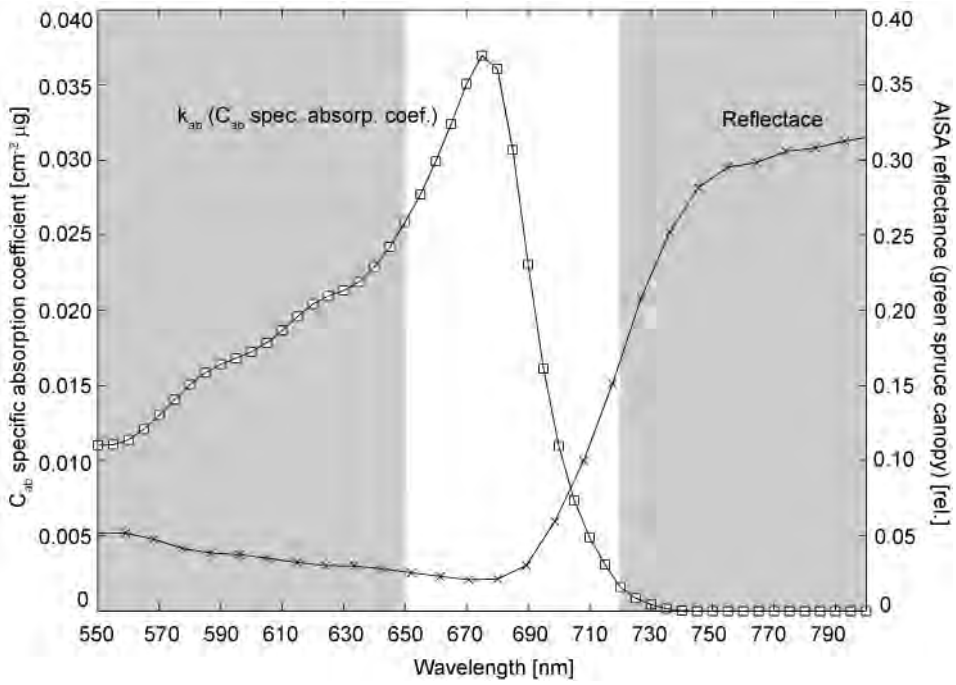

Figure 4.4 Selection of the spectral interval for continuum removal of chlorophyll sensitive wavelengths: start of the continuum at 650 nm (in the middle of the chlorophyll *a* and *b* (C_{ab}) specific absorption feature from 550 to 750 nm) and end of the continuum at 720 nm (in the middle of the red edge reflectance from 680 to 760 nm).

Table 4.1 Fixed and varied key input parameters for DART radiative transfer simulations of a Norway spruce scene.

Sun position of real solar noon (fixed)			
Zenith angle	θ_s	[°]	47.8
Azimuth angle (from North clockwise)	Φ_s	[°]	183.4
Scene parameters representing a 25-year-old Norway spruce forest stand			
Voxel size (fixed)		[m]	0.2
Horizontal dimensions (fixed)	x, y	[m]	6.0, 6.0
Slope (fixed)		[°]	13.5
Number of tree crowns (varied)			4-7
Canopy closure (varied)	CC	[%]	75-95 /in steps of 10/
Leaf area index (varied)	LAI	[m^2 m^{-2}]	4.0-9.0 /in steps of 1.0/
Simulated AISA Eagle spectral bands with Full-width-half-maximum – FWHM = 10 nm			
Central wavelengths of visible (VIS) bands (fixed)	λ_{VIS}	[nm]	652.1, 661.4, 670.7, 680.1, 689.4
Central wavelengths of near infrared (NIR) bands (fixed)	λ_{NIR}	[nm]	698.7, 708.1, 717.4

Table 4.2 Fixed input parameters for PROSPECT radiative transfer simulations of Norway spruce needle optical properties (C_w ~ leaf water column, C_m ~ leaf mass per area, N ~ leaf mesophyll structural parameter, C ~ needles of the current growing season, C+1 ~ needles of the previous growing season, and C++ ~ needles older than the previous growing season).

PROSPECT parameters	C_w	C_m	N
Needle types	[cm]	[g cm^{-2}]	[-]
Sunlit C	0.0475	0.0177	2.08
Sunlit C+1	0.0486	0.0206	2.08
Sunlit C++	0.0365	0.0233	2.08
Shaded C	0.0479	0.0118	2.02
Shaded C+1	0.0430	0.0172	2.02
Shaded C++	0.0461	0.0170	2.02

4.2.5 Retrieval of leaf chlorophyll content using optical indices and artificial neural network

We implemented and cross-compared five retrieval approaches estimating forest canopy C_{ab} from the airborne spectral AISA Eagle images using the PROSPECT-DART simulated LUT. The first approach employed the newly designed optical index $ANCB_{650–720}$, defined as the Area Under Curve of CR reflectance between 650 and 720 nm ($AUC_{650–720}$) normalized by the CR Band Depth at 670 nm (CBD_{670}). The $AUC_{650–720}$ was calculated according to the following equation:

$$AUC_{650-720} = \frac{1}{2}\sum_{j=1}^{n-1}(\lambda_{j+1} - \lambda_j)(\rho_{j+1} - \rho_j) \quad (4.1)$$

where ρ_j and ρ_{j+1} are values of the CR reflectance at the *j* and *j+1* bands, λ_j and λ_{j+1} are wavelengths of the *j* and *j+1* bands, and *n* is the number of used spectral bands. The results of three C_{ab} sensitive optical indices that have been used in the RT upscaling scheme in previous studies were additionally analyzed and compared with the $ANCB_{650–720}$ outcomes. The Normalized Difference optical index ($ND_{925\&710}$), computed between reflectance at 925 (ρ_{925}) and 710 (ρ_{710}) nm as:

$$ND_{925\&710} = (\rho_{925} - \rho_{710}) / (\rho_{925} + \rho_{710}), \quad (4.2)$$

was recommended as the best performing index for the C_{ab} retrieval of small broadleaf canopies from Hyperion satellite data by le Maire et al. (2008).

The Simple reflectance Ratio index ($SR_{750/710}$), computed as the red edge spectral transform:

$$SR_{750/710} = \rho_{750} / \rho_{710}, \quad (4.3)$$

where ρ_{750} and ρ_{710} is reflectance at 750 and 710 nm, respectively, was upscaled for C_{ab} estimation of Jack pine (*Pinus banksiana* Lamb.) stands using the PROSPECT and SPRINT RT models by Zarco-Tejada et al. (2004). Finally, Haboudane et al. (2002) proposed the ratio of TCARI and OSAVI optical indices as a LAI and soil background independent C_{ab} proxy for agricultural crops. The index is computed as the ratio of:

$$TCARI = 3[(\rho_{700} - \rho_{670}) - 0.2(\rho_{700} - \rho_{550})(\rho_{700} / \rho_{670})] \quad (4.4)$$

and

$$OSAVI = 1.16(\rho_{800} - \rho_{670})/(\rho_{800} - \rho_{670} + 0.16), \quad (4.5)$$

where ρ_{550}, ρ_{670}, ρ_{700} and ρ_{800} are the reflectance values at 550, 670, 700 and 800 nm. Recently, Zhang et al. (2008) applied TCARI/OSAVI upscaled by the PROSPECT and 4-SCALE RT models on Compact Airborne Spectrographic Imager (CASI) data to map C_{ab} of Black spruce (*Picea mariana* Mill.) stands in Canada. All four optical indices were computed for each PROSPECT-DART simulation and stored in our LUT. The empirical functions describing the closest relationship between the index values and the simulated C_{ab} were fitted in the PeakFit software package (Systat Software, Inc., USA). The best fitting equations (with the highest coefficient of determination R^2, significant at a given probability level *p*) were then applied per-pixel to the AISA Eagle imagery to estimate C_{ab} of the sunlit crown pixels.

Apart from optical indices, the ANN based retrieval approach has been successfully employed in LUT inversions of RT models (Bacour et al., 2006; Combal et al., 2003). Therefore, we decided to cross-compare the results of the optical indices with estimates from the computationally different ANN approach. After testing several ANN architectures in the MATLAB neural network toolbox (The MathWorks, Inc., USA), we chose a two-layer feed-forward back-propagation ANN. The first (input) layer was composed out of six neurons corresponding to the six simulated CR AISA Eagle wavebands and associated with a tan-sigmoidal transfer

function. A linear transfer function was assigned to the second (output) layer that contained only one neuron producing the C_{ab} estimate. Half of the PROSPECT-DART simulated LUT entries were randomly selected to train the predefined ANN. To avoid a scaling factor problem (each wavelength has a typical range of values) and to increase the convergence performance of the training procedure, the ANN inputs and outputs were standardized. Each input/output had a mean value of zero and standard deviation of one. The high-speed processing Levenberg–Marquardt optimization algorithm was applied for the network training. To prevent a potential over-training, an early stopping technique was implemented using a quarter of the randomly selected PROSPECT-DART LUT entries. Finally, the performance of the ANN was tested with the remaining quarter of the LUT entries. In particular, the root mean square error (RMSE) and the coefficient of determination R^2 were computed to test the ANN performance. The best performing ANN (i.e. not over-fitted and with the lowest possible RMSE and an R^2 close to one) was employed to retrieve C_{ab} from the AISA Eagle sunlit crown pixels.

To investigate the relationship of $ANCB_{650–720}$ and the three other optical indices with C_{ab} also in a case of broadleaf canopies, we performed additional PROSPECT-DART simulations for a virtual 1D homogeneous turbid medium of grassland and for a structurally more complex 3D canopy of a deciduous forest stand. The methodology and results of this RT exercise are provided in Appendix A3. In Appendix A4 we demonstrate differences in the statistical dependency of $ANCB_{650–720}$ on C_{ab} when established for sunlit or shaded pixels of Norway spruce crowns by RT models.

Table 4.3 Relative weights for sun-exposed and shaded crown parts per needle age-class used to compute the single mean leaf chlorophyll a & b content of sampled Norway spruce crown. (C ~ needles of the current growing season, C+1 ~ needles of the previous growing season, and C++ ~ needles older than the previous growing season).

Branch	Sun-exposed	Shaded
Age-class	[rel]	[rel.]
C	0.230	0.057
C+1	0.224	0.089
C++	0.095	0.306

4.2.6 Validation of leaf chlorophyll content estimates using ground truth measurements

Ten individual spruce trees were randomly selected in a transect crossing the experimental forest stand from East to West for the validation of the airborne C_{ab} maps (Figure 4.2a). The sampled crowns were localized with a decimeter accuracy using a DGPS device combined with the Field-Map system composed of laser telemeter, digital compass, and forest ecosystem mapping software (Institute of Forest Ecosystem Research, IFER Ltd., Czech Republic). Sampling took place in five days following the AISA Eagle acquisition date. Shoots of the three most recent age-classes were collected from a sun-exposed branch of the 3rd whorl (counted from top of the crown) and from a shaded branch (below 10th whorl) of each crown. Depending on their size, approximately twenty needles were randomly detached from each sampled shoot. Half of them were fresh-weighted, and scanned for a later calculation of their leaf hemisurface area according to the method described by Homolová et al. (2013a). The second half was frozen in liquid nitrogen, closed in a cooled dark container, and transported to the laboratory for a destructive C_{ab} analysis.

The laboratory C_{ab} measurements were carried out according to the standardized protocol established and verified in previous studies (Lhotáková et al., 2007; Malenovský et al., 2006a). On average, 0.5 g of the sampled frozen needles were bleached in 10 ml dimethylformamide (DMF), while keeping them in the dark and at 8° C for five consecutive days (Porra et al., 1989). The absorbance of the extracts was measured at wavelengths of 480, 647, and 664 nm using the Unicam Helios α spectrophotometer (Unicam Ltd., Cambridge, UK). A complementary needle sample was oven dried at 60° C for 48 hours and weighted to obtain the sample dry matter content. Leaf chlorophyll a & b concentrations in mg g^{-1} of dry matter were calculated according to the equations of Wellburn (1994). They were transformed in µg cm^{-2} using the measured specific leaf area (SLA), defined as the ratio of the hemisurface leaf area [cm^2] to the sample dry matter weight [g], according to Homolová et al. (2013a).

The crown representative C_{ab} value was computed as a weighted average of six needle samples (i.e. more than 10 needles of three age-classes collected from the 3rd and below the 10th whorl). Two types of measurements were collected to determine the weights: i) the biomass of each needle age-class within the vertical crown profile (i.e. percentage of the total age-class specific needle area per vertical crown level measured destructively in 2007 from six branches) and ii) the light extinction within the vertical crown profile measured with a CANFIB optical system (Global Change Research Centre AS CR, Czech Republic (Urban et al., 2007)). CANFIB consists of several light diffusers installed within a vertical crown profile and measuring the total incoming photosynthetically active radiation (PAR ~ radiation between 400 and 700 nm). The acquired relative PAR measurements expressing a fraction of the above canopy PAR per monitored crown level were coupled with the needle age-class

biomass of each sampled branch to create the average weights of each branch type and needle age-class (Table 4.3). Finally, the sampled trees were identified in the AISA Eagle image using their GPS locations. Their sunlit crown parts (between 15 and 25 pixels representing an area of 2.4–4.0 m^2 each) were manually selected (see their mean AISA HDRF in Figure 4.3) and their corresponding retrieved C_{ab} estimates were averaged and compared with the ground-measured dataset.

4.2.7 Statistical analysis assessing the accuracy of chlorophyll content estimates

To assess the performance of the trained ANN and the optical indices, we computed the following statistical indicators for the retrieved and the ground-measured C_{ab}: the coefficient of determination (R^2) of a linear function, the root mean square error (RMSE) including its systematic (RMSEs) and unsystematic (RMSEu) components, the relative RMSE (RRMSE; computed as RMSE normalized by the C_{ab} ground measured range) and the index of agreement (*d*). Additionally, the ANN C_{ab} estimates obtained for sunlit crown pixels of the AISA Eagle image were cross-compared with the $ANCB_{650–720}$, $ND_{925\&710}$, $SR_{750/710}$ and TCARI/OSAVI estimates. Assuming a one-to-one linear relationship between the number (N) of error free observations (O) and predictions (P), the RMSE of estimates and its systematic and unsystematic components can be calculated as follows (Willmott, 1981):

$$\mathrm{RMSE} = \sqrt{\sum_{i=1}^{N}(P_i - O_i)^2/N} \tag{4.6}$$

$$\mathrm{RMSE_S} = \sqrt{\sum_{i=1}^{N}(\widehat{P_i} - O_i)^2/N} \tag{4.7}$$

$$\mathrm{RMSE_U} = \sqrt{\sum_{i=1}^{N}(P_i - \widehat{P_i})^2/N} \tag{4.8}$$

where $\widehat{P_i} = a+bO_i$ and *a* and *b* are the coefficients of an ordinary least squares regression between O and P.

Both RMSE components are related to the RMSE through the following equation:

$$\mathrm{RMSE}^2 = \mathrm{RMSE}_S^2 + \mathrm{RMSE}_U^2 \quad (4.9)$$

These components offer complementary information to that of RMSE (and R^2) as they allow a deeper evaluation of the retrieval methods. If $RMSE_S$ prevails over $RMSE_U$, one can say that the retrieval method is affected by systematic errors and that it will yield biased C_{ab} estimations. On the contrary, if the RMSE is composed mostly by $RMSE_U$, then the retrieval method is as good as it can be. The index of agreement *d* complements information contained in RMSE, $RMSE_S$ and $RMSE_U$. It is expressed as:

$$d = 1 - \left(\sum_{i=1}^{N}(P_i - O_i)^2 / \sum_{i=1}^{N}(|'P_i| - |'O_i|)^2\right) \quad (4.10)$$

where $'P_i = P_i - \bar{O}$ and $'O_i = O_i - \bar{O}$. The index specifies the degree to which the observed deviations of the mean observations $\bar{O}$ correspond, both in magnitude and sign, to the predicted deviations of $\bar{O}$. It is a dimensionless indicator, where $d = 1.0$ indicates perfect agreement between the observed and estimated observations, and $d = 0.0$ connotes complete disagreement. A detailed description of $RMSE_s$, $RMSE_u$ and the index of agreement is provided in Willmott (1981).

4.3 Results and discussion

4.3.1 Sensitivity of continuum removed crown reflectance to C_{ab} and LAI

The CR bidirectional reflectance factors (BRFs) of the sunlit spruce crowns simulated between 650 and 720 nm in the coupled PROSPECT–DART model were plotted per C_{ab} level against the LAI values to investigate their sensitivity to both variables. Figure 4.5 illustrates that all CR BRFs of the simulated AISA Eagle bands are insensitive to LAI changes between 4 and 9 m^2 m^{-2}. Some sensitivity is observed for LAI values below six, where the BRF of spruce canopies is influenced by reflectance of photosynthetically inactive surfaces (woody elements) (Malenovský et al., 2008). Figure 4.5 also indicates that the most C_{ab} sensitive CR BRFs of the simulated AISA Eagle bands are located at 698.72 and 708.07 nm. The wavelengths between 650 and 690 nm are only sensitive to lower C_{ab} values, mostly below 40 µg cm^{-2}, and they become saturated with increasing C_{ab}, as previously shown by Daughtry et al. (2000). Consistently with Gitelson et al. (2003; 2006), our findings show that the most suitable (sensitive) wavelengths for C_{ab} estimation are located

around 710 nm (i.e. spectral interval 700–720 nm). Since the CR BRFs between 660 and 680 nm are rather stable and insensitive to moderate and high C_{ab}, they can be used as a normalization element of a continuum removal based C_{ab} estimator. Still, one has to keep in mind that such an estimator will retrieve the low C_{ab} estimates ($\leq$ 25 µg cm^{-2}) with a certain systematic error.

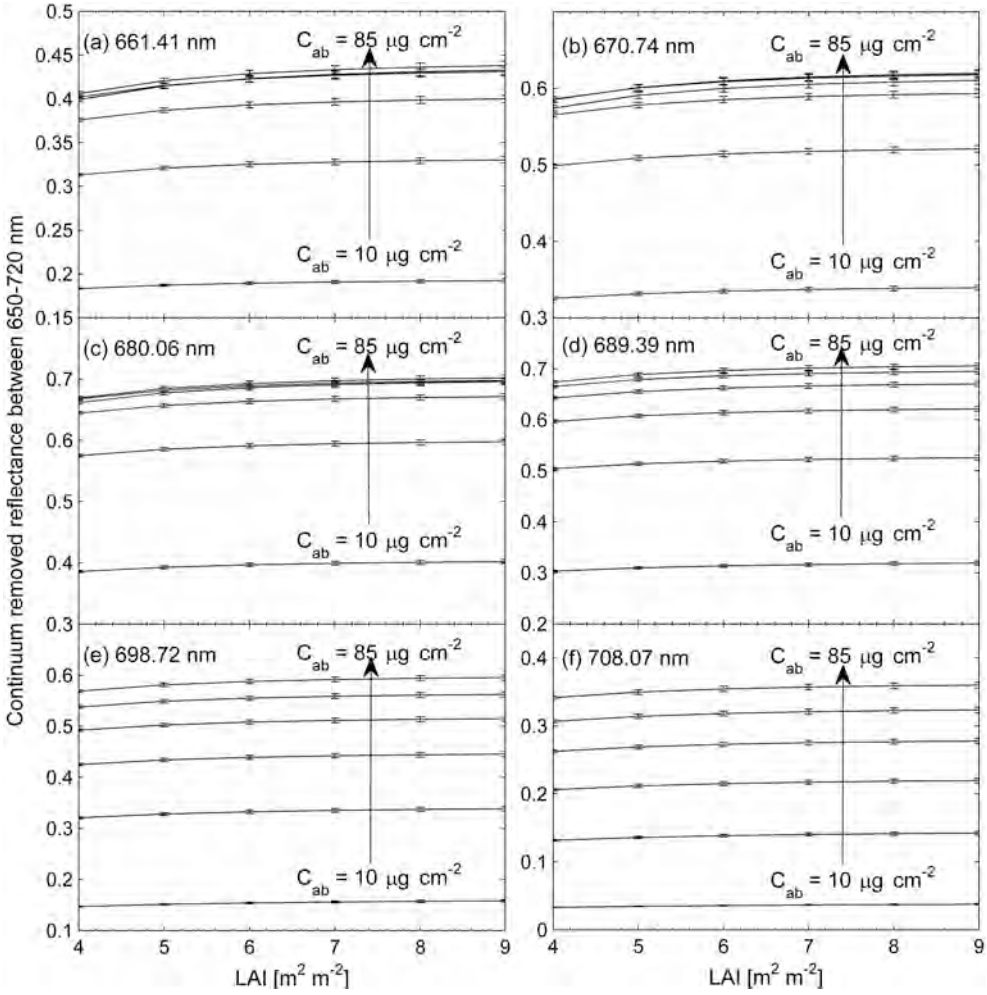

Figure 4.5 Sensitivity of continuum removed reflectance between 650 and 720 nm to leaf chlorophyll content (C_{ab}) and leaf area index for six spectral bands simulated by the PROSPECT-DART radiative transfer models at: 661.41 (a), 670.74 (b), 680.06 (c), 689.39 (d), 698.72 (e), and 708.07 nm (f). Each line corresponds with a simulated C_{ab} level (C_{ab} – 10, 25, 40, 55, 70 and 85 µg cm^{-2}). Small error bars represent positive and negative standard deviations driven by simulated canopy closures (CC – 75%, 85% and 95%).

4.3.2 Design of a continuum removal based C_{ab} optical index

Figure 4.6a shows that the area integrated under the simulated CR BRF curves of sunlit tree crowns between 650 and 720 nm ($AUC_{650\text{-}720}$) is exponentially related to C_{ab}. Nevertheless, due to the early saturation this exponential relationship cannot be exploited to estimate C_{ab} values above 40 μg cm^{-2} (e.g. $AUC_{650\text{-}720}$ equal to 30 corresponds with any C_{ab} from 55 up to 85 μg cm^{-2} depending on the actual LAI). Figure 4.6b indicates that the CR band depth of the strongest chlorophyll absorption between 660 and 680 nm, represented in our case by the CR band depth at 670 nm (CBD_{670}), is also insensitive to C_{ab} above 40 μg cm^{-2}, but the ratio of both variables $AUC_{650\text{-}720}/CBD_{670}$ exhibits a strong near-linear (exponential) relation to C_{ab} (Figure 4.6c). This new optical index, which we call 'Area under continuum-removed curve Normalized to the Chlorophyll absorption Band depth between 650 and 720 nm' ($ANCB_{650\text{-}720}$), can estimate C_{ab} of sunlit Norway spruce crowns independently from the LAI variation via the equation ($R^2 = 0.99$, $p < 0.001$):

$$\ln(C_{ab}) = 7.3903 - 7984.0135/(ANCB_{650\text{-}720})^2. \quad (4.11)$$

Notice in Figure 4.6c how $ANCB_{650\text{-}720}$ simulated with different LAI values concentrate for each C_{ab} value into one narrow (almost a single) point. This means, that for instance an $ANCB_{650\text{-}720}$ value around 48.4 will always predict C_{ab} of 55 μg cm^{-2} regardless the variation in actual forest stand LAI and canopy closure (CC).

Similar results were obtained also for other PROSPECT-DART simulated broadleaf canopies, i.e. homogeneous grassland and structurally heterogeneous deciduous forest stand (results in Appendix A3). The $ANCB_{650\text{-}720}$ of both broadleaf canopies is linearly dependent on C_{ab} ($R^2 = 0.95$ for grassland and $R^2 = 0.99$ for deciduous forest) and it maintains its LAI independency for C_{ab} estimates higher than 30 μg cm^{-2} (Figures A3.2c and A3.3c). A limited ability to retrieve C_{ab} below this threshold is due to spectral influence of the simulated background (bare soil), and in case of the grass canopy also due to the six leaf angle distributions (Table A3.1), both controlling the BRF continuum when C_{ab} absorption is too low. Because $ANCB_{650\text{-}720}$ is designed to exploit the variation in the CR reflectance due to changes in chlorophyll absorption between 650 and 720 nm, it should only be applied to pixels of pure vegetation canopy with a strong reflectance signal, i.e. in our case sunlit pixels of tree crowns. A comprehensive and systematic sensitivity analysis of $ANCB_{650–720}$ to mixed spectral information of different signal-to-noise ratios falls outside the scope of this study, but results in Appendix A3 suggest that an application of $ANCB_{650–720}$ to BRFs of canopies with a low LAI and C_{ab} (i.e. with a strong signal contribution from background bare soil) will result in unreliable C_{ab}

estimates. Also a significant presence of non-photosynthetic surfaces (e.g. tree trunks or manmade objects) or a high noise, which distorts the shape of the chlorophyll absorption feature between 650 and 720 nm, lead logically to an erroneous C_{ab} estimate. Although the analysis of the PROSPECT-DART simulated $ANCB_{650–720}$ for shaded crown parts revealed a similar empirical relationship with C_{ab} as for sunlit crowns (Appendix A4), the bottleneck for including the shaded pixels in the C_{ab} estimation is their low and spatially varying reflectance intensity and also an occasional noise in acquired airborne spectral data. Even though Figure 4.3 indicates acceptable radiometric quality of the AISA shaded crown pixels, our attempt to apply the C_{ab} retrieval in those pixels resulted in estimates of a random spatial variability (results not shown). We therefore deduce, that our shaded pixels are not suitable for the C_{ab} estimation due to the limited reflectance dynamic range and the locally specific shade intensity depending on recombination of various structural and geometrical forest stand parameters (e.g. foliar density, crown shape, tree height, slope, terrain configuration).

4.3.3 Chlorophyll estimation using optical indices and ANN

Three additional C_{ab} sensitive optical indices were computed from the PROSPECT-DART simulated LUT according to Eq. 4.2, 4.3, 4.4 and 4.5 and related statistically to the predefined C_{ab} classes (Figure 4.6d–f). The equation describing most accurately the dependency of $ND_{925\&710}$ on C_{ab} is a second order polynomial function ($R^2 = 0.92$, $p < 0.01$):

$$C_{ab} = 524.86(ND_{925\&710})^2 - 364.33(ND_{925\&710}) + 70.11 \quad (4.12)$$

$SR_{750/710}$ was related to C_{ab} linearly ($R^2 = 0.95$, $p < 0.01$) according to the following equation:

$$C_{ab} = 24.93(SR_{750/710}) - 36.38 \quad (4.13)$$

and TCARI/OSAVI can be used to retrieve C_{ab} through the following natural logarithm ($R^2 = 0.99$, $p < 0.001$):

$$C_{ab} = -56.01 \ln(TCARI/OSAVI) - 53.43. \quad (4.14)$$

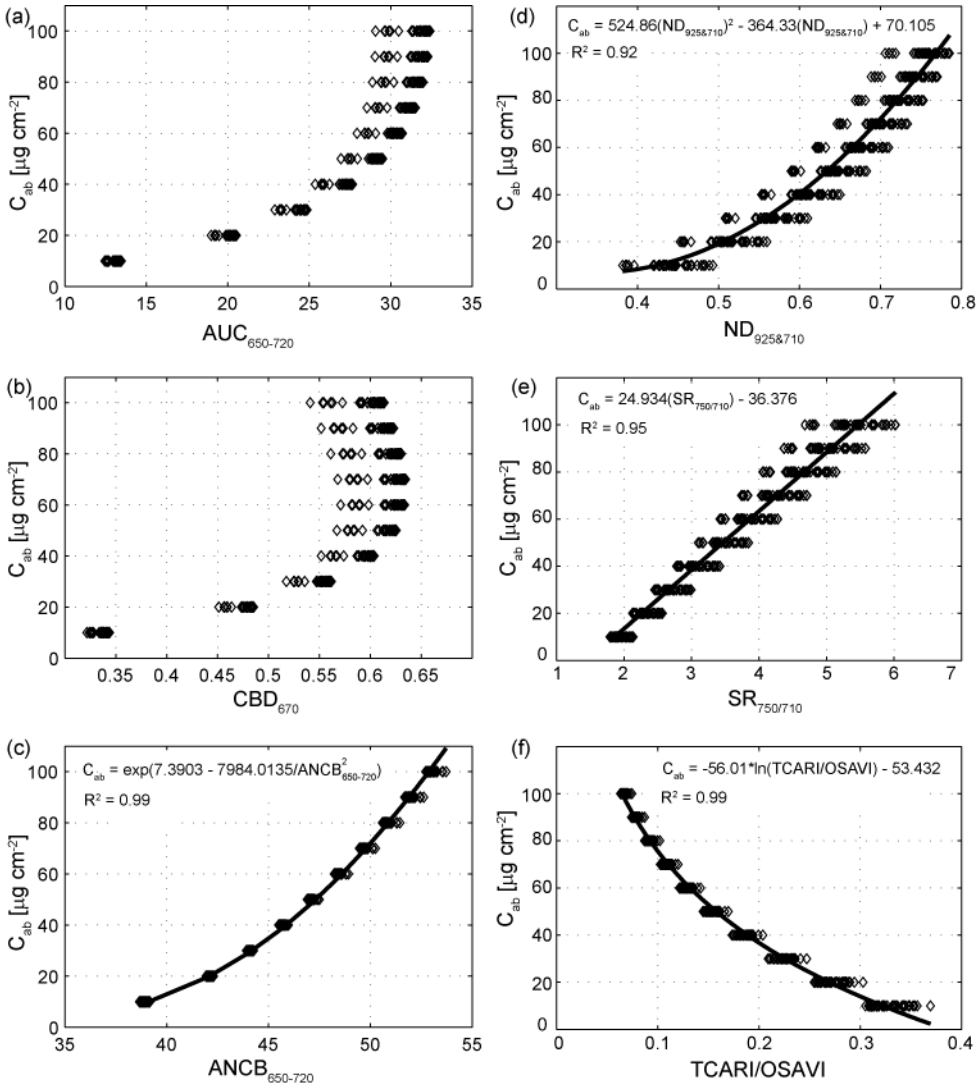

Figure 4.6 Design of the $ANCB_{650-720}$ optical index (c) using the Area Under Curve ($AUC_{650-720}$) of continuum removed reflectance (a) normalized by the Continuum Band Depth at 670 nm (CBD_{670}) (b); relation between leaf chlorophyll content (C_{ab}) and normalized difference between reflectance at 925 and 710 nm ($ND_{925\&710}$) (d), simple reflectance ratio between 750 and 710 nm ($SR_{750/710}$) (e) and ratio TCARI/OSAVI (f). The equations represent the best fitting functions with the highest coefficient of determination (R^2). A single diamond symbol represents one of the PROSPECT-DART simulated leaf area index (LAI) values (LAI between 4 and 9 with a step of 1) within three predefined canopy closures (CC – 75%, 85% and 95%).

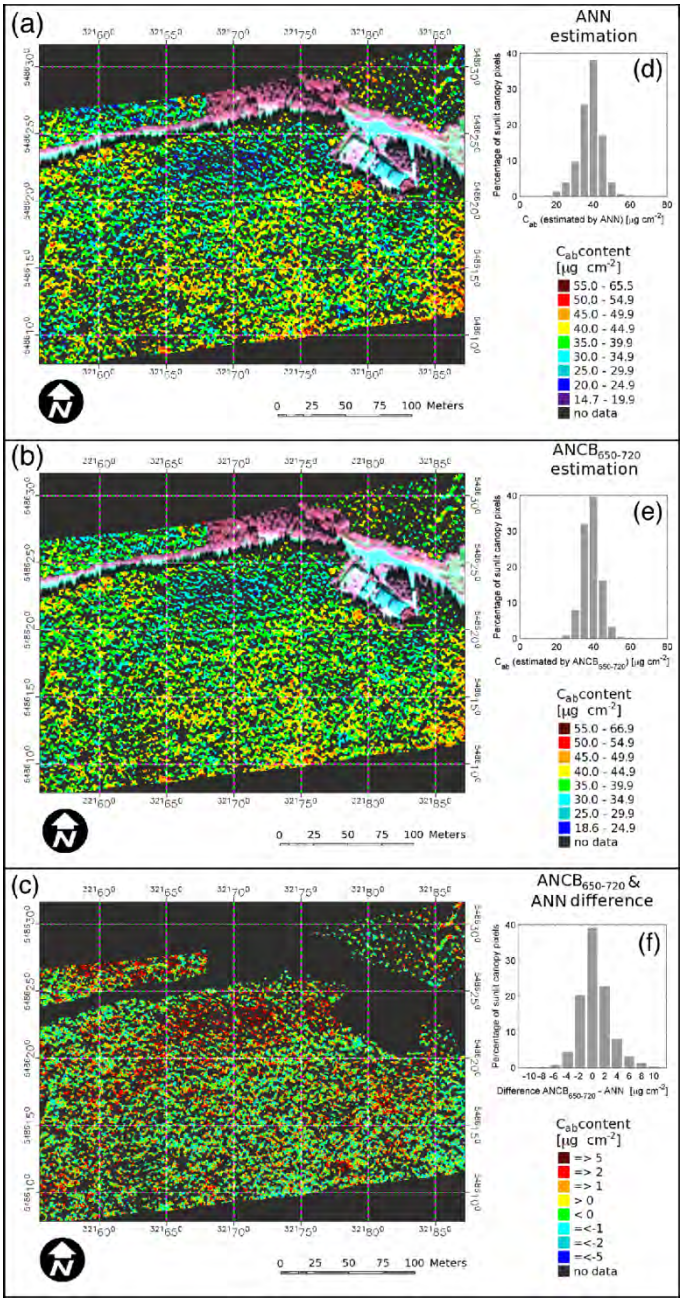

Figure 4.7 Leaf chlorophyll content of sunlit Norway spruce crown pixels estimated by ANN (a), ANCB$_{650-720}$ (b), and their reciprocal difference (ANCB$_{650-720}$ – ANN) (c), including histograms showing the percentage of pixels per C_{ab} class (d,e,f).

All three relationships are statistically significant, but only TCARI/OSAVI gains a variability that ensures a unique C_{ab} estimation for almost all the simulated LAI and CC combinations (Figure 4.6f). The variability of $ND_{925\&710}$ and $SR_{750/710}$ is quite high, which means that a given index value can correspond with up to four possible C_{ab} estimates (Figures 4.6d and e), depending on LAI and CC. The ANN was trained using continuum-removed AISA Eagle spectral bands of sunlit spruce crowns simulated with PROSPECT-DART models as described in Section 4.2.5. The accuracy assessment of the trained ANN revealed that it could estimate the simulated C_{ab} values with an RMSE of 0.40 µg cm^{-2} and with an R^2 of 0.99. The ANN and the empirical functions of optical indices stated in Eqs. 4.11, 4.12, 4.13 and 4.14 were consequently applied on the atmospherically corrected CR AISA Eagle spectral bands to retrieve C_{ab} of sunlit spruce crowns under investigation.

Figure 4.7 shows the C_{ab} maps and relative histograms of the ANN and $ANCB_{650–720}$ retrievals and also their reciprocal difference. Figure 4.7a and b demonstrate that the spatial pattern of both C_{ab} maps is similar, showing a large patch of low C_{ab} values at the highest elevation point of the study site (eastwards of the ecological station facility), which is exposed to a stronger environmental stress impact due to the weather conditions. C_{ab} maps produced by the $ND_{925\&710}$, $SR_{750/710}$ and TCARI/OSAVI empirical functions are having visually similar patterns (maps not shown), but their dynamic ranges and histogram distributions are shifted towards lower C_{ab} in case of $ND_{925\&710}$ and $SR_{750/710}$ or higher C_{ab} in case of TCARI/OSAVI (Figure 4.8a–c). We found that the lowest and the highest ANN C_{ab} estimates are equal to 14.7 µg cm^{-2} and 65.5 µg cm^{-2}, respectively, which match well with the values yielded by $ANCB_{650–720}$ (the lowest C_{ab} = 18.6 µg cm^{-2} and the highest C_{ab} = 66.9 µg cm^{-2}), but do not correspond so well with the estimates of the other three indices. For ANN and $ANCB_{650–720}$, the most frequent C_{ab} estimates are ranging between 40.0 and 44.9 µg cm^{-2} (Figures 4.7d and e), while for $ND_{925\&710}$ they range between 30.0 and 34.9 µg cm^{-2}, for $SR_{750/710}$ between 35.0 and 39.9 µg cm^{-2}, and for TCARI/OSAVI between 50.0 and 54.9 µg cm^{-2} (Figures 4.8a–c). The subtraction of the ANN C_{ab} map from the $ANCB_{650–720}$ C_{ab} map revealed an absolute mean difference of only 1.8 µg cm^{-2}, with the highest prediction differences ($\geq$ 5.0 µg cm^{-2}) appearing at the locations of low C_{ab} estimates (Figure 4.7c). The mean differences between ANN and the other three indices are higher, i.e. −9.01 µg cm^{-2} for $ND_{925\&710}$, −4.30 µg cm^{-2} for $SR_{750/710}$, and 13.29 µg cm^{-2} for TCARI/OSAVI. The histogram of the $ANCB_{650–720}$ − ANN C_{ab} difference shows a nearly symmetrical Gaussian distribution, with slightly higher frequencies for positive C_{ab} differences indicating a minor overestimation of $ANCB_{650–720}$ (Figure 4.7f). Almost 40% of the C_{ab} estimates produced by both methods are equal and about 40% are differing by only ± 2.0 µg cm^{-2}. Differences greater than ± 2.0 µg cm^{-2} are found for less than 20% of all the examined pixels (n = 151984). The histograms of the $ND_{925\&710}$ − ANN and $SR_{750/710}$ − ANN C_{ab} differences are also

symmetrical, but shifted significantly towards negative values, which suggests a systematic underestimation of both indices. Contrary to this, the TCARI/OSAVI – ANN histogram shows a strong shift towards higher C_{ab} values, i.e. an overestimation of C_{ab} retrieved by the index. These results demonstrate that, unlike the reflectance ratio based optical indices, both continuum removal-based methods (ANN and $ANCB_{650–720}$) produce consistent estimates.

A per-pixel statistical comparison of the ANN with the optical indices provided in Table 4.4a confirms a similar performance of the ANN and $ANCB_{650–720}$ methods (R^2 = 0.85, d = 0.95). The next two highest agreements are found between ANN and $SR_{750/710}$ (R^2 = 0.52, d = 0.75), and ANN and $ND_{925\&710}$ (R^2 = 0.51, d = 0.60), while TCARI/OSAVI seems to disagree with more than half of the ANN predictions (R^2 = 0.35, d = 0.45). The $ANCB_{650–720}$ results for C_{ab} values smaller than 30 µg cm^{-2} yield, however, systematically higher values than the ANN results (Figure 4.9d). This discrepancy can be attributed to the normalization of the index by the CBD_{670} term, which is not constant across the whole C_{ab} dynamic range, but slightly decreasing for C_{ab} values lower than 30 µg cm^{-2} (see Figures 4.5b and 4.6b). Figures 4.9a–c illustrates a greater mismatch between the ANN method and the remaining three ratio indices, with $ND_{925\&710}$ and $SR_{750/710}$ predicting in general lower and TCARI/OSAVI generating for most of the pixels higher C_{ab} estimates.

Table 4.4 Results of statistical analyses comparing the leaf chlorophyll a & b content (C_{ab}) estimated for sunlit spruce crown pixels of the AISA Eagle airborne image with four optical indices ($ANCB_{650-720}$, $ND_{925\&710}$, $SR_{750/710}$ and ratio TCARI/OSAVI) and with an artificial neural network (ANN) approach (a), and assessing their prediction accuracy when compared with ground measured crown C_{ab} values (b). (R^2 ~ coefficient of determination of the linear function, RMSE ~ root mean square error, RRMSE ~ relative RMSE computed for the actual chlorophyll range of 14.7 – 66.9 µg cm^{-2}, $RMSE_S$ ~ systematic RMSE, $RMSE_U$ ~ unsystematic RMSE, and d ~ index of agreement).

	R^2 [rel.]	RMSE [µg cm^{-2}]	RRMSE [%]	$RMSE_S$ [µg cm^{-2}]	$RMSE_U$ [µg cm^{-2}]	d [rel.]
(a) ANN AISA estimates vs.						
$ANCB_{650-720}$	0.85	2.42	4.64	1.59	1.82	0.95
$ND_{925\&710}$	0.51	10.42	19.96	9.03	5.20	0.60
$SR_{750/710}$	0.52	6.10	11.69	4.63	3.98	0.75
TCARI/OSAVI	0.35	14.93	28.60	13.32	6.74	0.45
(b) Ground measurements vs.						
ANN	0.72	2.18	4.18	0.77	2.04	0.92
$ANCB_{650-720}$	0.72	2.27	4.35	1.59	1.62	0.89
$ND_{925\&710}$	0.64	9.07	17.38	8.75	2.40	0.53
$SR_{750/710}$	0.71	4.16	7.97	3.82	1.64	0.75
TCARI/OSAVI	0.41	12.30	23.56	11.76	3.61	0.42

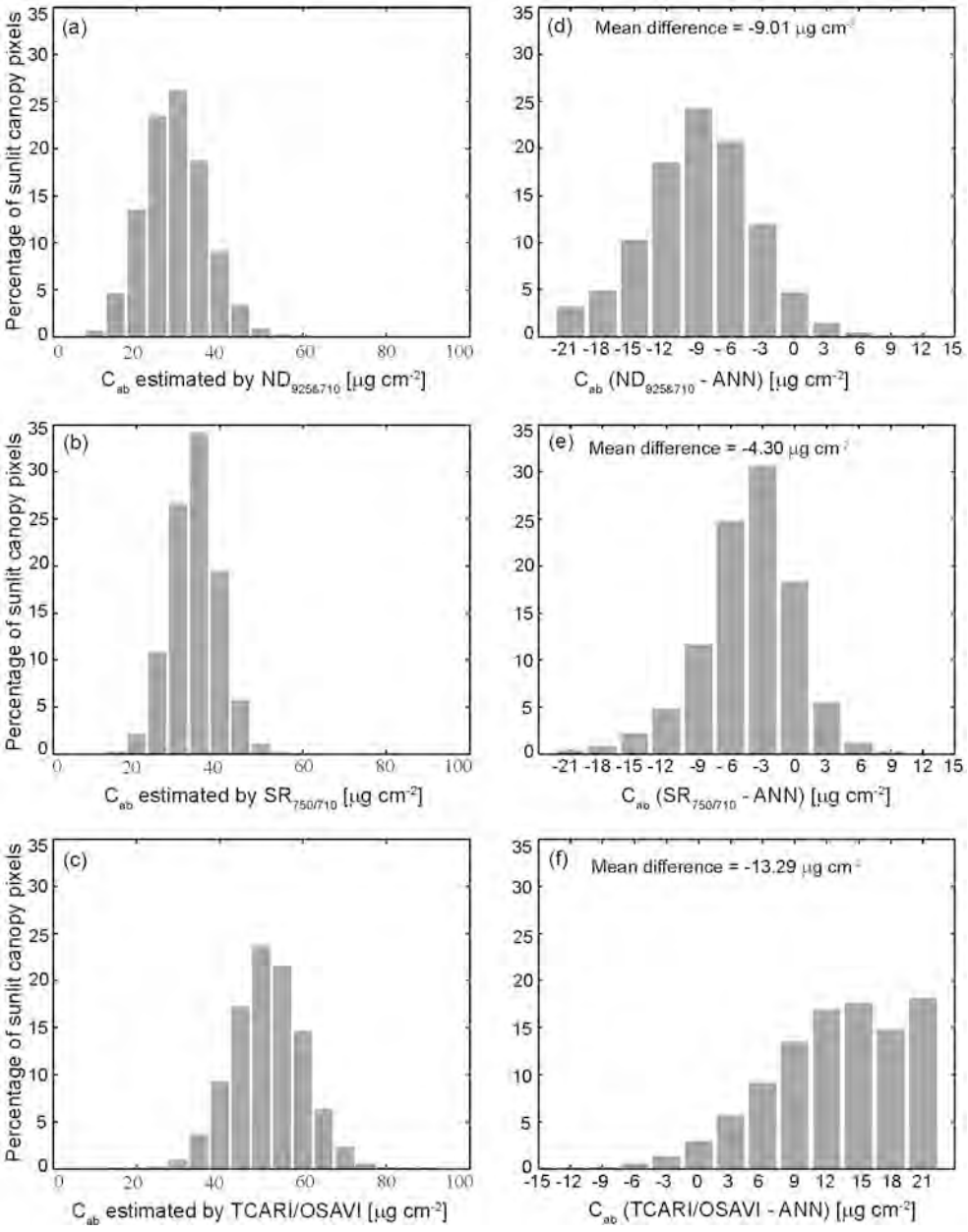

Figure 4.8 Histograms showing the percentage of sunlit crown pixels per C_{ab} value estimated by the normalized difference between reflectance at 925 and 710 nm ($ND_{925\&710}$) (a), simple reflectance ratio between 750 and 710 nm ($SR_{750/710}$) (b), ratio of TCARI/OSAVI indices (c), and the distribution of estimated C_{ab} differences computed between all three optical indices and ANN (d,e,f).

4.3.4 Comparison of airborne C_{ab} estimates with ground measurements

Needle samples of ten spruce crowns were collected during the flight campaign to generate the C_{ab} ground truth as described in Section 4.2.6. Unfortunately one of the sampled crowns had to be excluded from the original validation dataset due to the presence of a metallic meteorological tower standing next to the tree. Photons reflected from the metallic tower affected negatively the HDRF of the sampled spruce crown, which resulted in a systematic C_{ab} overestimation of about 17 μg cm^{-2} (results not shown).

The comparison of the C_{ab} values retrieved by all five estimation methods with the ground-measured C_{ab} of the nine remaining crowns is displayed in Figure 4.10. Indicators assessing statistical accuracy of all the prediction methods are available in Table 4.4b. The highest R^2 of 0.72 with the lowest RMSE indication and *d* of approximately 0.9 were obtained for ANN and $ANCB_{650–720}$. Both approaches resulted in virtually identical RMSE values of 2.18 μg cm^{-2} for the ANN (RRMSE of 4.18%) and 2.27 μg cm^{-2} for the $ANCB_{650–720}$ (RRMSE of 4.35%) retrieval (Figures 4.10a and b), with $RMSE_U$ higher than $RMSE_S$. The two RMSE components are for $ANCB_{650–720}$ almost equal, while $RMSE_U$ for ANN is about two times higher than $RMSE_S$, indicating an absence of systematic errors and a prevailing presence of random errors. The opposite situation is found for the other optical indices, with $RMSE_U$ being two to almost four times lower than $RMSE_S$. The second most accurate retrieval was performed with $SR_{750/710}$ (R^2 = 0.71, *d* = 0.75) (Figure 4.10e), followed by $ND_{925\&710}$ (R^2 = 0.64, *d* = 0.53) (Figure 4.10d), both underestimating C_{ab} by 4.16 and 9.07 μg cm^{-2}, respectively (RRMSE of 7.97 and 17.38%). The least accurate method is the TCARI/OSAVI estimation (R^2 = 0.41, *d* = 0.42) with an RMSE equal to 12.30 μg cm^{-2} (RRMSE of 23.56%) (Figure 4.10f). A visual investigation of the C_{ab} map revealed that the systematic overestimation of the TCARI/OSAVI retrieval is caused by pixels of a lower HDRF intensity located at the edge of spruce crowns. These AISA image pixels might be more affected by the background reflectance or they might contain a higher proportion of shadows than the one simulated by the RT models.

The results of our retrieval methods are, in general, comparable with previously published airborne C_{ab} mapping efforts in coniferous canopies. For instance, Zarco-Tejada et al. (2004) up-scaled the simple ratio $SR_{750/710}$ using the PROSPECT and SPRINT RT models to map C_{ab} of sunlit Jack pine crowns, achieving an RMSE of 8.1 μg cm^{-2} (RRMSE of 27.0%, computed for a C_{ab} range between 26.8 and 56.8 μg cm^{-2}). Our $SR_{750/710}$ retrieval achieved an RMSE of 4.16 μg cm^{-2} (RRMSE of 7.97%). Moorthy et al. (2008) reported an RMSE of 5.3 μg cm^{-2} (RRMSE of 26.20% for a pigment range of 25.7 – 45.9 μg cm^{-2}), when estimating C_{ab} of pine needles using coupled leaf (LIBERTY and PROSPECT) and canopy (SAILH) RT models. Zhang et al. (2008) estimated C_{ab} of Black spruce stands from CASI airborne data using PROSPECT and the 4-Scale geometrical–optical model with an accuracy of R^2

equal to 0.47 and an RMSE of 4.34 μg cm^{-2}. Our continuum removal based methods achieved the RMSE of almost two-folds lower than results of these studies. Finally, Schlerf et al. (2010) obtained an R^2 of 0.80 and RRMSE of 4.0% using a stepwise multiple linear regression predicting C_{ab} from continuum-removed Norway spruce reflectance functions of two HyMap airborne wavebands. Our ANN and $ANCB_{650–720}$ retrievals reached very similar RRMSE (Table 4.4b), with the systematic RMSE component always smaller than the unsystematic one. Still, it should be mentioned that none of the sampled crowns at our study site contained extremely low (≤ 15 μg cm^{-2}) or high (≥ 60 μg cm^{-2}) amounts of C_{ab}.

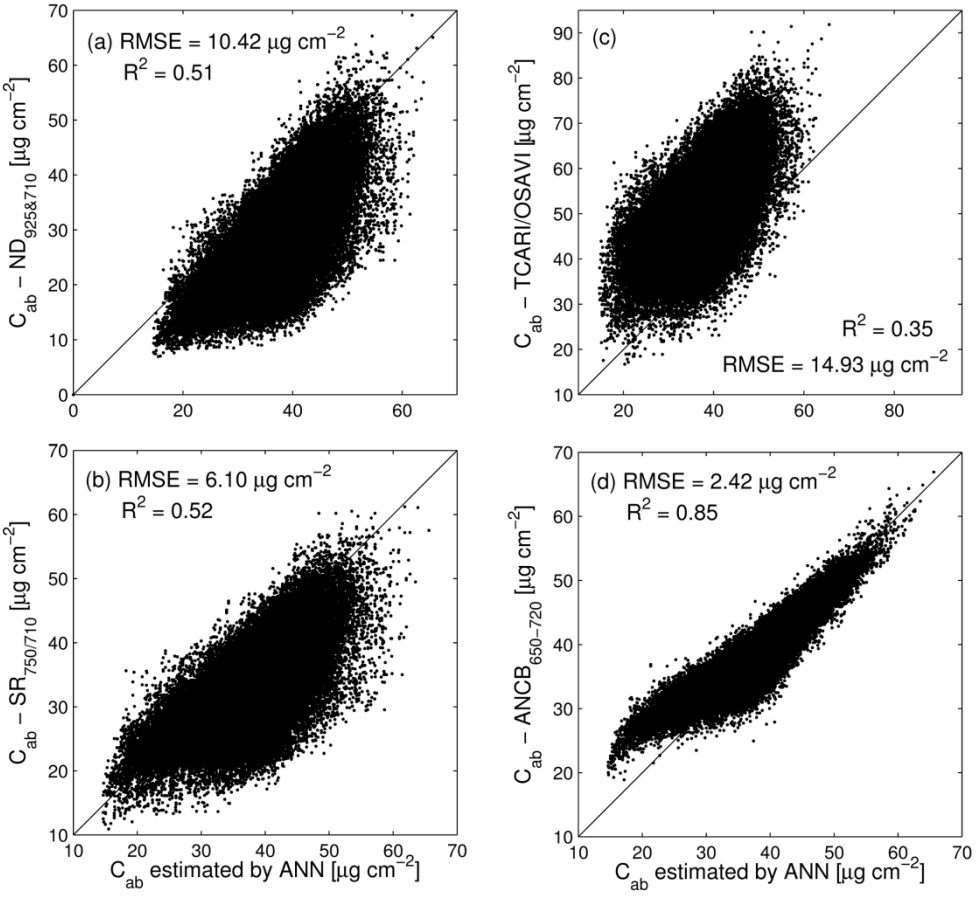

Figure 4.9 Scatterplot of leaf chlorophyll content (C_{ab}) retrieved by artificial neural network (ANN) plotted against the C_{ab} estimated of normalized difference ($ND_{925\&710}$) (a), simple reflectance ratio ($SR_{750/710}$) (b), ratio of TCARI/OSAVI indices (c), and $ANCB_{650\text{-}720}$ optical index (d). Each dot symbol represents one pixel of a sunlit tree crown indentified in the AISA Eagle image of the test site (R^2 – coefficient of determination, RMSE – root mean square error).

The cross-comparison of the C_{ab} values estimated for the nine ground-sampled crowns by $ANCB_{650–720}$ and ANN (Figure 4.10c) indicates a similar result to the one in Figure 4.9d. The figures show that although both approaches are based on continuum removal, the $ANCB_{650–720}$ estimates for low C_{ab} values are higher than those produced by the ANN. The ANN approach is, based on the validation results, slightly more accurate, but it is also more laborious and computationally intensive, especially during the training phase. Since ANN architecture contains several tuning parameters (e.g. the transitional functions between the neuron layers and their weights), it takes several hours and hundreds of training permutations to achieve the network of a desirable performance. The $ANCB_{650–720}$ approach is faster (it takes only few minutes to establish a relationship between the index and C_{ab} values), but still a comparably robust estimator, if applied to airborne images of high (sub-meter) spatial resolution that allows identification and exclusion of spectrally impure or noisy (e.g. deeply shadowed) canopy pixels.

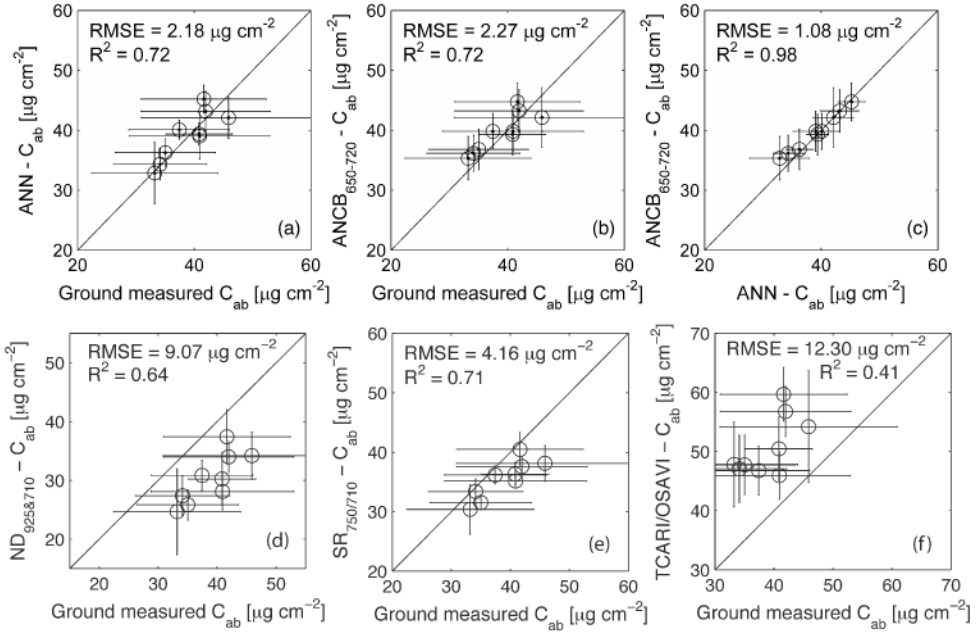

Figure 4.10 Validation of leaf chlorophyll content (C_{ab}) retrieved for the sampled spruce crowns from the AISA Eagle image using artificial neural network (ANN) (a), $ANCB_{650-720}$ optical index (b), normalized difference ($ND_{925\&710}$) (d), simple reflectance ratio ($SR_{750/710}$) (e), ratio of TCARI/OSAVI indices (f) and the reciprocal comparison of ANN and $ANCB_{650-720}$ estimations (c). Each circle represents one tree crown, horizontal bars represents two standard deviations of C_{ab} values either measured on the ground or retrieved by ANN and optical indices (R^2 – coefficient of determination, RMSE – root mean square error).

4.4 Conclusions

This study demonstrates that leaf-canopy radiative transfer modeling combined with continuum removal of red and red-edge reflectance (650 – 720 nm) can be successfully used for the retrieval of coniferous C_{ab} using airborne imaging spectroscopy data at sub-meter spatial resolution. Results are suggesting that the C_{ab} estimation based on the continuum removal transformation of several adjacent spectral bands is more robust than the retrieval using optical indices computed from few discrete reflectance bands. The selected spectral range was shown to be sufficient to accurately retrieve C_{ab} of closed forest canopies with a LAI above four. Nonetheless, a more generalized applicability of the method might be achieved, when further tested for sensors with different technical specifications (e.g. spectral sampling interval and full-width-half-maximum).

The newly proposed C_{ab} index $ANCB_{650–720}$ outperformed three selected reflectance ratio based optical indices ($ND_{925\&710}$, $SR_{750/710}$ and TCARI/OSAVI) and performed comparably to an ANN trained to retrieve the leaf C_{ab} of spruce crowns using the continuum removed PROSPECT-DART simulations. The only weakness in $ANCB_{650–720}$ performance is a subtle overestimation of C_{ab} values below 30 μg cm^{-2}. With the systematic RMSE being lower than the unsystematic one, the newly proposed index is similarly robust, but faster, than ANN as no time-consuming training is required. Because of this, we recommend using $ANCB_{650–720}$ for retrieving C_{ab} when both high vegetation fraction and high signal-to noise ratio (as in case of sunlit canopy pixels) are present.

Acknowledgements

This study was carried out within the ESA/PECS project no. 98029 (Global Change Research Centre, Academy of Sciences of the Czech Republic) using the CzeCOS infrastructure (LM2010007) supported by the CzechGlobe project (CZ.1.05/1.1.00/02.0073). Access to the MetaCentrum parallel computing clusters provided under the program ‘Projects of Large Infrastructure for Research, Development, and Innovations’ (LM2010005 funded by the Ministry of Education, Youth, and Sports of the Czech Republic) is acknowledged for facilitating our radiative transfer simulations. The work of authors from University of Zürich has been supported by the European Commission 6th Framework Programme project ECOCHANGE (GOCE-036866).

5

Comparison of remote sensing and plant trait-based modelling to predict ecosystem services in subalpine grasslands

This chapter is based on:

Homolová L, Schaepman ME, Lamarque P, Clevers JGPW, de Bello F, Thuiller W, Lavorel S (2013) Comparison of remote sensing and plant trait-based modelling to predict ecosystem services in subalpine grasslands.
Journal of Ecology (Submitted)

Abstract

1. There is a growing demand for spatially explicit assessment of multiple ecosystem services (ES) and remote sensing (RS) can provide valuable data to meet this challenge.

2. We used high spatial and spectral resolution RS images to assess multiple ES based on underpinning ecosystem properties (EP). We estimated five EP (green biomass, litter mass, crude protein content, species diversity and soil carbon content) from RS data using empirical RS methods and maps of ES were calculated as simple linear combinations of EP. Additionally, the RS-based results were compared with results of a plant trait-based statistical modelling approach that predicted EP and ES from land use, abiotic and plant trait data (modelling approach).

3. The RS approach was tested on subalpine grasslands located in the Central French Alps.

4. The comparison between the RS and the modelling approaches showed that RS-based results provided better insight into the fine-grained spatial distribution of EP and thereby ES, whereas the modelling approach reflected the land use signal that underpinned trait-based models of EP. The spatial agreement between the two approaches at a 20 m resolution varied between 16 and 22% for individual EP, but for the total ecosystem service supply it was only 7%.

5. The modelling approach identified the alpine grazed meadows land use class as hot spots and mown-grazed permanent meadows as cold spots. Whereas the RS-based hot spots were a small subset of those predicted by the modelling approach, cold spots were rather scattered, small patches with limited overlap with the modelling results.

6. *Synthesis*. Despite limitations associated with timing of assessment campaigns and in-situ data requirements, RS offers valuable data for spatially continuous mapping of EP and can thus supply RS-based proxies of ES. Although the RS approach was applied to a limited area and for one type of ecosystem (subalpine grasslands), we believe that the broader availability of high fidelity airborne and satellite RS data will promote RS-based assessment of ES to larger areas and other ecosystems.

5.1 Introduction

Human society benefits from a multitude of resources and processes that are supplied by ecosystems. They provide a vast range of services such as food, timber or clean water production, they regulate climate and diminish natural hazards, and they offer nonmaterial cultural assets (Burkhard et al., 2009; Costanza et al., 1997; de Groot et al., 2002; MEA, 2005). A concept of ecosystem services (ES) presents a way to quantify, analyze and manage the benefits obtained from ecosystems (MEA, 2005). Although the interest in ES is growing exponentially since the 1990's (Costanza et al., 1997; de Groot et al., 2002; Fisher et al., 2009; MEA, 2005), classification and consistent quantification of ES still remains a challenge (de Groot et al., 2010; Fisher et al., 2009; Wallace, 2007). Spatially explicit mapping of ES at different scales is required for sustainable land use planning and environmental decision making (Burkhard et al., 2012). Moreover, there is a growing interest in mapping of multiple ES and identification of areas with concentrated ES supply (Lavorel et al., 2011; Naidoo et al., 2008; O'Farrell et al., 2010).

The biggest challenge in spatially explicit mapping of ES is often a limited availability of primary data on ES (Eigenbrod et al., 2010). It is thus more common to use ES proxies – ecosystem properties, environmental variables or land cover / land use maps – which are naturally linked to ES and, at the same time, easier to obtain (Chan et al., 2006; Egoh et al., 2008; Eigenbrod et al., 2010; Lavorel et al., 2011). The mapping of ES is often based on land use or land cover data by transferring a single value of ES to each class (Burkhard et al., 2009; Costanza et al., 1997; Eigenbrod et al., 2010; Metzger et al., 2006). This approach is practical, but also less accurate as it neglects variability within a single class. Eigenbrod et al. (2010) showed that land cover based proxies of ES poorly correlated to primary data of biodiversity, recreation and carbon storage ES in England. Lavorel et al. (2011) showed that ecosystem properties (EP), which determined ES supply in subalpine grasslands, were better estimated when including spatial variations in environmental variables and plant traits than using a pure land use based model only. This spatially explicit approach required intensive in-situ measurements to calibrate linear regression models of plant traits and EP. Considering large variability of vegetation properties within land use classes (Garnier et al., 2007) and across landscapes due to environmental gradients (Albert et al., 2010), in-situ data is clearly a limiting factor in EP and ES mapping at larger spatial scales. Remote sensing (RS) gives a possibility to map spatial and temporal variation of ecosystem properties in a more extensive manner than individual in-situ measurements (Kokaly et al., 2009; Mulder et al., 2011; Ustin and Gamon, 2010).

An advantage of RS is that it provides variety of spatially continuous data at different spatial resolutions. RS data always represent a snapshot in time of

ecosystem state, but satellite RS offers high revisit frequency and thus a possibility to analyze EP and thereby ES variations not only in the spatial, but also in the temporal dimension. A variety of RS instruments with different spatial, spectral and temporal resolutions is nowadays available (Grace et al., 2007; Malenovský et al., 2009; Turner et al., 2003). Specifically, Ayanu et al. (2012) reviewed the suitability of existing satellite-based RS instruments and methods for ES assessment and concluded that more studies are needed to evaluate the validity of RS-based proxies for ES mapping.

In general, RS data can be used in two ways to support spatial assessment of ES. First, RS data serve to generate accurate and up-to-date land cover maps (Friedl et al., 2010), whereby different ES values are assigned to individual classes (Hu et al., 2008; Konarska et al., 2002; Lautenbach et al., 2011). Besides major limitations of land cover based assessment of ES, which were discussed earlier, Verburg et al. (2009) and Lavorel et al. (2011) suggested that ES should be better linked to actual land use that often differs from the actual land cover. Furthermore, the spatial resolution underlying land cover maps influences both the extent and the valuation of ES (Di Sabatino et al., 2013; Konarska et al., 2002).

The second way of using RS to support ES assessment is that RS data are directly used to estimate EP (e.g. biomass), which in turn serve as proxies for the actual ES (e.g. forage production) (Malmstrom et al., 2009). Especially those vegetation properties that play a key role in radiation absorption and scattering can be retrieved from the optical RS data achieving acceptable accuracies. These are for example chlorophyll content (Dash and Curran, 2004; Schlerf et al., 2010; Zarco-Tejada et al., 2004), water content (Clevers et al., 2010; Colombo et al., 2008; Serrano et al., 2000) and structural properties such as leaf area index (Fernandes et al., 2004) or fractional vegetation cover (Asner and Heidebrecht, 2002).

The most common RS method to study vegetation properties is to use field measurements to interpret RS images – empirical RS methods. Empirical RS methods build a statistical regression model between a limited number of in-situ data and a subset of spectral bands (Huber et al., 2008; Psomas et al., 2011; Serrano et al., 2002; Smith et al., 2002) or vegetation indices (Tian et al., 2011; Verstraete and Pinty, 1996). By nature, they are computationally fast, easy to implement and therefore suitable for feasibility case studies of smaller spatial extent. The major limitation is that established relationships are less transferable to the same area at a different time, to another location or to another sensor (Asner et al., 2003; Colombo et al., 2003; Grossman et al., 1996).

The objective of this research was to test the potential of high spatial and spectral resolution airborne RS data for mapping of ecosystem properties and services in subalpine grasslands. Using a common assessment of the supply of ES by subalpine grasslands based on their ecosystem properties, we estimated EP directly from RS data using empirical retrieval methods. The RS-based maps of EP and ES were

compared with estimates from the plant trait-based modelling approach combining mapped land use, abiotic variables and plant trait in-situ data (Lavorel et al., 2011). Furthermore, we discussed advantages and disadvantages of both approaches.

5.2 Material and methods

5.2.1 Study site and in-situ measurements

The study area is located in the Central French Alps, on the south facing slope of the Villar d'Arène municipality (45°02'22"N, 06°22'07"E). It spans an altitude gradient ranging from 1800 – 2100 m a.s.l. Floristic composition of the subalpine grasslands has been affected by a long history of agricultural and pastoral land use. A detailed description of the study area is given in Quétier et al. (2007a). Ecosystem properties (green biomass, litter mass, crude protein content, plant species diversity and soil carbon content) and plant traits (vegetation height, leaf dry matter content, nitrogen content and phosphorus content) were measured in 30 x 30 m permanent plots stratified by land use and altitude gradient during years 2004–2009. Detailed protocols for in-situ measurements are provided in Lavorel et al. (2011). Twenty-five plots were located within the area covered by the RS images (Figure 5.1a).

5.2.2 Remote sensing data

Airborne imaging spectroscopy (or hyperspectral RS) data were acquired using the AISA Dual system (Specim, Ltd. Finland) on July 23rd, 2008. We acquired six flight lines covering an area of about 4 x 2.5 km. The resulting ground pixel size was 0.8 m. In total 359 spectral bands covered the range of 400 – 2450 nm and an average spectral sampling interval between bands varied from 4.3 to 6.3 nm. We discarded about one third of the available spectral bands due to poor radiometric response and atmospheric disturbances. The AISA Dual images were pre-processed in three steps. The flight lines were first calibrated to at-sensor radiance values using sensor-specific radiometric calibration coefficients. Second, the flight lines were geometrically corrected using on-board navigation data and a local digital elevation model of 10 m spatial resolution. Subsequently, the images were orthorectified to a Universal Transverse Mercator (UTM, Zone 32N) map projection. Third, at-sensor radiance data were converted to hemispherical-directional reflectance factors (HDRF, see Schaepman-Strub et al. (2006) for terminology) by applying an atmospheric correction using the ATCOR-4 software (Richter and Schlapfer, 2002). A true colour composite of the fully corrected AISA Dual data is shown in Figure 5.1a.

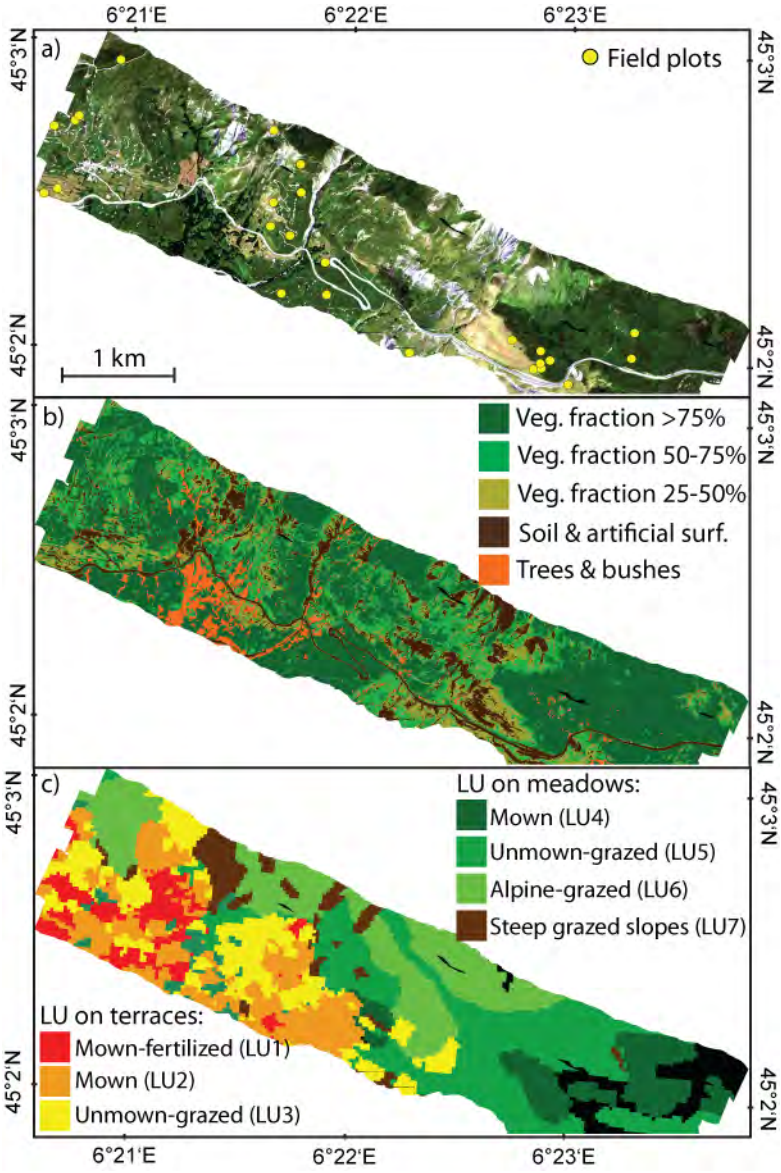

Figure 5.1 (a) True color display (R = 640 nm, G = 552 nm, B = 462 nm) of the AISA Dual mosaic with field plots. (b) Current land cover classification derived from supervised image classification and spectral unmixing. First three classes represent grassland-covered areas with indicated fraction of green vegetation. (c) Land use classification, which was adopted from Lavorel et al. (2011). Unclassified areas are in black.

We applied maximum likelihood classification (ENVI 4.8, ITT Visual Information Solutions) to distinguish grasslands from other land cover classes (trees and bushes, roads and urban areas, and bare soils and rocks). Subsequently, we applied a fully constrained spectral unmixing procedure (Zurita-Milla et al., 2007) on the classified grassland pixels, allowing them to be decomposed in relative fractions of three components: fractions of photosynthetic vegetation, non-photosynthetic vegetation, and soil. The actual land cover classification combined with the results of the spectral unmixing is shown in Figure 5.1b.

All pixels with a green vegetation fraction lower than 25% and pixels classified as trees/bushes, roads/urban areas, soils/rocks and heavily grazed or mown grasslands were masked out. In total about 25% of all AISA pixels were excluded from further analysis. Moreover, field plots located on the masked image area were also excluded and at the end maximum 18 plots remained for RS data interpretation.

5.2.3 Estimation of ecosystem properties

For clarity reasons we first introduce the main methodological steps (Figure 5.2) as this study combines and compares the RS approach (this study) with the plant trait-based modelling approach (Lavorel et al., 2011) to map multiple EP and ES. The second approach (further denoted as the modelling approach) was adopted from Lavorel et al. (2011). In this approach, five EP (green biomass, litter mass, crude protein content, species diversity and soil carbon) were modelled using general linear models combining the maps of land use, abiotic variables (topography and soil properties) and plant traits (vegetation height, leaf dry matter content, nitrogen and phosphorus content) (details in Lavorel et al. 2011). In these EP models, both abiotic and plant trait inputs were estimated based on land use and possible modifications reflecting effects of altitude or soil heterogeneity. The resulting maps of modelled EP were produced at a spatial resolution of 20 m and they were transformed to match the spatial extent of the AISA images (ArcGIS 10.0, ESRI Inc.).

The RS approach estimating EP from the AISA images was based on an empirical method, i.e. building a statistical regression model between in-situ measurements of EP and reflectance data (Cho et al., 2007; Darvishzadeh et al., 2008; Psomas et al., 2011; Ramoelo et al., 2013). We tested three empirical methods: i) narrow-band vegetation indices, i.e. normalized difference vegetation index (NDVI; eq. 5.1) and simple ratio (SR, eq. 5.2), ii) stepwise multiple linear regression (SML) and iii) partial least square regression (PLS).

We evaluated all possible two-pair band combinations (b_i, b_j) to build two types of narrow-band vegetation indices:

$$NDVI = (b_i - b_j) / (b_i + b_j) \quad (5.1)$$

$$SR = b_i / b_j \quad (5.2)$$

SML regression was applied to the full reflectance spectra (240 bands) and we evaluated all possible band combinations up to maximum of four spectral bands in order to avoid model overfitting (Psomas et al., 2011). Regression models with high multicollinearity among selected spectral bands (variance inflation factor VIF > 10) were eliminated. SML regression was implemented in R (version 2.15.0, R development core team, 2012) using the packages *leaps* and *regr0.*

PLS regression, a multivariate technique that reduces the large number of collinear spectral variables to a few non-correlated latent variables, was applied to full, non-transformed reflectance spectra using Matlab 7.11.0, function *plsregerss*.

The low number of in-situ EP data ($n \leq 18$) prevented using an independent subset for model calibration and validation. Therefore, all EP data were used to build empirical regression models. The overall capability of each empirical model to explain the variability in measured EP was evaluated by the coefficient of determination (R^2). The predictive power of a model has been assessed by estimating the root mean square error of prediction (RMSEP) using the leave-one-out cross-validation approach.

The best regression model estimating EP from RS data was selected according to the highest R^2 and lowest RMSEP and it was then applied to the entire RS image at the original spatial resolution of 0.8 m. Resulting maps of EP from RS images were normalized between 0 and 100 using 5^{th} and 95^{th} data percentiles as boundary values (Lavorel et al., 2011) and only then resampled to 20 m spatial resolution to match the results of the modelling approach.

Table 5.1 Coefficients used for combining individual ecosystem properties to a given ecosystem service.

	Ecosystem properties				
Ecosystem Service	Green biomass	Litter mass	Crude protein content	Species diversity	Soil carbon content
Agronomic	+1		+1		
Cultural		-1		+1	
C sequestration					+1
Total	Agronomic + Cultural + C sequestration ES				

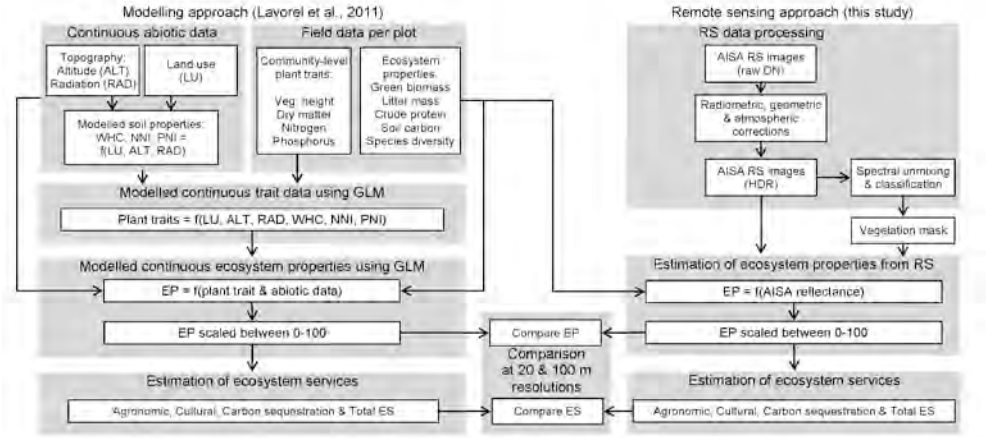

Figure 5.2 Conceptual framework for the remote sensing of ecosystem properties and services and the comparison with the modelling approach of Lavorel et al. (2011). Abbreviations: nitrogen nutrition index (NNI), phosphorus nutrition index (PNI), ecosystem properties (EP), ecosystem services (ES), remote sensing (RS), digital numbers (DN), hemispherical-directional reflectance (HDR).

5.2.4 Estimation of ecosystem services

Ecosystem services (i.e. agronomic value, cultural value and carbon sequestration) were related to ecosystem properties according to indicators identified by local stakeholders (Lamarque et al., 2011; Quétier et al., 2010) (Table 5.1). The original scheme relating EP and ES presented in Lavorel et al. (2011) was modified to overcome the inability of RS data to predict flowering onset, which was required to estimate the pollination ES and to incorporate date of flowering onset as part of the assessment of agronomic value. Maps of ES were produced as simple linear combinations of normalized EP maps using coefficients summarized in Table 5.1. Based on the three selected ES, which encompass the two most relevant services to local stakeholders (agronomic and cultural values), and one service of global relevance (carbon sequestration) (Lamarque et al., 2011), total ecosystem service supply was calculated as the sum of individual ES. The location of hot spots and cold spots of total ecosystem service supply was analyzed by applying the Getis-Ord-Gi* spatial statistic in ArcGIS 10.0, ESRI. The algorithm identifies statistically significant spatial clusters of high (hot spots) and low (cold spots) value by testing a null hypothesis whether the observed clustering is more pronounced than one would expect in a random distribution of those same values.

5.2.5 Comparison of remote sensing and modelling approaches

Spatial assessment of differences between the RS and the modelling approaches was implemented using Map Comparison Kit 3.2 (Visser and de Nijs, 2006) – a toolbox allowing spatial comparison of categorical maps using the fuzzy set theory (Hagen,

2003). The fuzzy approach has two great advantages as compared to a direct pixel-by-pixel comparison. It allows assessing the spatial neighbourhood of a pixel (i.e. closer pixels are more similar than distant pixels) and proximity among classes (i.e. some classes are more similar to each other than other classes) (Hagen, 2003). For the purpose of spatial comparison, all maps were classified by grouping values to equally spaced bins. The spatial comparison was repeated at two spatial resolutions: 20 m and 100 m pixel size in order to identify how the scale of heterogeneity affects the comparability of the RS and the modelling approaches.

Similarity between the RS and the modelling approaches was expressed spatially (similarity maps) and by calculating the percentage of average similarity (a fuzzy equivalent of overall classification accuracy obtained from a confusion matrix). Moreover, both approaches were compared by using descriptive statistics and frequency distributions calculated for the entire image area, as well as for the individual land use (LU) classes. We used the Wilcoxon-Mann-Whitney U test ($p \leq 0.05$) to identify statistically significant differences between the approaches.

The LU classification, which served to compare the RS and the modelling approaches, was fully adopted from Lavorel et al. (2011). The classification is shown in Figure 5.1c. Seven types of grasslands were classified within the area covered by the AISA images. Three LU classes were located on terraces that have been cultivated previously: fertilized and mown terraces (LU1), non-fertilized but mown terraces (LU2), and unmown terraces but grazed in spring and autumn (LU3). Two LU classes were located on never cultivated permanent meadows: mown grasslands (LU4), and unmown grasslands but grazed in summer (LU5). Finally, one class covered alpine-grazed meadows at altitudes above 2000 m a.s.l (LU6) and the last class represented grasslands growing on steep and grazed slopes (LU7).

5.3 Results

5.3.1 Ecosystem properties: comparison of remote sensing and modelling approaches

The best empirical models for predicting ecosystem properties from RS data are summarized in Table 5.2. The best model for green biomass estimation was based on a narrow-band NDVI index, whereas SML provided the most accurate solution for other EP. Interestingly, PLS did not outperformed SML despite the fact some studies found PLS being more powerful than SML or vegetation indices (Cho et al., 2007; Darvishzadeh et al., 2008). The prediction accuracy of the RS-based empirical models was moderate and of a similar order to those obtained from the modelling approach (Lavorel et al., 2011). Green biomass was estimated with the lowest accuracy among all EP ($R^2 = 0.54$), which was lower than the modelling approach ($R^2 = 0.70$). The prediction accuracy of the litter mass model ($R^2 = 0.60$) was comparable to the modelling approach ($R^2 = 0.61$). The prediction accuracy of the

crude protein content model (R^2 = 0.97) was higher than from the modelling approach (R^2 = 0.62), but the reliability of the RS-based model is strongly reduced due to low degrees of freedom, which resulted into an over-adjusted model. The prediction accuracies of the species diversity model (R^2 = 0.60) as well as of soil carbon content (R^2 = 0.73) were higher than for the modelling approach (both achieving R^2 = 0.31). Additionally, Figure 5.3 shows scatter plots between measured and RS-predicted EP, indicating that estimated EP from RS had a comparable range as in-situ measured EP.

Resulting maps of EP from the RS (left panels) and the modelling (middle panels) approaches at 20 m spatial resolution are presented in Figure 5.4. The visual comparison between approaches emphasises spatial consistency and continuity of the RS approach, contrasting with the land-use based pattern underpinning the modelling approach. The RS approach was thus highly sensitive to fine scale heterogeneity, which could be captured thanks to the high spatial resolution of the RS images. Therefore, the variability of RS-based EP within individual LU classes was up to ten times higher than the variability of the modelling approach (Appendix A5).

In contrast to the modelling approach, none the RS-based maps of EP clearly captured a distinct difference between grasslands growing on previously cultivated terraces (LU1-3 located in the S-W part of the image area) and grasslands at permanent meadows (LU4-7 located in the N-E part of the image area). Statistical analyses revealed that for all LU classes the mean EP value from the RS approach was always significantly different from the modelling approach (Wilcoxon-Mann-Whitney U test, $p \leq 0.05$). For instance the modelling approach substantially over - estimating (resp. under-estimating) green biomass for LU1 and LU5 (resp. LU3, LU6, LU7), and over-estimating species diversity for all land use types except LU3 and LU5 as compared to the RS approach (Appendix A5).

The spatial comparison between RS and modelling approaches based on the fuzzy set theory (Figure 5.4) indicated that the average similarity was around 20% at the spatial resolution of 20 m. Crude protein content, for which there was the lowest number of in-situ samples to calibrate RS images, was the EP with the lowest spatial agreement between the approaches (average fuzzy similarity calculated for entire image area was only 16.6%). Species diversity was the EP with the highest spatial agreement between the approaches (average fuzzy similarity reached up to 22.4%). In classes LU2, LU3 and LU7 the average similarity reached about 25%, whereas in LU1 (mown-fertilized terraces) it was only about 8%. We also investigated similarity of RS and modelling approaches at the spatial resolution of 100 m and the average fuzzy similarity increased from 20% up to 40% at the 100 m resolution (Figure A7.1).

Table 5.2 Summary of the best regression models estimating ecosystem properties from the AISA remote sensing data. Abbreviations: normalized difference vegetation index (NDVI), stepwise multiple linear regression (SML), an AISA band centred at wavelength λ (B_λ), degrees of freedom (d.f.), coefficient of determination (R^2), and root mean square error of prediction relative to mean observed value (RMSEP).

Ecosystem property	Model type	Predictive equation	d.f.	R^2	RMSEP [%]
Green biomass	NDVI	Gbio = 578.598*NDVI + 355.328 NDVI = $(B_{682} - B_{2441}) / (B_{682} - B_{2441})$	15	0.54	15.9
Litter mass	SML	Litt = $0.158*B_{871} - 0.180*B_{1158} + 0.242*B_{2308} - 73.153$	14	0.60	28.0
Crude protein content	SML	CPC = $-0.3876*B_{2038} + 0.5639*B_{2346} + 34.085$	2	0.97	1.5
Species diversity	SML	SDiv = $7.945e^{-04} * B_{706} - 5.031e^{-04} *B_{2447} - 3.825e^{-02}$	14	0.60	8.0
Soil carbon content	SML	Soilc = $-7.135e^{-03} * B_{734} + 12.352e^{-03} * B_{1328} - 8.101e^{-03} * B_{1686} + 2.9167$	13	0.73	8.4

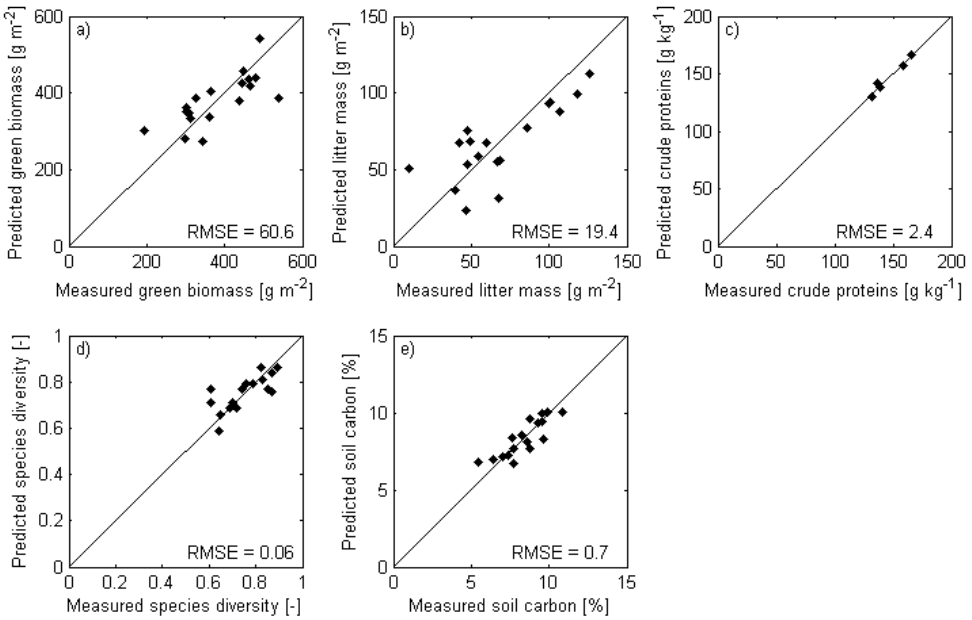

Figure 5.3 Comparison of in-situ measured and RS-predicted ecosystem properties: (a) green biomass [g m^{-2}], (b) litter mass [g m^{-2}], (c) crude protein content [g kg^{-1}], (d) species diversity [-], and (e) soil carbon content [%]. Predicted EP values represent here a mean value per plot calculated from pixels within a plot, which have green vegetation fraction > 25%. The solid line represents the one-to-one line.

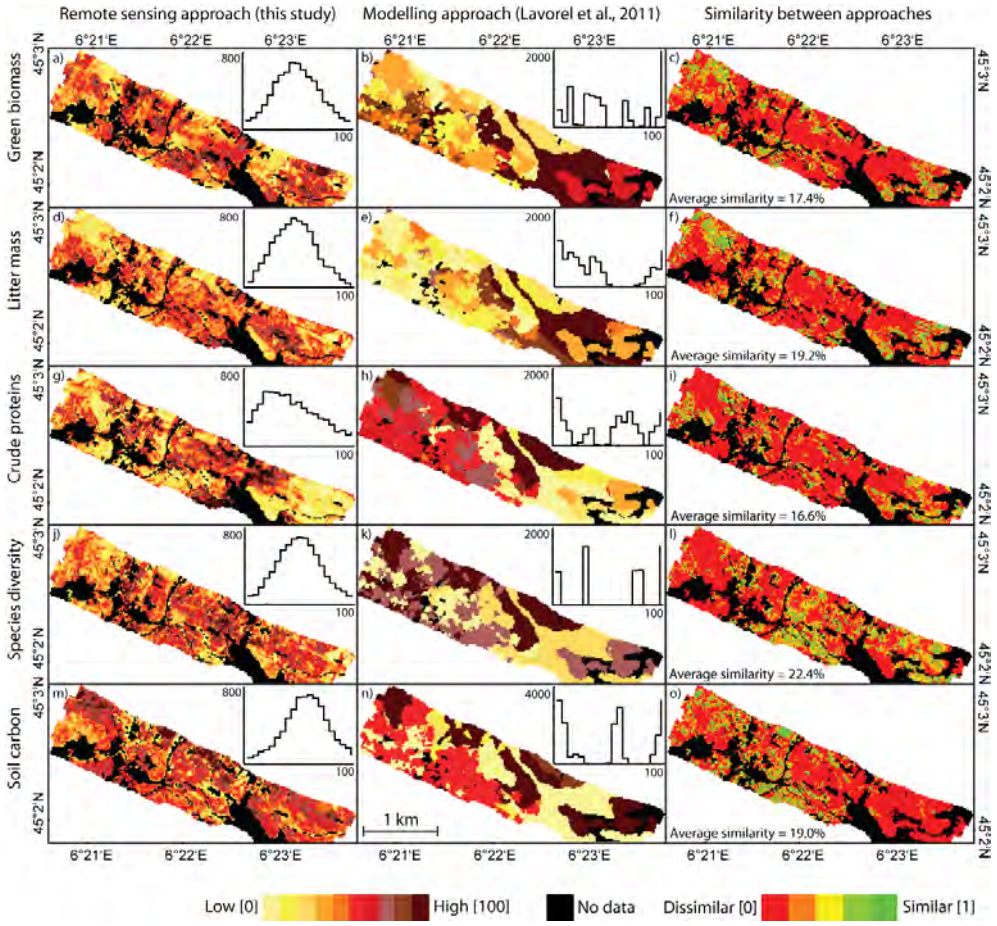

Figure 5.4 Ecosystem properties estimated from the remote sensing approach (this study) and from the modelling approach (Lavorel et al., 2011) at a spatial resolution of 20 m. The most right maps show similarity between remote sensing and modelling approach. Frequency histograms show the distribution of values within the image.

5.3.2 Ecosystem services: comparison of remote sensing and modelling approaches

Ecosystem services were calculated as simple linear combinations of ecosystem properties (Table 5.1). The agronomic ES was calculated as the sum of fodder quantity (green biomass) and fodder quality (crude proteins). The cultural ES was calculated as the difference of species diversity and litter mass. The climate regulation service through soil carbon sequestration was approximated by soil carbon content (therefore corresponding maps of the climate regulation service are presented only once in Figure 5.4m,n,o). Finally, total ES supply was calculated as the sum of

individual ES. Resulting maps of ES as derived from the RS (left panels) and the modelling (middle panels) approaches are presented in Figure 5.5.

The statistical analysis carried out at LU class level indicated that for almost all classes the mean ES value from the RS approach was significantly different from the modelling approach (Wilcoxon-Mann-Whitney U test, $p \leq 0.05$). In particular, the agronomic value was quite over-estimated (resp. under-estimated) by the modelling approach for LU1, LU2 and LU6 (resp. LU3 and LU7) as compared to the RS approach. The cultural value tended to be strongly over-estimated for all land use types except LU3 and especially LU5 (Appendix A6).

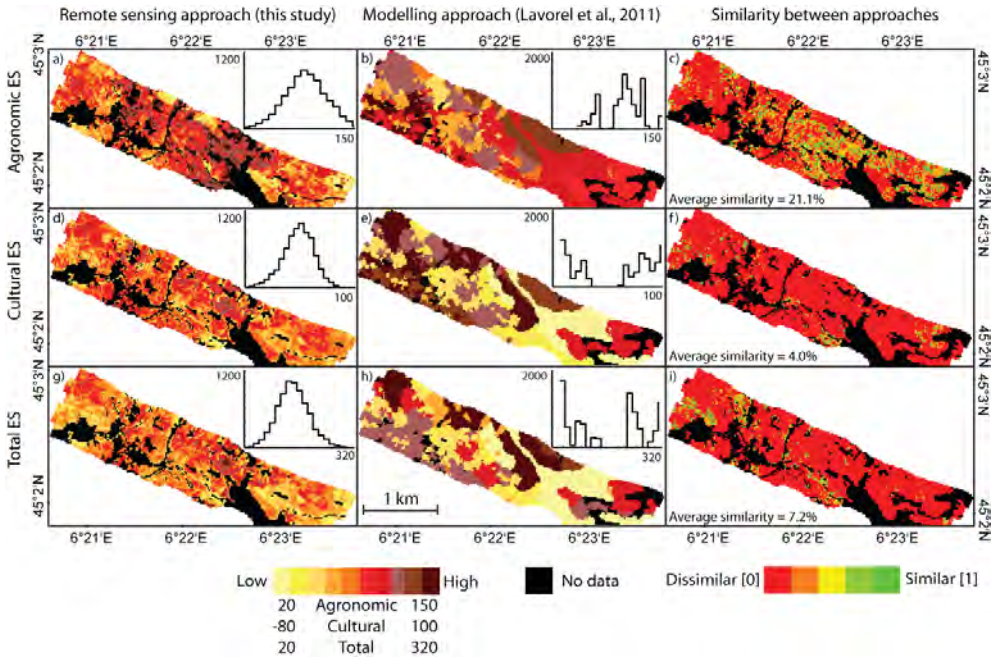

Figure 5.5 Ecosystem services estimated from the remote sensing approach (this study) and modelling approach (Lavorel et al., 2011) at a spatial resolution of 20 m. The most right maps show similarity between remote sensing and modelling approach. Frequency histograms show distribution of values within the image.

The spatial comparison between approaches based on the fuzzy set theory (Figure 5.5, right panels) indicated that the average similarity for the agronomic ES was around 20%, but for the cultural ES and the total ES it was less than 10%. Analogous to EP, LU classes with highest spatial agreement across ES were LU3 and LU7, where the average similarity reached about 20%. In LU1 (mown terraces) the spatial agreement was the lowest (about 2% only). At the spatial resolution of 100 m, the

average similarity increased up to 50% for agronomic ES and up to 30% for cultural and total ES compared to 20 m resolution (Figure A7.2).

Descriptive statistics for the total ecosystem service supply indicated that the modelling approach over-estimated (resp. under-estimated) total ES for LU1, LU2, LU 4 and LU6 (resp. LU3 and LU5) (Figure 5.6). Further spatial analysis of hot and cold spots of total ES supply (Figure 5.7) indicated that the area of hot/cold spots from the modelling approach was about double compared to the RS approach. The hot spots predicted by the RS approach appeared as a subset of those predicted by the modelling approach (40% overlap). This cannot be said about the cold spots of total ES supply, because only 17% of the RS-based cold spots overlapped with the modelling approach, and some different cold spots were predicted altogether. In general, the RS-based hot/cold spots were scattered, small patches across the study area, whereas the modelling approach identified the entirety of alpine grazed meadows (LU6) and unmown-grazed permanent meadows (LU5) as the hot spots and cold spots, respectively (Figure 5.7).

5.4 Discussion

5.4.1 Quality of empirical RS models of ecosystem properties

The major uncertainties of the empirical RS approach are related to RS, as well as in-situ data quality and representativeness. We minimized the uncertainties behind RS data by removing noisy bands and pixels with low vegetation signal, but uncertainties originating from atmospheric and topographic corrections remain. It is beyond the scope of this work to investigate their effects on the EP estimates. Therefore, we focus our discussion on uncertainties associated with in-situ EP measurements carried out at plot scale, and their matching to RS images.

Broad variability in EP was captured by stratifying field sampling plots according to land use and altitude (Lavorel et al., 2011). In this way, a small scale heterogeneity resulting in spectral variability within the image, for instance due to variability in soils and microclimatic conditions, was not fully captured. Analysis of the spectral representativeness of field plots indicated that about 25% of the pixels were outside the spectral range covered by the calibration dataset. Moreover, some field plots had to be removed, because they were located at areas with low green vegetation signal, due to mowing or grazing at the time of the RS campaign. This step negatively influenced mainly the litter mass model, because the plots that were removed had also higher values of litter mass (especially in LU5) and therefore the calibration range was reduced. Furthermore, there is always a risk that, by the nature of SLM, statistical model may be over-fitted to specific data points, and may therefore introduce prediction errors, especially for pixels outside of the calibration range.

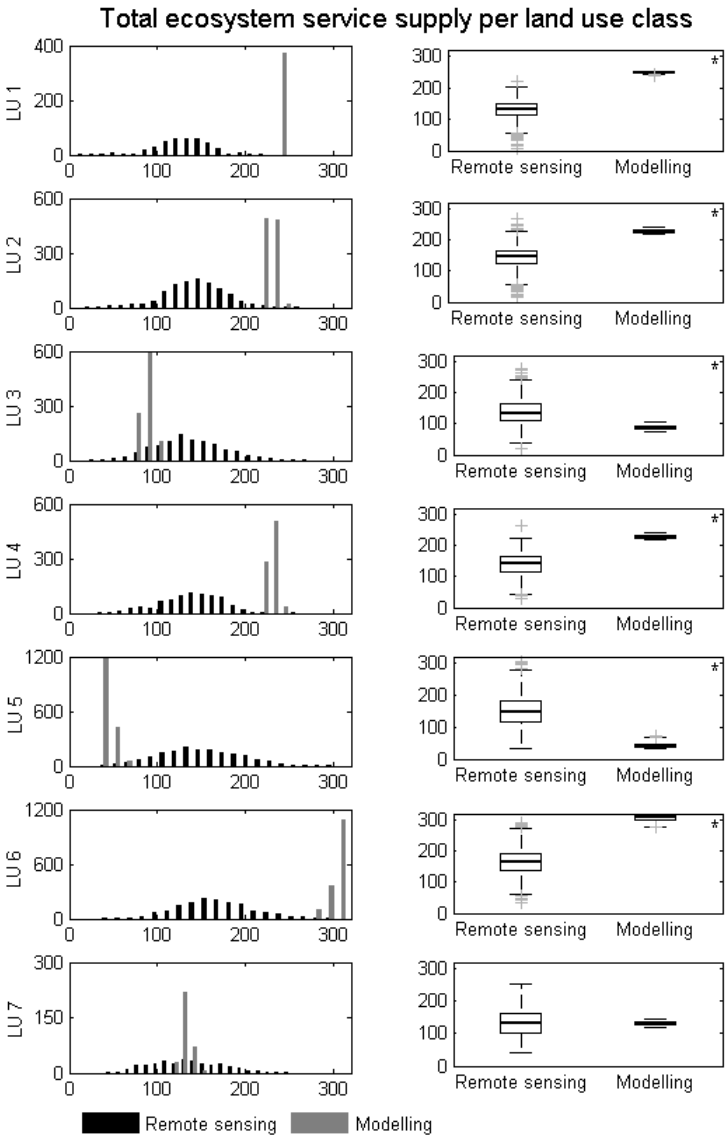

Figure 5.6 Comparison of remote sensing approach (this study) and modelling approach (Lavorel et al., 2011) to estimate total ecosystem service supply per land use class. The left panels show frequency distribution of the total ecosystem service. The right panels show boxplots, where central line in a box is median, box height is interquartile range representing 50% of the data, whiskers are minimum and maximum unless the observed values exceeded 1.5 times the interquartile range and in that case they are marked with crosses as outliers. The star symbol indicates that differences in median values between two approaches are significant ($p \leq 0.05$, Wilcoxon - Mann-Whitney U test).

Probably the strongest factor negatively influencing the quality of the RS empirical models was an asynchronous acquisition of in-situ EP data and RS images. In-situ EP data were collected between years 2004 and 2009, which smoothened variability among the vegetation seasons. In contrast, RS images represent one snapshot in time capturing the actual ecophysiological and development stage of grasslands during the second half of July 2008, which can not exactly be compared with inter-annual mean in-situ EP data (although 2008 appeared to be representative of an average year – Lavorel and Grigulis, 2013, unpublished data). Further, the date of RS acquisition was not optimal as compared to vegetation phenology and agricultural use. A good example that illustrates the temporal disparity is green biomass estimation in unmown-grazed summer meadows (LU5). Average green biomass value in this LU class was the highest for the modelling approach, but the lowest for the RS approach. This can be attributed to a large proportion of grassland pixels that were grazed at the date of RS acquisition, whereas the modelling approach was based on peak biomass measurements prior to mowing or grazing (first half of July). Likewise, in-situ crude protein content was estimated at peak vegetative growth in the middle of June, where differentiation among vegetation types is known to be greatest, whereas the later date for RS measurement resulted both in an average lower value (more advanced phenology) and a convergence among vegetation types (Duru, 1997). We can assume that both green biomass and crude protein content are the most dynamic EP within and between years and can be highly sensitive to disturbances such as drought in 2004 or vole outbreaks in 2009 – 2010.

5.4.2 Alternative RS solutions for ecosystem properties estimation

There are clear limitations and uncertainties behind the RS-based models of EP in this study. Being aware of them, still RS holds strong potential for EP mapping. We restricted our work to empirical approaches applied on airborne RS data, but there is large variety of other types of RS data and methods. Those might provide more suitable solutions to predict currently investigated or other EP, as well as some plant traits (Homolová et al., 2013b).

Green biomass and litter mass can be possibly related to the results of spectral unmixing, which allows subdividing the mixed nature of the spectral information into relative fractions of soil, photosynthetic vegetation (PV) and non-photosynthetic vegetation (NPV) (Asner et al., 2005; Roberts et al., 1993). We found a positive correlation between in-situ measurements on green biomass and the PV fraction ($r = 0.57$, results not shown), and between litter mass and the NPV fraction ($r = 0.81$, results not shown). This finding and similar patterns found by Numata et al. (2007) encourage a hypothesis that PV and NPV fractions can serve as proxies for green and dry vegetation biomass, respectively.

Crude protein content is essentially proportional to nitrogen content and a moderately strong relationship exists between nitrogen and chlorophyll content (Homolová et al., 2013b). Chlorophyll content is one of the vegetation properties that nowadays can be estimated from RS with high fidelity using a variety of chlorophyll-sensitive vegetation indices (Gitelson et al., 2006; Sims and Gamon, 2003) and physical retrieval methods based on radiative transfer modelling (Jacquemoud et al., 2009; Malenovský et al., 2013; Zhang et al., 2008).

In the case of species diversity, some authors suggested to approximate it by indicators of spectral heterogeneity derived from RS images (Rocchini, 2007; Rocchini et al., 2010). However, reported relationships between species and spectral diversity were moderately strong (r between 0.4 and 0.7) and usually found for data at a spatial resolution in the order of tens of meters (Rocchini, 2007). Therefore, this approach would be more suitable for areas with higher heterogeneity in land cover and for a larger scale assessment.

Mapping of soil properties is in general difficult in areas covered by vegetation (Bartholomeus et al., 2011). Some studies suggested that soil carbon content correlates with other vegetation properties such as leaf area index or canopy height (Li et al., 2010), but screening of our in-situ data did not indicate any significant relationship with measured plant traits or EP (results not shown). Here, soil carbon content was used as a proxy for the carbon sequestration service, given that in such mountain grasslands aboveground biomass senesces and largely decompose every year, RS based solutions that directly estimate carbon stocks sequestered by vegetation, i.e. primary productivity (Running et al., 2004; Zhao et al., 2005), may be considered for other types of ecosystems such as forests. Maps of primary productivity are delivered globally with a typical spatial resolution of 1 km, which is less suitable for local studies, but a large scale assessment of ecosystem carbon sequestration services can certainly benefit from it. Preferably still, RS data can also serve as an input into ecosystem models predicting carbon stocks (Porfirio et al., 2010).

Lastly, an important contribution of RS data is to update existing land use or land cover maps, which are often used as underlying spatial information for ES assessment (Eigenbrod et al., 2010; Metzger et al., 2006), and are highly dynamic (Verburg et al., 2009).

5.4.3 Assessing ecosystem services from RS data

The scheme combing the underlying EP of subalpine grasslands into ES was based on social evaluation as perceived by local stakeholders (Lamarque et al., 2011; Quétier et al., 2010). This makes it very specific for the actual study area, but we can assume that the scheme can be smoothly transferred to other subalpine regions with similar landscape management and ES demand (Lamarque et al., 2011). However, its applicability to more diverse landscapes needs to be further tested.

In general, little agreement was found between the approaches for the total ES supply (Figures 5.5i and 5.6). The hot spot analysis indicated more overlaps between the approaches for hot spots than for cold spots. The modelling approach clearly identified alpine grazed meadows (LU6) as ES hot spots. These grasslands provided a synergy between high species diversity, soil carbon and crude protein content and low litter mass. The cold spots were associated to unmown-grazed permanent meadows (LU5). These meadows exhibited high values for litter mass and green biomass and lower values for the three other EP.

The RS-based hot/cold spots were small scattered patches across the study area, rather than extensive patches associated with specific land use types. This contraction reflected the decrease in contrast among land uses in the RS as compared to the modelling approach (Appendix A6). The RS-based hot spots, similar to the modelling approach, were mainly associated with areas where high species diversity, high soil carbon and low litter mass were estimated from RS images. Moreover, they appeared to be a small subset of the hot spots identified by the modelling approach. In contrast, many RS-based cold spots could be associated to the combination of high litter mass and low values for all other EP, which was analogous to the modelling approach. The RS-based cold spots correspond well to pixels with lower vegetation fraction and are often scattered around roads and terrace banks, but they exhibited a small spatial overlap with the modelling approach.

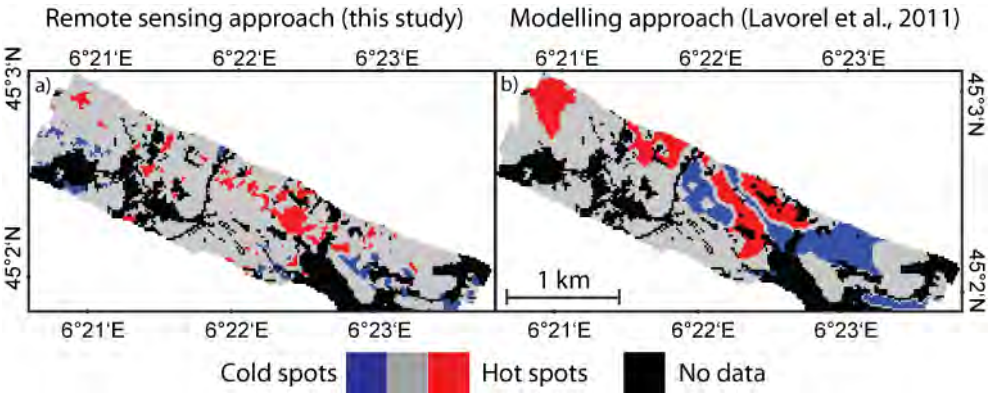

Figure 5.7 Location of hot spots and cold spots of the total ecosystem service supply in subalpine grasslands as derived by the remote sensing (b) and the modelling (b) approaches at a spatial resolution of 20 m.

5.4.4 Comparison of remote sensing and modelling approaches

The visual comparison of EP as well as ES at the spatial resolution of 20 m (cf. left and right panels in Figures 5.4 and 5.5 respectively) contrasted the spatial consistency and continuity of the RS approach with the land-used based pattern of the modelling approach. Indeed, in the modelling approach plant traits and abiotic variables incorporated into EP models were modelled themselves based on LU (Lavorel et al., 2011). Although the plant trait inputs of EP models provided additional information on the variability within single LU classes (Lavorel et al., 2011), still the variability was lower than in the RS approach. Moreover, the current LU classification accounts for broad classes of past and present land use (Quétier et al., 2007b), but the field sampling design did not capture finer variations within the classes resulting from specific land use history, and especially time since last mowing. Indeed, complementary sampling revealed that in particular within LU classes with grazing on former hay meadows (LU3, LU5), there was a significant effect of the date of mowing cessation, which influenced plant functional composition and associated EP such as green biomass, litter mass and species diversity (Caubet, 2009). Conversely, the sub-meter spatial resolution of the original RS images caused EP models to be sensitive to small scale variations driven by local topography, soils (esp. soil depth) and microclimatic conditions. In general, a higher spatial similarity between the approaches was found in those areas, where RS-based EP maps appear to be more homogeneous suggesting that these areas must have been spectrally homogeneous too.

Advantages and disadvantages of both approaches to quantify EP and consequently ES are closely related to attributes of in-situ measurements, as well as of underlying spatial data, which are related to spatial and temporal domains. The advantages/disadvantages are summarized in Table 5.3 and further discussed in following sections.

The spatial resolution of underlying spatial data plays an important role in assessment of ES. A coarser spatial resolution of the modelling approach (20 m) did not fully reflect spatial heterogeneity within the study area as it was discussed earlier. Moreover, it might have easily included non-vegetated areas assigning them an unrealistic value or left out small vegetation patches with high ES supply. Di Sabatino et al. (2013) demonstrated that land cover data at a spatial resolution of 20 to 30 m can still significantly underestimate total area of highly fragmented ecosystems such as water bodies. The high spatial resolution of RS data helped to eliminate non-vegetated areas, which usually have low EP and thereby ES values. Small-scale case studies like this one can certainly benefit from the high spatial resolution of airborne RS, but it is less applicable for larger scale studies. Satellite RS instruments that provide a good compromise between spectral and spatial resolutions (e.g., Landsat or Sentinel-2) still acquire data at a spatial resolution

between 10 and 60 m. Therefore, fusion of RS data of different spatial and spectral resolutions (Malenovský et al., 2007) can enhance spatial precision of ES mapping at large scales.

Table 5.3 Overview of advantages (+) and disadvantages (−) of the RS approach (this study) and the modelling approach (Lavorel et al., 2011) for assessment of ecosystem properties and services in subalpine grasslands.

	Remote sensing approach	Plant trait-based modelling approach
Input spatial data	(+) Higher spatial resolution from RS images Digital elevation model	(−) Coarser spatial resolution from Land use map Digital elevation model
Input field data	(+) Less field data needed (ecosystem properties) (+) Number of data can be reduced by employing physically-based RS retrieval methods (−) Measurement date needs to be close to RS acquisition	(−) More field data needed (plant traits, soil properties and ecosystem properties)
Input data pre-processing	(−) More data processing needed Laboratory analysis of field samples and radiometric, geometric, atmospheric corrections of RS images	(+) Less data processing needed Laboratory analysis of field samples only
Spatial domain	Determined by RS images, but (+) RS can be flexible on acquiring images at different spatial resolutions	Determined by land use map
Temporal domain	(−) Highly dependent on RS acquisition date, but (+) RS offers high multi-temporal flexibility, but (−) additional field data reflecting temporal variability are required	(+) Time independent (average), but (−) field data collection required during several vegetation seasons
Model transferability	(−) Limited transferability of empirical EP models to other sites, but (+) possibility of employing physically-based retrieval methods increases the universality	(+) Transferability of empirical trait-based EP models to other similar (e.g. grassland) sites

Both approaches addressed a temporal aspect of the analysis differently. As discussed earlier, the modelling approach is less dependent on inter-annual variability, because in-situ measurements of plant traits and EP were averaged across several vegetation seasons. Moreover, the underlying spatial information from the

LU classification is almost time independent as it reflects current and past land use management. In contrast, results of the RS approach are time specific, because a single snapshot of RS images reflects a particular development stage of vegetation and actual management activities. The RS approach is thus less generic than the modelling approach, but can in principle be extended to multi-temporal RS observations allowing long term monitoring and change detection of ES. Multi-temporal RS observations also potentially enable the incorporation of important intra-seasonally variable parameters such as phenology, which are important components of some ES (Lavorel et al., 2011).

The nature of the underlying spatial data to model EP differed between the approaches. The modelling approach builds only on two spatially explicit, independent landscape input variables (land use and elevation maps). These were used to predict the spatial distribution of all other abiotic and plant trait variables that further entered into EP models. In contrast, RS images offered initially 240 spectral bands, but these can be strongly correlated. The real spectral dimensionality of a single view imaging spectroscopy image varies between 3 and 12 (Laurent et al., 2011a; Verhoef, 2007), meaning that 3 to 12 vegetation properties can be retrieved.

The RS approach allowed skipping one important step of the modelling approach, in which plant traits and abiotic properties were estimated from LU and elevation maps. This step reduced the number of in-situ measurements by eliminating data on plant traits and abiotic properties. Nevertheless, in-situ measurements of EP will still remain a limiting factor for large scale and long term applications. The RS approach, on one hand, minimized propagation of errors related to the quality and a spatial resolution of the input in-situ and spatial (LU and elevation) data, but on the other hand it introduced other types of errors inherent to RS images and image processing (e.g. topographic and atmospheric corrections). Recent studies indicated that it is possible to retrieve some vegetation properties from top-of-atmosphere radiance data (Laurent et al., 2011b) reducing therefore uncertainties from atmospheric corrections.

A big disadvantage of the RS empirical methods is that transferability of regression equations to other test sites with different vegetation types or to other RS sensors is usually very limited (Asner et al., 2003; Colombo et al., 2003; Grossman et al., 1996). Similar constraints apply to some extent to the modelling approach, although trait based models provide robust inter-site predictions of EP (Fortunel et al., 2009). Luckily, RS offers also more universal solutions based on physical radiative transfer models, though their retrieval capacity is strictly limited to vegetation properties influencing the canopy radiation regime, e.g. leaf area index, chlorophyll content, water content (Baret and Buis, 2008; Colombo et al., 2008; Jacquemoud et al., 2009; Schlerf et al., 2005; Zarco-Tejada et al., 2004).

5.5 Conclusions

In this case study, we tested high spatial and spectral resolution RS data for the spatial assessment of ecosystem properties (EP) and multiple ecosystem services (ES) in subalpine grasslands. Furthermore, the RS-derived maps of EP and ES were compared with results of the plant trait-based modelling approach (Lavorel et al., 2011), which predicted EP using general linear models combining maps of land use, abiotic variables and plant traits. The prediction accuracy of the RS-based empirical EP models was good (R^2 = 0.54 – 0.73) and it was similar or better than those obtained from the modelling approach.

The average similarity between the RS and the modelling approaches at the 20 m spatial resolution varied between 16 and 22% for individual EP and for the total ecosystem service supply it was only around 7%. However, the spatial agreement increased by about 20 percentage points when increasing pixel size from 20 to 100 m, showing that some of the discrepancies among approaches resulted from their differences in intrinsic spatial resolution. Despite the fact that we found similarities in the bundles of EP underpinning the total ES in both approaches, the exact location differed as the RS-based hot/cold spots were smaller scattered patches within the study area, owing to decreased variability in EP within land use types in the RS as compared to the modelling approach. Overall, while the RS-based hot spots were a small subset of the hot spots identified by the modelling approach, for cold spots there was limited spatial overlap.

RS-based maps provided more detailed insight into the fine-scale spatial distribution of EP and thereby ES, although to some extent they might be oversensitive to small scale heterogeneity. RS results exhibited about ten times higher variability within individual LU classes than the modelling approach, which reflected by construction the underlying LU classification.

We are aware of the limitations of the RS approach presented in this study, which mainly originated from the asynchronous acquisition of RS and in-situ data, both in terms of specific year, and especially of timing within the vegetation season. But without any objective reference, it is hard to decide which of the two approaches is better, as both are imperfect assessments of a reality and both having their advantages and disadvantages. The underlying spatial data, RS images for the RS approach and LU map for the modelling approach, are the major source of the discrepancies between the two approaches. Therefore an approach that combines RS images, LU and elevation maps with in-situ EP data would probably the best compromise for accurate spatial assessment of multiple ES supplied by subalpine grasslands.

In general, future research should look for reliable links between ES and RS proxies. This will require more case studies, where RS and ES data (and EP determining ES) are acquired and analyzed together. The assessment of ES can already benefit from those vegetation properties that can be estimated from RS with

higher accuracy and for which RS methods are well established, e.g. chlorophyll content, leaf area index, fraction of absorbed photosynthetically active radiation, fractional vegetation cover. Besides the spatial and spectral domains of RS data that were explored in this study, future assessment of ES should also consider multi-temporal and multi-directional RS observations.

Acknowledgements

This work was supported by the European Commission 6th Framework Program project Ecochange (FP6-2006-GOCE-036866), ERA-Net BiodivERsA project VITAL, and contribute to EU FP7 project OPERAs (FP7-ENV-2012-308393). We thank Zbyněk Malenovský for his help with the AISA data acquisition and processing, Lucia Yáñez Rausell and the LECA team for field data collection, Daniel Wiedemeier and Parviz Fatehi for valuable advice on statistics.

6

Synthesis

6.1 Main results

Remote sensing of vegetation is a broad research field, where a lot of progress has been made in the last three decades. However, the complexity of interactions between vegetation and solar radiation, which are being constantly modulated by environmental factors, offers room for deeper investigation. Rather than solving one big research problem, this thesis builds a few bridges on a way leading to a better understanding of using imaging spectroscopy for ecologically driven applications in heterogeneous ecosystems (temperate coniferous forests and subalpine grasslands).The theoretical part of this thesis presented in Chapter 2 contributes to a critical evaluation of research achievements and challenges in RS of plant traits and encourages better communication between plant ecology and RS research communities. The applied part of this thesis contributes to improve our understanding of the structural and biochemical complexity in Norway spruce canopies (Chapters 3 and 4) and increases our knowledge of using imaging spectroscopy to assess ecosystem properties and capacity of subalpine grasslands in providing ecosystem services (Chapter 5). The work was performed at three plant hierarchical levels: the level of individual leaves (Chapter 3), plants (Chapter 4) and entire canopies (Chapter 5).

In this section, the main research questions of this thesis, which are elaborated in the core Chapters 2 – 5, are revisited and followed by a discussion on the main results.

1. What is the current state-of-the-art in using optical remote sensing for estimation of key plant traits used widely in plant ecology research?

Plant traits are widely used in plant ecology to understand the response of plants to various environmental pressures (e.g. climate change) and the effect of plants on ecosystem processes (e.g. biogeochemical cycles). Recent evidences are that plant ecologists agree on a set of key plant traits, which are relatively easy to measure in-situ and have a strong predictive response to ecosystem functions (Cornelissen et al., 2003). In-situ measurements do not allow spatially explicit and large scale mapping of key plant traits and therefore remote sensing based approaches are of great interest to the plant ecology community. In Chapter 2 the major achievements and challenges in RS estimation of key plant traits were reviewed. Our discussion was limited to eight traits with strongest potential to be mapped using RS (plant growth and life forms, flammability properties, photosynthetic pathways and photosynthesis activity, plant height, leaf lifespan and phenology, specific leaf area, leaf nitrogen and phosphorous).

Abilities to map plant traits using RS are constantly improving due to technological advancements. Nowadays, RS offers a large spectrum of data with different spatial, spectral and temporal resolutions, and image interpretation methods. Passive optical imaging spectroradiometers facilitate better mapping of traits related to leaf biochemistry and phenology. Multidirectional optical RS and active RS systems (laser scanners and radars) recently have gained more attention for their ability to describe traits related to the vegetation structure.

Classification techniques are common methods used to transfer RS data into thematic classes. However, they cannot be applied to all plant categorical traits, because not all underlying attributes of these traits show a clear response in RS data. For example, mapping of plant growth forms, which is determined by plant structure and phenology, cannot be fully resolved by RS, because some categories are spectrally too similar to be distinguished. Also individual attributes underlying a composed plant flammability trait cannot be resolved using RS, but there are many operational fire monitoring schemes that use RS data to assess combustibility of entire plant communities. RS of C3 and C4 photosynthetic pathways remains rare, but there is an intensive on-going RS research of global plant photosynthesis activity using proxies of fraction of absorbed photosynthetic radiation and light use efficiency.

Quantitative retrieval of continuous plant traits from RS is possible though not always straight forward. Plant height trait can be directly derived from laser scanning data achieving good accuracies (error of height estimation is usually below 10% of the mean canopy value for tall forest canopies, and up to 20% in lower canopies). Leaf phenology trait can be related to only four remotely sensed indicators (start, end, maximum peak and duration of the vegetation season) that can be retrieved from multi-temporal RS data of those canopies that periodically change their foliar apparatus. The spatial and temporal accuracy of these indicators is clearly related to the type of RS data with a typical spatial resolution ranging from 0.25 to 8 km and biweekly acquisition frequency.

Biochemical traits, phosphorus and nitrogen, can be retrieved quantitatively from optical RS data achieving moderately good accuracies (error of nitrogen estimation is around 15% of a mean canopy value, and 25% for phosphorus estimation). Both traits can be retrieved using empirical methods relying on a limited set of in-situ trait measurements. The reason which prevents them to be retrieved independently from in-situ data using physical methods based on radiative transfer modelling is that their weak absorption features are often masked by the spectral effects of leaf water and canopy structure. Similarly, the same confounding effects negatively influence retrievals of specific leaf area, the only biochemical trait from the reviewed key traits that can be estimated using physical retrieval methods. Despite this possibility the accuracy is highly variable and generally the lowest one from all reviewed biochemical traits (estimation error was around 45% of a mean canopy value). In

order to remove major inconsistencies in retrievals of leaf biochemical traits improved algorithms that effectively suppress the negative influence of water absorption (Ramoelo et al., 2011) and canopy structure (Knyazikhin et al., 2012) are needed.

Despite the fact that the discussion in Chapter 2 was limited to eight key plant traits mainly, some general findings irrespective from individual traits can be given. Both plant ecology and RS research fields face problems in using clear and standardized terminology. Although each research community puts efforts to standardize the terminology and improve communication within the field, remaining inconsistencies partly prevent successful integration of RS with plant ecology research. Another challenge common to both research fields is spatial scaling. The pixel size of RS images can vary from less than a meter to several kilometres, which is not always compatible with the spatial scale of in-situ trait measurements and trait-based analysis. Therefore, scaling schemes have to be applied on RS data (Malenovský et al., 2007) or in-situ trait measurements (Violle et al., 2007) prior to any RS-based analysis of plant traits.

The applicability of optical RS methods, however, goes beyond the eight key traits discussed in Chapter 2. Several well-established and thoughtfully validated RS-based plant traits and vegetation properties can support or even extend the current collection of key plant traits used in ecology (e.g., leaf chlorophyll and water content, leaf area index, fraction of absorbed photosynthetic radiation, and fractional vegetation cover). However, at the moment these are not considered key traits by the ecology community.

Recent developments in RS indicate that multiple trait mapping becomes possible when using combined retrieval schemes based on radiative transfer modelling that are optimized using spectral, spatial and directional domains simultaneously (Laurent et al., 2011). Also combination of data from multiple RS instruments (Asner et al., 2012; Cartus et al., 2012) is becoming more common and promising for complex vegetation studies and multiple trait mapping.

2. What is the variability of total-to-projected leaf area ratio of Norway spruce needles and what is the implication for remote sensing based estimates of crown averaged biochemical properties?

Plant ecologists recognize leaf area as one of the key plant traits, though it was not discussed in Chapter 2 as RS is not able to deliver this leaf trait. RS solutions are limited to estimation of leaf area index – a canopy property expressing total leaf area within a canopy per unit of land surface. Precise knowledge of total leaf area (LA_T) is required for vegetation photosynthesis and gas exchange related studies, as it is common to express photosynthesis rate or biochemical properties at leaf area basis. Moreover, RS methods estimating leaf biochemical traits often rely on in-situ

measurements that are usually expressed on leaf area basis too. In-situ measurement of LA_T is challenging for coniferous species due to their non-flat shape of needles. Therefore, the goal of Chapter 3 was to evaluate different laboratory methods to estimate LA_T of Norway spruce needles, to investigate the variability of the total-to-projected leaf area ratio (CF) within spruce canopies, and to explore the influence of an LA_T estimation error with respect to remotely sensed average crown chlorophyll content. In order to address these three goals a unique dataset of 270 spruce needle samples (from three needle age-classes, three canopy vertical levels and two spruce stands of different age and structure) were analyzed.

Total leaf area of spruce needles was estimated using six methods based on different geometrical models approximating a needle shape – one newly proposed and five existing ones. The new complex geometrical model proposed in this study provided accurate estimates of LA_T (RMSE < 5% of the average total leaf area), but a comparable accuracy was achieved using a simpler model. Therefore, the simpler parallelepiped model can be considered as more suitable for operational use in eco-physiology and RS research of leaf biochemistry. Other needle models that suggested an elliptic approximation of a needle shape underestimated LA_T by up to 60% and therefore were not suitable for spruce LA_T estimation.

High variability in the ratio of total-to-projected leaf area (CF) within spruce crowns was detected. Neither the age of the needles nor the age of the forest stand influenced the variability in CF significantly. The main source of variability in CF originated from the vertical sampling position. The highest CF of about 3.8 (close to square shaped needles) was found in the uppermost canopy layer and CF decreased to 2.5 (close to flat needles) in lower canopy layers. This result has an important implication for future sampling designs in spruce canopies; needle samples for LA_T measurements can be taken irrespective of their age (a mixed sample of several needle age classes), but shall be taken from several vertical canopy layers.

An example of estimating leaf chlorophyll content (C_{ab}) was taken to evaluate the impact of LA_T on crown averaged biochemical properties. The LA_T estimation methods themselves had a significant impact on crown averaged C_{ab}. Furthermore, crown averaged C_{ab} normalized to LA_T exponentially decreased with steadily increasing CF from two to four. Errors in crown C_{ab} associated with biased CF varied between 2 and 25 $\mu g\ cm^{-2}$. Considering that the realistic range of crown C_{ab} varies between 20 and 100 $\mu g\ cm^{-2}$, the error associated with a biased CF can reach up to 30% of the expected C_{ab} range.

The results of Chapter 3 suggested that more attention is needed for the accurate estimation of total leaf area when upscaling leaf level measurements of chlorophyll content to the level of entire crowns or canopies. This motivated us to develop a sophisticated upscaling scheme, which was applied in Chapter 4, to validate maps of chlorophyll content derived from airborne imaging spectroscopy.

3. What is the potential use of the continuum removal transformation for quantitative mapping of chlorophyll content of Norway spruce crowns using airborne data and radiative transfer modelling?

Continuous spectral data acquired by airborne imaging spectroradiometers provide enhanced possibilities to quantify leaf biochemical properties by investigating changes in the spectral continuum rather than in individual spectral bands. Therefore, the goal of Chapter 4 was to test the continuum removal (CR) transformation, a technique which enhances and normalizes spectrally contiguous absorption features, for estimation of leaf chlorophyll content (C_{ab}) in Norway spruce crowns. High spectral and spatial resolution airborne data allowed precise location of a C_{ab} absorption feature in the red part of the electromagnetic spectrum and accurate spatial delineation of individual sunlit crowns to strengthen the remotely sensed signal. The 3D canopy radiative transfer model DART coupled with the leaf-level model PROSPECT was used to simulate a database of canopy reflectance signatures in the region of the strongest C_{ab} absorption (between 650 and 720 nm) by altering the main model parameters (C_{ab}, leaf area index, canopy cover). This database was used to assess the sensitivity of CR spectra to C_{ab} variations and to evaluate perturbing effects of canopy structure.

Sensitivity analysis of CR spectra to C_{ab} revealed that area integrated under CR curve between 650 and 720 nm was exponentially related to C_{ab} and showed saturation for $C_{ab} > 40$ µg cm^{-2}. However, when the area integrated under CR curve was normalized to the CR band depth at 670 nm, the relationship to C_{ab} became significantly stronger and nearly linear. This result motivated us to formulate a new C_{ab} sensitive vegetation index called 'Area under continuum removed curve Normalized to the Chlorophyll absorption Band depth between 650 and 720 nm' ($ANCB_{650\text{-}720}$).

Validation against in-situ measured crown C_{ab} and cross-comparison of $ANCB_{650\text{-}720}$ with four other retrieval methods (artificial neural networks applied on CR spectra and three vegetation indices) revealed superior performance of the two CR-based methods compared to simple vegetation indices constructed from a few narrow bands. Although both CR-based retrieval methods exhibited similar accuracy, the $ANCB_{650\text{-}720}$ index is much faster to be implemented than the demanding training of a neural network.

The error associated with C_{ab} prediction using the $ANCB_{650\text{-}720}$ was similar or even lower as compared to other RS studies estimating C_{ab} of coniferous canopies using airborne imaging spectroscopy. Although one could object that our CR-based index was developed for conifers trees only, the robustness of the method was further evaluated using radiative transfer model simulations for broadleaf forest and grassland canopies. In both canopies, the predictive power of $ANCB_{650\text{-}720}$ was the strongest compared to the other three vegetation indices. Another potential limitation of the CR-based method is that it was applied on sunlit crown pixels, which could be

indentified thanks to the high spatial resolution of the RS images. However, additional analysis using radiative transfer model simulations confirmed that also shaded crown pixels convey a similar information content as sunlit pixels and therefore one can argue that $ANCB_{650-720}$ can be applied to a full crown spectrum.

The case study presented in Chapter 4 confirmed that the continuum removal technique applied to high spectral and spatial airborne imaging spectroscopy data is a powerful technique to estimate chlorophyll content in structurally complex forest canopies. The newly developed vegetation index based on CR – $ANCB_{650-720}$ index – is easy to implement, sensitive to broad variations in C_{ab} content, independent of leaf area index and for higher C_{ab} values also independent of leaf angle distribution variations. Its robustness was tested on simulated spectral data and in future it shall be expanded to real canopies using real imaging spectroscopy data.

4. What is the potential of airborne imaging spectroscopy to map ecosystem properties and services in subalpine grasslands in comparison with a plant trait-based modelling approach?

The concept of ecosystem services (ES) has become a widely investigated topic, because it presents a way to quantify, analyze and manage benefits that humans obtain from ecosystems. A challenge in ES mapping is lack of primary data on ES and therefore it is common to use proxies such as ecosystem properties (EP), environmental variables, land use and land cover maps, which are linked to ES and, at the same time, easier to obtain. In Chapter 5, a case study on ES mapping in subalpine grasslands using airborne imaging spectroscopy data was presented. RS images were used to derive five ecosystem properties (green biomass, litter mass, crude protein content, species diversity and soil carbon content) using empirical retrieval methods. Agronomic, cultural and total ES supplies of the subalpine grasslands were calculated as simple linear combinations of the underlying EP. Moreover, the RS approach was compared with the plant trait-based modelling approach presented by Lavorel et al. (2011), who estimated the underlying EP using a land use map, abiotic factors and plant trait data.

The best empirical models for predicting EP from RS images were based on a narrow-band NDVI index for green biomass, whereas stepwise linear regression models provided the most accurate solution for other EP. The prediction accuracy was good, R^2 ranged from 0.54 for the green biomass up to 0.73 for the soil carbon content model, which was similar to those obtained from the modelling approach. The major uncertainties of the RS-based models were related to the in-situ measured EP and how well they represented spectral variability and to the vegetation status captured by RS images. We found out that about 25% of the image pixels were outside the spectral range covered by the calibration dataset, which might introduce prediction errors. Probably the strongest factor negatively influencing the quality of

the RS empirical models was an asynchronous acquisition of EP data and RS images, both in terms of specific year, and especially of timing within the vegetation season. In-situ data on EP were collected between 2004 and 2009, which smoothened variability among the vegetation seasons. In contrast, RS images captured the actual development stage of subalpine grasslands in late summer 2008.

Visual comparison of EP and ES contrasted the spatial consistency and continuity of the RS approach with the land-use (LU) based pattern of the modelling approach. The RS approach was sensitive to fine scale heterogeneity, which could be captured thanks to the high spatial resolution of the RS images. Therefore, the variability of RS-based EP within individual LU classes was up to ten times higher than the variability from the modelling approach, where plant traits and abiotic variables incorporated into EP models were modelled themselves based on LU. Quantitative comparison using a fuzzy set theory indicated that the average similarity between the two approaches varied between 16 and 22%. The average similarity for the agronomic service was around 20%, but for the cultural and total ES it was below 10%. The spatial agreement between the two approaches significantly increased when the level of spatial aggregation increased from 20 m to 100 m. This suggested that the RS approach can detect finer spatial heterogeneity, which cannot be captured by the modelling approach.

In the modelling approach, due to the land use-based model structure, alpine grazed meadows were identified as hot spots, whereas mown-grazed permanent meadows were identified completely as cold spots of the total ES supply. The RS-based hot/cold spots were rather scattered patches within the study area. RS-based hot spots appeared to be a small subset of those identified by the modelling approach. However, it is not true for the RS-based cold spots, which corresponded to pixels with low vegetation signal (i.e., scattered pixels around roads and terrace banks), and exhibited small spatial overlap with the modelling approach.

The case study presented in Chapter 5 tested the potential of airborne imaging spectroscopy for spatial assessment of ecosystem properties as proxies for ecosystem services in subalpine grasslands and compared it with the plant trait-based modelling approach. Without any objective reference, it is hard to decide which of the two approaches is better, as both are an imperfect assessment of reality and both have their advantages and disadvantages. A strong point of the RS approach is the fine spatial resolution, which detected larger variability in vegetation properties driven by local topography and microclimatic conditions. An advantage of the modelling approach is that it is more or less independent from temporal vegetation changes as compared to the RS approach, which captures a specific development stage at one snapshot. Nevertheless, the RS approach can be extended to multi-temporal RS observations, as well as to other spatial resolutions. The RS approach allowed skipping one important step of the modelling approach, i.e. modelling of plant trait

and abiotic inputs of the EP models, which reduced the number of required in-situ measurements.

The applicability of the RS approach was limited only to a small study area and one vegetation type – subalpine grasslands – and therefore shall be expanded to more diverse landscapes. Underlying spatial data are most important for spatial assessment of EP and thereby ES; therefore, an approach that combines RS images, land use and elevation maps with in-situ EP measurements would probably be the most optimal compromise for accurate spatial assessment of multiple ES supplied by subalpine grasslands.

6.2 General conclusions

The underling base line of this research was to investigate potentials of airborne imaging spectroscopy for ecologically driven applications in structurally and functionally complex canopies. The main conclusions from the work presented in this thesis are as follows:

- Imaging spectroscopy supports better retrievals of plant traits related to leaf biochemistry, photosynthesis and phenology rather than traits related to vegetations structure. Major challenges in RS of plant traits are, first, to effectively suppress the negative influence of water absorption and canopy structure, which would facilitate accurate retrievals of biochemical and photosynthesis-related traits. Secondly, a challenge still is to match spatial scales of in-situ trait measurements and RS observations. Therefore, more coherent experiments, where in-situ measurements on plant traits and RS data at different spatial scales are acquired simultaneously, are needed.

- The main source of variability in total-to-projected leaf area ratio in spruce canopies originated from the vertical sampling position and not from needle age or forest stand age. Total leaf area estimation influenced crown averaged chlorophyll content. We found that an error associated with biased estimates of total leaf area can reach up to 30% of the expected chlorophyll range commonly found in forest canopies that can negatively influence validation of RS-based chlorophyll maps.

- Retrieval of spruce chlorophyll content based on a continuum removal technique outperformed commonly used vegetation indices. A newly designed vegetation index– $ANCB_{650\text{-}720}$– that builds on continuum removal for chlorophyll content prediction had a similar accuracy as an artificial neural network based on continuum removed bands, but the index was a lot easier to implement.

- Airborne imaging spectroscopy data proved to be partly successful in estimation of ecosystem properties that underline supply of ecosystem services in subalpine grasslands. Spatial comparison of the RS approach with plant trait-based modelling revealed relatively low spatial agreement. The RS approach showed more variability in ES driven by local topography and microclimatic conditions, which could not be detected by the trait-based modelling approach.

6.3 Reflection and outlook

This research addressed several specific problems, which contributed to improve our knowledge of using imaging spectroscopy in structurally and functionally complex canopies such as coniferous forest and subalpine grasslands. Using high resolution imaging spectroscopy, working at three hierarchical levels and with two types of contrasting ecosystems opens the door into the largest room ever – a room for improvement. Each chapter itself already suggested the main bottlenecks and future research directions. But instead of listing and discussing them all, we would like to narrow it down to only two generic topics: the interpretation of high resolution imaging spectroscopy data and the role of in-situ measurements of plant traits and canopy properties in RS of vegetation.

Interpretation of high resolution airborne imaging spectroscopy

In this thesis, airborne imaging spectroscopy data of high spectral as well as spatial resolutions were analysed. The spectral domain was interpreted in two ways: i) investigating the shape of a spectral signature using the continuum removal transformation (Chapter 4) and ii) investigating the large number of individual bands using statistical regression methods (Chapter 5). Although the statistical methods are widely used in RS research, the main bottleneck remains a high degree of redundancy and colinearity among individual bands. To overcome large redundancy, imaging spectroscopy data are often transformed into several uncorrelated bands, but this completely destroys the information content originating from the spectral shape. Results of Chapter 4 indicated that a vegetation index constructed from the shape of the continuum removed spectrum between 650 and 720 nm estimated spruce chlorophyll content with higher accuracy than traditional indices constructed from a few isolated narrow spectral bands. Therefore, I think that future studies shall explore more the shape of contiguous spectral signatures in relation to other major leaf biochemical traits such as water and nitrogen content or specific leaf area, rather than focusing on individual spectral bands.

The very high spatial resolution of airborne images analysed in this thesis was taken as an advantage to eliminate unwanted objects from the analysis and strengthen the signal originating from the vegetation canopy of interest. However, to some extent it can be perceived as a disadvantage too, because the spectral analysis might

become oversensitive to subtle spatial variations determined mainly by micro-topology and soil variability (as was likely the case in the grassland analysis in Chapter 5) or by mutual shadowing among individuals (as was the case in the spruce analysis in Chapter 4 and therefore the signal from sunlit and shaded crown parts was analysed separately).

The main asset of airborne imaging spectroscopy is that its high spatial and spectral resolution can be easily integrated to coarser resolutions and therefore used to study how relationships between vegetation properties and spectral data are maintained across different spatial, as well as, spectral scales.

Role of in-situ measurements in RS

Although RS intends to minimize efforts to map plant traits and ecosystem properties in-situ, the role of in-situ measurements in applied RS research is currently irreplaceable. Primary use of in-situ measurements of plant traits and vegetation properties as "ground truth" reference in RS is two-fold. They are either used to calibrate RS images (e.g., Chapter 5) or to validate the final RS-based maps of a given trait or property (e.g., Chapter 4). In this thesis, in-situ measurements were used both ways and we mainly struggled with a too low number of field observations ($n < 20$). The low number of observations causes that, first, the variability in field data is usually not fully captured. Crown averaged chlorophyll content of immature Norway spruce trees from Chapter 4 varied only between 35 and 45 $\mu g\ cm^{-2}$, which is a relatively narrow range and most likely did not fully represent the entire variability in a given spruce plantation. Secondly, the spectral variability captured by RS images cannot be fully explained by a limited dataset of in-situ measurements as demonstrated in Chapter 5, where in-situ data on ecosystem properties well represented about 75% of the image spectral variability.

Additionally, we were often wondering, how variability of leaf level traits within an individual (further illustrated on a single spruce tree) influences our quantification of in-situ "ground truth" data. Results of Chapter 3 indicated that large variability in leaf level traits such as chlorophyll content or specific leaf area exists inside individual spruce crowns. Especially in forest canopies, about 25% of plant trait variability can originate from within individual trees (Messier et al., 2010) and that is mainly due to the vertical light distribution inside canopies (Niinemets, 2010).

Following my research interest in spruce canopies, a preliminary test to investigate the influence of within-crown variability and upscaling schemes (from leaf to crown level) on crown averaged "ground truth" values of chlorophyll content was performed. The first results indicated that crown averages calculated from leaves sampled from the uppermost canopy layer were lower and exhibited the lowest agreement with estimates of chlorophyll content as presented in Chapter 4 in comparison to the case that leaf samples from the lower, shaded canopy layers were included (Homolová and Lukeš, 2011, unpublished data; Lukeš et al., 2009).

Particularly in coniferous forests, lower canopy layers and a forest floor become more apparent in nadir looking RS images due to the greater aggregation of foliage and increased scattering effects inside shoots as compared to broadleaf forests (Eriksson et al., 2006; Rautiainen and Stenberg, 2005).

Therefore, we think that more attention should be devoted to in-situ measurements of leaf traits in coniferous canopies and leaf sampling should not be restricted to the uppermost, sunlit canopy layer, as is often the case in RS studies (Huber et al., 2008; Moorthy et al., 2008). The contribution of lower canopy levels as well as a large within-crown variability should be better investigated and considered when measuring "ground truth" reference data. Especially 3D canopy radiative transfer models (Gastellu-Etchegorry et al., 2004) can be very helpful to investigate the importance of lower canopy layers and quantify their contribution to the remotely sensed signal (Eriksson et al., 2006).

Future RS studies of vegetation traits and properties should put more effort into their standardized in-situ measurements. They should make use of standardized in-situ measurement protocols that already exist for a set of key plant traits (Cornelissen et al., 2003; Pérez-Harguindeguy et al., 2013). However, standardized upscaling schemes to entire individuals or entire canopies, which are extremely important for example in RS studies of forest canopies, are not fully developed and established yet.

The literature review (Chapter 2) and the research presented in Chapter 5 indicate the potential future RS research direction towards a spatial ecology, i.e. spatially explicit mapping of plant traits, ecosystem properties and ecosystem services. Especially the work in Chapter 5 was motivated by a steadily increasing demand on the spatially explicit assessment of multiple landscape ecosystem services. We showed that some of the important ecosystem services can be mapped by linking them to ecosystem properties derived from RS data. A key feature of this study was combining in-situ measurements with remotely sensed spectral information, which provided insight into the spatial distribution of ecosystem properties and services. Although this case study was limited to a small area and only to one type of ecosystem (subalpine grasslands) it holds promise that it can be extended to larger and more diverse landscapes.

High quality RS data are certainly essential building elements for spatial ecology. In order to address the effects of climate and land use changes on biodiversity and ecosystems, their properties and services, the integration of in-situ and RS data will be ultimately required. A good example of such a research effort is the National Ecological Observatory Network (NEON) in the US (Kampe et al., 2010; Schimel, 2011). We hope that this interdisciplinary and integrative research efforts will slowly cross the national borders and spread worldwide. Also steadily improving RS technology becomes more available and therefore more existing ecological test sites will be able to facilitate proximal and remotely sensed spectral measurements.

Integration of in-situ and RS data is currently facing a major challenge: scaling. First, researchers need to fully understand the mechanism how leaf scattering properties with the interplay of canopy structure influence the canopy reflectance. This issue is for example addressed by the theory of spectral invariants (Knyazikhin et al., 2011; Rautiainen and Stenberg, 2005), which gains more attention within the RS community as recent studies tested it with in-situ measurements (Lukeš et al., 2011; Rautiainen et al., 2012). Solving the first scaling challenge will help to address another challenge: how relationships between plant traits and reflectance properties are maintained across spatial scales (from the level of leaves to entire canopies and ecosystems) and within time (during a vegetation season).

Appendices

Appendix A1 Literature review of remote sensing of leaf biochemical traits

Relevant peer-reviewed scientific articles presenting the estimation of important leaf functional biochemical traits (i.e. nitrogen and phosphorus concentration, leaf mass per area) using optical remote sensing (RS) methods were collected from Scopus using an appropriate set of keywords (e.g. “nitrogen content” and “remote sensing”). The reviewed papers are summarized in Table A1.1. We limit our search only to recent articles published since 2000, including some important studies published in the 1990’s. We included a paper only if it was cited more than five times before 2009 (not applied to articles published since 2009). From each article we extracted the following main features of the study: i) leaf functional trait, ii) vegetation type (broadleaf, conifers, crops, grasslands, mixed type), iii) trait units, iv) leaf or canopy scale of trait and RS measurements (leaf trait measurements of individual species are upscaled to the canopy level by calculating community weighted trait mean using species relative abundance; leaf RS measurements are acquired from individual leaves using laboratory or in-situ spectrometers, whereas canopy RS measurements are acquired by airborne or satellite spectrometers), v) RS spectrometer type (laboratory, field, airborne, spaceborne), vi) applied RS retrieval method, vii) coefficient of determination (R^2) reported for validation, viii) R^2 reported for calibration (i.e. building predictive relation between a trait and RS data), ix) relative root mean square error (RMSE) and x) the source (table or figure) from where the R^2 or RMSE was extracted. For those studies presenting results without the statistical accuracy indicators (R^2 and RMSE), we extracted the input data from figures and calculated the statistical results of the published relationship ourselves whenever possible. The absolute RMSE was converted to relative units by normalizing it to the mean observed trait value. Accuracy indicators (i.e. R^2 and RMSE) of remote sensing methods for the estimation of nitrogen, phosphorus concentration and content and leaf mass per area in different vegetation types are presented at Figure A1.1.

Table A1.1 Summary of important features extracted from articles presenting RS methods to estimate nitrogen (N), phosphorus (P) content or concentration and leaf mass per area (LMA) or specific leaf area (SLA). (Legend: Trait/Spect. Scales (L – leaf, C – canopy defines at which organization level trait / spectral data were measured); Sensor type (cf. original papers for exact sensors' acronyms, L – laboratory, F – field, A – airborne, and S – satellite); RS methods (R – reflectance, CR – continuum removal, FD – first derivative, LR – linear regression, MLR – multiple linear regression, SLR – stepwise linear regression, PLSR – partial least square regression, VI – vegetation index); R^2 val. and cal. (coefficient of determination for validation and calibration, n.a. – data not available), RMSE % (relative root mean square error), figure # / table # is the number in the original publication).

Trait	Veg. type	Trait units	Trait / Spect. scales	Sensor type	RS methods	R^2 val.	R^2 cal.	RMSE %	Fig. # / Tab. #	Reference
N	Broadlf.	%	L / C	AVIRIS (A)	Radiative transfer + empirical	0.91	n.a.	13.8	2a / -	(Asner and Vitousek, 2005)
N	Crops	mg g^{-1}	L / C	CASI (A)	LR with R@550nm	n.a.	0.78	n.a.	eq. 10	(Boegh et al., 2002)
N	Mixed	%	L / L	NIRSys 6500 (L)	PLSR of log(1/R)	0.87	0.97	25.8	2a,3a / -	(Bolster et al., 1996)
N	Crops	mg g^{-1}	L / C	CASI (A)	LR - VI (DCNI)	0.51	n.a.	15.7	sec.3.5.2	(Chen et al., 2010b)
N	Crops	mg g^{-1}	L / C	FieldSpec (F)	LR - VI (DCNI)	0.62	0.64	13.7	fig.7a / sec.3.5.1	(Chen et al., 2010b)
N	Crops	%	L / L	GER 3700 (L)	LR with red edge	n.a.	0.86	n.a.	6e / -	(Cho and Skidmore, 2006)
N	Grassl.	%	L / L	GER 3700 (L)	LR with red edge	n.a.	0.47	n.a.	6e / -	(Cho and Skidmore, 2006)
N	Grassl.	%	L / C	GER 3700 (F)	LR with red edge	n.a.	0.82	n.a.	6e / -	(Cho and Skidmore, 2006)
N	Grassl.	g m^{-2}	C/C	FieldSpec (F)	LR – VI	0.77	n.a.	23.8	5,6 / v	(Clevers and Kooistra, 2012)
N	Crops	g m^{-2}	C/C	CropScan (F)	LR – VI	0.85	n.a.	42.3	8,9 / vi	(Clevers and Kooistra, 2012)
N	Broadlf.	%	C / C	Hyperion (S)	PLSR of log(1/R)	0.64	n.a.	13.1	3 / 4	(Coops et al., 2003)
N	Crops	%	L / C	FieldSpec (F)	LR – VI (MCARI/ MTVI2)	n.a.	0.48	n.a.	- / 3	(Eitel et al., 2007)
N	Crops	%	L / C	FieldSpec (F)	LR with red edge	0.75	n.a.	17.8	5a / -	(Feng et al., 2008)
N	Crops	g m^{-2}	L / C	FieldSpec (F)	LR with FD@742nm	0.87	n.a.	17.4	6a / -	(Feng et al., 2008)
N	Mixed	%	L / C	GER 3700 (F)	LR – VI (NDVI-based)	0.72	n.a.	n.a.	- / 2	(Ferwerda et al., 2005)
N	Mixed	%	L / L	GER 3700 (L)	SLR of FD	0.86	n.a.	n.a.	- / 4	(Ferwerda and Skidmore, 2007)

Table A1.1 Continues

Trait	Veg. type	Trait units	Trait / Spect. scales	Sensor type	RS methods	R^2 val.	R^2 cal.	RMSE %	Fig. # / Tab. #	Reference
N	Crops	%	L / C	SD2000 (F)	LR – VI (NDVI-based)	n.a.	0.56	n.a.	4e / 3	(Hansen and Schjoerring, 2003)
N	Crops	g m^{-2}	C / C	SD2000 (F)	LR – VI (NDVI-based)	n.a.	0.69	n.a.	4f / 3	(Hansen and Schjoerring, 2003)
N	Conifer.	%	L / C	HyMap (A)	CR	0.45	n.a.	8.5	7b / 3	(Huber et al., 2008)
N	Broadlf.	%	L / C	HyMap (A)	CR	0.29	n.a.	9.7	- / 3	(Huber et al., 2008)
N	Conifer.	kg ha^{-1}	C / C	AVIRIS (A)	SLR of FD	0.9	n.a.	24.8	5c / -	(Johnson et al., 1994)
N	Conifer.	mg cm^{-2}	L / C	AVIRIS (A)	SLR of FD	0.85	n.a.	20.0	6a / -	(Johnson et al., 1994)
N	Crops	g m^{-2}	C / C	CropScan TM (F)	LR	n.a.	0.82	n.a.	5 / -	(Jongschaap and Booij, 2004)
N	Grassl.	%	L / C	CAO (A)	Neural networks	0.41	0.53	13.2	5 / 2	(Knox et al., 2011)
N	Mixed	%	C / C	AVIRIS (A)	MLR of FD	0.87	n.a.	8.7	4a / 7	(Martin and Aber, 1997)
N	Mixed	%	C / C	AVIRIS (A)	PLSR	0.83	n.a.	13.1	- / 2 sec3.2	(Martin et al., 2008)
N	Mixed	%	C / C	Hyperion (S)	PLSR	0.82	n.a.	17.0	- / 2 sec3.2	(Martin et al., 2008)
N	Grassl.	mg g^{-1}	L / C	GER 3700 (F)	LR with red edge	0.89	n.a.	n.a.	- / 3	(Mutanga and Skidmore, 2007)
N	Grassl.	%	L / C	GER 3700 (F)	SLR of CR	0.52	n.a.	24.4	4 / -	(Mutanga et al., 2004)
N	Mixed	%	C / C	AVIRIS (A)	PLSR of FD of log(1/R)	n.a.	0.79	n.a.	2a / -	(Ollinger et al., 2008)
N	Mixed	%	C / C	MODIS (S)	PLSR of FD of log(1/R)	n.a.	0.88	n.a.	2b / -	(Ollinger et al., 2008)
N	Mixed	%	C / C	AVIRIS (A)	PLSR of FD of log(1/R)	0.79	0.83	11.9	6b / 2	(Ollinger and Smith, 2005)
N	Mixed	%	C / C	Hyperion (S)	PLSR of FD of log(1/R)	0.60	0.82	15.6	6a / 2	(Ollinger and Smith, 2005)
N	Crops	g m^{-2}	C / C	AVIS (A)	LR – VI (CAI)	n.a.	0.77	n.a.	6b / -	(Oppelt and Mauser, 2004)
N	Crops	kg ha^{-1}	C / C	IKONOS (S)	LR - VI (NDVI)	n.a.	0.70	n.a.	- / 6	(Reyniers and Vrindts, 2006)

Table A1.1 Continues

Trait	Veg. type	Trait units	Trait / Spect. scales	Sensor type	RS methods	R^2 val.	R^2 cal.	RMSE %	Fig. # / Tab. #	Reference
N	Crops	kg ha^{-1}	C / C	CropScan TM (F)	LR - VI (NDVI)	n.a.	0.75	n.a.	- / 7	(Reyniers and Vrindts, 2006)
N	Mixed	%	L / C	AVIRIS (A)	LR - VI (NDNI)	n.a.	0.34	n.a.	2a / -	(Serrano et al., 2002)
N	Mixed	%	C / C	AVIRIS (A)	SLR of FD	0.75	n.a.	34.4	1a / 3	(Serrano et al., 2002)
N	Conifer.	%	C / C	HyMap (A)	SLR of CR	0.56	n.a.	4.9	2d / 4	(Schlerf et al., 2010)
N	Conifer.	%	L / L	FieldSpec (L)	SLR of CR	0.47	n.a.	7.0	2b / 3	(Schlerf et al., 2010)
N	Mixed	%	C / C	AVIRIS (A)	PLSR of FD of log(1/R)	0.79	0.83	10.4	- / 2	(Smith et al., 2003)
N	Mixed	%	C / C	Hyperion (S)	PLSR of FD of log(1/R)	0.6	0.82	15.7	- / 2	(Smith et al., 2003)
N	Mixed	%	C / C	AVIRIS (A)	PLSR of FD of log(1/R)	0.82	n.a.	13.4	- / 3	(Smith et al., 2002)
N	Broadlf.	%	C / C	AVIRIS (A)	PLSR of FD	0.86	n.a.	3.1	2b / -	(Townsend et al., 2003)
N	Broadlf.	%	C / C	Hyperion (S)	PLSR of FD	0.83	n.a.	3.6	2a / -	(Townsend et al., 2003)
N	Broadlf.	mg g^{-1}	L / L	NIRSystem 6500 (L)	SLR of log(1/R)	0.85	n.a.	4.6	- / 2	(Yoder and Pettigrew-Crosby, 1995)
N	Broadlf.	g m^{-2}	C / C	GER (F)	SLR of log (1/R)	0.63	n.a.	n.a.	- / 3	(Yoder and Pettigrew-Crosby, 1995)
N	Conifer.	%	L / C	AVIRIS (A)	SLR	0.55	n.a.	13.9	7a / -	(Zagolski et al., 1996)
P	Mixed	%	L / L	GER 3700 (L)	SLR of FD	0.51	n.a.	n.a.	- / 4	(Ferwerda and Skidmore, 2007)
P	Grassl.	%	L / C	CAO (A)	Neural networks	0.79	0.57	17.6	5 / 2	(Knox et al., 2011)
P	Grassl.	%	L / C	HyMap (A)	Neural networks	0.63	n.a.	28.0	3 / 4	(Mutanga and Kumar, 2007)
P	Grassl.	%	L / C	GER 3700 (F)	SLR of CR	0.70	n.a.	11.0	4 / -	(Mutanga et al., 2004)
P	Crops	%	L / C	FieldSpec (F)	LR - VI (NDVI-based)	0.30	n.a.	23.4	- / 4	(Pimstein et al., 2011)
P	Crops	g m^{-2}	C / C	FieldSpec (F)	LR - VI (NDVI-based)	0.61	n.a.	36.6	4bd / 5	(Pimstein et al., 2011)

Table A1.1 Continues

Trait	Veg. type	Trait units	Trait / Spect. scales	Sensor type	RS methods	R^2 val.	R^2 cal.	RMSE %	Fig. # / Tab. #	Reference
P	Crops	g m^{-2}	C / C	FieldSpec (F)	PLSR of FD	0.81	n.a.	25.6	5d / 6	(Pimstein et al., 2011)
P	Crops	%	L / C	FieldSpec (F)	PLSR of FD	0.46	n.a.	18.6	5b / 6	(Pimstein et al., 2011)
P	Broadlf.	%	L / C	AVIRIS (A)	Radiative transfer & empirical	n.a	n.a.	n.a.	3b / -	(Porder et al., 2005)
P	Grassl.	%	C / C	FieldSpec (F)	SLR of water-removed R	0.64	n.a.	17.6	- / 1	(Ramoelo et al., 2011)
LMA	Mixed	g cm^{-2}	L / L	Perkin-Elmer (L)	PROSPECT inver.	n.a.	n.a.	28.0	- / 2	(Baret and Fourty, 1997)
LMA	Mixed	g cm^{-2}	L / L	Varian Cary 17 DI (L)	PROSPECT inver.	0.48	n.a.	42.1	6 / 2	(Baret and Fourty, 1997)
LMA	Broadlf.	g cm^{-2}	L / L	FieldSpec (L)	PROSPECT inver.	0.01	n.a.	n.a.	4b / -	(Colombo et al., 2008)
LMA	Broadlf.	g cm^{-2}	L / C	MIVIS (A)	PROSAIL inver.	0.00	n.a.	23.9	8c / -	(Colombo et al., 2008)
LMA	Mixed	g cm^{-2}	L / L	Perkin-Elmer (L)	MLR	0.84	n.a.	17.0	6 / -	(Fourty and Baret, 1998)
LMA	Broadlf.	g m^{-2}	L / L	FieldSpec (L)	LR – VI (NDVI-based)	n.a.	n.a.	47.1	5a / 4	(le Maire et al., 2008)
LMA	Broadlf.	g m^{-2}	L / L	FieldSpec (L)	LR – VI (NDVI-based)	n.a.	n.a.	28.0	5b,c / 4	(le Maire et al., 2008)
LMA	Broadlf.	g m^{-2}	C / C	FieldSpec (F), Hyperion (S)	LR – VI (NDVI-based))	n.a.	n.a.	11.8	7 / 5	(le Maire et al., 2008)
SLA	Broadlf.	m^2 kg^{-1}	C / C	Landsat TM (S)	LR - VI (red/nir)	n.a.	0.91	n.a.	5a / 9	(Lymburner et al., 2000)
SLA	Broadlf.	m^2 kg^{-1}	C / C	Landsa tTM (S)	LR - VI (SLAVI)	n.a.	0.84	n.a.	5c / 9	(Lymburner et al., 2000)
LMA	Mixed	g cm^{-2}	L / L	Perkin-Elmer (L)	PROSPECT inver.	0.38	n.a.	n.a.	2a / -	(Riaño et al., 2005)
LMA	Mixed	g cm^{-2}	C / C	GER 2600 (F)	PROSPECT-Lillesaeter inver.	0.12	n.a.	n.a.	5a / -	(Riaño et al., 2005)
LMA	Conifer.	g cm^{-2}	L / C	DAIS 7915 (A)	PROSPECT-GeoSAIL inver.	0.15	n.a.	22.2	3d / -	(Schaepman et al., 2004)
LMA	Conifer.	g m^{-2} *LAI	C / C	DAIS 7915 (A)	PROSPECT-GeoSAIL inver.	0.79	n.a.	30.6	3f / -	(Schaepman et al., 2004)

Table A1.1 Continues

Trait	Veg. type	Trait units	Trait / Spect. scales	Sensor type	RS methods	R^2 val.	R^2 cal.	RMSE %	Fig. # / Tab. #	Reference
LMA	Crops	g cm^{-2} *LAI	C / C	HyMap (A)	PROSAIL inver.	0.86	n.a.	144.8	4d / 4	(Vohland et al., 2010)
LMA	Crops	g cm^{-2} *LAI	C / C	HyMap (A)	PROSAIL inver.	0.72	n.a.	134.5	4d / 4	(Vohland et al., 2010)
LMA	Crops	g cm^{-2} *LAI	C / C	HyMap (A)	PROSAIL inver.	0.85	n.a.	69.0	4d / 4	(Vohland et al., 2010)
LMA	Crops	g cm^{-2}	L / C	HyMap (A)	PROSAIL inver.	0.10	n.a.	38.5	- / 7	(Vohland et al., 2010)
LMA	Crops	g cm^{-2}	L / C	HyMap (A)	PROSAIL inver.	0.25	n.a.	69.2	- / 7	(Vohland et al., 2010)
LMA	Crops	g cm^{-2}	L / C	HyMap (A)	PROSAIL inver.	0.72	n.a.	51.3	- / 7	(Vohland et al., 2010)
LMA	Mixed	g cm^{-2}	L / L	FieldSpec (L)	LR – VI (NDVI-based)	0.68	0.64	n.a.	5 / 2	(Wang et al., 2011)

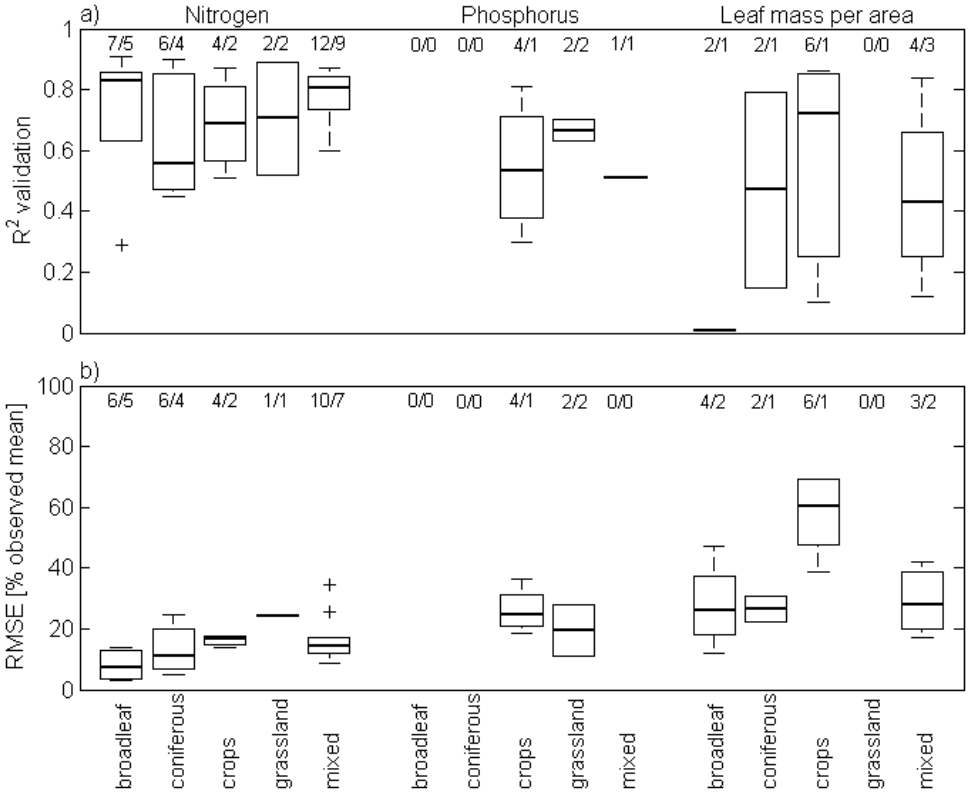

Figure A1.1 Performance of remote sensing methods for the estimation of nitrogen, phosphorus concentration and content and leaf mass per area in different vegetation types evaluated by using the coefficient of determination R^2 (a) and relative root mean square error RMSE (b). (Legend: Central line in a box is median, box height is the interquartile range (i.e. 50% of the data) and whiskers represent minimum and maximum unless the observed values exceed 1.5 of the interquartile range in that case they are marked as outliers (crosses). Number (in format of x/y) above each box indicates number of reported accuracy indicators (x) and corresponding number of scientific articles (y) they were extracted from.).

Appendix A2 Relationship between leaf chlorophyll and nitrogen content in montane grass species.

Leaf samples of 27 plant species growing at two study sites located in the area of Col de Lautaret, in the central French Alps (within 5 km from the Joseph Fourier alpine station, 45°02'09"N, 06°24'04"E) were collected during the vegetation season of 2008. The first test site is located on the south facing slopes above the village Villar-d'Arène (1800 – 2100 m a.s.l.). A detailed description of this site, which is affected by a long history of agricultural and pastoral land use, is given in Quétier et al. (2007a). The second test site is located in a valley between Lautaret and Galibier Pass (2000 – 2800 m a.s.l.). The prevailing vegetation cover is mosaic of bare rocks and alpine meadow species.

Leaf trait data of 27 dominant subalpine and alpine species, i.e. specific leaf area, leaf chlorophyll and nitrogen content, were measured in July 2008. Well developed individuals that were growing under sun exposed conditions, were collected from three locations along the altitude gradient at each study site. Depending on species occurrence, we collected 5 to 20 samples per species. Specific leaf area (SLA) was calculated as one-sided fresh leaf area per unit dry mass ($cm^2\ g^{-1}$). Leaf chlorophyll *a* and *b* were determined spectrophotometrically from an extract of grinded leaves in ethanol according to Wellburn (1994) following methods proposed by Porra, et al. (1989). Leaf nitrogen was obtained from dried and grinded leaves samples of 3 – 5 mg, which were analysed with a FlashEA 1112 elemental analyser (Thermo Fisher Scientific Inc., Milan, Italy). Both, leaf total chlorophyll and nitrogen per unit dry mass were multiplied by SLA to obtain final leaf chlorophyll ($\mu g\ cm^{-2}$) and nitrogen ($mg\ cm^{-2}$) content. Correlation coefficients and linear relationships established between leaf chlorophyll and nitrogen content of 27 subalpine and alpine species is presented at Figure A2.1.

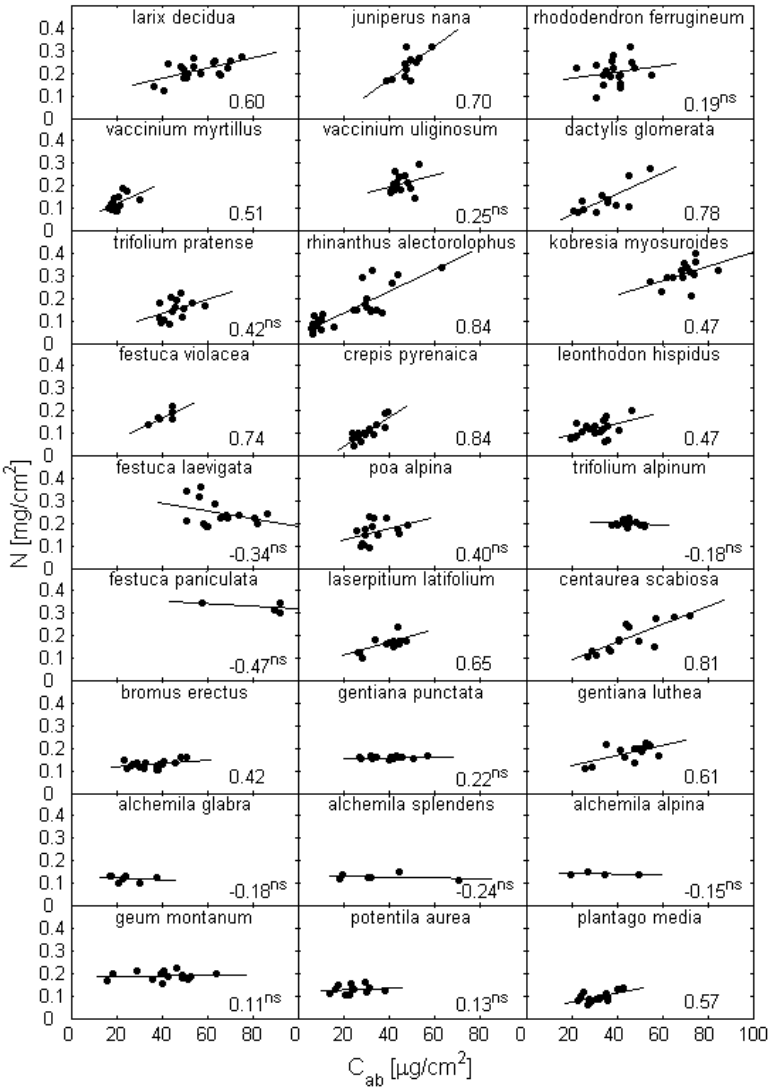

Figure A2.1 Relationship between leaf chlorophyll (C_{ab} [µg cm^{-2}]) and nitrogen (N [mg cm^{-2}]) content for 27 dominant subalpine and alpine species. For each relationship we report Pearson's correlation coefficient, the superscript "ns" indicates that the correlation is not significant ($p \leq 0.1$).

Appendix A3 Chlorophyll sensitivity of $ANCB_{650-720}$ and other three optical indices in the case of broadleaf canopies

To compare the C_{ab} sensitivity of the newly proposed $ANCB_{650–720}$ and three previously published optical indices also in a case of broad-leaf plants, we simulated a top-of-the-canopy bi-directional reflectance factor (BRF) of two structurally different broadleaf canopies: i) a homogeneous grassland (scenario SC1) and ii) a heterogeneous deciduous forest (scenario SC2). The simulations were performed using the radiative transfer models PROSPECT-4 (Feret et al., 2008) and DART (Gastellu-Etchegorry et al., 2004). The sun-sensor geometry of the broadleaf simulations was kept as for the Norway spruce simulations, i.e. sun zenith angle equal to 47.8° and sun azimuth angle equal to 183.4°. Only the canopy reflectance observed from nadir was considered in this sensitivity test. We simulated canopy BRF at 11 discrete wavelengths corresponding to the AISA Eagle spectral bands with the following central wavelengths: 551, 652, 661, 670, 680, 689, 708, 717, 745, and 802 nm (full width half maximum of 10 nm).

The optical properties of the soil background and woody materials were measured during the field campaign at Bílý Kříž test site in the ASD integrating sphere coupled with the ASD FieldSpec PRO spectroradiometer (ASD, Inc., USA); their spectral signatures are shown in Figure A3.1. The leaf optical properties were simulated with the PROSPECT model (version 4). The input parameters are summarized in Table A3.1. The variable of interest C_{ab} was kept free, ranging between 10 and 85 μg cm^{-2} increasing with a step of 15 μg cm^{-2}. In total, 216 different combinations of structurally simple 1-D homogeneous turbid medium of grassland canopy were simulated within scenario SC1 by varying the leaf chlorophyll content (C_{ab}), leaf area index (LAI) and leaf angle distribution (LAD). Scenario SC2, representing a structurally heterogeneous 3-D canopy of a mixed deciduous forest, was constructed from two horizontal leaf layers: i) the understory layer modeled as small spherical bushes and ii) the overstory layer modeled as ellipsoidal crowns with woody trunks. We executed 108 different canopy realizations of SC2 by varying the input parameters C_{ab}, LAI and canopy cover. An overview of fixed and varying input parameters for both scenarios is provided in Table A3.1. All four chlorophyll sensitive optical indices ($ANCB_{650–720}$, $ND_{925\&710}$, $SR_{750/710}$ and TCARI/OSAVI) were computed from the simulated canopy BRF (in case of SC2 only from sunlit crown pixels) and plotted against C_{ab} to investigate their relationship.

The dependency of $AUC_{650–720}$ and CBD_{670} on C_{ab} is for both scenarios very similar to Norway spruce crowns (Figures 4.5a and b) and also empirical relations between the indices and C_{ab} are statistically significant (Figure A3.2 and A3.3). However, a large variability in computed values of $ND_{925\&710}$ and $SR_{750/710}$ is seen in the case of SC1. Since this variability is not observed for SC2, it is logically caused by six different leaf angle distributions. $ANCB_{650–720}$ and TCARI/OSAVI are less influenced by the changing leaf angle distribution, varying mainly for C_{ab} lower than

40 µg cm^{-2}. For both scenarios, $ANCB_{650–720}$ showed the strongest C_{ab} predictive power (R^2 = 0.95 and 0.99, p < 0.01 and 0.001) described by a linear function. However, $ANCB_{650-720}$ predictions for C_{ab} values bellow 20 µg cm^{-2} are for both broadleaf canopies less reliable than those of Norway spruce crowns (Figures A3.2c and A3.3c).

Table A3.1 Key input parameters of the PROSPECT-DART radiative transfer simulations conducted for sensitivity analyses of chlorophyll estimating indices for two broadleaf canopies: grassland (SC1) and deciduous forest (SC2). (NA ~ not applicable).

Parameters	Units	SC1 (grassland)	SC2 (deciduous forest)	
			Bushes	Trees
Leaf level (PROSPECT)				
Chlorophyll content	[µg cm^{-2}]	10, 25, 40, 55, 70, 85	10, 25, 40, 55, 70, 85	
Water content	[g cm^{-2}]	0.0175	0.0199	0.0199
Leaf mass per area	[g cm^{-2}]	0.0084	0.0043	0.0066
Structural parameter N	[-]	1.75	1.83	2.66
Canopy level (DART)				
Canopy height	[m]	0.5 ± 0.15	1.5 ± 0.2	8.0 ± 1.5
Crown shape		NA	Spherical	Ellipsoidal
Trunk diameter	[m]	NA	NA	0.15
Proportion of leaf cells	[%]	100	80	60
Leaf angle distribution	[-]	Erectophile, Spherical, Planophile, Uniform, Extremophile Plagiophile	Spherical	Planophile
Leaf area index	[-]	1, 2, 3, 4, 5, 6	4, 5, 6, 7, 8, 9	
Canopy cover	[%]	100	45, 65, 85	

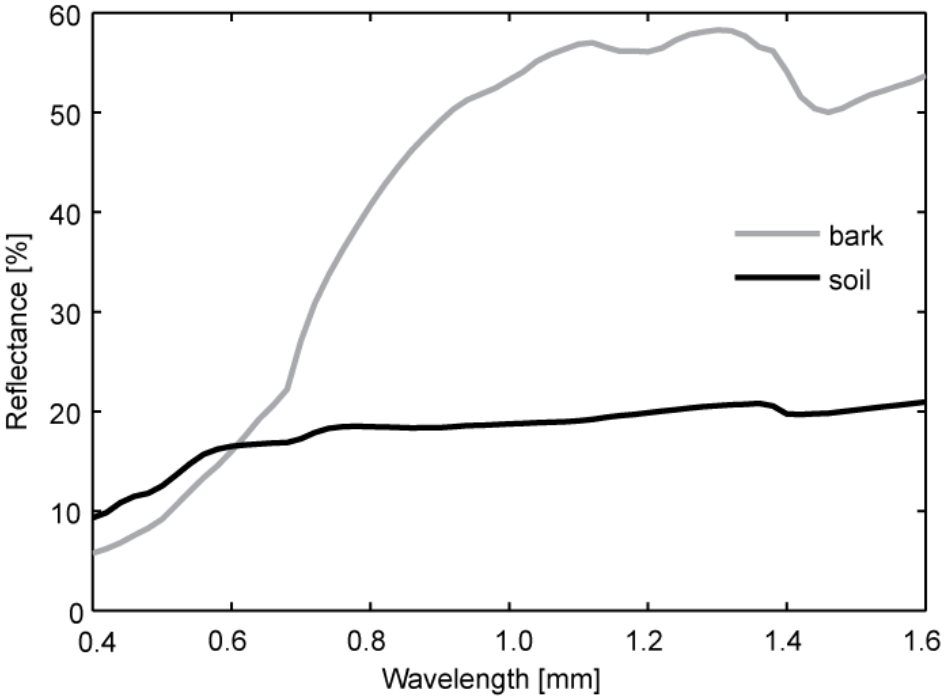

Figure A3.1 Reflectance signatures of soil background and tree bark as used in PROSPECT-DART radiative transfer simulations of broadleaf canopy scenarios (SC1 and SC2).

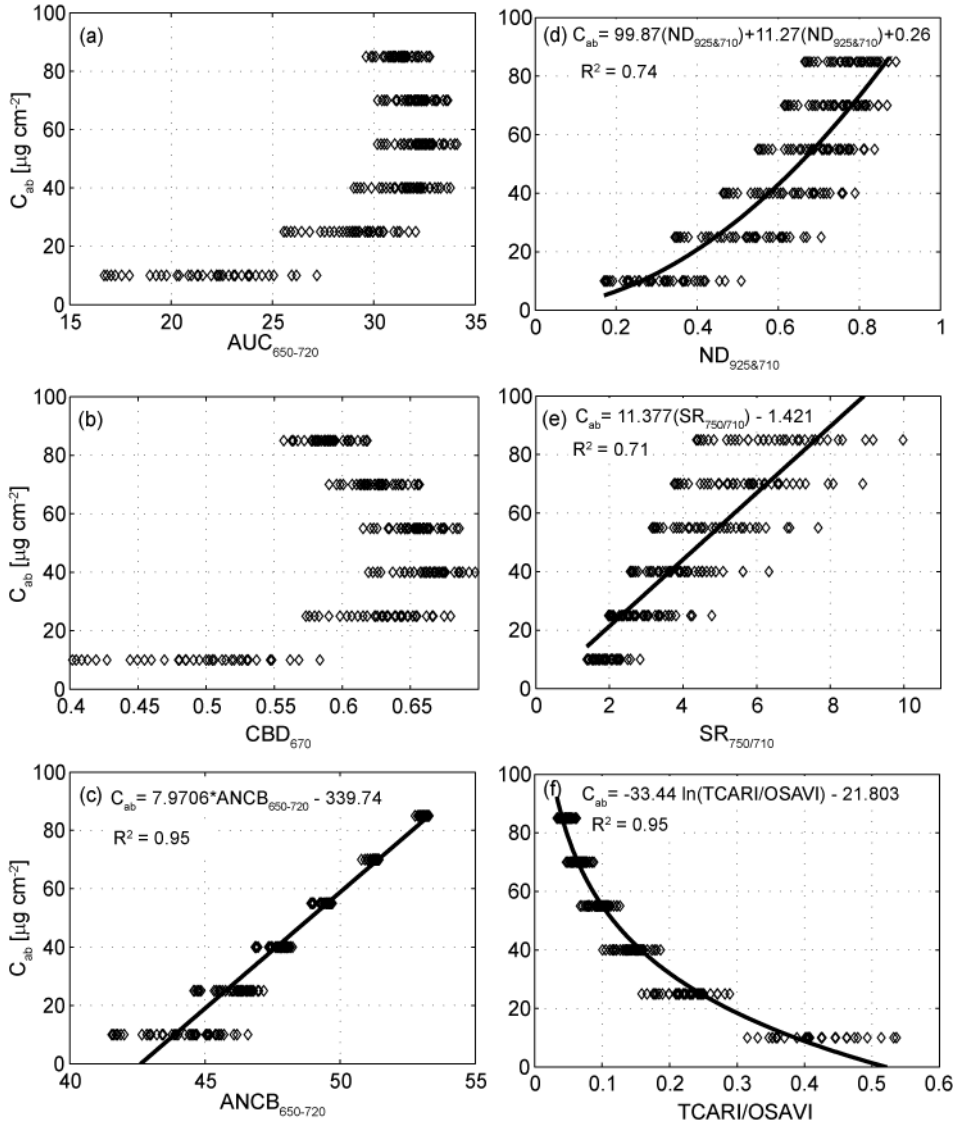

Figure A3.2 Relationship between leaf chlorophyll content (C_{ab}) and the Area Under Curve ($AUC_{650-720}$) of continuum removed reflectance between 650 and 720 nm (a), Continuum Band Depth at 670 nm (CBD_{670}) (b), $ANCB_{650-720}$ optical index (c), Normalized Difference ($ND_{925\&710}$) (d), Simple reflectance Ratio ($SR_{750/710}$) (e), and ratio of TCARI/OSAVI indices (f) computed from PROSPECT-DART radiative transfer simulations for a homogenous grassland (scenario SC1). (R^2 is coefficient of determination of the best fitting mathematical function).

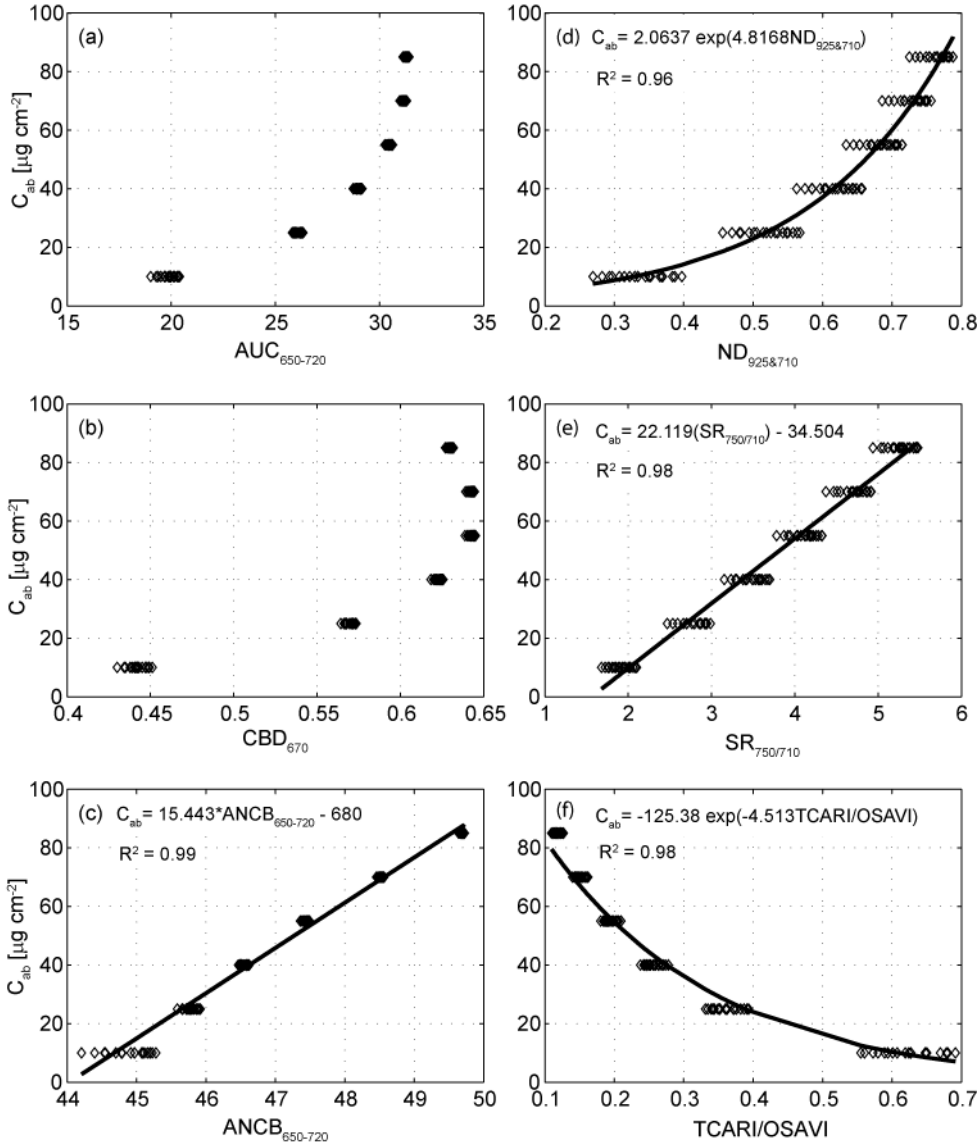

Figure A3.3 Relationship between leaf chlorophyll content (C_{ab}) and the Area Under Curve ($AUC_{650-720}$) of continuum removed reflectance between 650 and 720 nm (a), Continuum Band Depth at 670 nm (CBD_{670}) (b), $ANCB_{650-720}$ optical index (c), Normalized Difference ($ND_{925\&710}$) (d), Simple reflectance Ratio ($SR_{750/710}$) (e), and ratio of TCARI/OSAVI indices (f) computed from PROSPECT-DART radiative transfer simulations for a heterogeneous deciduous forest stand (scenario SC2). (R^2 is coefficient of determination of the best fitting mathematical function).

Appendix A4 Comparison of the $ANCB_{650-720} - C_{ab}$ relationship for sunlit and shaded spruce crowns parts simulated with PROSPECT and DART

Similar to the structurally heterogeneous 3-D canopy of a mixed broadleaf forest (Appendix A3), 108 Norway spruce scenes parameterized according to Tables 4.1 and 4.2 were simulated with spruce-adapted PROSPECT and DART models for a leaf chlorophyll content varying between 10 and 85 µg cm^{-2} increasing with a step of 15 µg cm^{-2}. Pixels of sunlit and shaded crown parts were separated using a maximum likelihood classification. $AUC_{650–720}$, CBD_{670} and $ANCB_{650–720}$ were computed from the top-of-the-canopy bi-directional reflectance factor (BRF) averaged per simulation and plotted against the predefined C_{ab} classes to investigate potential differences in C_{ab} empirical relationships for sunlit and shaded pixels. Figure A4.1 demonstrates that the $AUC_{650–720}$ and CBD_{670} values of shaded crown parts vary more than those of sunlit parts. $ANCB_{650–720}$ is, nevertheless, reducing this variability and producing the statistically significant exponential relationship ($R^2 = 0.99$, $p < 0.001$) of very similar shape as for sunlit parts (Figure A4.1c). Based on this result, one could propose to use the whole spruce crowns for C_{ab} estimation regardless their sunlit or shaded appearance. It is, however, important to stress out that the presented relationships were obtained from the radiative transfer modeling of a generalized spruce forest stand, which omitted any kind of image noise. Depending on radiometric specifications of an airborne sensor, the reflectance signal of shaded pixels may contain a higher portion of a random noise. The presence of noise, the spatially specific forest canopy shade intensity, and importantly the limited reflectance dynamic range (Figure 4.3 indicates that reflectance of shaded pixels is twice lower than of sunlit crown pixels) will predominantly result in C_{ab} estimates of low accuracy.

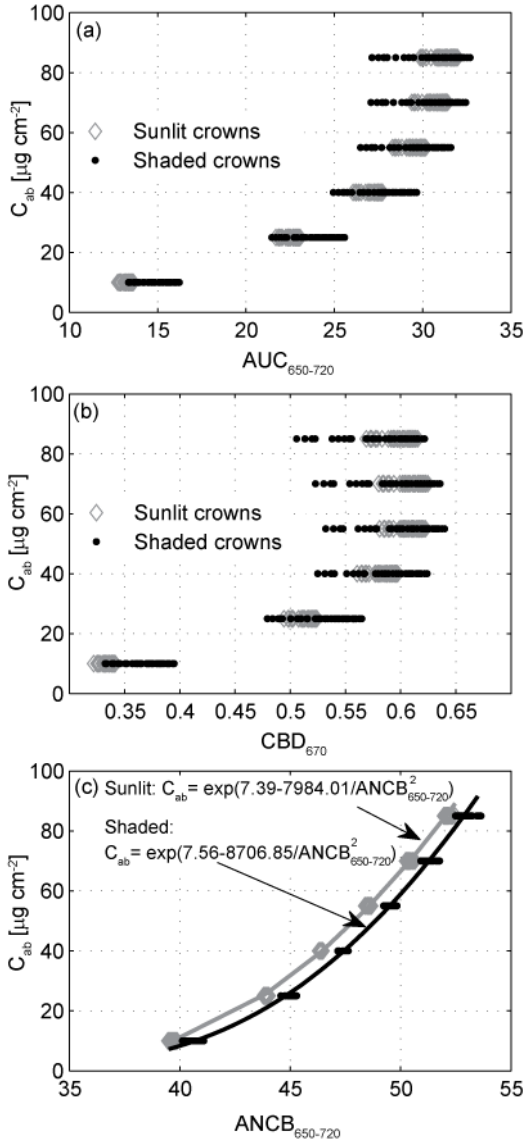

Figure A4.1 The $ANCB_{650-720}$ optical index (c) computed from the Area Under Curve ($AUC_{650-720}$) of continuum-removed reflectance (a) and Continuum Band Depth at 670 nm (CBD_{670}) (b) separately from sunlit and shaded Norway spruce crown pixels. The equations represent the best fitting exponential functions (coefficient of determination R^2 = 0.99, significance probability level $p<0.01$). A single diamond/dot symbol represents one of the PROSPECT-DART simulated leaf area index values (LAI □ <4,9> with a step of 1) within three predefined canopy closures (CC □ 75, 85 and 95%).

Appendix A5 Descriptive statistics: comparison of the remote sensing and the modelling approaches to estimate ecosystem properties per land use class.

The evaluated ecosystem properties are: (a) green biomass, (b) litter mass, (c) crude protein content, (d) species diversity and (e) soil carbon content. The left panels show frequency distribution of a given ecosystem property for the remote sensing approach (black bars) and for the modelling approach (grey bars). The right panels show boxplots, where central line in a box is median, box height is interquartile range representing 50% of the data, whiskers are minimum and maximum unless the observed values exceeded 1.5 times the interquartile range and in that case they are marked with crosses as outliers. The star symbol indicates that differences in median values between two approaches are significant ($p \leq 0.05$, Wilcoxon -Mann-Whitney U test).

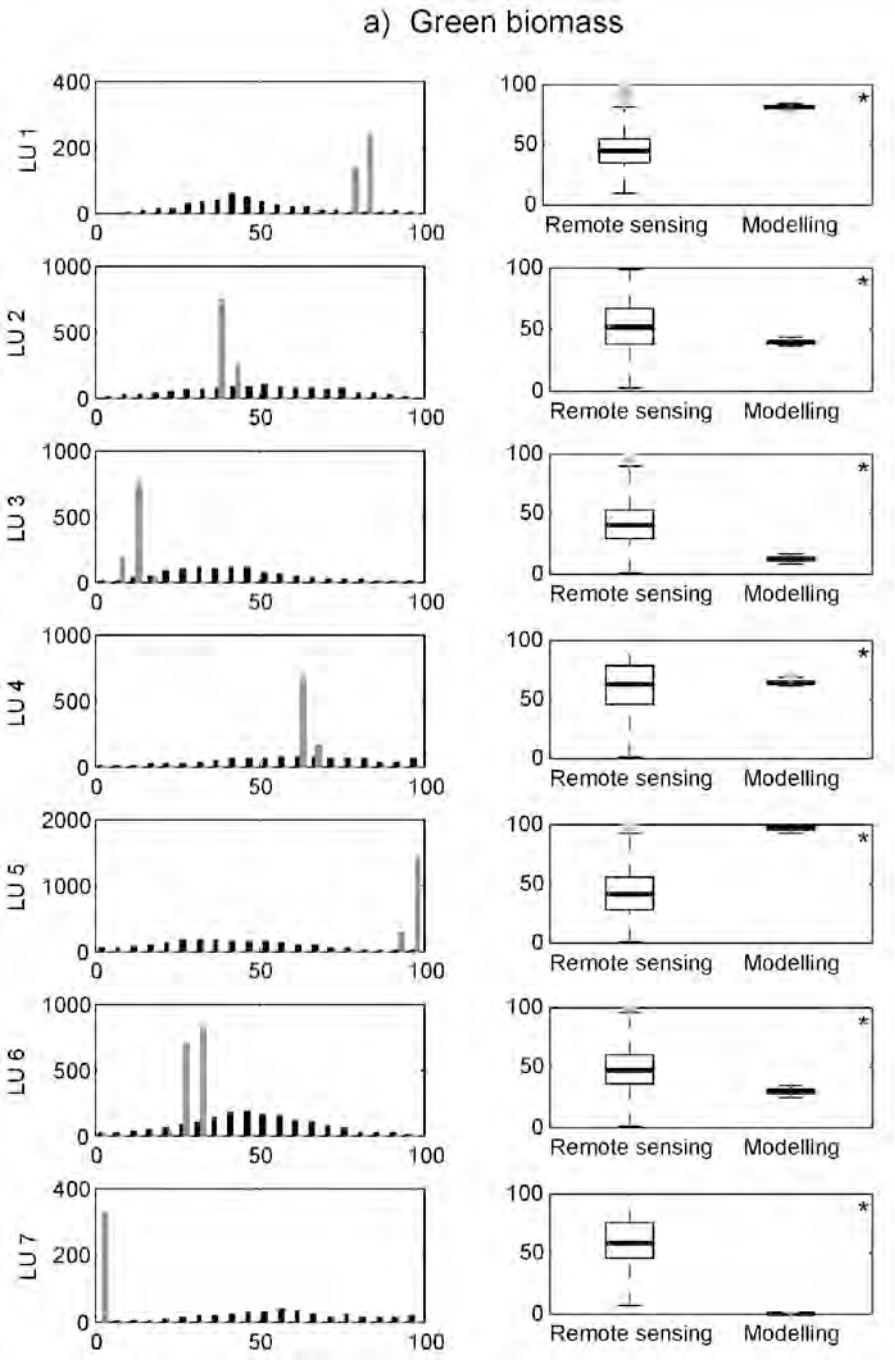
a) Green biomass
LU 1
LU 2
LU 3
LU 4
LU 5
LU 6
LU 7
Remote sensing
Modelling

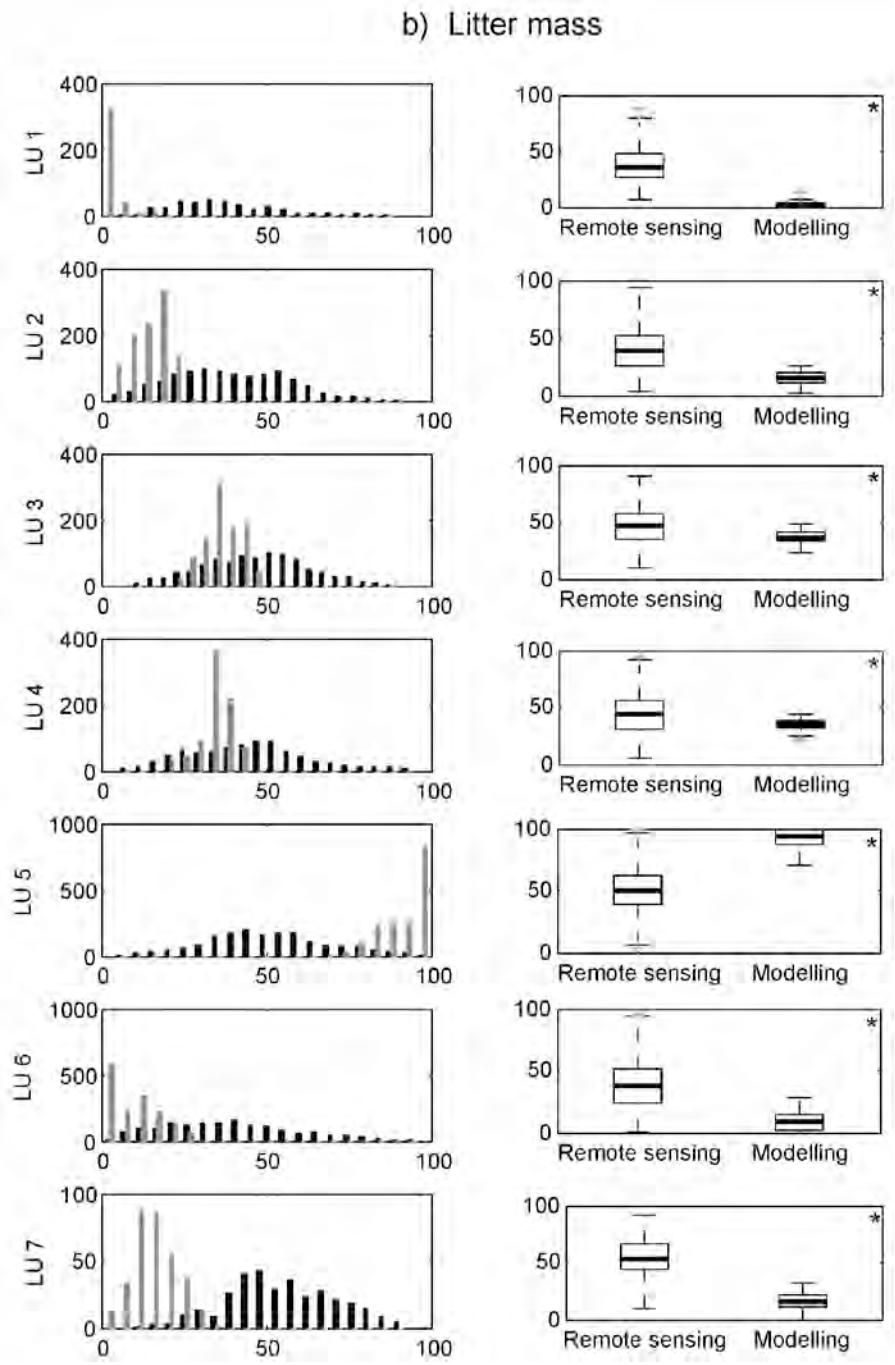
b) Litter mass
LU 1
LU 2
LU 3
LU 4
LU 5
LU 6
LU 7
Remote sensing
Modelling

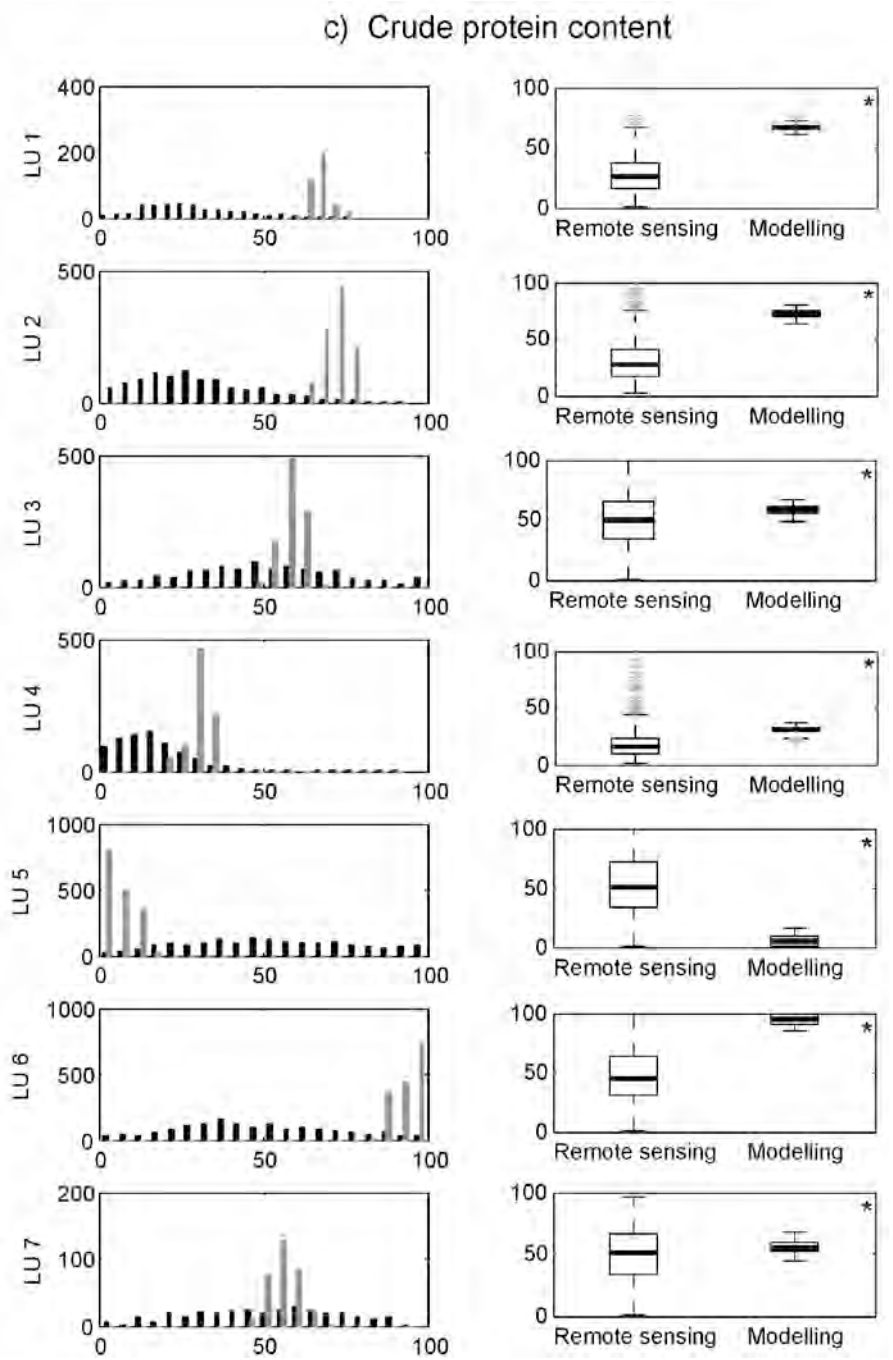
c) Crude protein content
LU 1
LU 2
LU 3
LU 4
LU 5
LU 6
LU 7
Remote sensing
Modelling

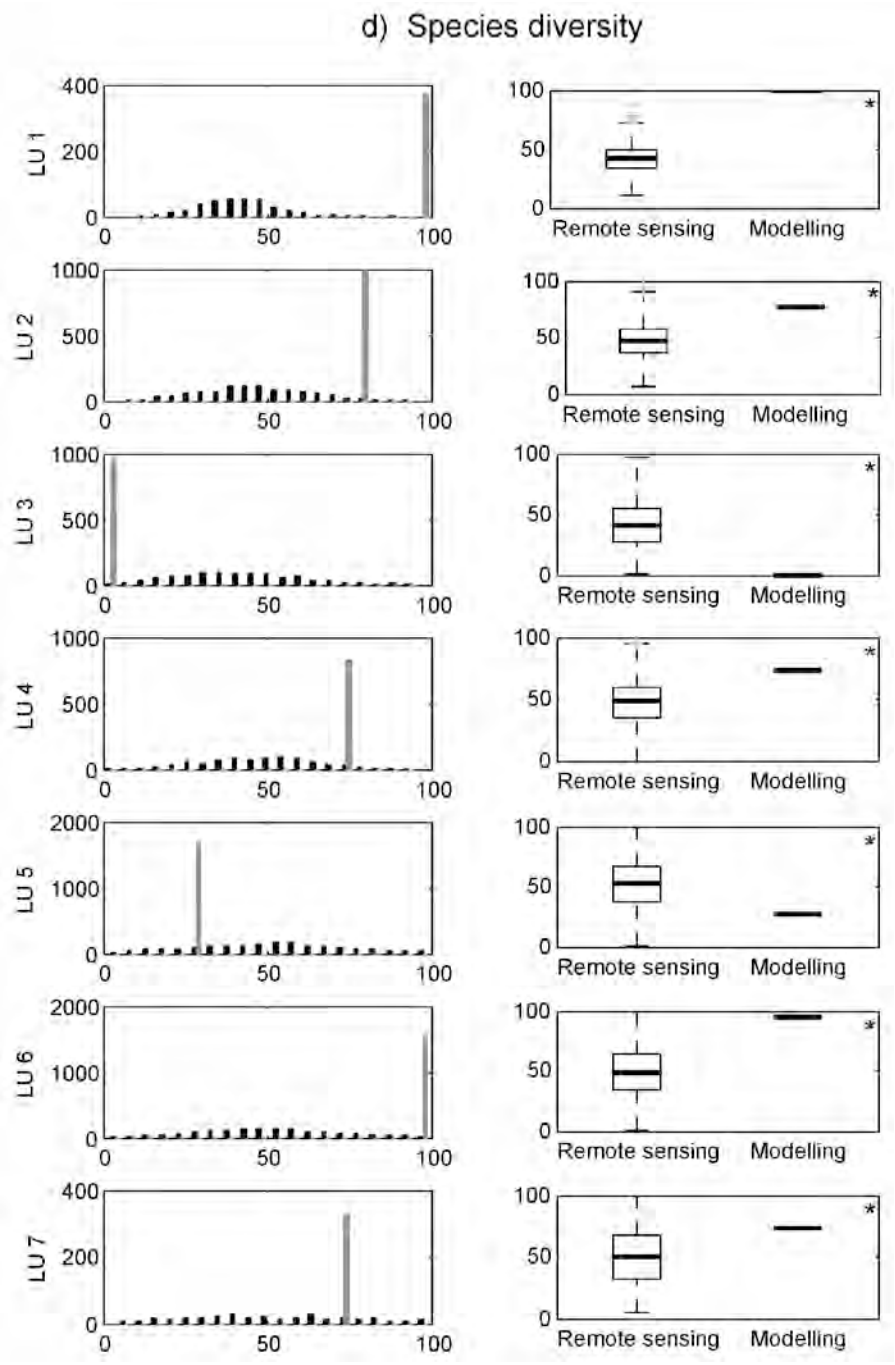
d) Species diversity
LU 1
LU 2
LU 3
LU 4
LU 5
LU 6
LU 7
Remote sensing
Modelling

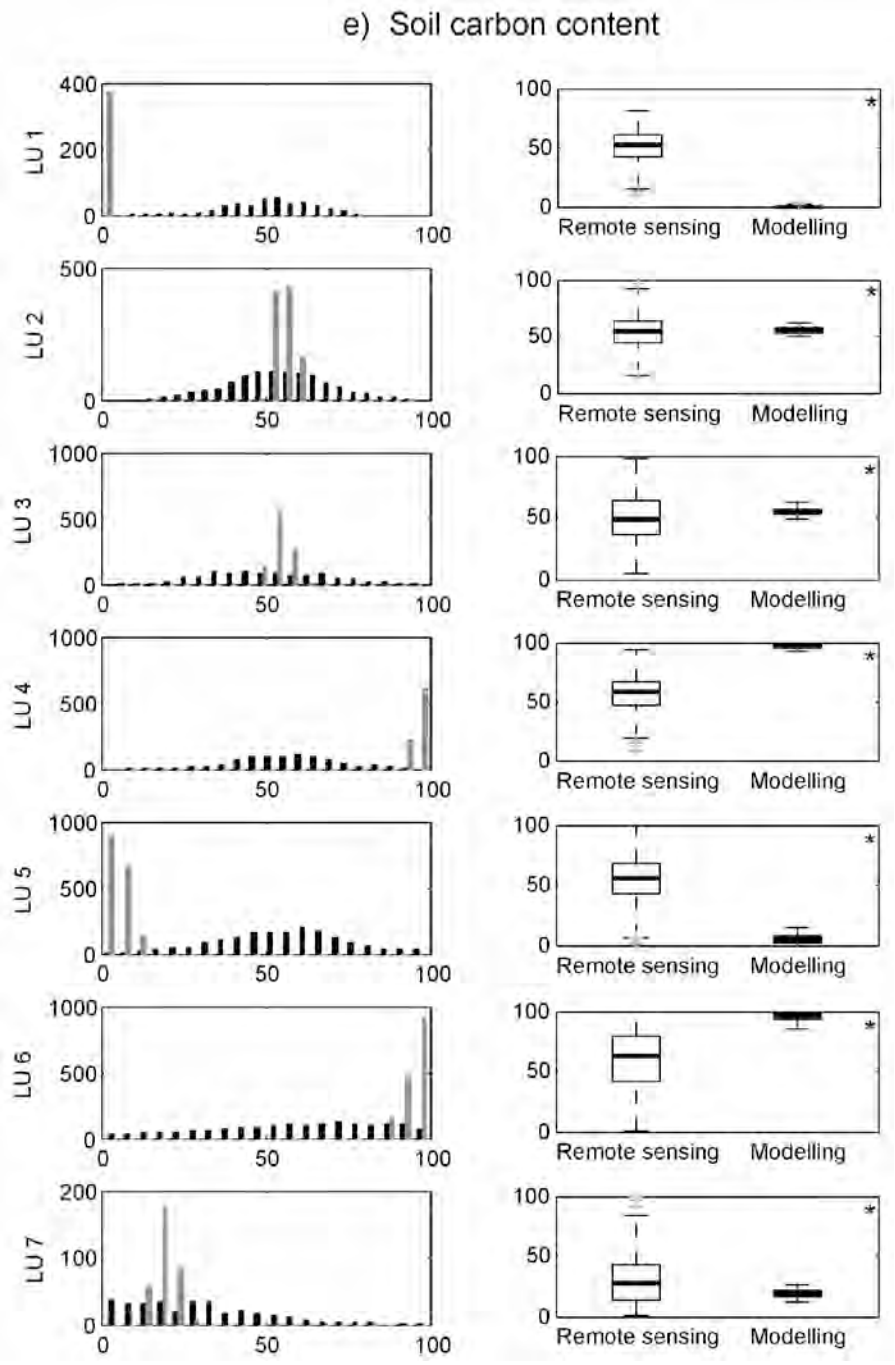
e) Soil carbon content
LU 1
LU 2
LU 3
LU 4
LU 5
LU 6
LU 7
Remote sensing
Modelling

Appendix A6 Descriptive statistics: comparison of the remote sensing and the modelling approaches to estimate ecosystem services per land use class.

The evaluated ecosystem properties are: (a) agronomic and (b) cultural value. The left panels show frequency distribution of a given ecosystem service for the remote sensing approach (black bars) and for the modelling approach (grey bars). The right panels show boxplots, where central line in a box is median, box height is interquartile range representing 50% of the data, whiskers are minimum and maximum unless the observed values exceeded 1.5 times the interquartile range and in that case they are marked with crosses as outliers. The star symbol indicates that differences in median values between two approaches are significant ($p < 0.05$, Wilcoxon-Mann-Whitney U test).

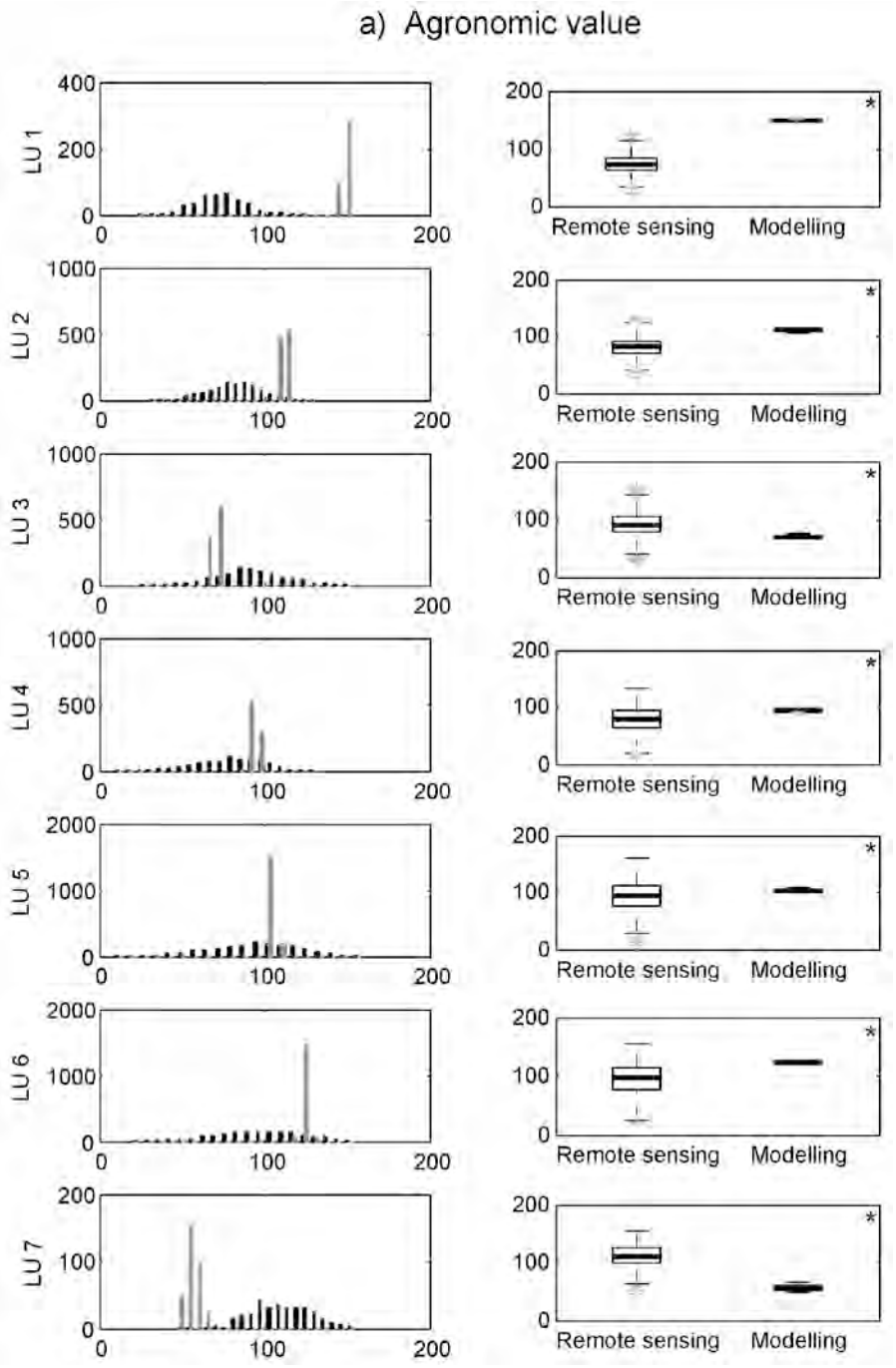
a) Agronomic value
LU 1
LU 2
LU 3
LU 4
LU 5
LU 6
LU 7
Remote sensing
Modelling

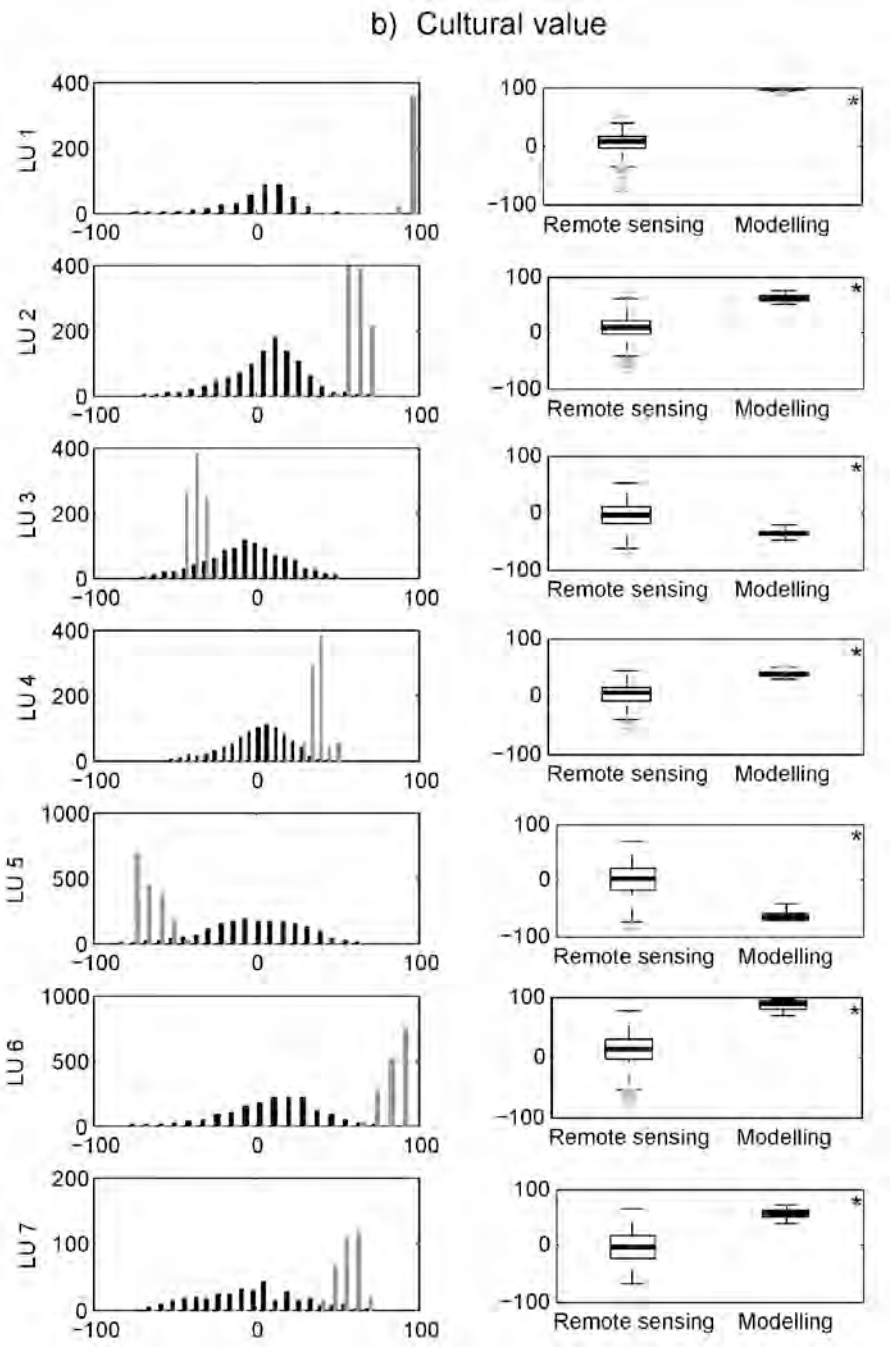
b) Cultural value
LU 1
LU 2
LU 3
LU 4
LU 5
LU 6
LU 7
Remote sensing
Modelling

Appendix A7 Ecosystem properties and services estimated from the remote sensing and the modelling approachs at a spatial resolution of 100 m.

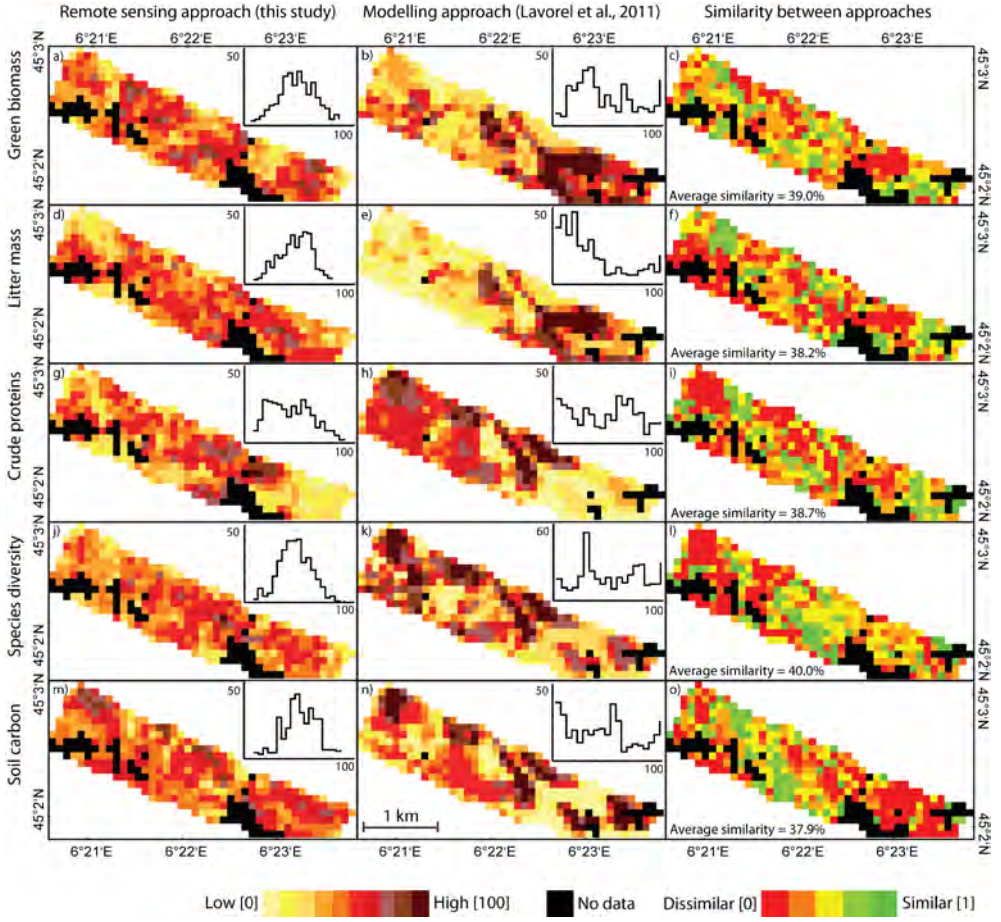

Figure A7.1 Ecosystem properties estimated from the remote sensing approach (Chapter 5) and from the modelling approach (Lavorel et al., 2011) at a spatial resolution of 100 m. The most right maps show similarity between the approaches. Frequency histograms show the distribution of values within the image.

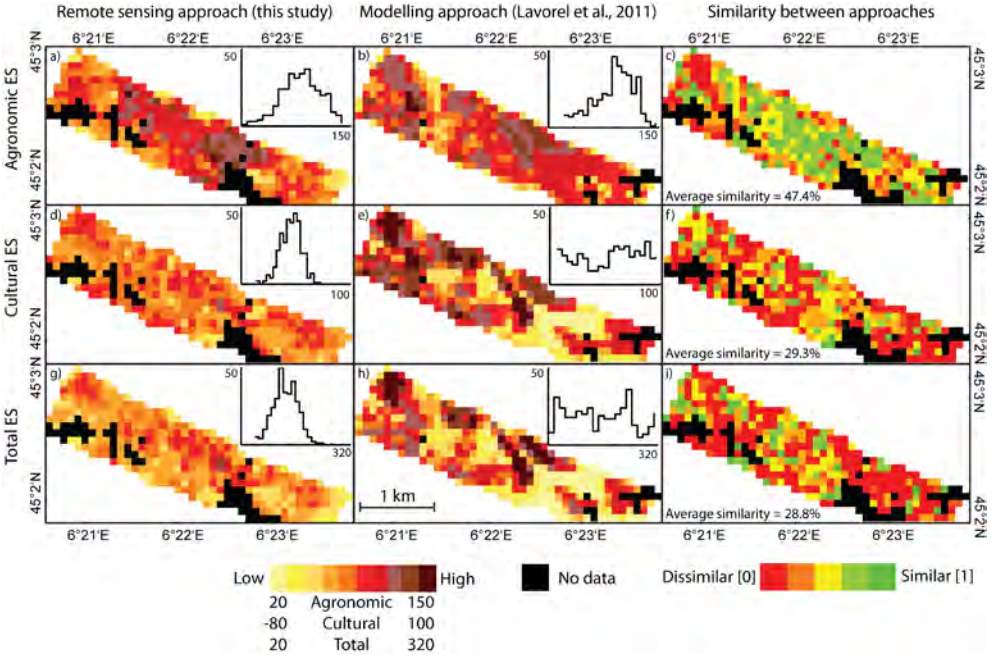

Figure A7.2 Ecosystem services estimated from the remote sensing approach (Chapter 5) and from the modelling approach (Lavorel et al., 2011) at a spatial resolution of 100 m. The most right maps show similarity between the approaches. Frequency histograms show the distribution of values within the image.

References

Ač A, Malenovský Z, Hanuš J, Tomášková I, Urban O, Marek MV (2009) Near-distance imaging spectroscopy investigating chlorophyll fluorescence and photosynthetic activity of grassland in the daily course. Functional Plant Biology 36, 1006-1015.

Albert CH, Thuiller W, Yoccoz NG, Soudant A, Boucher F, Saccone P, Lavorel S (2010) Intraspecific functional variability: Extent, structure and sources of variation. Journal of Ecology 98, 604-613.

Arino O, Bicheron P, Achard F, Latham J, Witt R, Weber JL (2008) GLOBCOVER - The most detailed portrait of Earth. ESA Bulletin - European Space Agency, 24-31.

Arroyo LA, Pascual C, Manzanera JA (2008) Fire models and methods to map fuel types: The role of remote sensing. Forest Ecology and Management 256, 1239-1252.

Asner GP (1998) Biophysical and biochemical sources of variability in canopy reflectance. Remote Sensing of Environment 64, 234-253.

Asner GP, Elmore AJ, Hughes RF, Warner AS, Vitousek PM (2005) Ecosystem structure along bioclimatic gradients in Hawai'i from imaging spectroscopy. Remote Sensing of Environment 96, 497-508.

Asner GP, Heidebrecht KB (2002) Spectral unmixing of vegetation, soil and dry carbon cover in arid regions: Comparing multispectral and hyperspectral observations. International Journal of Remote Sensing 23, 3939-3958.

Asner GP, Hicke JA, Lobell DB (2003) Per-pixel analysis of forest structure: Vegetation indices, spectral mixture analysis and canopy reflectance modeling, in: Wulder MA, Franklin SE (Eds.), Remote sensing of forest environments. Concepts and case studies. Kluwer Academic Publishers, Boston, pp. 209-254.

Asner GP, Knapp DE, Boardman J, Green RO, Kennedy-Bowdoin T, Eastwood M, Martin RE, Anderson C, Field CB (2012) Carnegie Airborne Observatory-2: Increasing science data dimensionality via high-fidelity multi-sensor fusion. Remote Sensing of Environment 124, 454-465.

Asner GP, Martin RE, Tupayachi R, Emerson R, Martinez P, Sinca F, Powell GVN, Wright SJ, Lugo AE (2011) Taxonomy and remote sensing of leaf mass per area (LMA) in humid tropical forests. Ecological Applications 21, 85-98.

Asner GP, Vitousek PM (2005) Remote analysis of biological invasion and biogeochemical change. Proceedings of the National Academy of Sciences of the United States of America 102, 4383-4386.

Ayanu YZ, Conrad C, Nauss T, Wegmann M, Koellner T (2012) Quantifying and mapping ecosystem services supplies and demands: A review of remote sensing applications. Environmental Science and Technology 46, 8529-8541.

Bacour C, Baret F, Béal D, Weiss M, Pavageau K (2006) Neural network estimation of LAI, fAPAR, fCover and LAI×Cab, from top of canopy MERIS reflectance data: Principles and validation. Remote Sensing of Environment 105, 313-325.

Baret F, Buis S (2008) Estimating canopy characteristics from remote sensing obsrvations: Review of methods and associated problems, in: Liang S (Ed.), Advances in Land Remote Sensing: System, Modeling, Inversion and Application. Springer, pp. 173-201.

Baret F, Fourty T (1997) Estimation of leaf water content and specific leaf weight from reflectance and transmittance measurements. Agronomie 17, 455-464.

Baret F, Hagolle O, Geiger B, Bicheron P, Miras B, Huc M, Berthelot B, Niño F, Weiss M, Samain O, et al. (2007) LAI, fAPAR and fCover CYCLOPES global products derived from VEGETATION. Part 1: Principles of the algorithm. Remote Sensing of Environment 110, 275-286.

Bartholomé E, Belward AS (2005) GLC2000: A new approach to global land cover mapping from earth observation data. International Journal of Remote Sensing 26, 1959-1977.

Bartholomeus H, Kooistra L, Stevens A, van Leeuwen M, van Wesemael B, Ben-Dor E, Tychon B (2011) Soil Organic Carbon mapping of partially vegetated agricultural fields with imaging spectroscopy. International Journal of Applied Earth Observation and Geoinformation 13, 81-88.

Barton CVM, North PRJ (2001) Remote sensing of canopy light use efficiency using the photochemical reflectance index - Model and sensitivity analysis. Remote Sensing of Environment 78, 264 - 273.

Beerling DJ, Fry JC (1990) A comparison of the accuracy, variability and speed of five different methods for estimating leaf area. Annals of Botany 65, 483-488.

Blackburn GA (2007) Hyperspectral remote sensing of plant pigments. Journal of Experimental Botany 58, 855-867.

Boegh E, Soegaard H, Broge N, Hasager CB, Jensen NO, Schelde K, Thomsen A (2002) Airborne multispectral data for quantifying leaf area index, nitrogen concentration, and photosynthetic efficiency in agriculture. Remote Sensing of Environment 81, 179-193.

Bolster KL, Martin ME, Aber JD (1996) Determination of carbon fraction and nitrogen concentration in tree foliage by near infrared reflectance: A comparison of statistical methods. Canadian Journal of Forest Research-Revue Canadienne De Recherche Forestiere 26, 590-600.

Bonan GB (2008) Forests and climate change: Forcings, feedbacks, and the climate benefits of forests. Science 320, 1444-1449.

Bond BJ, Farnsworth BT, Coulombe RA, Winner WE (1999) Foliage physiology and biochemistry in response to light gradients in conifers with varying shade tolerance. Oecologia 120, 183-192.

Brandtberg T, Warner TA, Landenberger RE, McGraw JB (2003) Detection and analysis of individual leaf-off tree crowns in small footprint, high sampling density lidar data from the eastern deciduous forest in North America. Remote Sensing of Environment 85, 290-303.

Broge NH, Leblanc E (2001) Comparing prediction power and stability of broadband and hyperspectral vegetation indices for estimation of green leaf area index and canopy chlorophyll density. Remote Sensing of Environment 76, 156-172.

Buonasera K, Lambreva M, Rea G, Touloupakis E, Giardi MT (2011) Technological applications of chlorophyll a fluorescence for the assessment of environmental

pollutants. Analytical and Bioanalytical Chemistry 401, 1139-1151.

Burkhard B, Kroll F, Müller F, Windhorst W (2009) Landscapes' capacities to provide ecosystem services – a concept for land-cover based assessments. Landscape Online 15, 1-22.

Burkhard B, Kroll F, Nedkov S, Müller F (2012) Mapping ecosystem service supply, demand and budgets. Ecological Indicators 21, 17-29.

Buschmann C (2007) Variability and application of the chlorophyll fluorescence emission ratio red/far-red of leaves. Photosynthesis Research 92, 261-271.

Canadell JG, Le Quéré C, Raupach MR, Field CB, Buitenhuis ET, Ciais P, Conway TJ, Gillett NP, Houghton RA, Marland G (2007) Contributions to accelerating atmospheric CO2 growth from economic activity, carbon intensity, and efficiency of natural sinks. Proceedings of the National Academy of Sciences of the United States of America 104, 18866-18870.

Cartus O, Kellndorfer J, Rombach M, Walker W (2012) Mapping canopy height and growing stock volume using airborne lidar, ALOS PALSAR and Landsat ETM+. Remote Sensing 4, 3320-3345.

Caubet S (2009) Approche fonctionnelle diachronique et pluriscalaire des queyrellins de Villar d'Arène, Laboratoire d'ecologie Alpine. Université Montpellier II, Grenoble, p. 85.

Cescatti A, Zorer R (2003) Structural acclimation and radiation regime of silver fir (Abies alba Mill.) shoots along a light gradient. Plant, Cell and Environment 26, 429-442.

Chan KMA, Shaw MR, Cameron DR, Underwood EC, Daily GC (2006) Conservation planning for ecosystem services. PLoS Biology 4, 2138-2152.

Chen JM, Pavlic G, Brown L, Cihlar J, Leblanc SG, White HP, Hall RJ, Peddle DR, King DJ, Trofymow JA, et al. (2002) Derivation and validation of Canada-wide coarse-resolution leaf area index maps using high-resolution satellite imagery and ground measurements. Remote Sensing of Environment 80, 165-184.

Chen M, Schliep M, Willows RD, Cai ZL, Neilan BA, Scheer H (2010a) A red-shifted chlorophyll. Science 329, 1318-1319.

Chen P, Haboudane D, Tremblay N, Wang J, Vigneault P, Li B (2010b) New spectral indicator assessing the efficiency of crop nitrogen treatment in corn and wheat. Remote Sensing of Environment 114, 1987-1997.

Cheng YB, Zarco-Tejada PJ, Riaño D, Rueda CA, Ustin SL (2006) Estimating vegetation water content with hyperspectral data for different canopy scenarios: Relationships between AVIRIS and MODIS indexes. Remote Sensing of Environment 105, 354-366.

Chmura DJ, Tjoelker MG (2008) Leaf traits in relation to crown development, light interception and growth of elite families of loblolly and slash pine. Tree Physiology 28, 729-742.

Cho MA, Skidmore A, Corsi F, van Wieren SE, Sobhan I (2007) Estimation of green grass/herb biomass from airborne hyperspectral imagery using spectral indices and partial least squares regression. International Journal of Applied Earth Observation and Geoinformation 9, 414-424.

Cho MA, Skidmore AK (2006) A new technique for extracting the red edge position from hyperspectral data: The linear extrapolation method. Remote Sensing of Environment 101, 181-193.

Chopping MJ (2008) Terrestrial applications of multiangle remote sensing, in: Liang S (Ed.), Advances in Land Remote Sensing: System, Modeling, Inversion and Application. Springer, pp. 95-144.

Chopping M, Moisen GG, Su L, Laliberte A, Rango A, Martonchik JV, Peters DPC (2008) Large area mapping of southwestern forest crown cover, canopy height, and biomass using the NASA Multiangle Imaging Spectro-Radiometer. Remote Sensing of Environment 112, 2051-2063.

Chuvieco E, Riaño D, Aguado I, Cocero D (2002) Estimation of fuel moisture content from multitemporal analysis of Landsat Thematic Mapper reflectance data: Applications in fire danger assessment. International Journal of Remote Sensing 23, 2145-2162.

Clark ML, Clark DB, Roberts DA (2004) Small-footprint lidar estimation of sub-canopy elevation and tree height in a tropical rain forest landscape. Remote Sensing of Environment 91, 68-89.

Clark RN, Roush TL (1984) Reflectance spectroscopy: quantitative analysis techniques for remote sensing applications. Journal of Geophysical Research 89, 6329-6340.

Clevers JGPW (1989) Application of a weighted infrared-red vegetation index for estimating leaf area index by correcting for soil moisture. Remote Sensing of Environment 29, 25-37.

Clevers JGPW, Kooistra L (2012) Using hyperspectral remote sensing data for retrieving canopy chlorophyll and nitrogen content. IEEE Journal of Selected Topics in Applied Earth Observations and Remote Sensing 5, 574-583.

Clevers JGPW, Kooistra L, Schaepman ME (2008) Using spectral information from the NIR water absorption features for the retrieval of canopy water content. International Journal of Applied Earth Observation and Geoinformation 10, 388-397.

Clevers JGPW, Kooistra L, Schaepman ME (2010) Estimating canopy water content using hyperspectral remote sensing data. International Journal of Applied Earth Observation and Geoinformation 12, 119-125.

Cohen WB, Goward SN (2004) Landsat's role in ecological applications of remote sensing. BioScience 54, 535-545.

Colombo R, Bellingeri D, Fasolini D, Marino CM (2003) Retrieval of leaf area index in different vegetation types using high resolution satellite data. Remote Sensing of Environment 86, 120-131.

Colombo R, Meroni M, Marchesi A, Busetto L, Rossini M, Giardino C, Panigada C (2008) Estimation of leaf and canopy water content in poplar plantations by means of hyperspectral indices and inverse modeling. Remote Sensing of Environment 112, 1820-1834.

Combal B, Baret F, Weiss M, Trubuil A, Mace D, Pragnere A, Myneni R, Knyazikhin Y, Wang L (2003) Retrieval of canopy biophysical variables from bidirectional reflectance: Using prior information to solve the ill-posed inverse problem. Remote Sensing of Environment 84, 1-15.

Coops NC, Hilker T, Hall FG, Nichol CJ, Drolet GG (2010) Estimation of light-use efficiency of terrestrial ecosystems from space: A status report. BioScience 60, 788-797.

Coops NC, Smith ML, Martin ME, Ollinger SV (2003) Prediction of eucalypt foliage nitrogen content from satellite-derived hyperspectral data. IEEE Transactions on Geoscience and Remote Sensing 41, 1338-1346.

Cornelissen JHC, Lavorel S, Garnier E, Díaz S, Buchmann N, Gurvich DE, Reich PB, Ter Steege H, Morgan HD, van der Heijden MGA, et al. (2003) A handbook of protocols for standardised and easy measurement of plant functional traits worldwide. Australian Journal of Botany 51, 335-380.

Costanza R, D'Arge R, de Groot R, Farber S, Grasso M, Hannon B, Limburg K, Naeem S, O'Neill RV, Paruelo J, et al. (1997) The value of the world's ecosystem services and natural capital. Nature 387, 253-260.

Curran PJ (1989) Remote sensing of foliar chemistry. Remote Sensing of Environment 30, 271-278.

Curran PJ, Dungan JL, Peterson DL (2001) Estimating the foliar biochemical concentration of leaves with reflectance spectrometry testing the Kokaly and Clark methodologies. Remote Sensing of Environment 76, 349-359.

D'Odorico P, Gonsamo A, Pinty B, Gobron N, Schaepman M, Coops NC, Mendez E (2013) Intercomparison of fractional absorbed photosynthetically active radiation products derived from satellite data over Europe. (submitted).

Dahlgren JP, Von Zeipel H, Ehrlén J (2007) Variation in vegetative and flowering phenology in a forest herb caused by environmental heterogeneity. American Journal of Botany 94, 1570-1576.

Damm A, Elber J, Erler A, Giol G, Hamdi K, Hutjes R, Košvancová M, Meroni M, Miglietta F, Moersch A, et al. (2010) Remote sensing of sun-induced fluorescence to improve modeling of diurnal courses of gross primary production (GPP). Global Change Biology 16, 171-186.

Danson FM, Morsdorf F, Koetz B (2009) Airborne and terrestrial laser scanning for measuring vegetation canopy structure, in: Heritage GL, Large ARG (Eds.), Laser Scanning for the Environmental Sciences. Wiley-Blackwell, Oxford, UK, pp. 201-219.

Darvishzadeh R, Skidmore A, Schlerf M, Atzberger C, Corsi F, Cho M (2008) LAI and chlorophyll estimation for a heterogeneous grassland using hyperspectral measurements. ISPRS Journal of Photogrammetry and Remote Sensing 63, 409-426.

Dash J, Curran PJ (2004) The MERIS terrestrial chlorophyll index. International Journal of Remote Sensing 25, 5403-5413.

Dash J, Jeganathan C, Atkinson PM (2010) The use of MERIS Terrestrial Chlorophyll Index to study spatio-temporal variation in vegetation phenology over India. Remote Sensing of Environment 114, 1388-1402.

Datt B (1998) Remote sensing of chlorophyll a, chlorophyll b, chlorophyll a+b, and total carotenoid content in eucalyptus leaves. Remote Sensing of Environment 66, 111-121.

Daughtry CST, Walthall CL, Kim MS, de Colstoun EB, McMurtrey JE (2000) Estimating corn leaf chlorophyll concentration from leaf and canopy reflectance. Remote Sensing of Environment 74, 229-239.

Davenport IJ, Bradbury RB, Anderson GQA, Hayman GRF, Krebs JR, Mason DC, Wilson JD, Veck NJ (2000) Improving bird population models using airborne remote sensing. International Journal of Remote Sensing 21, 2705-2717.

Davidson A, Csillag F (2001) The influence of vegetation index and spatial resolution on a two-date remote sensing-derived relation to C4 species coverage. Remote Sensing of Environment 75, 138-151.

Dawson TP, Curran PJ, North PRJ, Plummer SE (1999) The propagation of foliar biochemical absorption features in forest canopy reflectance: A theoretical analysis. Remote Sensing of Environment 67, 147-159.

de Bello F, Lepš J, Sebastia MT (2006) Variations in species and functional plant diversity along climatic and grazing gradients. Ecography 29, 801-810.

de Beurs KM, Henebry GM (2010) Spatio-temporal statistical emthods for modeling land surface phenology, in: Hudson IL, Keatley MR (Eds.), Phenological Research: Methods for Environmental and Climate Change Analysis. Springer, pp. 177-208.

de Groot RS, Alkemade R, Braat L, Hein L, Willemen L (2010) Challenges in integrating the concept of ecosystem services and values in landscape planning, management and decision making. Ecological Complexity 7, 260-272.

de Groot RS, Wilson MA, Boumans RMJ (2002) A typology for the classification, description and valuation of ecosystem functions, goods and services. Ecological Economics 41, 393-408.

de Jong R, Verbesselt J, Schaepman ME, de Bruin S (2012) Trend changes in global greening and browning: Contribution of short-term trends to longer-term change. Global Change Biology 18, 642-655.

Delbart N, le Toan T, Kergoat L, Fedotova V (2006) Remote sensing of spring phenology in boreal regions: A free of snow-effect method using NOAA-AVHRR and SPOT-VGT data (1982-2004). Remote Sensing of Environment 101, 52-62.

Di Sabatino A, Coscieme L, Vignini P, Cicolani B (2013) Scale and ecological dependence of ecosystem services evaluation: Spatial extension and economic value of freshwater ecosystems in Italy. Ecological Indicators 32, 259-263.

Díaz S, Cabido M (1997) Plant functional types and ecosystem function in relation to global change. Journal of Vegetation Science 8, 463-474.

Díaz S, Hodgson JG, Thompson K, Cabido M, Cornelissen JHC, Jalili A, Montserrat-Martí G, Grime JP, Zarrinkamar F, Asri Y, et al. (2004) The plant traits that drive ecosystems: Evidence from three continents. Journal of Vegetation Science 15, 295-304.

Dirnböck T, Dullinger S, Grabherr G (2003) A regional impact assessment of climate and land-use change on alpine vegetation. Journal of Biogeography 30, 401-417.

Disney M, Lewis P, Saich P (2006) 3D modelling of forest canopy structure for remote sensing simulations in the optical and microwave domains. Remote Sensing of Environment 100, 114-132.

Disney MI, Lewis P, North PRJ (2000) Monte Carlo ray tracing in optical canopy reflectance modelling. Remote Sensing Reviews 18, 163-196.

Doney SC, Fabry VJ, Feely RA, Kleypas JA (2009) Ocean acidification: The other CO2 problem. Annual Review of Marine Science 1, 169-192.

Duru M (1997) Leaf and stem in vitro digestibility for grasses and dicotyledons of meadow plant communities in spring. Journal of the Science of Food and Agriculture 74, 175-185.

Egoh B, Reyers B, Rouget M, Richardson DM, le Maitre DC, van Jaarsveld AS (2008) Mapping ecosystem services for

planning and management. Agriculture, Ecosystems and Environment 127, 135-140.

Ehleringer JR, Cerling TE, Helliker BR (1997) C4 photosynthesis, atmospheric CO2, and climate. Oecologia 112, 285-299.

Eigenbrod F, Armsworth PR, Anderson BJ, Heinemeyer A, Gillings S, Roy DB, Thomas CD, Gaston KJ (2010) The impact of proxy-based methods on mapping the distribution of ecosystem services. Journal of Applied Ecology 47, 377-385.

Eitel JUH, Long DS, Gessler PE, Smith AMS (2007) Using in-situ measurements to evaluate the new RapidEye™ satellite series for prediction of wheat nitrogen status. International Journal of Remote Sensing 28, 4183-4190.

Erdfelder E, Faul F, Buchner A (1996) GPOWER: A general power analysis program. Behavior Research Methods, Instruments, and Computers 28, 1-11.

Erdody TL, Moskal LM (2010) Fusion of LiDAR and imagery for estimating forest canopy fuels. Remote Sensing of Environment 114, 725-737.

Eriksson HM, Eklundh L, Kuusk A, Nilson T (2006) Impact of understory vegetation on forest canopy reflectance and remotely sensed LAI estimates. Remote Sensing of Environment 103, 408-418.

Falkowski MJ, Smith AMS, Gessler PE, Hudak AT, Vierling LA, Evans JS (2008) The influence of conifer forest canopy cover on the accuracy of two individual tree measurement algorithms using lidar data. Canadian Journal of Remote Sensing 34, S338-S350.

Feng W, Yao X, Zhu Y, Tian YC, Cao WX (2008) Monitoring leaf nitrogen status with hyperspectral reflectance in wheat. European Journal of Agronomy 28, 394-404.

Fensholt R, Sandholt I, Rasmussen MS (2004) Evaluation of MODIS LAI, fAPAR and the relation between fAPAR and NDVI in a semi-arid environment using in situ measurements. Remote Sensing of Environment 91, 490-507.

Feret JB, Francois C, Asner GP, Gitelson AA, Martin RE, Bidel LPR, Ustin SL, le Maire G, Jacquemoud S (2008) PROSPECT-4 and 5: Advances in the leaf optical properties model separating photosynthetic pigments. Remote Sensing of Environment 112, 3030-3043.

Fernandes RA, Miller JR, Chen JM, Rubinstein IG (2004) Evaluating image-based estimates of leaf area index in boreal conifer stands over a range of scales using high-resolution CASI imagery. Remote Sensing of Environment 89, 200-216.

Ferwerda JG, Skidmore AK (2007) Can nutrient status of four woody plant species be predicted using field spectrometry? ISPRS Journal of Photogrammetry and Remote Sensing 62, 406-414.

Ferwerda JG, Skidmore AK, Mutanga O (2005) Nitrogen detection with hyperspectral normalized ratio indices across multiple plant species. International Journal of Remote Sensing 26, 4083-4095.

Field CB, Randerson JT, Malmstrom CM (1995) Global net primary production: Combining ecology and remote sensing. Remote Sensing of Environment 51, 74-88.

Fisher B, Turner RK, Morling P (2009) Defining and classifying ecosystem services for decision making. Ecological Economics 68, 643-653.

Foody GM, Dash J (2007) Discriminating and mapping the C3 and C4 composition of grasslands in the northern Great Plains, USA. Ecological Informatics 2, 89-93.

Fortunel C, Garnier E, Joffre R, Kazakou E, Quested H, Grigulis K, Lavorel S, Ansquer P, Castro H, Cruz P, et al. (2009) Leaf traits capture the effects of land use changes and climate on litter decomposability of grasslands across Europe. Ecology 90, 598-611.

Fourty TH, Baret F (1998) On spectral estimates of fresh leaf biochemistry. International Journal of Remote Sensing 19, 1283-1297.

Friedl MA, Sulla-Menashe D, Tan B, Schneider A, Ramankutty N, Sibley A, Huang X (2010) MODIS Collection 5 global land cover: Algorithm refinements and characterization of new datasets. Remote Sensing of Environment 114, 168-182.

Galloway JN, Townsend AR, Erisman JW, Bekunda M, Cai Z, Freney JR, Martinelli LA, Seitzinger SP, Sutton MA (2008) Transformation of the nitrogen cycle: Recent trends, questions, and potential solutions. Science 320, 889-892.

Gamon JA, Peñuelas J, Field CB (1992) A narrow-waveband spectral index that tracks diurnal changes in photosynthetic efficiency. Remote Sensing of Environment 41, 35-44.

Garbulsky MF, Peñuelas J, Gamon J, Inoue Y, Filella I (2011) The photochemical reflectance index (PRI) and the remote sensing of leaf, canopy and ecosystem radiation use efficiencies. A review and meta-analysis. Remote Sensing of Environment 115, 281-297.

Garnier E, Lavorel S, Ansquer P, Castro H, Cruz P, Dolezal J, Eriksson O, Fortunel C, Freitas H, Golodets C, et al. (2007) Assessing the effects of land-use change on plant traits, communities and ecosystem functioning in grasslands: A standardized methodology and lessons from an application to 11 European sites. Annals of Botany 99, 967-985.

Garnier E, Shipley B, Roumet C, Laurent G (2001) A standardized protocol for the determination of specific leaf area and leaf dry matter content. Functional Ecology 15, 688-695.

Gastellu-Etchegorry JP, Bruniquel-Pinel V (2001) A modeling approach to assess the robustness of spectrometric predictive equations for canopy chemistry. Remote Sensing of Environment 76, 1-15.

Gastellu-Etchegorry JP, Demarez V, Pinel V, Zagolski F (1996) Modeling radiative transfer in heterogeneous 3-D vegetation canopies. Remote Sensing of Environment 58, 131-156.

Gastellu-Etchegorry JP, Martin E, Gascon F (2004) DART: a 3D model for simulating satellite images and studying surface radiation budget. International Journal of Remote Sensing 25, 73-96.

Gitelson AA (2002) Assessing carotenoid content in plant leaves with reflectance spectroscopy. Photochemistry and Photobiology 75, 272-281.

Gitelson AA, Gritz Y, Merzlyak MN (2003) Relationships between leaf chlorophyll content and spectral reflectance and algorithms for non-destructive chlorophyll assessment in higher plant leaves. Journal of Plant Physiology 160, 271-282.

Gitelson AA, Keydan GP, Merzlyak MN (2006) Three-band model for noninvasive estimation of chlorophyll, carotenoids, and anthocyanin contents in higher plant leaves. Geophysical Research Letters 33, L11402.

Gitelson AA, Merzlyak MN, Lichtenthaler HK (1996) Detection of red edge position and chlorophyll content by

reflectance measurements near 700 nm. Journal of Plant Physiology 148, 501-508.

Glenn NF, Spaete LP, Sankey TT, Derryberry DR, Hardegree SP, Mitchell J (2011) Errors in LiDAR-derived shrub height and crown area on sloped terrain. Journal of Arid Environments 75, 377-382.

Gobron N, Pinty B, Verstraete MM, Widlowski JL (2000) Advanced vegetation indices optimized for up-coming sensors: design, performance, and applications. IEEE Transactions on Geoscience and Remote Sensing 38, 2489-2505.

Gobron N, Verstraete M (2009) Assesment of the status of the development of the standards for the terrestrial essential climate variables: FAPAR - Fraction of Absorbed Photosynehtetically Active Radiation. Global Terrestrial Observing System, FAO, Rome, Italy, p. 24.

Goetz AFH (2009) Three decades of hyperspectral remote sensing of the Earth: A personal view. Remote Sensing of Environment 113.

Grace J, Nichol C, Disney M, Lewis P, Quaife T, Bowyer P (2007) Can we measure terrestrial photosynthesis from space directly, using spectral reflectance and fluorescence? Global Change Biology 13, 1484-1497.

Grêt-Regamey A, Brunner SH, Kienast F (2012) Mountain ecosystem services: Who cares? Mountain Research and Development 32, S23-S34.

Grime JP (1998) Benefits of plant diversity to ecosystems: Immediate, filter and founder effects. Journal of Ecology 86, 902-910.

Grossman YL, Ustin SL, Jacquemoud S, Sanderson EW, Schmuck G, Verdebout J (1996) Critique of stepwise multiple linear regression for the extraction of leaf biochemistry information from leaf reflectance data. Remote Sensing of Environment 56, 182-193.

Guanter L, Estellés V, Moreno J (2007) Spectral calibration and atmospheric correction of ultra-fine spectral and spatial resolution remote sensing data. Application to CASI-1500 data. Remote Sensing of Environment 109, 54-65.

Guanter L, Frankenberg C, Dudhia A, Lewis PE, Gómez-Dans J, Kuze A, Suto H, Grainger RG (2012) Retrieval and global assessment of terrestrial chlorophyll fluorescence from GOSAT space measurements. Remote Sensing of Environment 121, 236-251.

Guo J, Trotter CM (2004) Estimating photosynthetic light-use efficiency using the photochemical reflectance index: Variations among species. Functional Plant Biology 31, 255-265.

Haboudane D, Miller JR, Tremblay N, Zarco-Tejada PJ, Dextraze L (2002) Integrated narrow-band vegetation indices for prediction of crop chlorophyll content for application to precision agriculture. Remote Sensing of Environment 81, 416-426.

Hagen A (2003) Fuzzy set approach to assessing similarity of categorical maps. International Journal of Geographical Information Science 17, 235-249.

Hakala T, Suomalainen J, Kaasalainen S, Chen Y (2012) Full waveform hyperspectral LiDAR for terrestrial laser scanning. Optics Express 20, 7119-7127.

Hallik L, Kull O, Niinemets Ü, Aan A (2009) Contrasting correlation networks between leaf structure, nitrogen and chlorophyll in herbaceous and woody canopies. Basic and Applied Ecology 10, 309-318.

Hamada Y, Stow DA, Coulter LL, Jafolla JC, Hendricks LW (2007) Detecting Tamarisk species (Tamarix spp.) in riparian habitats of Southern California using high spatial resolution hyperspectral imagery. Remote Sensing of Environment 109, 237-248.

Hansen PM, Schjoerring JK (2003) Reflectance measurement of canopy biomass and nitrogen status in wheat crops using normalized difference vegetation indices and partial least squares regression. Remote Sensing of Environment 86, 542-553.

Harris A, Dash J (2010) The potential of the MERIS Terrestrial Chlorophyll Index for carbon flux estimation. Remote Sensing of Environment 114, 1856-1862.

Hatch MD (1987) C4 photosynthesis: a unique blend of modified biochemistry, anatomy and ultrastructure. BBA Reviews On Bioenergetics 895, 81-106.

Hernández-Clemente R, Navarro-Cerrillo RM, Suárez L, Morales F, Zarco-Tejada PJ (2011) Assessing structural effects on PRI for stress detection in conifer forests. Remote Sensing of Environment 115, 2360-2375.

Hernández-Clemente R, Navarro-Cerrillo RM, Zarco-Tejada PJ (2012) Carotenoid content estimation in a heterogeneous conifer forest using narrow-band indices and PROSPECT+DART simulations. Remote Sensing of Environment 127, 298-315.

Hestir EL, Khanna S, Andrew ME, Santos MJ, Viers JH, Greenberg JA, Rajapakse SS, Ustin SL (2008) Identification of invasive vegetation using hyperspectral remote sensing in the California Delta ecosystem. Remote Sensing of Environment 112, 4034-4047.

Hilker T, Coops NC, Hall FG, Black TA, Wulder MA, Nesic Z, Krishnan P (2008a) Separating physiologically and directionally induced changes in PRI using BRDF models. Remote Sensing of Environment 112, 2777-2788.

Hilker T, Coops NC, Wulder MA, Black TA, Guy RD (2008b) The use of remote sensing in light use efficiency based models of gross primary production: A review of current status and future requirements. Science of the Total Environment 404, 411-423.

Holmgren J, Nilsson M, Olsson H (2003) Estimation of tree height and stem volume on plots using airborne laser scanning. Forest Science 49, 419-428.

Homolová L, Lukeš P, Malenovský Z, Lhotáková Z, Kaplan V, Hanuš J (2013a) Measurement methods and variability assessment of the Norway spruce total leaf area: Implications for remote sensing. Trees - Structure and Function 27, 111-121.

Homolová L, Malenovský Z, Clevers JGPW, García-Santos G, Schapeman ME (2013b) Review of optical-based remote sensing for plant trait mapping. Ecological Complexity in press.

Hopkinson C, Chasmer L, Young-Pow C, Treitz P (2004) Assessing forest metrics with a ground-based scanning lidar. Canadian Journal of Forest Research 34, 573-583.

Hu H, Liu W, Cao M (2008) Impact of land use and land cover changes on ecosystem services in Menglun, Xishuangbanna, Southwest China. Environmental Monitoring and Assessment 146, 147-156.

Huber S, Kneubühler M, Psomas A, Itten K, Zimmermann NE (2008) Estimating foliar biochemistry from hyperspectral data in mixed forest canopy. Forest Ecology and Management 256, 491-501.

Huete A, Didan K, Miura T, Rodriguez EP, Gao X, Ferreira LG (2002) Overview of the radiometric and biophysical performance of the MODIS vegetation indices. Remote Sensing of Environment 83, 195-213.

Hyde P, Dubayah R, Walker W, Blair JB, Hofton M, Hunsaker C (2006) Mapping forest structure for wildlife habitat analysis using multi-sensor (LiDAR, SAR/InSAR, ETM+, Quickbird) synergy. Remote Sensing of Environment 102, 63-73.

IPCC (2007) Climate change 2007: The physical science basis. Contribution of Working Group I to the Fourth Assessment Report of the Intergovernmental Panel on Climate Change, in: Solomon S, Qin D, Manning M, Chen Z, Marquis M, Averyt KB, Tignor M, Miller HL (Eds.). Cambridge University Press, Cambridge UK and New York, USA, p. 996.

Irisarri JGN, Oesterheld M, Verón SR, Paruelo JM (2009) Grass species differentiation through canopy hyperspectral reflectance. International Journal of Remote Sensing 30, 5959-5975.

Jacquemoud S, Baret F (1990) PROSPECT: A model of leaf optical properties spectra. Remote Sensing of Environment 34, 75-91.

Jacquemoud S, Ustin SL, Verdebout J, Schmuck G, Andreoli G, Hosgood B (1996) Estimating leaf biochemistry using the PROSPECT leaf optical properties model. Remote Sensing of Environment 56, 194-202.

Jacquemoud S, Verhoef W, Baret F, Bacour C, Zarco-Tejada PJ, Asner GP, Francois C, Ustin SL (2009) PROSPECT + SAIL models: A review of use for vegetation characterization. Remote Sensing of Environment 113, S56-S66.

Jakubowski MK, Guo Q, Kelly M (2013) Tradeoffs between lidar pulse density and forest measurement accuracy. Remote Sensing of Environment 130, 245-253.

Jia GJ, Burke IC, Goetz AFH, Kaufmann MR, Kindel BC (2006) Assessing spatial patterns of forest fuel using AVIRIS data. Remote Sensing of Environment 102, 318-327.

Johnson JD (1984) A rapid technique for estimating total surface area of pine needles. Forest Science 30, 913-921.

Johnson LF, Billow CR (1996) Spectrometric estimation of total nitrogen concentration in Douglas-fir foliage. International Journal of Remote Sensing 17, 489-500.

Johnson LF, Hlavka CA, Peterson DL (1994) Multivariate analysis of AVIRIS data for canopy biochemical estimation along the oregon transect. Remote Sensing of Environment 47, 216-230.

Joiner J, Yoshida Y, Vasilkov AP, Corp LA, Middleton EM (2011) First observations of global and seasonal terrestrial chlorophyll fluorescence from space. Biogeosciences 8, 637-651.

Jongschaap REE, Booij R (2004) Spectral measurements at different spatial scales in potato: Relating leaf, plant and canopy nitrogen status. International Journal of Applied Earth Observation and Geoinformation 5, 205-218.

Joos F, Spahni R (2008) Rates of change in natural and anthropogenic radiative forcing over the past 20,000 years. Proceedings of the National Academy of Sciences of the United States of America 105, 1425-1430.

Jordan CF (1969) Derivation of leaf area index from quality of light on the forest floor. Ecology 50, 663-666.

Julien Y, Sobrino JA (2009) Global land surface phenology trends from GIMMS database. International Journal of Remote Sensing 30, 3495-3513.

Kaartinen H, Hyyppä J, Yu X, Vastaranta M, Hyyppä H, Kukko A, Holopainen M, Heipke C, Hirschmugl M, Morsdorf F, et al. (2012) An international comparison of individual tree detection and extraction using airborne laser scanning. Remote Sensing 4, 950-974.

Kalacska M, Bohlman S, Sanchez-Azofeifa GA, Castro-Esau K, Caelli T (2007) Hyperspectral discrimination of tropical dry forest lianas and trees: Comparative data reduction approaches at the leaf and canopy levels. Remote Sensing of Environment 109, 406-415.

Kalina J, Urban O, Čajánek M, Kurasová I, Špunda V, Marek MV (2001) Different responses of Norway spruce needles from shaded and exposed crown layers to the prolonged exposure to elevated CO2 studied by various chlorophyll a fluorescence techniques. Photosynthetica 39, 369-376.

Kampe TU, Johnson BR, Kuester MA, Keller M (2010) NEON: The first continental-scale ecological observatory with airborne remote sensing of vegetation canopy biochemistry and structure. Journal of Applied Remote Sensing 4, art. no. 043510.

Kattge J, Díaz S, Lavorel S, Prentice IC, Leadley P, Bönisch G, Garnier E, Westoby M, Reich PB, Wright IJ, et al. (2011) TRY - a global database of plant traits. Global Change Biology 17, 2905-2935.

Kimes DS, Kirchner JA (1982) Radiative transfer model for heterogeneous 3-D scenes. Applied Optics 21, 4119-4129.

Kimes DS, Knyazikhin Y, Privette JL, Abuelgasim AA, Gao F (2000) Inversion methods for physically-based models. Remote Sensing Reviews 18, 381-439.

Klein Goldewijk K, Beusen A, van Drecht G, de Vos M (2011) The HYDE 3.1 spatially explicit database of human-induced global land-use change over the past 12,000 years. Global Ecology and Biogeography 20, 73-86.

Kleyer M, Bekker RM, Knevel IC, Bakker JP, Thompson K, Sonnenschein M, Poschlod P, van Groenendael JM, Klimeš L, Klimešová J, et al. (2008) The LEDA Traitbase: A database of life-history traits of the Northwest European flora. Journal of Ecology 96, 1266-1274.

Knox NM, Skidmore AK, Prins HHT, Asner GP, van der Werff HMA, de Boer WF, van der Waal C, de Knegt HJ, Kohi EM, Slotow R, et al. (2011) Dry season mapping of savanna forage quality, using the hyperspectral Carnegie Airborne Observatory sensor. Remote Sensing of Environment 115, 1478-1488.

Knyazikhin Y, Schull MA, Stenberg P, Mõttus M, Rautiainen M, Yang Y, Marshak A, Latorre Carmona P, Kaufmann RK, Lewis P, et al. (2012) Hyperspectral remote sensing of foliar nitrogen content. Proceedings of the National Academy of Sciences 110, E185-E192.

Knyazikhin Y, Schull MA, Xu L, Myneni RB, Samanta A (2011) Canopy spectral invariants. Part 1: A new concept in remote sensing of vegetation. Journal of Quantitative Spectroscopy and Radiative Transfer 112, 727-735.

Koch B (2010) Status and future of laser scanning, synthetic aperture radar and hyperspectral remote sensing data for forest biomass assessment. ISPRS Journal of Photogrammetry and Remote Sensing 65, 581-590.

Koetz B, Schaepman M, Morsdorf F, Bowyer P, Itten K, Allgower B (2004) Radiative transfer modeling within a heterogeneous canopy for estimation of forest fire fuel properties. Remote Sensing of Environment 92, 332-344.

Kokaly RF (2001) Investigating a physical basis for spectroscopic estimates of leaf nitrogen concentration. Remote Sensing of Environment 75, 153-161.

Kokaly RF, Asner GP, Ollinger SV, Martin ME, Wessman CA (2009) Characterizing canopy biochemistry from imaging spectroscopy and its application to ecosystem studies. Remote Sensing of Environment 113, S78-S91.

Kokaly RF, Clark RN (1999) Spectroscopic determination of leaf biochemistry using band-depth analysis of absorption features and stepwise multiple linear regression. Remote Sensing of Environment 67, 267-287.

Kokaly RF, Despain DG, Clark RN, Livo KE (2003) Mapping vegetation in Yellowstone National Park using spectral feature analysis of AVIRIS data. Remote Sensing of Environment 84, 437-456.

Konarska KM, Sutton PC, Castellon M (2002) Evaluating scale dependence of ecosystem service valuation: A comparison of NOAA-AVHRR and Landsat TM datasets. Ecological Economics 41, 491-507.

Körner C (1999) Alpine Plant Life: functional plant ecology of high mountain ecosystems. Springer-Verlag Berlin Heidelberg Germany.

Kraft NJB, Valencia R, Ackerly DD (2008) Functional traits and niche-based tree community assembly in an Amazonian forest. Science 322, 580-582.

Kross A, Fernandes R, Seaquist J, Beaubien E (2011) The effect of the temporal resolution of NDVI data on season onset dates and trends across Canadian broadleaf forests. Remote Sensing of Environment 115, 1564-1575.

Kumar L, Schmidt K, Dury SJ, Skidmore A (2001) Imaging spectrometry and vegetation sciences, in: van der Meer FD, de Jong SM (Eds.), Imaging Spectrometry. Basic principles and prospective applications. Kluwer Academic Publishers, Dordrecht, The Netherlands, pp. 111-155.

Kurokawa H, Peltzer DA, Wardle DA (2010) Plant traits, leaf palatability and litter decomposability for co-occurring woody species differing in invasion status and nitrogen fixation ability. Functional Ecology 24, 513-523.

Lamarque P, Tappeiner U, Turner C, Steinbacher M, Bardgett RD, Szukics U, Schermer M, Lavorel S (2011) Stakeholder perceptions of grassland ecosystem services in relation to knowledge on soil fertility and biodiversity. Regional Environmental Change 11, 791-804.

Lasaponara R, Lanorte A (2007) Remotely sensed characterization of forest fuel types by using satellite ASTER data. International Journal of Applied Earth Observation and Geoinformation 9, 225-234.

Laurent VCE, Verhoef W, Clevers JGPW, Schaepman ME (2011a) Estimating forest variables from top-of-atmosphere radiance satellite measurements using coupled radiative transfer models. Remote Sensing of Environment 115, 1043-1052.

Laurent VCE, Verhoef W, Clevers JGPW, Schaepman ME (2011b) Inversion of a coupled canopy-atmosphere model using multi-angular top-of-atmosphere radiance data: A forest case study. Remote Sensing of Environment 115, 2603-2612.

Lautenbach S, Kugel C, Lausch A, Seppelt R (2011) Analysis of historic changes in regional ecosystem service provisioning using land use data. Ecological Indicators 11, 676-687.

Lavorel S, Garnier E (2002) Predicting changes in community composition and ecosystem functioning from plant traits: Revisiting the Holy Grail. Functional Ecology 16, 545-556.

Lavorel S, Grigulis K, Lamarque P, Colace M, Garden D, Girel J, Pellet G, Douzet R (2011) Using plant functional traits to understand the landscape distribution of multiple ecosystem services. Journal of Ecology 99, 135-147.

Lavorel S, Grigulis K, McIntyre S, Williams NSG, Garden D, Dorrough J, Berman S, Quétier F, Thébault A, Bonis A (2008) Assessing functional diversity in the field - Methodology matters! Functional Ecology 22, 134-147.

le Maire G, François C, Dufrêne E (2004) Towards universal broad leaf chlorophyll indices using PROSPECT simulated database and hyperspectral reflectance measurements. Remote Sensing of Environment 89, 1-28.

le Maire G, François C, Soudani K, Berveiller D, Pontailler JY, Bréda N, Genet H, Davi H, Dufrêne E (2008) Calibration and validation of hyperspectral indices for the estimation of broadleaved forest leaf chlorophyll content, leaf mass per area, leaf area index and leaf canopy biomass. Remote Sensing of Environment 112, 3846-3864.

le Toan T, Quegan S, Davidson MWJ, Balzter H, Paillou P, Papathanassiou K, Plummer S, Rocca F, Saatchi S, Shugart H, et al. (2011) The BIOMASS mission: Mapping global forest biomass to better understand the terrestrial carbon cycle. Remote Sensing of Environment 115, 2850-2860.

LeBauer DS, Treseder KK (2008) Nitrogen limitation of net primary productivity in terrestrial ecosystems is globally distributed. Ecology 89, 371-379.

Lefsky MA (2002) Lidar remote sensing for ecosystem studies. BioScience 52, 19-30.

Lhotáková Z, Albrechtová J, Malenovský Z, Rock BN, Polák T, Cudlín P (2007) Does the azimuth orientation of Norway spruce (Picea abies/L./Karst.) branches within sunlit crown part influence the heterogeneity of biochemical, structural and spectral characteristics of needles? Environmental and Experimental Botany 59, 283-292.

Li P, Wang Q, Endo T, Zhao X, Kakubari Y (2010) Soil organic carbon stock is closely related to aboveground vegetation properties in cold-temperate mountainous forests. Geoderma 154, 407-415.

Liang L, Schwartz MD (2009) Landscape phenology: An integrative approach to seasonal vegetation dynamics. Landscape Ecology 24, 465-472.

Liang S (2004) Quantitative remote sensing of land surfaces. John Wiley & Sons, Inc., Hoboken, New Jersey.

Lindberg E, Olofsson K, Holmgren J, Olsson H (2012) Estimation of 3D vegetation structure from waveform and discrete return airborne laser scanning data. Remote Sensing of Environment 118, 151-161.

Liu J, Miller JR, Haboudane D, Pattey E (2004) Exploring the relationship between red edge parameters and crop variables for precision agriculture, Proceedings IEEE International Geoscience and Remote Sensing Symposium (IGARSS '04), Fairbanks, Alaska, USA, pp. 1276-1279.

Lobell DB, Asner GP, Law BE, Treuhaft RN (2002) View angle effects on canopy reflectance and spectral mixture analysis of coniferous forests using AVIRIS. International Journal of Remote Sensing 23, 2247-2262.

Lukeš P, Malenovský Z, Hanuš J, Kaplan V, Homolová L, Pokorný R (2009) Challenges in accuracy assessment of Norway spruce leaf chlorophyll content estimated from airborne and satellite imaging spectroscopy data, Workshop on the retrieval of geophysical variables using high spatial resolution optical imagery, ESA/ESTEC Noordwijk, The Netherlands, 14-15 Oct 2009.

Lukeš P, Rautiainen M, Stenberg P, Malenovský Z (2011) Empirical test of the spectral invariants theory using imaging spectroscopy data from a coniferous forest. International Journal of Applied Earth Observation and Geoinformation 13, 668-675.

Luyssaert S, Inglima I, Jung M, Richardson AD, Reichstein M, Papale D, Piao SL, Schulze ED, Wingate L, Matteucci G, et al. (2007) CO2 balance of boreal, temperate, and tropical forests derived from a global database. Global Change Biology 13, 2509-2537.

Lymburner L, Beggs PJ, Jacobson CR (2000) Estimation of canopy-average surface-specific leaf area using Landsat TM data. Photogrammetric Engineering and Remote Sensing 66, 183-191.

Magnani F, Mencuccini M, Borghetti M, Berbigier P, Berninger F, Delzon S, Grelle A, Hari P, Jarvis PG, Kolari P, et al. (2007) The human footprint in the carbon cycle of temperate and boreal forests. Nature 447, 848-850.

Magnusson M, Fransson JES, Holmgren J (2007) Effects on estimation accuracy of forest variables using different pulse density of laser data. Forest Science 53, 619-626.

Malenovský Z, Albrechtová J, Lhotáková Z, Zurita-Milla R, Clevers J, Schaepman ME, Cudlín P (2006a) Applicability of the PROSPECT model for Norway spruce needles. International Journal of Remote Sensing 27, 5315-5340.

Malenovský Z, Bartholomeus HM, Acerbi-Junior FW, Schopfer JT, Painter TH, Epema GF, Bregt AK (2007) Scaling dimensions in spectroscopy of soil and vegetation. International Journal of Applied Earth Observation and Geoinformation 9, 137-164.

Malenovský Z, Homolová L, Zurita-Milla R, Lukeš P, Kaplan V, Hanuš J, Gastellu-Etchegorry JP, Schaepman ME (2013) Retrieval of spruce leaf chlorophyll content from airborne image data using continuum removal and radiative transfer. Remote Sensing of Environment 131, 85-102.

Malenovský Z, Martin E, Homolová L, Gastellu-Etchegorry JP, Zurita-Milla R, Schaepman ME, Pokorný R, Clevers JGPW, Cudlín P (2008) Influence of woody elements of a Norway spruce canopy on nadir reflectance simulated by the DART model at very high spatial resolution. Remote Sensing of Environment 112, 1-18.

Malenovský Z, Mishra KB, Zemek F, Rascher U, Nedbal L (2009) Scientific and technical challenges in remote sensing of plant canopy reflectance and fluorescence. Journal of Experimental Botany 60, 2987-3004.

Malenovský Z, Rott H, Cihlar J, Schaepman ME, García-Santos G, Fernandes R, Berger M (2012) Sentinels for science: Potential of Sentinel-1, -2, and -3 missions for scientific observations of ocean, cryosphere, and land. Remote Sensing of Environment 120, 91-101.

Malenovský Z, Ufer C, Lhotaková Z, Clevers JGPW, Schaepman ME, Albrechtová J, Cudlín P (2006b) A new hyperspectral index for chlorophyll estimation of a forest canopy: area under curve normalised to maximal band depth between 650-725 nm. EARSeL eProceedings 5, 161-172.

Mallet C, Bretar F (2009) Full-waveform topographic lidar: State-of-the-art. ISPRS Journal of Photogrammetry and Remote Sensing 64, 1-16.

Malmstrom CM, Butterfield HS, Barber C, Dieter B, Harrison R, Qi J, Riaño D, Schrotenboer A, Stone S, Stoner CJ, et al. (2009) Using remote sensing to evaluate the influence of grassland restoration activities on ecosystem forage provisioning services. Restoration Ecology 17, 526-538.

Martin ME, Aber JD (1997) High spectral resolution remote sensing of forest canopy lignin, nitrogen, and ecosystem processes. Ecological Applications 7, 431-443.

Martin ME, Newman SD, Aber JD, Congalton RG (1998) Determining forest species composition using high spectral resolution remote sensing data. Remote Sensing of Environment 65, 249-254.

Martin ME, Plourde LC, Ollinger SV, Smith ML, McNeil BE (2008) A generalizable method for remote sensing of canopy nitrogen across a wide range of forest ecosystems. Remote Sensing of Environment 112, 3511-3519.

Martínez B, Camacho F, Verger A, García-Haro FJ, Gilabert MA (2013) Intercomparison and quality assessment of MERIS, MODIS and SEVIRI FAPAR products over the Iberian Peninsula. International Journal of Applied Earth Observation and Geoinformation 21, 463-476.

Mayaux P, Eva H, Gallego J, Strahler AH, Herold M, Agrawal S, Naumov S, de Miranda EE, di Bella CM, Ordoyne C, et al. (2006) Validation of the global land cover 2000 map. IEEE Transactions on Geoscience and Remote Sensing 44, 1728-1737.

McCallum I, Wagner W, Schmullius C, Shvidenko A, Obersteiner M, Fritz S, Nilsson S (2010) Comparison of four global FAPAR datasets over Northern Eurasia for the year 2000. Remote Sensing of Environment 114, 941-949.

MEA (2005) Millennium Ecosystem Assessment. Ecosystem and Human Well-being: Synthesis. Island Press, Washington, DC., 155.

Melillo JM, McGuire AD, Kicklighter DW, Moore III B, Vorosmarty CJ, Schloss AL (1993) Global climate change and terrestrial net primary production. Nature 363, 234-240.

Meroni M, Colombo R (2006) Leaf level detection of solar induced chlorophyll fluorescence by means of a subnanometer resolution spectroradiometer. Remote Sensing of Environment 103, 438-448.

Meroni M, Rossini M, Guanter L, Alonso L, Rascher U, Colombo R, Moreno J (2009) Remote sensing of solar-induced chlorophyll fluorescence: Review of methods and applications. Remote Sensing of Environment 113, 2037-2051.

Messier J, McGill BJ, Lechowicz MJ (2010) How do traits vary across ecological scales? A case for trait-based ecology. Ecology Letters 13, 838-848.

Metzger MJ, Rounsevell MDA, Acosta-Michlik L, Leemans R, Schröter D (2006) The vulnerability of ecosystem services to land use change. Agriculture, Ecosystems and Environment 114, 69-85.

Milton EJ, Schaepman ME, Anderson K, Kneubühler M, Fox N (2009) Progress in field spectroscopy. Remote Sensing of Environment 113, S92-S109.

Mitchard ETA, Saatchi SS, Woodhouse IH, Nangendo G, Ribeiro NS, Williams M, Ryan CM, Lewis SL, Feldpausch TR, Meir P (2009) Using satellite radar backscatter to predict above-ground woody biomass: A consistent relationship across four different African landscapes. Geophysical Research Letters 36.

Monteith JL (1972) Solar-radiation and productivity in tropical ecosystems. Journal of Applied Ecology 9, 747-766.

Montesano PM, Cook BD, Sun G, Simard M, Nelson RF, Ranson KJ, Zhang Z, Luthcke S (2013) Achieving accuracy requirements for forest biomass mapping: A

spaceborne data fusion method for estimating forest biomass and LiDAR sampling error. Remote Sensing of Environment 130, 153-170.

Mooney HA, Winner WE, Pell EJ (1991) Response of plants to multiple stresses. Academic Press, Inc., San Diego, California, USA.

Moorthy I, Miller JR, Noland TL (2008) Estimating chlorophyll concentration in conifer needles with hyperspectral data: An assessment at the needle and canopy level. Remote Sensing of Environment 112, 2824-2838.

Morsdorf F, Mårell A, Koetz B, Cassagne N, Pimont F, Rigolot E, Allgöwer B (2010) Discrimination of vegetation strata in a multi-layered Mediterranean forest ecosystem using height and intensity information derived from airborne laser scanning. Remote Sensing of Environment 114, 1403-1415.

Moya I, Camenen L, Evain S, Goulas Y, Cerovic ZG, Latouche G, Flexas J, Ounis A (2004) A new instrument for passive remote sensing: 1. Measurements of sunlight-induced chlorophyll fluorescence. Remote Sensing of Environment 91, 186-197.

Mulder VL, de Bruin S, Schaepman ME, Mayr TR (2011) The use of remote sensing in soil and terrain mapping - A review. Geoderma 162, 1-19.

Mutanga O, Kumar L (2007) Estimating and mapping grass phosphorus concentration in an African savanna using hyperspectral image data. International Journal of Remote Sensing 28, 4897-4911.

Mutanga O, Skidmore AK (2007) Red edge shift and biochemical content in grass canopies. ISPRS Journal of Photogrammetry and Remote Sensing 62, 34-42.

Mutanga O, Skidmore AK, Prins HHT (2004) Predicting in situ pasture quality in the Kruger National Park, South Africa, using continuum-removed absorption features. Remote Sensing of Environment 89, 393-408.

Mutlu M, Popescu SC, Stripling C, Spencer T (2008) Mapping surface fuel models using lidar and multispectral data fusion for fire behavior. Remote Sensing of Environment 112, 274-285.

Myneni RB (1991) Modeling radiative transfer and photosynthesis in three-dimensional vegetation canopies. Agricultural and Forest Meteorology 55, 323-344.

Myneni RB, Asrar G, Hall FG (1992) A three-dimensional radiative transfer method for optical remote sensing of vegetated land surfaces. Remote Sensing of Environment 41, 105-121.

Myneni RB, Dong J, Tucker CJ, Kaufmann RK, Kauppi PE, Liski J, Zhou L, Alexeyev V, Hughes MK (2001) A large carbon sink in the woody biomass of northern forests. Proceedings of the National Academy of Sciences of the United States of America 98, 14784-14789.

Myneni RB, Hoffman S, Knyazikhin Y, Privette JL, Glassy J, Tian Y, Wang Y, Song X, Zhang Y, Smith GR, et al. (2002) Global products of vegetation leaf area and fraction absorbed PAR from year one of MODIS data. Remote Sensing of Environment 83, 214-231.

Myneni RB, Williams DL (1994) On the relationship between FAPAR and NDVI. Remote Sensing of Environment 49, 200-211.

Næsset E, Gobakken T, Holmgren J, Hyyppä H, Hyyppä J, Maltamo M, Nilsson M, Olsson H, Persson Å, Söderman U (2004) Laser scanning of forest resources: The nordic experience. Scandinavian Journal of Forest Research 19, 482-499.

Naidoo R, Balmford A, Costanza R, Fisher B, Green RE, Lehner B, Malcolm TR, Ricketts TH (2008) Global mapping of ecosystem services and conservation priorities. Proceedings of the National Academy of Sciences of the United States of America 105, 9495-9500.

Nemani R, Hashimoto H, Votava P, Melton F, Wang W, Michaelis A, Mutch L, Milesi C, Hiatt S, White M (2009) Monitoring and forecasting ecosystem dynamics using the Terrestrial Observation and Prediction System (TOPS). Remote Sensing of Environment 113, 1497-1509.

Niinemets Ü (1997) Distribution patterns of foliar carbon and nitrogen as affected by tree dimensions and relative light conditions in the canopy of Picea abies. Trees - Structure and Function 11, 144-154.

Niinemets Ü (2007) Photosynthesis and resource distribution through plant canopies. Plant, Cell and Environment 30, 1052-1071.

Niinemets Ü (2010) A review of light interception in plant stands from leaf to canopy in different plant functional types and in species with varying shade tolerance. Ecological Research 25, 693-714.

Niinemets Ü, Kull O (1995) Effects of light availability and tree size on the architecture of assimilative surface in the canopy of Picea abies: Variation in needle morphology. Tree Physiology 15, 307-315.

Normile D (2009) Round and round a guide to the carbon cycle. Science 325, 1642-1643.

Numata I, Roberts DA, Chadwick OA, Schimel J, Sampaio FR, Leonidas FC, Soares JV (2007) Characterization of pasture biophysical properties and the impact of grazing intensity using remotely sensed data. Remote Sensing of Environment 109, 314-327.

O'Farrell PJ, Reyers B, le Maitre DC, Milton SJ, Egoh B, Maherry A, Colvin C, Atkinson D, de Lange W, Blignaut JN, et al. (2010) Multi-functional landscapes in semi arid environments: Implications for biodiversity and ecosystem services. Landscape Ecology 25, 1231-1246.

Okin GS, Roberts DA, Murray B, Okin WJ (2001) Practical limits on hyperspectral vegetation discrimination in arid and semiarid environments. Remote Sensing of Environment 77, 212-225.

Ollinger SV (2011) Sources of variability in canopy reflectance and the convergent properties of plants. New Phytologist 189, 375-394.

Ollinger SV, Richardson AD, Martin ME, Hollinger DY, Frolking SE, Reich PB, Plourde LC, Katul GG, Munger JW, Oren R, et al. (2008) Canopy nitrogen, carbon assimilation, and albedo in temperate and boreal forests: Functional relations and potential climate feedbacks. Proceedings of the National Academy of Sciences of the United States of America 105, 19336-19341.

Ollinger SV, Smith ML (2005) Net primary production and canopy nitrogen in a temperate forest landscape: An analysis using imaging spectroscopy, modeling and field data. Ecosystems 8, 760-778.

Oppelt N, Mauser W (2004) Hyperspectral monitoring of physiological parameters of wheat during a vegetation period using AVIS data. International Journal of Remote Sensing 25, 145-159.

Orwin KH, Buckland SM, Johnson D, Turner BL, Smart S, Oakley S, Bardgett RD (2010) Linkages of plant traits to soil properties and the functioning of temperate grassland. Journal of Ecology 98, 1074-1083.

Palmroth S, Stenberg P, Smolander S, Voipio P, Smolander H (2002) Fertilization has little effect on light-interception efficiency of Picea abies shoots. Tree Physiology 22, 1185-1192.

Patenaude G, Milne R, Dawson TP (2005) Synthesis of remote sensing approaches for forest carbon estimation: Reporting to the Kyoto Protocol. Environmental Science and Policy 8, 161-178.

Paula S, Arianoutsou M, Kazanis D, Tavsanoglu Ç, Lloret F, Buhk C, Ojeda F, Luna B, Moreno JM, Rodrigo A, et al. (2009) Fire-related traits for plant species of the Mediterranean Basin. Ecology 90, 1420.

Pauli H, Gottfried M, Reiter K, Klettner C, Grabherr G (2007) Signals of range expansions and contractions of vascular plants in the high Alps: Observations (1994-2004) at the GLORIA master site Schrankogel, Tyrol, Austria. Global Change Biology 13, 147-156.

Peñuelas J, Filella I, Gamon JA (1995) Assessment of photosynthetic radiation-use efficiency with spectral reflectance. New Phytologist 131, 291-296.

Pérez-Harguindeguy N, Díaz S, Garnier E, Lavorel S, Poorter H, Jaureguiberry P, Bret-Harte MS, Cornwell WK, Craine JM, Gurvich DE, et al. (2013) New handbook for standardised measurement of plant functional traits worldwide. Australian Journal of Botany 61, 167-234.

Perterer J, Körner C (1990) Das Problem der Bezugsgrösse bei physiologisch-ökologischen Untersuchungen an Koniferennadeln. (The problem of reference parameters in physiologic-ecological research with conifer needles). Forstw Cbl 109, 220-241.

Pimstein A, Karnieli A, Bansal SK, Bonfil DJ (2011) Exploring remotely sensed technologies for monitoring wheat potassium and phosphorus using field spectroscopy. Field Crops Research 121, 125-135.

Písek J, Chen JM, Nilson T (2011) Estimation of vegetation clumping index using MODIS BRDF data. International Journal of Remote Sensing 32, 2645-2657.

Pokorný R (2002) Index listové plochy v porostech lesních dřevin (Leaf area index of forest canopies), Faculty of Forestry and Wood Technology. Mendel University in Brno, Brno, The Czech Republic, p. 135.

Pokorný R, Marek MV (2000) Test of accuracy of LAI estimation by LAI-2000 under artificially changed leaf to wood area proportions. Biologia Plantarum 43, 537-544.

Porder S, Asner GP, Vitousek PM (2005) Ground-based and remotely sensed nutrient availability across a tropical landscape. Proceedings of the National Academy of Sciences of the United States of America 102, 10909-10912.

Porfirio LL, Steffen W, Barrett DJ, Berry SL (2010) The net ecosystem carbon exchange of human-modified environments in the Australian Capital Region. Regional Environmental Change 10, 1-12.

Porra RJ, Thompson WA, Kriedemann PE (1989) Determination of accurate extinction coefficients and simultaneous equations for assaying chlorophylls a and b extracted with four different solvents: verification of the concentration of chlorophyll standards by atomic absorption spectroscopy. Biochemica and Biophysica Acta 975, 384-394.

Psomas A, Kneubühler M, Huber S, Itten K, Zimmermann NE (2011) Hyperspectral remote sensing for estimating aboveground biomass and for exploring species richness patterns of grassland habitats. International Journal of Remote Sensing 32, 9007-9031.

Quétier F, Lavorel S, Thuiller W, Davies I (2007a) Plant-trait-based modeling assessment of ecosystem-service sensitivity to land-use change. Ecological Applications 17, 2377-2386.

Quétier F, Rivoal F, Marty P, de Chazal J, Thuiller W, Lavorel S (2010) Social representations of an alpine grassland landscape and socio-political discourses on rural development. Regional Environmental Change 10, 119-130.

Quétier F, Thabault A, Lavorel S (2007b) Plant traits in a state and transition framework as markers of ecosystem response to land-use change. Ecological Monographs 77, 33-52.

Ramoelo A, Skidmore AK, Schlerf M, Heitkönig IMA, Mathieu R, Cho MA (2013) Savanna grass nitrogen to phosphorous ratio estimation using field spectroscopy and the potential for estimation with imaging spectroscopy. International Journal of Applied Earth Observation and Geoinformation 23, 334-343.

Ramoelo A, Skidmore AK, Schlerf M, Mathieu R, Heitkönig IMA (2011) Water-removed spectra increase the retrieval accuracy when estimating savanna grass nitrogen and phosphorus concentrations. ISPRS Journal of Photogrammetry and Remote Sensing 66, 408-417.

Rautiainen M, Heiskanen J, Eklundh L, Möttus M, Lukeš P, Stenberg P (2010) Ecological applications of physically based remote sensing methods. Scandinavian Journal of Forest Research 25, 325-339.

Rautiainen M, Mõttus M, Yáñez-Rausell L, Homolová L, Malenovský Z, Schaepman ME (2012) A note on upscaling coniferous needle spectra to shoot spectral albedo. Remote Sensing of Environment 117, 469-474.

Rautiainen M, Stenberg P (2005) Application of photon recollision probability in coniferous canopy reflectance simulations. Remote Sensing of Environment 96, 98-107.

Rautiainen M, Stenberg P, Nilson T, Kuusk A (2004) The effect of crown shape on the reflectance of coniferous stands. Remote Sensing of Environment 89, 41-52.

Reed BC, Brown JF, VanderZee D, Loveland TR, Merchant JW, Ohlen DO (1994) Measuring phenological variability from satellite imagery. Journal of Vegetation Science 5, 703-714.

Reich PB, Kloeppel BD, Ellsworth DS, Walters MB (1995) Different photosynthesis-nitrogen relations in deciduous hardwood and evergreen coniferous tree species. Oecologia 104, 24-30.

Reyniers M, Vrindts E (2006) Measuring wheat nitrogen status from space and ground-based platform. International Journal of Remote Sensing 27, 549-567.

Riaño D, Vaughan P, Chuvieco E, Zarco-Tejada PJ, Ustin SL (2005) Estimation of fuel moisture content by inversion of radiative transfer models to simulate equivalent water thickness and dry matter content: Analysis at leaf and canopy level. IEEE Transactions on Geoscience and Remote Sensing 43, 819-826.

Richardson AD, Braswell BH, Hollinger DY, Jenkins JP, Ollinger SV (2009) Near-surface remote sensing of spatial and temporal variation in canopy phenology. Ecological Applications 19, 1417-1428.

Richter R, Schlapfer D (2002) Geo-atmospheric processing of airborne imaging spectrometry data. Part 2: atmospheric/topographic correction. International Journal of Remote Sensing 23, 2631-2649.

Roberts DA, Smith MO, Adams JB (1993) Green vegetation, nonphotosynthetic vegetation, and soils in AVIRIS data. Remote Sensing of Environment 44, 255-269.

Rocchini D (2007) Effects of spatial and spectral resolution in estimating ecosystem α-diversity by satellite imagery. Remote Sensing of Environment 111, 423-434.

Rocchini D, Balkenhol N, Carter GA, Foody GM, Gillespie TW, He KS, Kark S, Levin N, Lucas K, Luoto M, et al. (2010) Remotely sensed spectral heterogeneity as a proxy of species diversity: Recent advances and open challenges. Ecological Informatics 5, 318-329.

Rochdi N, Fernandes R, Chelle M (2006) An assessment of needles clumping within shoots when modeling radiative transfer within homogeneous canopies. Remote Sensing of Environment 102, 116-134.

Rockström J, Steffen W, Noone K, Persson Å, Chapin III FS, Lambin EF, Lenton TM, Scheffer M, Folke C, Schellnhuber HJ, et al. (2009) A safe operating space for humanity. Nature 461, 472-475.

Ross JK (1981) The radiation regime and architecture of plant stands. W. Junk, The Hague, Netherlands.

Roux-Fouillet P, Wipf S, Rixen C (2011) Long-term impacts of ski piste management on alpine vegetation and soils. Journal of Applied Ecology 48, 906-915.

Running SW, Nemani RR, Heinsch FA, Zhao M, Reeves M, Hashimoto H (2004) A Continuous Satellite-Derived Measure of Global Terrestrial Primary Production. BioScience 54, 547-560.

Saatchi S, Halligan K, Despain DG, Crabtree RL (2007) Estimation of forest fuel load from radar remote sensing. IEEE Transactions on Geoscience and Remote Sensing 45, 1726-1740.

Sampson PH, Zarco-Tejada PJ, Mohammed GH, Miller JR, Noland TL (2003) Hyperspectral remote sensing of forest condition: Estimating chlorophyll content in tolerant hardwoods. Forest Science 49, 381-391.

Sánchez-Azofeifa GA, Castro K, Wright SJ, Gamon J, Kalacska M, Rivard B, Schnitzer SA, Feng JL (2009) Differences in leaf traits, leaf internal structure, and spectral reflectance between two communities of lianas and trees: Implications for remote sensing in tropical environments. Remote Sensing of Environment 113, 2076-2088.

Schaepman-Strub G, Schaepman ME, Painter TH, Dangel S, Martonchik JV (2006) Reflectance quantities in optical remote sensing-definitions and case studies. Remote Sensing of Environment 103, 27-42.

Schaepman ME (2007) Spectrodirectional remote sensing: From pixels to processes. International Journal of Applied Earth Observation and Geoinformation 9, 204-223.

Schaepman ME (2009) Imaging Spectrometers, in: Warner TA, Duane Nellis M, Foody GM (Eds.), The SAGE Handbook of Remote Sensing. SAGE, London (UK), pp. 166-178.

Schaepman ME, Koetz B, Schaepman-Strub G, Zimmermann NE, Itten KI (2004) Quantitative retrieval of biogeophysical characteristics using imaging spectroscopy - A mountain forest case study. Community Ecology 5, 93-104.

Schaepman ME, Ustin SL, Plaza AJ, Painter TH, Verrelst J, Liang S (2009) Earth system science related imaging spectroscopy - An assessment. Remote Sensing of Environment 113, S123-S137.

Schimel D (2011) The era of continental-scale ecology. Frontiers in Ecology and the Environment 9, 311.

Schimel DS, Asner GP, Moorcroft P (2013) Observing changing ecological diversity in the Anthropocene. Frontiers in Ecology and the Environment 11, 129-137.

Schlerf M, Atzberger C, Hill J (2005) Remote sensing of forest biophysical variables using HyMap imaging spectrometer data. Remote Sensing of Environment 95, 177-194.

Schlerf M, Atzberger C, Hill J, Buddenbaum H, Werner W, Schüler G (2010) Retrieval of chlorophyll and nitrogen in Norway spruce (Picea abies L. Karst.) using imaging spectroscopy. International Journal of Applied Earth Observation and Geoinformation 12, 17-26.

Schmidt KS, Skidmore AK (2003) Spectral discrimination of vegetation types in a coastal wetland. Remote Sensing of Environment 85, 92-108.

Schwartz MD, Hanes JM (2010) Intercomparing multiple measures of the onset of spring in eastern North America. International Journal of Climatology 30, 1614-1626.

Sellin A (2000) Estimating the needle area from geometric measurements: Application of different calculation methods to Norway spruce. Trees - Structure and Function 14, 215-222.

Serrano L, Gamon JA, Berry J (1997) Estimation of leaf area with an integrating sphere. Tree Physiology 17, 571-576.

Serrano L, Peñuelas J, Ustin SL (2002) Remote sensing of nitrogen and lignin in Mediterranean vegetation from AVIRIS data: Decomposing biochemical from structural signals. Remote Sensing of Environment 81, 355-364.

Serrano L, Ustin SL, Roberts DA, Gamon JA, Peñuelas J (2000) Deriving water content of chaparral vegetation from AVIRIS data. Remote Sensing of Environment 74, 570-581.

Shipley B, Vu TT (2002) Dry matter content as a measure of dry matter concentration in plants and their parts. New Phytologist 153, 359-364.

Siebke K, Ball MC (2009) Non-destructive measurement of chlorophyll b:a ratios and identification of photosynthetic pathways in grasses by reflectance spectroscopy. Functional Plant Biology 36, 857-866.

Sims DA, Gamon JA (2002) Relationships between leaf pigment content and spectral reflectance across a wide range of species, leaf structures and developmental stages. Remote Sensing of Environment 81, 337-354.

Sims DA, Gamon JA (2003) Estimation of vegetation water content and photosynthetic tissue area from spectral reflectance: A comparison of indices based on liquid water and chlorophyll absorption features. Remote Sensing of Environment 84, 526-537.

Sitch S, Smith B, Prentice IC, Arneth A, Bondeau A, Cramer W, Kaplan JO, Levis S, Lucht W, Sykes MT, et al. (2003) Evaluation of ecosystem dynamics, plant geography and terrestrial carbon cycling in the LPJ dynamic global vegetation model. Global Change Biology 9, 161-185.

Skidmore AK, Ferwerda JG, Mutanga O, van Wieren SE, Peel M, Grant RC, Prins HHT, Balcik FB, Venus V (2010) Forage quality of savannas - Simultaneously mapping foliar protein and polyphenols for trees and grass using hyperspectral imagery. Remote Sensing of Environment 114, 64-72.

Skole D, Tucker C (1993) Tropical deforestation and habitat fragmentation in the Amazon: Satellite data from 1978 to 1988. Science 260, 1905-1910.

Smith GM, Milton EJ (1999) The use of the empirical line method to calibrate remotely sensed data to reflectance. International Journal of Remote Sensing 20, 2653-2662.

Smith ML, Martin ME, Plourde L, Ollinger SV (2003) Analysis of hyperspectral data for estimation of temperate forest canopy nitrogen concentration: Comparison between an airborne (AVIRIS) and a spaceborne (Hyperion) sensor. IEEE Transactions on Geoscience and Remote Sensing 41, 1332-1337.

Smith ML, Ollinger SV, Martin ME, Aber JD, Hallett RA, Goodale CL (2002) Direct estimation of aboveground forest productivity through hyperspectral remote sensing of canopy nitrogen. Ecological Applications 12, 1286-1302.

Smith WK, Schoettle AW, Cui M (1991) Importance of the method of leaf area measurement to the interpretation of gas exchange of complex shoots. Tree Physiology 8, 121-127.

Smolander S, Stenberg P (2003) A method to account for shoot scale clumping in coniferous canopy reflectance models. Remote Sensing of Environment 88, 363-373.

Špunda V, Čajánek M, Kalina J, Lachetová I, Šprtová M, Marek MV (1998) Mechanistic differences in utilization of absorbed excitation energy within photosynthetic apparatus of Norway spruce induced by the vertical distribution of photosynthetically active radiation through the tree crown. Plant Science 133, 155-165.

Stagakis S, Markos N, Sykioti O, Kyparissis A (2010) Monitoring canopy biophysical and biochemical parameters in ecosystem scale using satellite hyperspectral imagery: An application on a Phlomis fruticosa Mediterranean ecosystem using multiangular CHRIS/PROBA observations. Remote Sensing of Environment 114, 977-994.

Stenberg P (1996) Simulations of the effects of shoot structure and orientation on vertical gradients in intercepted light by conifer canopies. Tree Physiology 16, 99-108.

Stenberg P, Kangas T, Smolander H, Linder S (1999) Shoot structure, canopy openness, and light interception in Norway spruce. Plant, Cell and Environment 22, 1133-1142.

Still CJ, Berry JA, Collatz GJ, DeFries RS (2003) Global distribution of C3 and C4 vegetation: Carbon cycle implications. Global Biogeochemical Cycles 17, 6-1.

Stöckli R, Vidale PL (2004) European plant phenology and climate as seen in a 20-year AVHRR land-surface parameter dataset. International Journal of Remote Sensing 25, 3303-3330.

Stow DA, Hope A, McGuire D, Verbyla D, Gamon J, Huemmrich F, Houston S, Racine C, Sturm M, Tape K, et al. (2004) Remote sensing of vegetation and land-cover change in Arctic Tundra Ecosystems. Remote Sensing of Environment 89, 281-308.

Straatsma M, Middelkoop H (2007) Extracting structural characteristics of herbaceous floodplain vegetation under leaf-off conditions using airborne laser scanner data. International Journal of Remote Sensing 28, 2447-2467.

Svenson SE, Davies FT (1992) Comparison of methods for estimating surfface area of water-stressed and fully hydrated pine needle segments for gas exchange analysis. Tree Physiology 10, 417-421.

Thomas CD, Cameron A, Green RE, Bakkenes M, Beaumont LJ, Collingham YC, Erasmus BFN, Ferreira De Siqueira M, Grainger A, Hannah L, et al. (2004) Extinction risk from climate change. Nature 427, 145-148.

Tian YC, Yao X, Yang J, Cao WX, Hannaway DB, Zhu Y (2011) Assessing newly developed and published vegetation indices for estimating rice leaf nitrogen concentration with ground- and space-based hyperspectral reflectance. Field Crops Research 120, 299-310.

Townsend PA, Foster JR, Chastain Jr RA, Currie WS (2003) Application of imaging spectroscopy to mapping canopy nitrogen in the forest of the central Appalachian mountains using Hyperion and AVIRIS. IEEE Transactions on Geoscience and Remote Sensing 41, 1347-1354.

Treuhaft RN, Law BE, Asner GP (2004) Forest attributes from radar interferometric structure and its fusion with optical remote sensing. BioScience 54, 561-571.

Tucker CJ (1979) Red and photographic infrared linear combinations for monitoring vegetation. Remote Sensing of Environment 8, 127-150.

Tucker CJ, Pinzon JE, Brown ME, Slayback DA, Pak EW, Mahoney R, Vermote EF, El Saleous N (2005) An extended AVHRR 8-km NDVI dataset compatible with MODIS and SPOT vegetation NDVI data. International Journal of Remote Sensing 26, 4485-4498.

Turner DP, Cohen WB, Kennedy RE, Fassnacht KS, Briggs JM (1999) Relationships between leaf area index and Landsat TM spectral vegetation indices across three temperate zone sites. Remote Sensing of Environment 70, 52-68.

Turner W, Spector S, Gardiner N, Fladeland M, Sterling E, Steininger M (2003) Remote sensing for biodiversity science and conservation. Trends in Ecology and Evolution 18, 306-314.

UN (2011) United Nations, Department of Economics and Social Affairs, Population Division. World Population Prospects: The 2010 Revisions, Highlights and Advance Tables. Working Paper No. ESA/P/WP.220, New York: United Nations.

Underwood E, Ustin S, DiPietro D (2003) Mapping nonnative plants using hyperspectral imagery. Remote Sensing of Environment 86, 150-161.

Underwood EC, Mulitsch MJ, Greenberg JA, Whiting ML, Ustin SL, Kefauver SC (2006) Mapping invasive aquatic vegetation in the Sacramento-San Joaquin Delta using hyperspectral imagery. Environmental Monitoring and Assessment 121, 47-64.

Urban O, Janouš D, Acosta M, Czerný R, Marková I, Navrátil M, Pavelka M, Pokorný R, Šprtová M, Zhang R, et al. (2007) Ecophysiological controls over the net ecosystem exchange of mountain spruce stand. Comparison of the response in direct vs. diffuse solar radiation. Global Change Biology 13, 157-168.

Ustin SL, Gamon JA (2010) Remote sensing of plant functional types. New Phytologist 186, 795-816.

Ustin SL, Gitelson AA, Jacquemoud S, Schaepman M, Asner GP, Gamon JA, Zarco-Tejada P (2009) Retrieval of foliar information about plant pigment systems from high resolution spectroscopy. Remote Sensing of Environment 113, S67-S77.

Ustin SL, Roberts DA, Gamon JA, Asner GP, Green RO (2004) Using imaging spectroscopy to study ecosystem processes and properties. BioScience 54, 523-534.

van der Zande D, Hoet W, Jonckheere I, van Aardt J, Coppin P (2006) Influence of measurement set-up of ground-based LiDAR for derivation of tree structure. Agricultural and Forest Meteorology 141, 147-160.

van Kleunen M, Weber E, Fischer M (2010) A meta-analysis of trait differences between invasive and non-invasive plant species. Ecology Letters 13, 235-245.

van Leeuwen M, Nieuwenhuis M (2010) Retrieval of forest structural parameters using LiDAR remote sensing. European Journal of Forest Research 129, 749-770.

van Wijk MT, Williams M (2005) Optical instruments for measuring leaf area index in low vegetation: Application in arctic ecosystems. Ecological Applications 15, 1462-1470.

Verburg PH, van de Steeg J, Veldkamp A, Willemen L (2009) From land cover change to land function dynamics: A major challenge to improve land characterization. Journal of Environmental Management 90, 1327-1335.

Verhoef W (2007) A Bayesian optimisation approach for model inversion of hyperspectral-multidirectional observations: The blance with a priori information., in: Schaepman ME, Liang S, Groot NE, Kneubuhler M (Eds.), 10th Intl. Symposium on Physical Measurements and Spectral Signatures in Remote Sensing (ISPMSRS'07), Davos, Switzerland, pp. 499-504.

Verhoef W, Bach H (2007) Coupled soil-leaf-canopy and atmosphere radiative transfier modeling to simulate hyperspectral multi-angular surface reflectance and TOA radiance data. Remote Sensing of Environment 109, 166-182.

Verrelst J, Schaepman ME, Malenovský Z, Clevers JGPW (2010) Effects of woody elements on simulated canopy reflectance: Implications for forest chlorophyll content retrieval. Remote Sensing of Environment 114, 647-656.

Verstraete MM, Pinty B (1996) Designing optimal spectral indexes for remote sensing applications. IEEE Transactions on Geoscience and Remote Sensing 34, 1254-1265.

Vile D, Garnier É, Shipley B, Laurent G, Navas ML, Roumet C, Lavorel S, Díaz S, Hodgson JG, Lloret F, et al. (2005) Specific leaf area and dry matter content estimate thickness in laminar leaves. Annals of Botany 96, 1129-1136.

Violle C, Navas ML, Vile D, Kazakou E, Fortunel C, Hummel I, Garnier E (2007) Let the concept of trait be functional! Oikos 116, 882-892.

Visser H, de Nijs T (2006) The map comparison kit. Environmental Modelling and Software 21, 346-358.

Vohland M, Mader S, Dorigo W (2010) Applying different inversion techniques to retrieve stand variables of summer barley with PROSPECT + SAIL. International Journal of Applied Earth Observation and Geoinformation 12, 71-80.

Wallace KJ (2007) Classification of ecosystem services: Problems and solutions. Biological Conservation 139, 235-246.

Wang L, Qu JJ, Hao X, Hunt Jr ER (2011) Estimating dry matter content from spectral reflectance for green leaves of different species. International Journal of Remote Sensing 32, 7097-7109.

Waring RH (1983) Estimating forest growth and efficiency in relation to canopy leaf area. Advances in Ecological Research 13, 327-354.

Wellburn AR (1994) The spectral determination of chlorophyll a and chlorophyll b, as well as total carotenoids, using various solvents with spectrophotometers of different resolution. Journal of Plant Physiology 144, 307-313.

White MA, de Beurs KM, Didan K, Inouye DW, Richardson AD, Jensen OP, O'Keefe J, Zhang G, Nemani RR, van Leeuwen WJD, et al. (2009) Intercomparison, interpretation, and assessment of spring phenology in North America estimated from remote sensing for 1982-2006. Global Change Biology 15, 2335-2359.

Widlowski JL, Pinty B, Gobron N, Verstraete MM, Diner DJ, Davis AB (2004) Canopy structure parameters derived from multi-angular remote sensing data for terrestrial carbon studies. Climatic Change 67, 403-415.

Widlowski JL, Pinty B, Lavergne T, Verstraete MM, Gobron N (2006) Horizontal radiation transport in 3-D forest canopies at multiple spatial resolutions: Simulated impact on canopy absorption. Remote Sensing of Environment 103, 379-397.

Widlowski JL, Robustelli M, Disney M, Gastellu-Etchegorry JP, Lavergne T, Lewis P, North PRJ, Pinty B, Thompson R, Verstraete MM (2008) The RAMI On-line Model Checker (ROMC): A web-based benchmarking facility for canopy reflectance models. Remote Sensing of Environment 112, 1144-1150.

Willmott CJ (1981) On the validation of models. Physical Geography 2, 184-194.

Wright IJ, Reich PB, Westoby M, Ackerly DD, Baruch Z, Bongers F, Cavender-Bares J, Chapin T, Cornelissen JHC, Diemer M, et al. (2004) The worldwide leaf economics spectrum. Nature 428, 821-827.

Wulder MA, White JC, Nelson RF, Næsset E, Ørka HO, Coops NC, Hilker T, Bater CW, Gobakken T (2012) Lidar sampling for large-area forest characterization: A review. Remote Sensing of Environment 121, 196-209.

Xiao X, Hollinger D, Aber J, Goltz M, Davidson EA, Zhang Q, Moore III B (2004) Satellite-based modeling of gross primary production in an evergreen needleleaf forest. Remote Sensing of Environment 89, 519-534.

Xie YC, Sha ZY, Yu M (2008) Remote sensing imagery in vegetation mapping: A review. Journal of Plant Ecology 1, 9-23.

Yoder BJ, Pettigrew-Crosby RE (1995) Predicting nitrogen and chlorophyll content and concentrations from reflectance spectra (400-2500 nm) at leaf and canopy scales. Remote Sensing of Environment 53, 199-211.

Youngentob KN, Roberts DA, Held AA, Dennison PE, Jia X, Lindenmayer DB (2011) Mapping two Eucalyptus subgenera using multiple endmember spectral mixture analysis and continuum-removed imaging spectrometry data. Remote Sensing of Environment 115, 1115-1128.

Zagolski F, Pinel V, Romier J, Alcayde D, Fontanari J, Gastellu-Etchegorry JP, Giordano G, Marty G, Mougin E, Joffre R (1996) Forest canopy chemistry with high spectral resolution remote sensing. International Journal of Remote Sensing 17, 1107-1128.

Zarco-Tejada PJ, Berni JAJ, Suárez L, Sepulcre-Cantó G, Morales F, Miller JR (2009) Imaging chlorophyll fluorescence with an airborne narrow-band multispectral camera for vegetation stress detection. Remote Sensing of Environment 113, 1262-1275.

Zarco-Tejada PJ, Miller JR, Harron J, Hu B, Noland TL, Goel N, Mohammed GH, Sampson P (2004) Needle chlorophyll content estimation through model inversion using hyperspectral data from boreal conifer forest canopies. Remote Sensing of Environment 89, 189-199.

Zarco-Tejada PJ, Miller JR, Noland TL, Mohammed GH, Sampson PH (2001) Scaling-up and model inversion methods with narrowband optical indices for chlorophyll content estimation in closed forest canopies with hyperspectral data. IEEE Transactions on Geoscience and Remote Sensing 39, 1491-1507.

Zarco-Tejada PJ, Pushnik JC, Dobrowski S, Ustin SL (2003) Steady-state chlorophyll a fluorescence detection from canopy derivative reflectance and double-peak red-edge effects. Remote Sensing of Environment 84, 283-294.

Zhang Y, Chen JM, Miller JR, Noland TL (2008) Leaf chlorophyll content retrieval from airborne hyperspectral remote sensing imagery. Remote Sensing of Environment 112, 3234-3247.

Zhao M, Heinsch FA, Nemani RR, Running SW (2005) Improvements of the MODIS terrestrial gross and net primary production global data set. Remote Sensing of Environment 95, 164-176.

Zurita-Milla R, Clevers JGPW, Schaepman ME, Kneubuehler M (2007) Effects of MERIS L1b radiometric calibration of regional land cover mapping and land products. Internation Journal of Remote Sensing 28, 653-673.

Summary

Terrestrial vegetation is an important component of the Earth's biosphere and therefore playing an essential role in climate regulation, carbon sequestration, and it provides large variety of services to humans. For a sustainable management of terrestrial ecosystems it is essential to understand vegetation responses to various pressures, to monitor and to predict the spatial extent and the rate of ecosystem changes. Remote sensing (RS) therefore offers a unique opportunity for spatially continuous, and for some type of RS data, also frequent monitoring of terrestrial ecosystems.

RS of vegetation is a broad research field, where a lot of progress has been made in the last three decades. However, the complexity of interactions between vegetation and solar radiation, constantly modulated by environmental factors, offers room for deeper investigation. Rather than solving one big research problem, this thesis built a few bridges on a way leading towards better understanding of using airborne imaging spectroscopy for ecological analysis in temperate coniferous forests and subalpine grasslands. The research was divided into a theoretical and an applied part. The theoretical part contributed to a critical evaluation of research achievements and challenges in optical RS of plant traits (Chapter 2). The applied part addressed three research topics: i) investigating variability of total to projected leaf area ratio in spruce canopies and its implications on RS of chlorophyll content (Chapter 3), ii) testing chlorophyll retrieval methods based on continuum removal in spruce canopies (Chapter 4), and iii) exploring potentials of imaging spectroscopy to map ecosystem properties and the capacity of subalpine grasslands in providing ecosystem services in comparison with a plant trait-based modelling approach (Chapter 5).

In Chapter 2, we reviewed achievements and challenges in RS estimation of key plant traits and we concentrated our discussion on eight traits with the strongest potential to be mapped using RS (plant growth and life forms, flammability properties, photosynthetic pathways and photosynthesis activity, plant height, leaf lifespan and phenology, specific leaf area, leaf nitrogen and phosphorous). The review indicated that imaging spectroscopy facilitates better retrievals of plant traits related to leaf biochemistry, photosynthesis and phenology rather than traits related to vegetations structure. Estimation of the canopy structure related traits (e.g. plant height) can certainly benefit from increasing synergies between imaging spectroscopy and active RS (radar or laser scanning). One of major challenges in RS of plant traits is to effectively suppress the negative influences of water absorption and canopy structure, which would facilitate more accurate retrievals of biochemical and photosynthesis-related traits. Secondly, a successful integration of RS and plant ecology concepts would require careful matching of spatial scales of in-situ trait data with RS observations.

In Chapter 3, measurement methods and variability of total to projected leaf area within spruce crowns were investigated. Comparison of six laboratory methods revealed that methods using an elliptic approximation of a needle shape underestimated total leaf area compared to methods using a parallelepiped approximation. The variability in total to projected leaf area was primarily driven by the vertical sampling position and less by needle age or forest stand age. We found that total leaf area estimation has an important implication on RS of leaf chlorophyll content. An error associated with biased estimates of total leaf area can reach up to 30% of the expected chlorophyll range commonly found in forest canopies and therefore negatively influences the validation of RS-based chlorophyll maps.

In Chapter 4, potentials of the continuum removal transformation for mapping of chlorophyll content in spruce canopies were investigated. We tested two methods based on continuum removal: artificial neural networks and an optical index. The optical index was newly designed here and it was based on the spectral continuum between 650 and 720 nm. Both continuum removal based methods exhibited superior accuracy in chlorophyll retrieval compared to commonly used narrow-band vegetation indices (e.g. NDVI, TCARI/OSAVI). The newly designed index was equally accurate, but certainly provided a more operational approach as compared to the neural network.

In Chapter 5, mapping of ecosystem properties that underline ecosystem services provided by subalpine grasslands using RS methods was tested and further compared with a statistical plant trait-based modelling approach. Imaging spectroscopy in combination with empirical retrieval methods was partly successful to map ecosystem properties. The prediction accuracy at the calibration phase was comparable to the trait-based modelling approach. Spatial comparison between the two approaches revealed rather small agreement. The average fuzzy similarity between the approaches was around 20% for ecosystem properties, but in case of the total ecosystem service supply it decreased below 10%. However, the RS approach detected more variability in ecosystem properties and thereby in services, which was driven by local topography and microclimatic conditions, which could not be detected by the plant trait-based approach.

Especially Chapters 2 and 5 indicated that one of the future RS research directions may be in spatial ecology, i.e. spatially explicit mapping of plant traits, ecosystem properties and ecosystem services. High quality RS data are certainly essential building elements for spatial ecology. But in order to address the effects of climate and land use changes on biodiversity and ecosystems, their properties and services, the integration of in-situ and RS data will be ultimately required. Therefore, more coherent experiments, where in-situ and RS data are measured simultaneously at different spatial scales, are needed in the future.

Samenvatting

Terrestrische vegetatie vormt een belangrijk onderdeel van de biosfeer op aarde en speelt dus een essentiële rol in de regulering van het klimaat en de koolstofvastlegging, en het biedt een grote verscheidenheid aan diensten voor de mens. Voor een duurzaam beheer van terrestrische ecosystemen is het essentieel om de vegetatiereactie op verschillende invloeden te begrijpen, en om de ruimtelijke omvang en het tempo van veranderingen in een ecosysteem te monitoren en te voorspellen. Remote sensing (RS) biedt daarom een unieke mogelijkheid voor ruimtelijk continue, en voor sommige type RS-gegevens ook frequente, monitoring van terrestrische ecosystemen.

RS van vegetatie is een breed terrein van onderzoek, waar in de afgelopen drie decennia veel vooruitgang is geboekt. Echter, de complexiteit van de interacties tussen vegetatie en zonnestraling, voortdurend gewijzigd door omgevingsfactoren, biedt ruimte voor nader onderzoek. In plaats van het oplossen van één groot onderzoeksprobleem, bouwt dit proefschrift een paar bruggen op een weg die leidt tot een beter begrip van het gebruik van beeldvormende spectroscopie vanuit vliegtuigen voor ecologische analyse in gematigde naaldbossen en sub-alpiene graslanden. Het onderzoek is opgedeeld in een theoretisch en een toegepast deel. Het theoretische deel draagt bij aan een kritische evaluatie van onderzoeksresultaten en aan uitdagingen in de optische RS van planteigenschappen (Hoofdstuk 2). Het toegepaste deel besteedt aandacht aan drie onderzoeksthema's: i) het onderzoeken van de variabiliteit in de verhouding van totaal ten opzichte van geprojecteerd bladoppervlak bij sparren en de implicaties ervan op de RS van het chlorofylgehalte (Hoofdstuk 3), ii) het testen van methoden voor het bepalen van het chlorofylgehalte bij sparren op basis van de zogenaamde ‘continuum removal’ techniek (Hoofdstuk 4), en iii) het verkennen van de mogelijkheden van beeldvormende spectroscopie voor het karteren van ecosysteem-eigenschappen en het vermogen van sub-alpiene graslanden om ecosysteemdiensten te leveren in vergelijking met een modelbenadering gebaseerd op planteigenschappen (Hoofdstuk 5).

In hoofdstuk 2 wordt een overzicht gegeven van resultaten en uitdagingen voor het schatten van de belangrijkste planteigenschappen met behulp van RS en concentreren we onze discussie op acht eigenschappen met de beste potentie om met behulp van RS in kaart te worden gebracht (plantengroei en levensvorm, ontvlambaarheid, fotosyntheseprocessen en -activiteit, planthoogte, levensduur en fenologie van bladeren, specifiek bladoppervlak, stikstofgehalte en fosforgehalte in het blad). Het overzicht leert dat beeldvormende spectroscopie de bepaling van planteigenschappen gerelateerd aan de biochemische samenstelling van bladeren, fotosynthese en fenologie beter mogelijk maakt dan eigenschappen gerelateerd aan vegetatiestructuur. Schatting van aan vegetatiestructuur-gerelateerde kenmerken (bijv. planthoogte) kan zeker profiteren van de synergie van beeldvormende spectroscopie en actieve RS (radar of laser scanning). Een van de grote uitdagingen in de RS van planteigenschappen is om de negatieve invloeden van absorptie door water en van vegetatiestructuur effectief te onderdrukken, hetgeen nauwkeuriger

bepalingen van biochemische en fotosynthese-gerelateerde kenmerken zou vergemakkelijken. Ten tweede zou een succesvolle integratie van RS en concepten uit de plantenecologie een zorgvuldige afstemming van ruimtelijke schalen van in-situ data met RS observaties vereisen.

In hoofdstuk 3 worden meetmethoden en variabiliteit in de verhouding van totaal ten opzichte van geprojecteerd bladoppervlak bij sparren onderzocht. Uit vergelijking van zes laboratoriumtechnieken blijkt dat methoden met behulp van een elliptische benadering van de naaldvorm het totale bladoppervlak onderschatten in vergelijking tot methoden met behulp van een parallellepipedum benadering. De variabiliteit in de verhouding van totaal ten opzichte van geprojecteerd bladoppervlak wordt voornamelijk bepaald door de verticale positie van bemonstering en minder door de leeftijd van de naalden of van de bosopstand. De schatting van het totale bladoppervlak is van groot belang voor de RS van het chlorofylgehalte van het blad. Een systematische fout in schattingen van het totale bladoppervlak kan oplopen tot 30% van de verwachte range in chlorofylgehaltes gevonden in bossen en heeft dus een negatieve invloed op de validatie van op RS gebaseerde chlorofylkaarten.

In hoofdstuk 4 worden de mogelijkheden van de ‘continuum removal’ transformatie voor het karteren van het chlorofylgehalte bij sparren onderzocht. Wij hebben twee methoden op basis van ‘continuum removal’ getest: kunstmatige neurale netwerken en een optische index. De optische index is nieuw ontworpen en is gebaseerd op het spectrale continuüm tussen 650 en 720 nm. Beide ‘continuum removal’ methoden geven een superieure nauwkeurigheid in het afleiden van het chlorofylgehalte vergeleken met veelgebruikte smalle-band vegetatie indices (bv. NDVI, TCARI / OSAVI). De nieuw ontworpen index is even nauwkeurig, maar geeft zeker een meer operationele benadering vergeleken met het neurale netwerk.

In hoofdstuk 5 wordt het in kaart brengen van ecosysteem-eigenschappen, die ecosysteemdiensten van sub-alpiene graslanden onderstrepen en die verkregen zijn met behulp van RS methoden, getest en verder vergeleken met een statistische modelbenadering gebaseerd op planteigenschappen. Beeldvormende spectroscopie in combinatie met empirische bepalingsmethoden is deels succesvol in het karteren van ecosysteem-eigenschappen. De voorspellingsnauwkeurigheid in de kalibratiefase is vergelijkbaar met de modelbenadering gebaseerd op planteigenschappen. Ruimtelijke vergelijking tussen de twee benaderingen blijkt vrij weinig overeenstemming op te leveren. De gemiddelde ‘fuzzy’ overeenstemming tussen de benaderingen is ongeveer 20% voor ecosysteem-eigenschappen, maar in het geval van de totale levering van ecosysteemdiensten daalt deze beneden 10%. De RS aanpak detecteert echter meer variabiliteit in ecosysteem-eigenschappen en daardoor ook in ecosysteemdiensten, hetgeen gedreven wordt door lokale topografie en micro-klimatologische condities, die niet kunnen worden gedetecteerd door de planteigenschappen-benadering.

Vooral de hoofdstukken 2 en 5 tonen aan dat een van de toekomstige RS onderzoeksrichtingen de ruimtelijke ecologie zou kunnen zijn, d.w.z. het ruimtelijk

expliciet bepalen van planteigenschappen, ecosysteem-eigenschappen en ecosysteemdiensten. Hoge kwaliteit RS gegevens vormen zeker essentiële bouwstenen voor de ruimtelijke ecologie. Maar om de gevolgen aan te pakken van klimaatverandering en landgebruiksveranderingen op biodiversiteit en op ecosystemen, hun eigenschappen en diensten, zal uiteindelijk de integratie van in-situ en RS-gegevens nodig zijn. Daarom zijn meer samenhangende experimenten, waarbij in-situ en RS data gelijktijdig op verschillende schaalniveaus worden gemeten, in de toekomst nodig.

Shrnutí

Vegetace je nezbytnou součásti zemské biosféry, podílí se na regulaci klimatu a poskytuje lidem celou řadu hmotných i nehmotných přínosů (ekosystémové služby). Lidská společnost by proto měla usilovat o trvale udržitelné využívání ekosystémů a hospodaření v nich. Toho lze dosáhnout tehdy, pokud budeme schopni pochopit, jakým způsobem vegetace reaguje na různé stresové podněty, a budeme monitorovat současný stav ekosystémů a předvídat jejich změny v prostoru, čase i co se týče jejich funkce. Vhodným nástrojem pro studium ekosystémů jsou tak moderní metody optického dálkového průzkumu Země (DPZ), které poskytují prostorové informace o zemském povrchu.

Studium vegetace s použitím metod optického DPZ je široké pole vědecké činnosti, která se rozvíjí již 30 let. Avšak vzájemné působení slunečního záření a vegetace je proces natolik komplexní, že neustále poskytuje prostor pro nové vědecké bádaní a zlepšování metod DPZ. Tato disertační práce řeší několik oddělených vědeckých otázek, které zapadají do mozaiky poznání toho, jak letecká obrazová spektroskopie (úzce specifický typ dat DPZ) může přispět ke studiu ekosystémů, jako jsou jehličnaté lesy a horské louky. Disertační práce je rozdělena do dvou částí, teoretické a praktické. Teoretická část kriticky hodnotí současné metody optického DPZ a jejich využití v rámci monitorování stavu a vlastností vegetace (kapitola 2). Praktická část pak řeší tři následující témata: i) jak se mění poměr celkové a projekční listové plochy v porostech smrku ztepilého a jaký vliv mají tyto změny na mapování obsahu chlorofylu z dat obrazové spektroskopie (kapitola 3), ii) vývoj nového metodického postupu pro odhad obsahu chlorofylu v porostech smrku ztepilého z dat obrazové spektroskopie (kapitola 4), a iii) srovnání dvou metod pro mapování ekosystémových vlastností a služeb horských lučních ekosystémů, kde první metoda je založena na prostorových datech obrazové spektroskopie a druhá metoda na pozemních měření vlastností horských luk a způsobu využití půdy (kapitola 5).

Literární rešerše, která je prezentována v druhé kapitole, shrnuje současný stav využití metod optického DPZ v rámci studia vegetace a jejích vlastností. Diskuzi jsme zaměřili především na osm hlavních vlastností vegetace, které se hojně používají při studiu funkce rostlin v ekosystémech a u nichž je zároveň velká pravděpodobnost, že mohou být studovány za pomocí DPZ. Tyto vlastnosti jsou životní formy rostlin, vlastnosti rostlin rozhodující o jejich vznícení, fotosyntéza, její aktivita a rozlišení C3 a C4 rostlin, fenologie rostlin, výška, specifická listová plocha, obsah dusíku a obsah fosforu v listech. Data optické spektroskopie jsou častěji využívána pro studium fyziologických a fenologických vlastností rostlin. Zatímco metody DPZ zaměřené na studium morfologických vlastností rostlin a struktury porostů spíše využívají data aktivního DPZ (radar a laserové skenovaní) a jejich propojení s optickými daty. Hlavním problémem při studiu vlastností vegetace

z dat DPZ je vliv vody a struktury vegetace na kvalitu signálu v infračervených vlnových délkách. Tudíž jedním z hlavních úkolů studia vegetací pomocí metod DPZ je efektivně potlačit tyto negativní vlivy ovlivňující infračervená pásma. Pro ekologicky zaměřené aplikace používající metody optického DPZ je taktéž nezbytné sladit prostorové rozlišení dat DPZ a pozemních měření vlastností rostlin a ekosystémových procesů.

Ve třetí kapitole jsme se zaměřili na studium listové plochy v porostech smrku ztepilého. Studovali jsme, jakým způsobem lze co nejpřesněji změřit celkovou a projekční plochu jehlic, jak se mění poměr mezi celkovou a projekční listovou plochu v rámci koruny smrku, a jakým způsobem se chyby v měření listové plochy promítají do odhadů obsahu chlorofylu z dat obrazové spektrometrie. V této studii jsme srovnali šest metod výpočtu celkové plochy jehlic na základě jejich morfologických znaků a zjednodušeného geometrického modelu jehlice. Metody, které použily elipsoid jako základ geometrického modelu jehlice, výrazně podhodnocovaly celkovou plochu jehlic ve srovnání s metodami, které použily hranol nebo složeninu komolých kuželů jako základ geometrického modelu jehlic. Dále jsme zjistili, že poměr mezi celkovou a projekční plochou jehlic se mění v rámci koruny smrků a to hlavně ve vertikálním směru v závislosti na intenzitě slunečního osvitu. Vliv věku jehlic a průměrného stáří porostu na poměr mezi celkovou a projekční listovou plochou je minimální. Právě výpočet celkové plochy jehlic má i výrazný vliv na přesnost odhadů obsahu chlorofylu z dat DPZ, neboť obsah chlorofylu je často vyjádřen na jednotku listové plochy. Míra chyby z odhadu celkové listové plochy jehlic smrku ztepilého, která se může dále promítnout do obsahu chlorofylu, může činit až 30% z celkového rozsahu běžných hodnot obsahu chlorofylu ve smrkových porostech

Ve čtvrté kapitole jsme se zaměřili na vývoj metodiky odhadu obsahu chlorofylu ve smrkových porostech z dat letecké obrazové spektrometrie s velmi vysokým prostorovým a spektrálním rozlišením. Právě velmi vysoké spektrální rozlišení leteckých snímků umožnilo stanovit metodiku odhadu chlorofylu na tvaru spektrální křivky odrazivosti a využít tak transformaci spektrálního kontinua (tzv. „kontinuum removal“). Transformovaná spektrální informace pomocí „continuum removal“ byla poté využita ve dvou výpočetních modulech, i) jako nově navržený optický vegetační index v rozmezí 650 a 720 nm a ii) jako vstupní data do umělé neuronové sítě. Oba přístupy založené na transformaci spektrálního kontinua dokázaly odhadnout obsah chlorofylu ve smrkových porostech s vyšší přesností než běžně používané vegetační indexy jako NDVI nebo TCARI/OSAVI. I když oba přístupy založené na transformaci spektrálního kontinua vykazovaly podobně přesné výsledky odhadu chlorofylu, nově navržený vegetační index byl početně jednodušší a praktičtější než metoda použití neuronových sítí.

V páté kapitole jsme se pak zaměřili na srovnání dvou metodických přístupů pro ohodnocení ekosystémových služeb v rámci horských lučních ekosystémů. V obou

případech byly ekosystémové služby vztaženy k vlastnostem horských lučních ekosystémů jako nadzemní zelená a suchá biomasa, obsah proteinů, druhová rozmanitost a obsah uhlíku v půdě. Oba přístupy se právě odlišovaly v metodice, jak tyto vlastnosti lučních ekosystémů byly modelovány v prostoru. Jeden přístup byl založen na prostorových datech z letecké obrazové spektroskopie a druhý přístup na prostorových datech jako digitální model terénu a mapy využití půdy. Srovnání obou přístupů ukázalo, že pouze 20% z naší zájmové lokality vykazovalo shodu obou přístupů, co se týče již výše zmíněných modelovaných vlastností lučních ekosystémů. Co se týče služeb poskytovaných horskými loukami, tak pouze 10% z celkové plochy naší zájmové lokality vykazovalo shodu mezi oběma přístupy. Výhodou metodiky založené na datech letecké obrazové spektroskopie bylo, že dokázala zachytit mnohem vyšší variabilitu ekosystémových vlastností v prostoru, což odráží vysokou rozmanitost terénu a mikroklimatických podmínek v rámci studované lokality.

Prostorově zaměřené analýzy v ekologii se budou neustále rozvíjet. Jak nastínily kapitoly 2 a 5, stanou se data optického DPZ, zejména pak obrazové spektroskopie, základním stavebním kamenem pro moderní ekologii (mapování a monitorování stavu ekosystémů a jejich vlastností). Každopádně vývoj takovýchto přístupů bude vyžadovat sladění a souhru metod DPZ s ekologickými metodami a více příležitostí, kdy budou pozemní data ekosystémových vlastností a data dálkového průzkumu Země měřena současně a v různých prostorových měřítkách.

Acknowledgements

Reflecting back on my PhD time with some of distance, I have to say that it was an exciting though sometimes painful experience, but it certainly was an interesting and worthy way that I decided to walk on. There have been many people, supervisors, colleagues, friends and my closest family, who supported me during that time and now I would like to use this opportunity to say "Thank You".

First of all, I would like to express my sincere thanks to my supervisors, Michael Schaepman and Jan Clevers. Although our interactions were sometimes scarce due to the fact that we rarely shared the same geographical location, I appreciate your encouragement and valuable comments to my work. I am very grateful to Michael for the opportunity spending last two years at Remote Sensing Laboratories in Zurich.

I would like to thank to all of my co-authors for the constructive comments and feedback on my papers. It was my pleasure to keep on working with my former colleagues from the remote sensing group of Czechglobe – Petr Lukeš, Jan Hanuš and Věroš Kaplan. I would like to thank to Zbyněk Malenovský for his partial coordination during my first year in Zurich and his valuable feedback on my papers. And I wish to thank to Sandra Lavorel and Pénélope Lamarque from Laboratoire d'Ecologie Alpine, who helped me a lot with my last paper on ecosystem services

In order to keep the PhD spirit up, I'm more than grateful to all my friends, who gave me an opportunity to take a break from it and spent pleasurable moments in their company. I would like to thank to my office mates from RSL for a friendly working atmosphere. Thanks to Jirka I know how Lapland looks in winter. Thanks to Monika, Pawel and Agatka I discovered beauties of Poland. Livia pushed me beyond my physical limits when asking for more pilates and jogging. And it was always very happy to meet every now and then a couple of friends from the Czech Republic and therefore my greetings and thanks go to Jana, Blanka, Honza, Jarka and their families. My special thanks go to Scotland to my good friend Andrea, who always recharged me with her overwhelming positive energy. Last but not least, I wish to express my deepest gratitude to my best PhD mates and good friends, Lucia, Petra, Valerie and Titia. Girls, your support and nice time we spent together were priceless.

Most importantly, I want to say big "DĚKUJI" to my family. My deepest respect and gratitude flies to my parents and grandparents for their never ending support, love and endless hours on skype when reporting news from home. I want to thank to my brothers Jirka and Tomáš and to my cousins Víťa and Zuzka, who always find time to visit me wherever I was living. And I owe my deep loving thanks to Daniel who supported me with friendship, love, energy, inspiration and chocolate during last years of my PhD. I truly believe that getting know you is the most valuable outcome of this project.

Short biography

Lucie was born in Velké Meziříčí, located nearby Brno in the Czech Republic on July 19th, 1981. She attended the local primary school, as well as the gymnasium in Velké Meziříčí, where she graduated in 1999. Besides her regular studies she attended painting and handcrafting classes and handcrafting remained her most enjoyable and relaxing hobby until now.

In 1999 she started her master studies at *Czech University of Life Sciences Prague*. She studied master curriculum in *Landscape engineering* at *Faculty of forestry and environment.* After the fourth year of her master studies she decided to get an international experience and thanks to the Erasmus student exchange program she could spend one year in the Netherlands at *Wageningen University*. At the end, she extended her stay in Wageningen by one more year and in 2005 she obtained her first master degree in *Geo-Information Science*. Her master thesis was about leaf area index estimation in Norway spruce forests using airborne imaging spectroscopy and radiative transfer modelling.

After she graduated in Wageningen, Lucie moved back to the Czech Republic. She finished her master studies of Landscape engineering and started a part time research job at *Academy of Sciences, Institute of Systems Biology and Ecology* (nowadays called *Global Change Research Centre*). Her major responsibilities were field measurements of forest biochemical and spectral properties and further data processing. She was contributing to the ESA/PECS project on spectral-spatial scaling of forest biochemical properties to support forthcoming GMES Sentinel 2 mission.

In February 2008 Lucie joined *Marie Curie Research Training Network (Hyper-I-Net)* and at the same time she started her PhD curriculum at *Wageningen University*. Within the Hyper-I-Net network Lucie spent two years in *Specim, Ltd.* (Finland), a leading company in imaging spectroscopy. Lucie was trained in calibration of airborne imaging spectroradiometers and she explored the use of downwelling irradiance sensor for atmospheric correction of airborne images. In February 2010 Lucie moved to Poland, where she spent nine months at *University of Warsaw*. Since 2011 Lucie was located at *University of Zurich* in Switzerland, where she continued working on her PhD thesis, which is successfully finished by now.

In the course of five years of her PhD, Lucie lived in three countries with contrasting cultural background. Besides moving around Europe and exploring Finnish, Polish and Swiss cultures, food and landscapes Lucie worked on various research topics presented in this thesis. She attended several courses, summer schools and international conferences.

List of publications

Peer reviewed journals

Homolová L, Schaepman ME, Lamarque P, Clevers JGPW, de Bello F, Thuiller W, Lavorel S (2013) Comparison of remote sensing and plant trait-based modelling to predict ecosystem services in subalpine grasslands. *Journal of Ecology* (Submitted)

Pottier J, Malenovský Z, Psomas A, **Homolová L**, Schaepman ME, Choler P, Thuiller W, Guisan A, Zimmermann NE (2013) Modelling plant species distribution and diversity in alpine grasslands using airborne imaging spectroscopy. *Biology Letters* (Submitted)

Homolová L, Malenovský Z, Clevers JGPW, García-Santos G, Schaepman ME (2013) Review of optical-based remote sensing for plant trait mapping. *Ecological Complexity* 15: 1-16

Malenovský Z, **Homolová L**, Zurita-Milla R, Lukeš P, Kaplan V, Hanuš J, Gastellu-Etchegorry J-P, Schaepman ME (2013) Retrieval of spruce leaf chlorophyll content from airborne image data using continuum removal and radiative transfer. *Remote Sensing of Environment*, 131, 85-102.

Homolová L, Lukeš P, Malenovský Z, Lhotáková Z, Kaplan V, Hanuš J (2013) Measurement methods and variability assessment of the Norway spruce total leaf area: implications for remote sensing. *Trees Structure and Functions*, 27, 111-121.

Rautiainen M, Mõttus M, Yáñez-Rausell L, **Homolová L**, Malenovský Z, Schaepman ME (2012) A note on upscaling coniferous needle spectra to shoot spectral albedo. *Remote Sensing of Environment*, 117, 469-474

Malenovský Z, Martin E, **Homolová L**, Gastellu-Etchegorry J-P, Zurita-Milla R, Schaepman ME, Pokorný R, Clevers JGPW, Cudlín P (2008) Influence of woody elements of a Norway spruce canopy on nadir reflectance simulated by the DART model at very high spatial resolution. *Remote Sensing of Environment*, 112(1), 1-18

Other scientific publications

Homolová L, Alanko-Huotari K, Schaepman ME (2009) Sensitivity of the ground-based downwelling irradiance recorded by the FODIS sensor in respect of different angular positions. *1st IEEE Workshop on Hyperspectral Image and Signal Processing: Evolution in Remote Sensing (WHISPERS)*. Grenoble, France

Yañez-Rausell L, **Homolová L**, Malenovský Z, Schaepman ME (2008) Geometrical and structural parameterization of forest canopy radiative transfer by LIDAR measurements. *The International Archives of the Photogrammetry, Remote Sensing and Spatial Information Sciences XXI ISPRS Congress*. Beijing, China

Homolová L, Malenovský Z, Lhotáková Z, Kaplan V, Hanuš J (2007) Optical differences between sun exposed and shaded Norway spruce needles. *5th EARSeL SIG IS workshop on Imaging Spectroscopy: innovation in environmental research*. Bruges, Belgium

Homolová L, Malenovský Z, Hanuš J, Tomášková I, Dvořáková M, Pokorný R (2007) Comparison of different ground techniques to map leaf area index of Norway spruce forest canopy. *10th International Symposium on Physical Measurements and Spectral Signatures in Remote Sensing*. Davos, Switzerland

PE&RC PhD Education Certificate

With the educational activities listed below the PhD candidate has complied with the educational requirements set by the C.T. de Wit Graduate School for Production Ecology and Resource Conservation (PE&RC) which comprises of a minimum total of 32 ECTS (= 22 weeks of activities)

Review of literature (6 ECTS)

- Review of optical-based remote sensing for plant functional ecology

Writing of project proposal (4.5 ECTS)

- Mapping of plant functional groups of alpine grassland ecosystems using airborne imaging spectroscopy and soil-vegetation-atmosphere radiative transfer modelling (2008)

Post-graduate courses (7.5 ECTS)

- Advanced IDL programming course; WUR-CGI, NL (2008)
- Inverse modelling for improving environmental and ecological models; University of Amsterdam, NL (2009)
- 2nd Hyper-I-Net summer school on Earth sciences and applications using imaging spectroscopy; WUR-CGI, NL (2008)
- 3rd Hyper-I-Net summer school on hyperspectral data: from images to information; University of Pavia, I (2009)
- 4th Hyper-I-Net summer school on calibration; DLR, D (2010)
- Atmospheric correction over land using ATCOR; DLR, D (2011)

Competence strengthening / skills courses (1.2 ECTS)

- Techniques for writing and presenting scientific papers; WUR, NL (2009)

Laboratory training and working visits (3.9 ECTS)

- Radiometric calibration of hyperspectral sensors; Specim Ltd., FI (2008)
- Training in atmosphere radiative transfer MODTRAN & ATCOR; RSL, University of Zürich, CH (2009)

PE&RC Annual meetings, seminars and the PE&RC weekend (1.6 ECTS)

- PE&RC Day: Scaling from molecules to ecosystems (2008)
- PE&RC Symposium: 3rd remote sensing symposium of Dutch network of PhD students; Oral presentation (2011)

Discussion groups / local seminars / other scientific meetings (4.2 ECTS)

- Meetings of AISA research & development group; Specim Ltd., FI (2008 and 2009)
- Hyper-I-Net mid–term review meeting; DLR, D (2009)
- Plant facility and terrestrial LIDAR workshop; WUR-CGI, NL (2011)
- Colloquium in Remote Sensing; RSL, University of Zürich, CH (2012)
- "Friday's food for thought"- an interdisciplinary discussion club; Geography department; University of Zürich, CH (2011 and 2012)

International symposia, workshops and conferences (3.5 ECTS)

- 2nd PHYSENSE workshop of the Nordic network on physically-based remote sensing of forests; Helsinki, FI (2011)
- 9th Swiss geoscience meeting; poster presentation; Zürich, CH (2011)
- A European perspective on the future of biodiversity and ecosystems - final conference of the Ecochange FP6 project; poster presentation; Zürich, CH (2012)

Lecturing / supervision of practical's/ tutorials; 1 day (0.3 ECTS)

- Verification of remote sensing products: guest lecture; University of Warsaw, PL (2010)